frontiers | Research Topics

Zoonotic diseases originating from wildlife: Emergence/ re-emergence, evolution, prevalence, pathogenesis, prevention, and treatment

Edited by
Hongliang Chai, Quan Liu, Natasha N. Gaudreault and Zhang Wan Jiang

Published in
Frontiers in Microbiology

ISSN 1664-8714
ISBN 978-2-83252-045-1
DOI 10.3389/978-2-83252-045-1

About Frontiers

Frontiers is more than just an open access publisher of scholarly articles: it is a pioneering approach to the world of academia, radically improving the way scholarly research is managed. The grand vision of Frontiers is a world where all people have an equal opportunity to seek, share and generate knowledge. Frontiers provides immediate and permanent online open access to all its publications, but this alone is not enough to realize our grand goals.

Frontiers journal series

The Frontiers journal series is a multi-tier and interdisciplinary set of open-access, online journals, promising a paradigm shift from the current review, selection and dissemination processes in academic publishing. All Frontiers journals are driven by researchers for researchers; therefore, they constitute a service to the scholarly community. At the same time, the *Frontiers journal series* operates on a revolutionary invention, the tiered publishing system, initially addressing specific communities of scholars, and gradually climbing up to broader public understanding, thus serving the interests of the lay society, too.

Dedication to quality

Each Frontiers article is a landmark of the highest quality, thanks to genuinely collaborative interactions between authors and review editors, who include some of the world's best academicians. Research must be certified by peers before entering a stream of knowledge that may eventually reach the public - and shape society; therefore, Frontiers only applies the most rigorous and unbiased reviews. Frontiers revolutionizes research publishing by freely delivering the most outstanding research, evaluated with no bias from both the academic and social point of view. By applying the most advanced information technologies, Frontiers is catapulting scholarly publishing into a new generation.

What are Frontiers Research Topics?

Frontiers Research Topics are very popular trademarks of the *Frontiers journals series*: they are collections of at least ten articles, all centered on a particular subject. With their unique mix of varied contributions from Original Research to Review Articles, Frontiers Research Topics unify the most influential researchers, the latest key findings and historical advances in a hot research area.

Find out more on how to host your own Frontiers Research Topic or contribute to one as an author by contacting the Frontiers editorial office: frontiersin.org/about/contact

Zoonotic diseases originating from wildlife: Emergence/re-emergence, evolution, prevalence, pathogenesis, prevention, and treatment

Topic editors

Hongliang Chai — Northeast Forestry University, China
Quan Liu — First Affiliated Hospital of Jilin University, China
Natasha N. Gaudreault — Kansas State University, United States
Zhang Wan Jiang — Chinese Academy of Agricultural Sciences (CAAS), China

Citation

Chai, H., Liu, Q., Gaudreault, N. N., Jiang, Z. W., eds. (2023). *Zoonotic diseases originating from wildlife: Emergence/re-emergence, evolution, prevalence, pathogenesis, prevention, and treatment*. Lausanne: Frontiers Media SA.
doi: 10.3389/978-2-83252-045-1

Table of contents

frontiers | Frontiers in Microbiology

TYPE Editorial
PUBLISHED 14 March 2023
DOI 10.3389/fmicb.2023.1165365

OPEN ACCESS

EDITED AND REVIEWED BY
Axel Cloeckaert,
Institut National de Recherche Pour l'Agriculture, l'Alimentation et l'Environnement (INRAE), France

*CORRESPONDENCE
Hongliang Chai
✉ hongliang_chai@hotmail.com
Quan Liu
✉ liuquan1973@hotmail.com
Natasha N. Gaudreault
✉ nng5757@vet.k-state.edu
Wanjiang Zhang
✉ wanjiang09@126.com

SPECIALTY SECTION
This article was submitted to Infectious Agents and Disease, a section of the journal Frontiers in Microbiology

RECEIVED 14 February 2023
ACCEPTED 16 February 2023
PUBLISHED 14 March 2023

CITATION
Chai H, Liu Q, Gaudreault NN and Zhang W (2023) Editorial: Zoonotic diseases originating from wildlife: Emergence/re-emergence, evolution, prevalence, pathogenesis, prevention, and treatment.
Front. Microbiol. 14:1165365.
doi: 10.3389/fmicb.2023.1165365

Editorial: Zoonotic diseases originating from wildlife: Emergence/re-emergence, evolution, prevalence, pathogenesis, prevention, and treatment

Hongliang Chai[1]*, Quan Liu[2]*, Natasha N. Gaudreault[3]* and Wanjiang Zhang[4]*

[1]College of Wildlife and Protected Area, Northeast Forestry University, Harbin, China, [2]Department of Infectious Diseases and Center of Infectious Diseases and Pathogen Biology, Key Laboratory of Organ Regeneration and Transplantation of the Ministry of Education, Key Laboratory of Zoonotic Diseases, The First Hospital of Jilin University, Changchun, China, [3]Department of Diagnostic Medicine/Pathobiology, College of Veterinary Medicine, Kansas State University, Manhattan, KS, United States, [4]State Key Laboratory of Veterinary Biotechnology, Harbin Veterinary Research Institute, Chinese Academy of Agricultural Sciences, Harbin, China

KEYWORDS

zoonotic diseases, wildlife, evolution, prevalence, pathogenesis, prevention, treatment, emergence/re-emergence

Editorial on the Research Topic
Zoonotic diseases originating from wildlife: Emergence/re-emergence, evolution, prevalence, pathogenesis, prevention, and treatment

Wild animals carry a variety of pathogens and can serve as natural reservoirs of pathogens because they live in complex environments. Wildlife diseases not only pose a serious threat to animal health, especially rare and endangered wild animals, but also cause important zoonoses that threaten public health, such as AIDS, Ebola, avian influenza, and others. It has been reported that 60.3% of emerging human infectious diseases are animal-borne, of which 71.8% have originated from wildlife. In addition, due to the habits of wildlife migration, wild animals and birds are major disease spreaders, as they can transmit many zoonotic diseases across regions and country borders, intercontinentally and globally. Meanwhile, many mosquitoes and ticks carried by wildlife are also major vectors of diseases (vector-borne diseases), facilitating disease spread, causing huge economic losses to poultry and livestock, and bringing major public health problems to human beings. With this context, we launched this Research Topic on 10 January 2022. Frontiers in Microbiology published 12 articles, involving 139 authors from nine countries. Despite the diversity of 10 zoonotic diseases, the contributions fall into three research areas: viral diseases, bacterial diseases, and parasitic diseases.

Viral diseases

The first area of research, viral diseases, included avian influenza, AIDS, COVID-19, parvovirus infection, hemorrhagic fever with renal syndrome (HFRS), Monkeypox (MPX), and tick-borne encephalitis virus. Emerging infectious diseases are one of the main threats to public health, with the potential to cause a pandemic when the infectious agent manages to spread globally. Miranda et al. reviewed three major pandemics: the influenza pandemic, the human immunodeficiency virus (HIV) pandemic, and the COVID-19 pandemic. They analyzed these pandemics' historical and epidemiological contexts and the determinants of their emergence. Furthermore, they compared pharmaceutical and non-pharmaceutical interventions that had been used to slow down these three pandemics and focus on the technological advances that were made in the progress. Finally, they discussed the evolution of epidemiological modeling, which has become an essential tool to support public health policymaking and they discuss it in the context of these three pandemics. While these pandemics were caused by distinct viruses that started in different periods and different regions of the globe, their work showed that many of the determinants of their emergence and countermeasures used to halt transmission were common. Therefore, it is important to further improve and optimize such approaches and adapt them to future-threatening emerging infectious diseases.

Since it was first identified in 1956, the H11 subvariant influenza virus has been reported worldwide for several decades. Jiang, Li, et al. isolated a strain of H11N3 avian influenza virus (AIV) from poultry feces in live poultry markets in the southeast coastal region of China. Considering that H11 subvariants were known to cause human infections and to enrich the knowledge of the H11 subvariant avian influenza virus, genetics, pathogenicity, and transmissibility of the isolate were studied. Phylogenetic analysis indicated that the H11N3 isolate was of Eurasian origin and carried genes that were closely related to duck H7N2 and H4N6. The receptor-binding preference analysis revealed that the H11N3 isolate only acquired a binding affinity for avian-derived receptors. In the respiratory system of mice, the isolated virus could directly infect mice without adaptation. In addition, results from transmission experiments and the detection of antibodies in guinea pigs demonstrated that the H11N3 influenza virus can efficiently transmit through the respiratory tract in mammalian models. Direct infection of the H11N3 influenza virus without adaptation in mouse models and aerosol transmission between guinea pig models confirmed its pandemic potential in mammals, underscoring the importance of monitoring rare influenza virus subtypes in future studies.

To date, there have been three epidemic waves of H5N8 avian influenza worldwide. The current third epidemic wave began in October 2020 and has expanded to at least 46 countries. Jiang, Liu, et al. conducted active and passive surveillance to monitor H5N8 viruses from wild birds in China. Genetic analysis of 10 H5N8 viruses isolated from wild birds identified two different genotypes. Animal challenge experiments indicated that the H5N8 isolates were highly pathogenic in chickens, and mildly pathogenic in ducks, while pathogenicity varied in Balb/c mice. Moreover, there were significant differences in antigenicity as compared to the Re-11 vaccine strain, and vaccinated chickens were not completely protected against the high dose of the H5N8 virus. With the use of the new matched vaccine and increased poultry immune density, surveillance should be intensified to monitor the emergence of mutant strains and potential worldwide spread *via* wild birds.

Avian-to-mammal transmission and mammalian adaptation of AIV are threats to public health and are of great concern. The H3 subtype of the influenza virus has low pathogenicity and is widely distributed in humans, canines, equines, and avians. In 2018–2019, Yao et al. isolated six H3N2 subtype influenza viruses from 329 samples acquired from ducks in China as part of an ongoing virus surveillance program. One strain of the H3N2 virus was a novel reassortant influenza virus containing HA and PB2 segments from the canine H3N2 virus. The findings suggested that the viruses studied have undergone multiple reassortment events. Their results provided a framework for understanding the molecular basis of host-range shifts of influenza viruses and indicated that dogs were potential "mixing vessels" for influenza virus transmission.

COVID-19 has emerged as a major public health challenge worldwide. A comprehensive understanding of clinical characteristics and immune responses in COVID-19 asymptomatic carriers and symptomatic patients was of great significance to the countermeasures of COVID-19 patients. Li et al. described the clinical information and laboratory findings of 43 individuals from Hunan Province, China, including 13 COVID-19 asymptomatic carriers, 10 symptomatic patients, and 20 healthy controls from 25 January to 18 May 2020. Their results showed that for cytokines, significantly higher Th1 cytokines including IL-2, IL-8, IL-12p70, IFN-γ, and TNF-α as well as Th2 cytokines including IL-10 and IL-13 were observed in symptomatic patients compared with asymptomatic carriers. Compared with symptomatic patients, higher N-specific IgG4/IgG1 ratios and RBD-specific/N-specific IgG1 ratios were observed in asymptomatic carriers. Comparable nAbs were detected in both asymptomatic carriers and symptomatic COVID-19 patients. In the symptomatic group, nAbs in patients with underlying diseases were weaker than those of patients without underlying diseases. Their retrospective study enriches and verifies the clinical characteristics and serology diversities in COVID-19 asymptomatic carriers and symptomatic patients.

The fact that wild felines are carriers of pernicious infectious viruses should be a major concern due to the potential cross-species transmission between the felines and human or domestic animals. Huang et al. screened four infectious viruses: feline parvovirus (FPV), feline coronavirus (FCoV), canine distemper virus (CDV), and influenza A virus (IAV) in the blood samples of 285 captive Siberian tigers and the spleen samples from two deceased lions, which were collected from 2019 to 2021 in three Siberian Tigers Parks from the northeast of China. The results showed that FPV circulated in the captive Siberian tigers and lions in northeastern China, and this provided valuable information for the study of FPV epidemiology in wild felines.

To analyze the clinical significance of serum ferritin, procalcitonin (PCT), and C-reactive protein (CRP) in hemorrhagic fever with renal syndrome patients, Che et al. analyzed the demographical, clinical, and laboratory data in 373 HFRS patients in northeastern China retrospectively. The levels of serum ferritin

and PCT in severe patients ($n = 108$) were significantly higher than those in mild patients ($n = 265$, $p < 0.001$) and associated with HFRS severity. The serum ferritin level in non-survivors ($n = 14$) was significantly higher than in survivors ($n = 359$, $p < 0.001$). They found that serum ferritin and PCT had a robust association with HFRS severity and mortality, which might be promising predictors, and CRP was an effective biomarker to assess bacterial co-infection in HFRS.

Monkeypox was first reported in humans in 1970, and outbreaks were restricted and highly localized to endemic regions of western and central Africa. However, after the first reported case in the UK in early May 2022, Karim et al. believed that the pattern of epidemic spreading in the geographical regions was much larger compared to the past, posing a risk that MPX might become entrenched beyond endemic areas. This virus is less transmissible than SARS-CoV-2, as it is transmitted mainly through personal, close, often skin-to-skin contact with infectious MPX rash, body fluids, or scabs from an individual with MPX. Infections usually present with chills, fever, fatigue, muscle aches, headache, sore throat, skin lesions, and lymphadenopathy. Currently, there are no antivirals approved for MPX. However, an antiviral drug called "tecovirimat" which was approved for the treatment of smallpox has been made accessible to treat MPX. Moreover, to prevent MPX, there are two vaccines available that are approved by FDA: Bavarian Nordic JYNNEOS and ACAM2000 vaccine. Contact tracing is absent in the case of an MPX outbreak and there is a lack of information from the data systems rapid manner. Additionally, test capacity needs to be increased. Like SARS-CoV-2, global demand for vaccines for the MPX outbreak far exceeds availability.

The geographic range of tick-borne encephalitis virus (TBEV) and the human incidence is increasing throughout Europe putting many non-endemic regions and countries at risk of outbreaks. In the spring of 2020, there was an outbreak of TBE in Ain, Eastern France, where the virus had never been detected before. Gonzalez et al. investigated the suspected farm using an integrative One Health approach. They confirmed the alimentary origin of the TBE outbreak and witnessed in real-time the seroconversion of recently exposed individuals and the excretion of the virus in goat milk. In addition, they identified a wooded focus area where and around which there was a risk of TBEV exposure, provided the first TBEV isolate which was a source of dietary contamination in France, obtained its full-length genome sequence, and found that it did not cluster very closely neither with the isolate circulating in Alsace nor with any other isolate within the European lineage. TBEV is now a notifiable human disease in France, which facilitates surveillance of TBEV incidence and distribution throughout France.

Bacterial diseases

The bacterial diseases in our Research Topic included *Bartonella* infection and *pseudotuberculosis*. Rodents are the primary natural reservoirs of *Bartonella* spp. and some are zoonotic causative agents. Hence, surveillance of *Bartonella* sp. infection in rodents is very important for the prevention of human bartonellosis. Jian et al. captured rodents and collected their spleen samples for *Bartonella* sp. DNA detection and identification by amplifying the 16S rRNA, gltA, and ftsz genes using semi-nested polymerase chain reaction (PCR). The results indicated that *Bartonella* sp. DNA was detected in seven *Rattus norvegicus* individuals with a detection rate of 6.7% in Chengde City, while bacterial DNA in 31 *Apodemus agrarius* individuals with a detection rate of 28.4% in Handan City. The DNA detection rate across the rodents' genders and ages was not statistically significant. Furthermore, sequence analysis of the above-mentioned three genes demonstrated that at least eight *Bartonella* species were circulating in Hebei Province, of which three, including *Bartonella rattimassiliensis*, *Bartonella grahamii*, and *Bartonella tribocorum* are human pathogens, thus suggesting the existence of a major public health risk. Overall, these results revealed the detection rate and genetic diversity of *Bartonella* species infection in rodents in Hebei Province, which could be potentially helpful for the prevention of bartonellosis caused by rodent-associated *Bartonella* species. Their study highlighted the urgent need for the surveillance of *Bartonella* infection in rodents and ectoparasites that affect both rodents and humans and could cause fever of unknown origin or endocarditis.

Yersinia pseudotuberculosis is a foodborne zoonotic bacterium that is pathogenic to guinea pigs, rabbits, and mice. It also causes *pseudotuberculosis* in humans. Dong et al. found out that Ebselen (EbSe) exhibited synergistic antibacterial activity with silver nitrate (Ag+) against *Y. pseudotuberculosis* YpIII strain with high efficacy *in vitro* using UV-vis, DTNB, LSCM, FCM, ETM, and WB assays. The depletion of total glutathione (GSH) amount and inhibition of thioredoxin reductase (TrxR) activity in the thiol-dependent redox system revealed the destructiveness of EbSe-Ag+-caused intracellular oxidative stress. Furthermore, a YpIII-caused mice gastroenteritis model was constructed, and EbSe-Ag+ significantly reduced bacterial loads with low toxicity, downregulated the expression levels of interferon (IL)-1β and tumor necrosis factor-α, and upregulated the expression level of IL-10 on-site, demonstrating the *in vivo* antibacterial activity and immune-modulatory property of EbSe-Ag+. Collectively, these results provided academic fundamentals for further analysis and development of EbSe-Ag+ as the antibacterial agent for *pseudotuberculosis* control.

Parasitic diseases

The third area of research was parasitic diseases. *Echinococcus multilocularis*, the causative agent of alveolar echinococcosis (AE), severely threatens human health and livestock farming. The first line of chemotherapeutic drug for AE is albendazole, which limits the rapid extension of *E. multilocularis* metacestodes, but is rarely curative for AE, with severe side effects in long-term use. Thus, the development of new anti-echinococcal drugs is mandated. Pseudolaric acid B (PAB) has long been used to treat fungal-infected dermatosis and exerted anti-tumor, -fertility, -angiogenesis, -tubulin, and antiparasitic activity. However, the effect of PAB against *Echinococcus* spp. remains unclear. Gao et al. found that after exposure to PAB at 20 μg/ml, a significant reduction of the survival rate and substantial ultrastructural destructions in *E. multilocularis* protoscoleces were observed *in vitro*. Furthermore, the wet weight of *E. multilocularis* cysts in

the infected mice was significantly decreased after treatment with PAB (40, 20, or 10 mg/kg) for 12 weeks. Meanwhile, a significant increase of both protein and mRNA expression of transforming growth factor-beta 1 (TGF-β1) was detected in the serum and liver of the infected mice, whereas PAB administration lowered its expression significantly. The toxicity tests demonstrated that PAB displayed lower cytotoxicity to human liver and kidney cells (HL-7702 and HK-2 cell) with IC_{50} = 25.29 and 42.94 μg/ml than albendazole with IC_{50} = 3.71 and 21.22 μg/ml *in vitro*, and caused lower hepatoxicity and nephrotoxicity in mice than ABZ. Their findings indicated that PAB possesses a potent anti-echinococcal effect with lower toxicity than albendazole, implying it is a potential chemotherapeutic agent for AE. Additionally, their study demonstrated that the suppressive effect of PAB on the parasite may involve the down-regulation of TGF-β1 signaling.

In conclusion, these articles find that the spillover of pathogens from wildlife to domestic animals or humans can lead to the rapid evolution of the pathogen. Under the immune stress in new hosts, pathogens can evolve and acquire new biological properties which may pose a serious threat to the health of domestic animals and humans. Pathogens carried by wild animals and birds are not only transmitted across proximal hosts but can also spread over wide ranges geographically *via* wildlife migration. Understanding the risks of wildlife-borne zoonotic diseases is necessary to increase awareness and facilitate the application of preventive and control measures to reduce disease spread.

Author contributions

All authors listed have made a substantial, direct, and intellectual contribution to the work and approved it for publication.

Conflict of interest

The authors declare that the research was conducted in the absence of any commercial or financial relationships that could be construed as a potential conflict of interest.

Publisher's note

frontiers | Frontiers in Microbiology

ORIGINAL RESEARCH
published: 05 April 2022
doi: 10.3389/fmicb.2022.857800

Emergence and Evolution of Novel Canine-Avian Reassortant H3N2 Influenza A Viruses in Duck in Leizhou Peninsula, China

Qiucheng Yao[1†], Wenhong Mai[1†], Yuexiao Lian[2†], Mengdi Zhang[1], Qiang Yao[3], Caiyun Huang[4], Ye Ge[1] and Zhihui Zhao[1*]*

[1] College of Coastal Agricultural Sciences, Guangdong Ocean University, Zhanjiang, China, [2] Guangdong Laboratory Animals Monitoring Institute and Guangdong Key Laboratory of Laboratory Animals, Guangzhou, China, [3] China Animal Disease Prevention and Control Center, Beijing, China, [4] Central People's Hospital of Zhanjiang, Zhanjiang, China

OPEN ACCESS

Edited by:
Hongliang Chai,
Northeast Forestry University, China

Reviewed by:
Yanbing Li,
Harbin Veterinary Research Institute (CAAS), China
Guimei He,
East China Normal University, China
Daxin Peng,
Yangzhou University, China

***Correspondence:**
Ye Ge
geye_perfect@126.com
Zhihui Zhao
zhzhao@jlu.edu.cn

[†] These authors have contributed equally to this work

Specialty section:
This article was submitted to Infectious Agents and Disease, a section of the journal Frontiers in Microbiology

Received: *19 January 2022*
Accepted: *28 February 2022*
Published: *05 April 2022*

Citation:
Yao Q, Mai W, Lian Y, Zhang M, Yao Q, Huang C, Ge Y and Zhao Z (2022) Emergence and Evolution of Novel Canine-Avian Reassortant H3N2 Influenza A Viruses in Duck in Leizhou Peninsula, China. Front. Microbiol. 13:857800. doi: 10.3389/fmicb.2022.857800

Avian-to-mammal transmission and mammalian adaptation of avian influenza virus (AIV) are threats to public health and of great concern. The H3 subtype of influenza virus has low pathogenicity and is widely distributed in humans, canines, equines and avians. In 2018–2019, we isolated six H3N2 subtype influenza viruses from 329 samples acquired from ducks on the Leizhou Peninsula, China, as part of an ongoing virus surveillance program. All viruses were analyzed by whole-genome sequencing with subsequent genetic comparison and phylogenetic analysis. Phylogenetic analysis demonstrated that reassortment of these viruses has occurred among different hosts and subtypes. Some of the H3 AIV isolates have similar genes as subtypes H5 and H7 of highly pathogenic avian influenza viruses (HPAIVs). Most importantly, one strain of H3N2 virus is a novel reassortant influenza virus containing HA and PB2 segments from canine H3N2 virus. The time of most recent common ancestor (tMRCA) data indicated that this reassortant H3N2 virus might have emerged in 2011–2018. The findings suggest that the viruses studied here have undergone multiple reassortment events. Our results provide a framework for understanding the molecular basis of host-range shifts of influenza viruses and we should pay more attention to canine which lived with avian together.

Keywords: avian influenza virus, H3N2, canine originated, evolution, reassortment

INTRODUCTION

Avian influenza virus (AIV) is a negative-sense RNA virus that belongs to the Orthomyxoviridae family and includes subtypes with a wide range of hosts, primarily birds and mammals (Zhu et al., 2015; Lycett et al., 2019). AIVs are divided into two categories: lowly pathogenic AIVs (LPAIVs) and highly pathogenic AIVs (HPAIVs) (Sun et al., 2017). HPAIVs are leading threats on commercial poultry farms, causing massive economic losses and posing high risks to public health. HPAIVs

Abbreviations: AIV, avian influenza virus; HA, hemagglutinin gene; NA, neuraminidase gene; PB2, polymerase PB2 gene; PB1, polymerase PB1 and putative PB1-F2 protein genes; PA, polymerase PA and PA-X protein (PA-X) genes; M, matrix protein 2 and matrix protein 1 genes; NP, nucleocapsid protein gene; NS, nuclear export protein (NEP) and non-structural protein 1 (NS1) genes.

often cause severe disease outbreaks in domestic poultry and wild birds and can cause outbreaks in humans. LPAIVs usually cause only asymptomatic infection, where infected animals seem healthy, or mild disease in poultry; however, LPAIVs also pose a threat to human health, as they can provide HPAIVs with gene segments, allowing novel HPAIVs or other viruses to arise through genetic rearrangement and recombination and cause severe infection (Peng et al., 2013; Sun et al., 2017). However, as LPAIVs usually do not cause disease or death in animals, they are low-priority targets for animal disease control, which allows them to evolve silently in nature.

H3N2 influenza viruses are the main causes of epidemics and have spread widely in humans since 1968. The H3N2 subtype of influenza virus is widespread in humans, canines, ferrets, swine, and domestic and wild birds. Although the H3N2 subtype is categorized as an LPAIV, it actively circulates in humans. Some avian-origin H3N2 viruses have been transmitted to dogs, causing severe respiratory disease. In 2007, Song et al. (2008) and Zhang et al. (2015) isolated H3N2 strains of avian origin from dogs with severe respiratory diseases and reported that this subtype of AIV could bind the SAα 2,3-gal receptor (revealing that this subtype can be transmitted from poultry to dogs and steadily persist in dogs). During 2009–2010, 12 avian-origin H3N2 strains were isolated from dogs in northern China. Analysis of eight gene segments of the isolates indicated that all eight segments were from H3N2 AIVs from southern China and Korea (Sun et al., 2013a). These studies show that the H3N2 subtype has spread globally and that dogs play an important role as intermediate hosts.

Virus ecology and evolution play central roles in disease emergence. A critical feature of the ecology and epidemiology of AIVs is interspecies transmission (Webster, 1998). Different lineages of influenza virus have jumped to different hosts or undergone reassortment, sometimes resulting in pandemics. During its circulation among migratory wild birds, H3N2 AIV can donate its gene segments to other viruses. Studies have clearly revealed H3N2 viruses transmitted among guinea pigs and ferrets via respiratory droplets and a severe influenza outbreak occurring as a result in chickens in China in 2017 (Guan et al., 2019). In addition, different lineages of H3N2 influenza viruses have been found in several animals, including horses, birds, pigs and dogs, and they not only have accelerated AIV reassortment and interspecies transmission to humans but also provide potential for other zoonotic infections, posing high risks to the poultry industry and public health (Peng et al., 2013; Parrish et al., 2015; Yang et al., 2015; Zhu et al., 2015; Cui et al., 2016; Li et al., 2016; Sun et al., 2017).

In this study, we investigated the phylogenetic and evolutionary dynamics of H3N2 AIV in the Leizhou Peninsula to accurately identify its origin and genotypes as well as its cross-species transmission and spread in new host populations. Notably, our results enhance our understanding of what has sustained canine and avian transmission of H3N2 influenza virus and the mechanism of emergence of novel influenza viruses in new hosts. Our research provides basic and valuable information for achieving the comprehensive control of AIVs and has great significance for the maintenance of human health.

MATERIALS AND METHODS

Sample Collection

A total of 329 oropharyngeal and cloacal swab samples were collected from apparently healthy ducks on six duck farms on the Leizhou Peninsula, China. In addition, tissue samples were collected from diseased or dead poultry on farms during the study. Each oropharyngeal or cloacal swab was placed into a collection tube containing 1 ml of phosphate-buffered saline (PBS; containing 1,000 U/ml penicillin and 2,000 μg/ml streptomycin). The sample tubes were stored in a handheld portable 4°C refrigerator, transported to the laboratory within 24 h and then immediately frozen at −80°C.

Virus Isolation and Identification

The samples were inoculated into 9–11-day-old SPF chicken embryos using a virus isolation manual. After 48 h of culture, the allantoic fluid of the surviving chicken embryos was harvested and tested for hemagglutination activity with 1% chicken red blood cells (cRBCs). The viruses were purified three times by serial dilution and inoculated into 9–11 days old SPF chicken embryos. The hemagglutinin (HA) subtype was identified by the hemagglutination inhibition (HI) method and sequencing. Neuraminidase (NA) subtypes were determined by direct sequencing. RNA extraction, RT-PCR, subtyping of extracted RNA (Invitrogen) and reverse transcription of viral RNA (Invitrogen) were performed according to the manufacturers' instructions. RT-PCR was performed according to the method routine (Shi et al., 2018). The primers used in these studies to identify HA and NA subtypes by RT-PCR would be supported if necessary. Sanger sequencing was used to determine the whole-genome sequences of the AIV isolates. The data were merged and assembled.

Sequence Information

A total of 100 HA sequences of the H3 subtype of AIV; 138 NA sequences of the N2 subtype of AIV; and 67 H3N2 canine influenza virus (CIV) HA and NA, 10 H3N2 feline influenza virus (FIV) HA and NA, 1 H7N2 FIV HA or 1 H7N2 FIV NA, and 82 H3N8 equine influenza virus (EIV) HA and NA coding regions were collected from the GISAID database[1] and the NCBI GenBank database[2].

Alignment and Model Selection

The length of each segment after alignment was as follows: HA, 1,698 nucleotides (nt); M, 1,044 nt; NA, 1,407 nt; NP, 1,494 nt; NS, 1,051 nt; PA, 2,148 nt; PB1, 2,271 nt; and PB2, 2,277 nt. BLASTn was performed locally with default parameters against the downloaded sequences using each of the H3N2 genome sequences from this study as a query. The first 100 gene sequences in the BLAST output were collected. For each gene, multiple sequence alignment was performed using Muscle and included the H3N2 sequences from this study.

[1]https://www.gisaid.org

[2]https://www.ncbi.nlm.nih.gov/

Phylogenetic analysis was performed for two rounds using RAxML. In the first round, 1,000 bootstrap replicates were run, and the best-fit model according to the Bayesian information criterion (BIC) of each gene segment was selected as the nucleotide substitution model (Kalyaanamoorthy et al., 2017). Based on the phylogenetic topologies obtained and their bootstrap values, we selected a few representative reference sequences and formed eight smaller data sets. TempEst (version 1.5.1) was used to analyze the temporal signal in the selected sequences.

Phylogenetic and Evolutionary Dynamics Analyses

Phylogenetic analysis was repeated using the method described above. For all eight datasets, sequences without full alignment length were removed. A phylogenetic tree was reconstructed by the maximum likelihood (ML) method in RAxML under the GTRGAMMA model with 1,000 bootstrap replicates. The time of the most common ancestor (tMRCA) was estimated with the BEAST package (v1.8.4) with the suitable nucleotide substitution model and clock model and a constant size coalescent model. A Markov chain Monte Carlo (MCMC) run of 50,000,000 states sampling each 5,000 steps was performed to obtain an effective sample size (ESS) of $\geq$ 200. Each tree was run twice independently and combined using LogCombiner. After a burn-in of 10%, the final tree was summarized using TreeAnnotator and visualized in FigTree. Root-to-tip genetic distance analysis was performed based on the ML tree against sampling dates using TempEst. The maximum clade credibility (MCC) trees of each segment were built using the same methods as above. The tMRCA and evolutionary rates were estimated using the Bayesian MCMC process. The MCC trees were reconstructed with 10% burn-in and annotated with FigTree (v1.4.1).

Amino Acid Analysis

Amino acid changes associated with canine infection of H3N2 CIV and H3N8 CIV were analyzed using MEGA 7.0. Consensus sequences were aligned, and mutations were recorded. The positions of the mutations of each enzootic cluster were confirmed manually. The number of amino acid changes in each enzootic cluster was counted.

RESULTS

Sampling, Virus Isolation, and Sequencing

Based on HA testing and RT-PCR, in total, six H3N2 subtype AIVs were isolated from samples collected from ducks on the Leizhou Peninsula, Guangdong Province, China, from 2018 to 2019. One strain was isolated in 2018, and the other five strains were isolated in 2019. The exact isolation time, place and host of each isolate are listed in **Table 1**. We analyzed the complete genome sequences of these H3N2 subtype AIVs and submitted them to the GenBank database. To date, the H3N2 subtype of AIV has been detected in many species, such as humans, avians, canines, and felines, and in the environment. Avians are the second largest reservoir of H3N2, with chickens, ducks, geese, and wild birds being the main hosts. Among them, wild birds represent more than half of H3N2 hosts (**Figures 1A,B**).

Phylogenetic Analysis of H3N2 Avian Influenza Virus

Phylogenetic analysis of the eight AIV genes in this study was performed to assess their relationships with corresponding genes in domestic poultry, wild birds and other animals using data from both the NCBI and GISAID databases. The criterion for grouping the viruses was the identity above 95%, which were belong to one group. The results revealed that the eight genes (PB2, PB1, PA, HA, NP, NA, M, and NS) were distributed in Eurasian lineages.

The surface genes (HA and NA) of the viruses we named XY3/H3N2, XY44/H3N2, and XY46/H3N2 exhibited the highest sequence homologies with A/duck/Guangdong/F352/2018 (H3N2) and A/duck/Guangdong/F1172/2018 (H3N2). The HA and NA sequences of the PY8/H3N2 virus exhibited the highest homology with A/canine/Guangdong/3/2018 (H3N2) and A/chicken/nantong/02/2017 (H9N2), respectively (**Figures 2A,B**). However, the inner genes (PB1, PA, M, NS) of the strains PY8/H3N2, XY3/H3N2, XY44/H3N2, and XY46/H3N2 exhibited the highest sequence homology with A/Environment/Guangdong/zhanjiang/C18277136 (H5N6), A/Environment/Guangdong/zhanjiang/C18277135/2018 (H5N6), A/Environment/Guangdong/zhanjiang/C17277346/2017 (H5N6), and A/duck/Guangxi/04.10JX013/2015 (Mixed) (H6N2), respectively (**Figures 3B,C,E,F**). For the PB2 gene sequence, XY3/H3N2, XY44/H3N2, and XY46/H3N2 exhibited the highest homology with A/Environment/Guangdong/zhanjiang/C17277335/2017 (H5N6), whereas PY8/H3N2 exhibited the highest homology with A/canine/Beijing/20170512-122/2017 (H3N2) (**Figure 3A**). For the NP gene, PY8/H3N2, XY3/H3N2, and XY44/H3N2 exhibited the highest homology with A/Environment/Guangdong/zhanjiang/C17277346/2017 (H5N6), whereas XY46/H3N2 exhibited the highest homology with A/environment/Guangxi/79509/2014 (H3N2) (**Figure 3D**). In conclusion, XY3/H3N2, XY44/H3N2, XY46/H3N2 and PY8/H3N2 were closely related to H5-subtype AIVs.

For the A1-2/H3N2 and SN3/H3N2 strains, we analyzed the sequences of the eight gene segments and found that the surface genes (HA and NA) of these two viruses had the highest homology with A/Environment/Hunan/46780/2015 (H3N8) and A/duck/Guangdong/F138/2017 (H3N2), respectively. However, the inner genes (PA, NP, and M) exhibited the highest homology with A/duck/Jiangxi/01.14NCJD040-P/2015 (Mixed) (H1N3), A/Environment/Guangdong/zhanjiang/C17277335/2017 (H5N6), and A/duck/Huzhou/4227/2013 (H7N7), respectively. With respect to the sequences of the inner genes PB2, PB1, and NS, the novel isolated virus A1-2/H3N2 had the highest homology with A/Envrionment/Guangdong/zhanjiang/C17277346/2017 (H5N6), A/canine/Guangdong/1/2018 (H3N2), and A/chicken/Ganzhou/GZ43/2016 (H3N2), respectively, whereas SN3/H3N2 had the highest homology

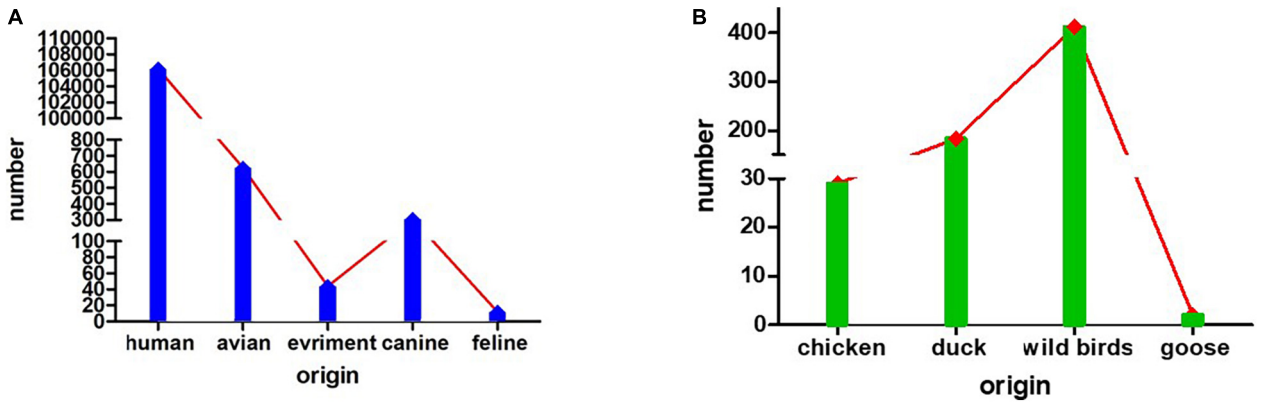

FIGURE 1 | The numbers of isolated H3N2 viruses. **(A)** The numbers of H3N2 viruses isolated from humans, avians, the environment, canines and felines. **(B)** The numbers of H3N2 viruses isolated from avians, such as chickens, ducks, wild birds, and geese.

TABLE 1 | Information of the 6 avian influenza viruses.

No.	Virus name	Abbreviation	Time	Place	Host
1	A/duck/Guangdong/A1-2/2019 (H3N2)	A1-2/H3N2	2018.10	Wuling duck farm, Suixi, Zhanjiang, Guangdong Province	Duck
2	A/duck/Guangdong/SN3/2019 (H3N2)	SN3/H3N2	2019.03	Shannei duck farm, Suixi, Zhanjiang, Guangdong Province	Duck
3	A/duck/Guangdong/PY8/2019 (H3N2)	PY8/H3N2	2019.10	Puyang duck farm, Leizhou, Zhanjiang, Guangdong Province	Duck
4	A/duck/Guangdong/XY3/2019 (H3N2)	XY4/H3N2	2019.10	Xiayang duck farm, Leizhou, Zhanjiang, Guangdong Province	Duck
5	A/duck/Guangdong/XY44/2019 (H3N2)	XY44/H3N2	2019.10	Xiayang duck farm, Leizhou, Zhanjiang, Guangdong Province	Duck
6	A/duck/Guangdong/XY46/2019 (H3N2)	XY46/H3N2	2019.10	Xiayang duck farm, Leizhou, Zhanjiang, Guangdong Province	Duck

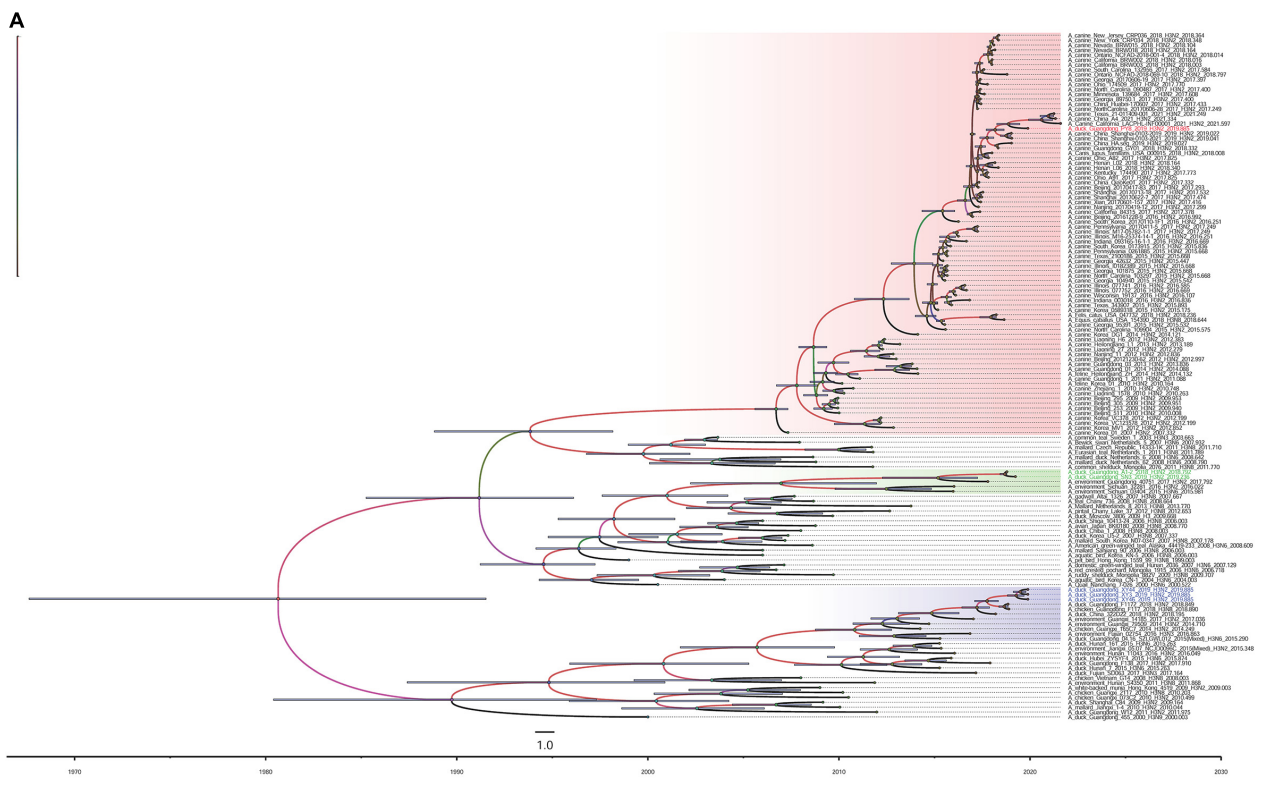

FIGURE 2 | (Continued)

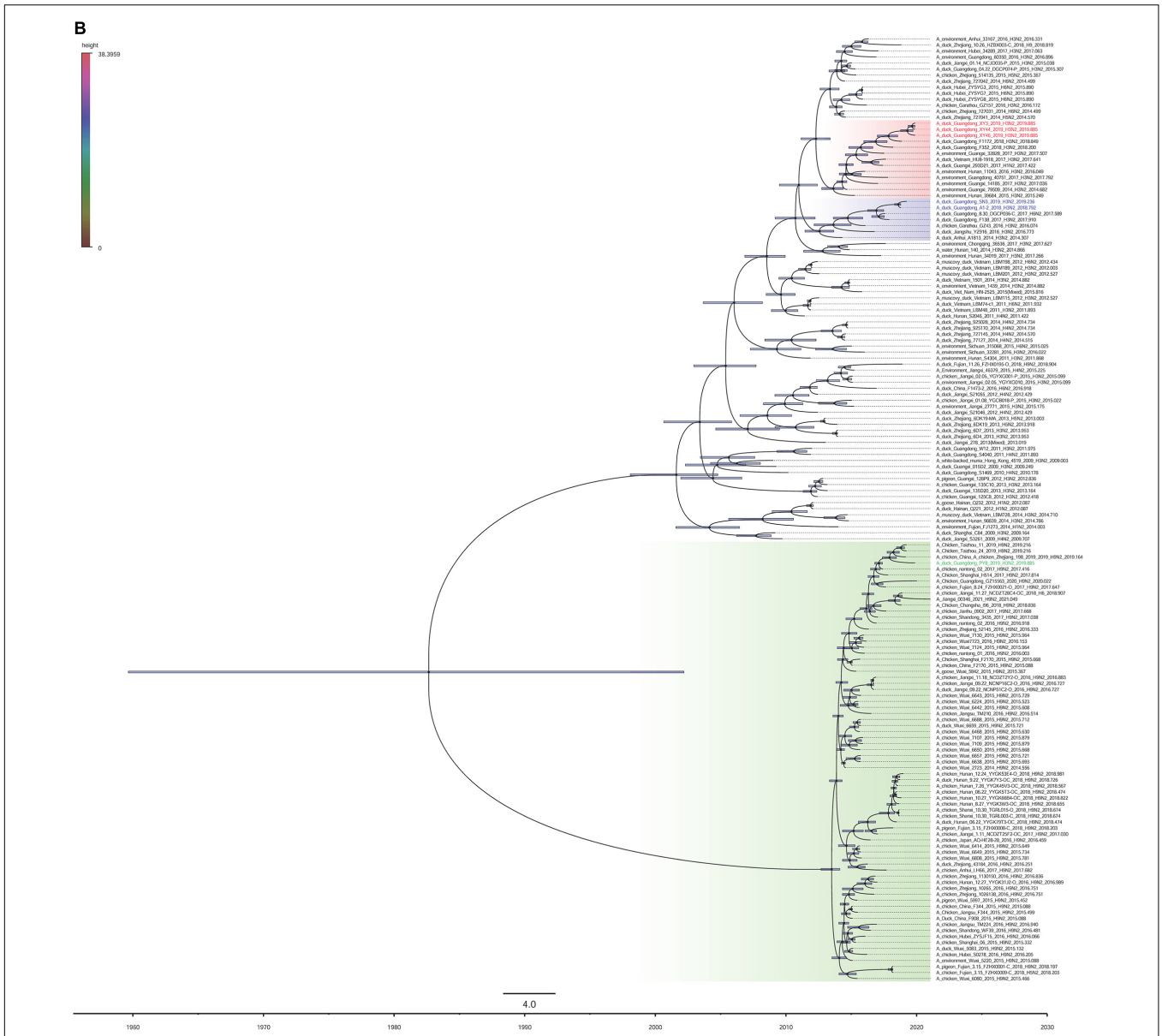

FIGURE 2 | Maximum clade credibility trees of the coding sequences of 2 segments. Node bars indicate the 95% highest posterior density (HPD) of node height. The influenza A virus strains isolated in this study are colored red, blue, and green. Each branch was colored by posterior probability. The segments shown are **(A)** hemagglutinin (HA); **(B)** neuraminidase (NA).

with A/Environment/Guangxi/28753/2014 (H3N2), A/duck/Hubei/ZYSYF2/2015 (H3N6) and A/Environment/Guangxi/79509/2014 (H3N2), respectively. We noticed that both viruses showed close relationships with the H1, H5, and H7 subtypes of AIVs. A Bayesian MCMC method was then utilized to estimate the evolutionary rate for each gene segment (**Table 2**).

Insights Into the Origin of H3N2 Avian Influenza Virus

To determine the origins of the six isolated H3N2 viruses, we sequenced the six inner gene and constructed individual ML phylogenetic trees (**Figures 3A–F**). The PB1, PA, NP, M, and NS gene segments of PY8/H3N2 were closely related to those of an H5N6 strain isolated from the environment in Zhanjiang, China (**Figures 3B–F**). The HA and PB2 gene sequences were closely related to sequences of strains isolated from canines in Beijing and Guangdong, respectively, in China (**Figures 2A**, **3A**). The NA gene sequences were closely related to sequences from an H9N2 strain isolated from chicken in Nantong, China (**Figure 2B**). The PB2, PB1, PA, NP, and M sequences of XY3/H3N2, XY44/H3N2 and XY46/H3N2 were all closely related to those of an H5N6 strain isolated from the environment in Zhanjiang, China. The HA and NA sequences were closely related to those of H3N2 and

H6N2 strains, respectively, isolated from Guangdong ducks. The PB1 gene segments of A1-2/H3N2 and SN3/H3N2 were closely related to those of duck H3N6 isolated in Hubei Province, China. The PB2 gene segments of A1-2/H3N2 and SN3/H3N2 were closely related to those of environment-isolated strains of H5N6 from Zhanjiang and H3N2 from Guangxi, respectively. The PA gene segments A1-2/H3N2 and SN3/H3N2 were closely related to a sequence of duck H1N3 from Jiangxi Province, China.

The NP, M and HA gene segments of A1-2/H3N2 and SN3/H3N2 were closely related to sequences of an H5N6 strain isolated from the environment in Zhanjiang, a H7N7 strain from duck in Huzhou and an H3N8 strain isolated from the environment from Hunan, China, respectively. The N2 gene segments of A1-2/H3N2 and SN3/H3N2 were closely related to a sequence of an H3N2 strain isolated from duck in Guangdong, as were those of XY3/H3N2, XY44/H3N2 and XY46/H3N2. The NS gene segments of A1-2/H3N2 and SN3/H3N2 were closely related to those of an H3N2 strain from Ganzhou chicken and an H3N2 strain from the environment in Guangxi, China (**Table 1**). These results showed that the six H3N2 viruses were all reassortant strains carrying gene segments from various influenza A virus subtypes and various hosts, including avians and mammals (canines).

BEAST software was used to determine the tMRCA. Reassortment events to produce the novel H3N2 viruses occurred between 2007 and 2019 (**Figures 2A,B**). The time span was long, especially for the PY8/H3N2 virus. Most of the gene sequences arose in 2017–2019; however, some of them emerged earlier. The PB1 sequence of the A1-2/H3N2 strain emerged in June 2007, and the PB2 sequence of the PY8/H3N2 strain emerged in August 2011 (**Table 2**). The correlation coefficient of HA and NA were 0.8361 and 0.9716, respectively. The correlation coefficient of the other genes were all above 0.7 (**Table 2**). In addition, using BEAST software to determine the tMRCA, we found that the PB2, PB1, NP and M segments of the H5N6 viruses isolated from the environment in Zhanjiang most likely emerged in April-July 2017 and that the PA gene segments emerged in June 2013. These findings indicated that these H3N2 genes were possibly in circulation in the Zhanjiang poultry AIV gene pool at the beginning of 2013. Furthermore, these findings indicated that the novel waterfowl-origin H3N2 viruses are reassortant influenza viruses containing segments from a multitude of subtypes and different host species (various wild waterfowl, domestic poultry). In this study, the mean substitution rate of the H3N2 HA gene was 2.42×10^{-3} ($1.7195–3.1847 \times 10^{-3}$, 95% HPD) substitutions/site/year, and among the eight genes of H3N2 AIV, the HA gene was characterized by a slow evolution rate. The fastest rate was detected for the NP gene, at 4.55×10^{-3} ($3.6033–5.5667 \times 10^{-3}$, 95% HPD) substitutions/site/year (**Table 1**).

Molecular Characterization of Surface Genes

We analyzed the genome sequences of the surface genes of the six isolated viruses to determine whether the viruses had acquired genetic markers associated with mammalian pathogenicity, virulence, or adaptation to new hosts. None of the six isolated viruses had consecutive basic amino acids in

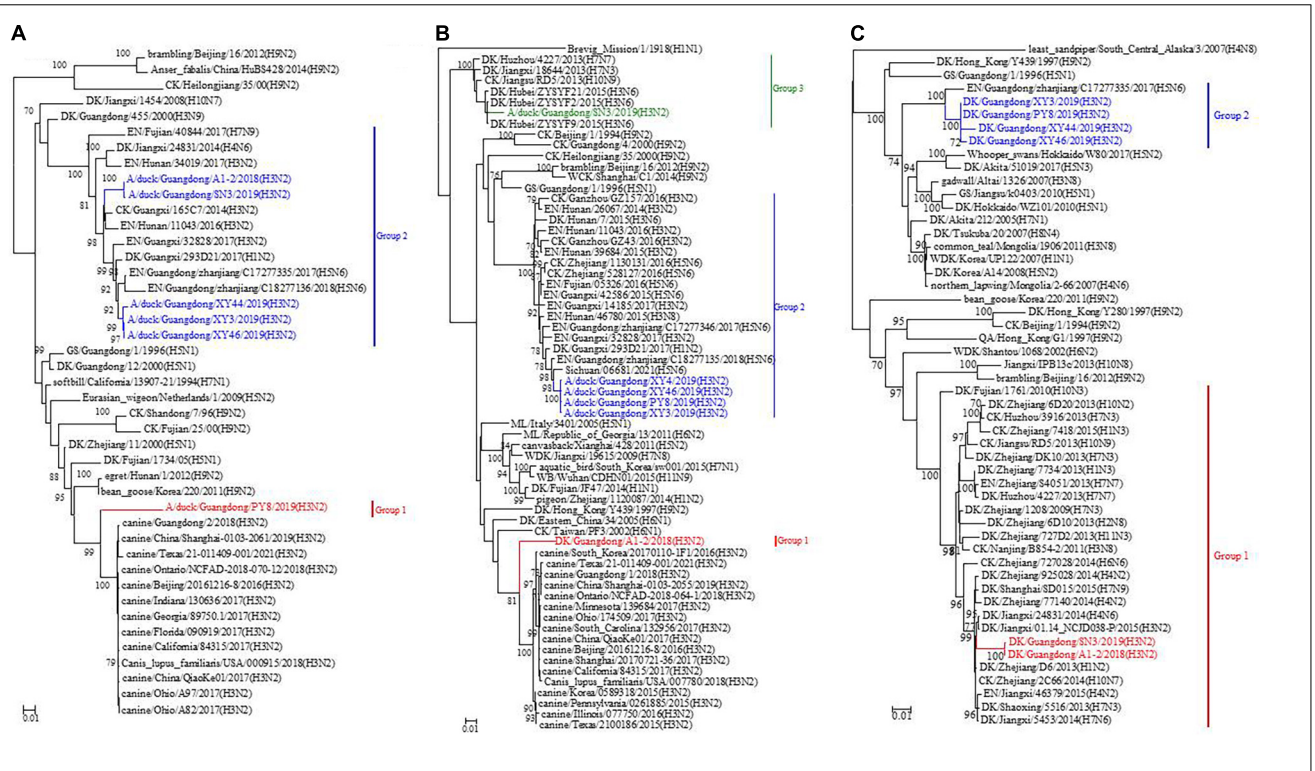

FIGURE 3 | (Continued)

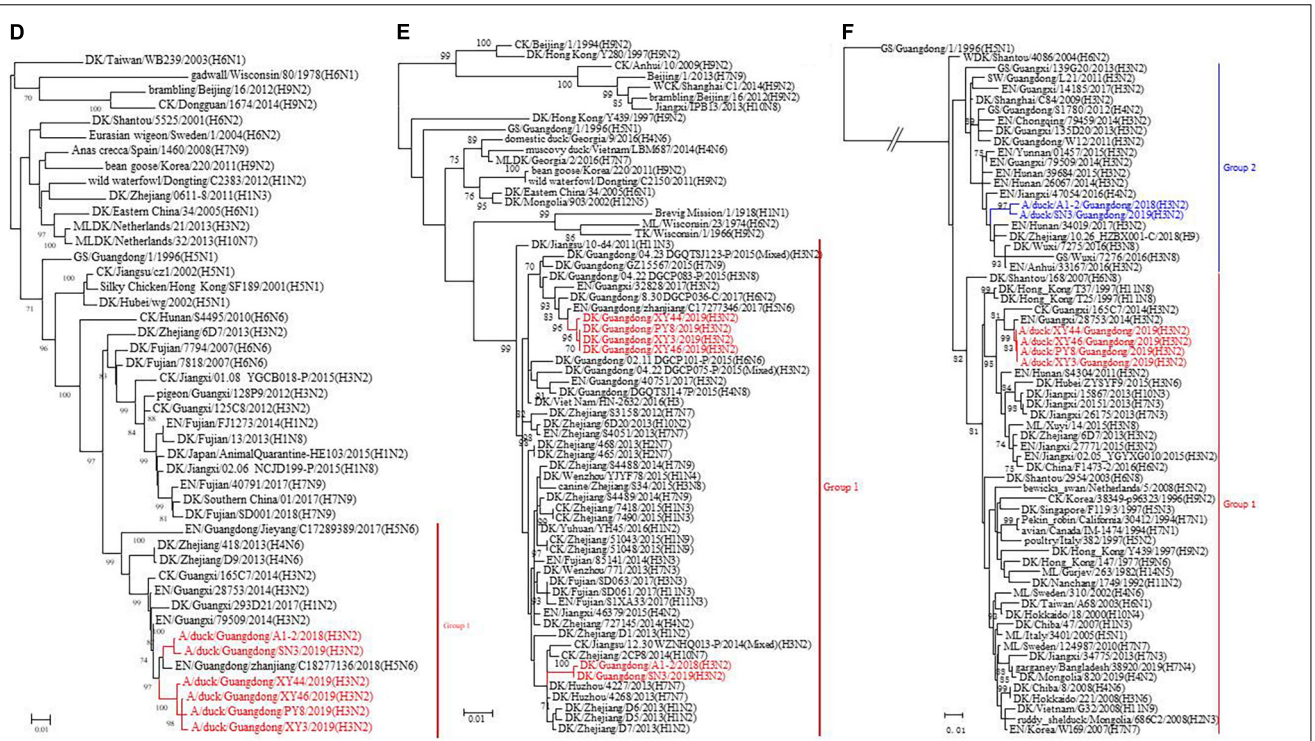

FIGURE 3 | Phylogenetic analysis of the surface genes of H3N2-subtype AIVs isolated from 2018 to 2019 using the maximum likelihood method. **(A)** PB2, **(B)** PB1, **(C)** PA, **(D)** NP, **(E)** M, and **(F)** NS. Phylogenetic trees were generated with the MAGE 7.0 software package. The evolutionary history was inferred using the maximum likelihood method based on the Tamura-Nei model. The tree with the highest log likelihood (–10541.1792) is shown. The percentage of trees in which the associated taxa clustered together is shown next to the branches. The initial tree(s) for the heuristic search were obtained by applying the neighbor-joining method to a matrix of pairwise distances estimated using the maximum composite likelihood (MCL) approach. The tree is drawn to scale, and the branch lengths indicate the number of substitutions per site. All positions containing gaps and missing data were eliminated. The phylogenetic trees of the 6 genes were obtained without a root tree. The sequences of viruses listed in black were downloaded from available databases. The viruses listed in red, blue, and green were sequenced in this study. CK, chicken; DK, duck; GS, goose; SW, swine; ML, mallard; WDK, wild duck; EN, environment.

their sequences. The HA protein sequences belonging to A1-2/H3N2, SN3/H3N2, XY3/H3N2, XY44/H3N2, and XY46/H3N2 shared the cleavage site are PEKQTR↓GLF; that of PY8/H3N2 had a different cleavage site (PERQTR↓GLF). The cleavage site of PY8/H3N2 is the same as that of a CIV isolated from Jiangsu, China (Lin et al., 2012). However, the protein sequences of all the strains corresponded to low-pathogenicity AIV. The amino acid substitutions Q226L and G228S (H3 numbering, which is used throughout the manuscript) are the key substitutions that play an important role in recognizing the receptors of humans (Ge et al., 2018; Guan et al., 2019; Shi et al., 2020). The substitution of A138S in the HA protein could contribute to the virulence of influenza virus to mammalian hosts (Le et al., 2019). In this study, no substitutions of A138S, Q226L, or G228S were detected in any of the six isolated viruses. Some researchers demonstrated that the amino acid substitution 155T in the HA protein altered the binding of the human-type receptor in the H9N2 virus and that the H9N2 virus was the donor of inner gene segments to the H7N9 and H10N8 viruses, which infected humans in China (Li et al., 2014; Guan et al., 2019). We compared the protein sequences of the six isolated viruses and found that all of them exhibited the 155T substitution, which indicated that these H3N2 AIVs may have an increased ability to bind the human-type receptor.

Some studies proved that the deletion of amino acids at positions 63–65 confers the virus enhanced lethality against mice (Sun et al., 2013b; Shi et al., 2020). All six isolated strains except PY8/H3N2 lacked deletions in the NA protein sequence. Some substitutions in the NA protein sequence, including V116A, E119G, Q136L, R152K, H274Y, and R292K, have been shown to confer AIV acquired resistance against neuraminidase inhibitors (Boltz et al., 2010; Hurt et al., 2010; Gubareva et al., 2017; Kode et al., 2019a; Shi et al., 2020). We found none of the above mutations in the NA active sites. Kode et al. (2019b) found the novel I117T substitution in HPAIV and showed that it conferred reduced susceptibility to oseltamivir and zanamivir. Interestingly, we also found this mutation in our six isolated viruses (**Table 3**).

Molecular Characterization of Inner Genes

The six viruses identified here also possessed the amino acid substitution 251R in polymerase basic 2 (PB2), which has frequently been identified in human influenza viruses. Of note, 251R and 590S in PB2 are known determinants of adaptation

TABLE 2 | Evolution rate and time of most recent common ancestor for each of the eight segments.

Segment	Correlation coefficient	Best-fit model	Strains	Mean evolutionrate (substitution /site/year)	95% HPD interval	Most recent common ancestor	tMRCA§	95% HPD interval	Posterior probability
PB2	0.9654	GTR+F+I+G4	PY8	2.74E-03	2.1746E-3, 3.331E-3	Beijing canine H3N2 strain	August 2011	(January 2007, September 2015)	0.9827
			XY3			Zhanjiang environment H5N6 strain	October 2018	(July 2015, May 2017)	0.9973
			XY44						
			XY46						
			A1-2			Zhanjiang environment H5N6 strain	July 2018	(January 2018, October 2018)	0.4138
			SN3			Guangxi environment H3N2 strain			
PB1	0.9592	GTR+F+G4	PY8	3.36E-03	2.59E-3, 4.1063E-3	Zhanjiang environment H5N6 strain	September 2016	(January 2016, May 2017)	1
			XY3						
			XY44						
			XY46						
			A1-2			Guangdong canine H3N2 strain	September 2005	(April 2000, January 2011)	
			SN3			Hubei duck H3N6 strain	January 2014	(October 2013, March 2014)	
PA	0.8372	GTR+F+G4	PY8	2.22E-03	1.976E-3, 2.4213E-3	Zhanjiang environment H5N6 strain	June 2013	(March 2012, August 2014)	1
			XY3						
			XY44						
			XY46						
			A1-2 SN3			Jiangxi duck H1N3 strain	August 2013	(January 2013, April 2014)	0.866
HA	0.8361	TIM+F+G4	PY8	2.958E-03	2.4021E-3, 3.5226E-3	Guangdong canine H3N2 strain	November 2018	(April 2018, June 2019)	0.9994
			XY3			Guangdong duck H3N2 strain	October 2017	(February 2017, May 2018)	0.9398
			XY44						
			XY46						
			A1-2 SN3			Hunan environment H3N8 strain	March 2015	(April 2012, April 2017)	1
NP	0.9567	TVM+F+G4	PY8	4.55E-03	3.6033E-3, 5.5667E-3	Zhanjiang environment H5N6 strain	January 2016	(January 2015, December 2016)	1
			XY3						
			XY44						
			XY46			Guangxi environment H3N2 strain			
			A1-2 SN3			Zhanjiang environment H5N6 strain	December 2016	(March 2016, August 2017)	0.996
N2	0.9716	GTR+F+I+G4	PY8	3.58E-03	2.9104E-3, 4.2725E-3	Nantong chicken H9N2 strain	December 2017	(May 2017, June 2018)	1
			XY3			Guangdong duck H3N2 strain	November 2017	(December 2016, July 2018)	
			XY44						
			XY46						
			A1-2 SN3				December 2016	(April 2016, June 2017)	
M	0.8319	SYM+G4	PY8	3.32E-03	2.1996E-3, 4.5981E-3	Zhanjiang environment H5N6 strain	December 2016	(June 2016, June 2017)	1

(Continued)

TABLE 2 | (Continued)

Segment	Correlation coefficient	Best-fit model	Strains	Mean evolutionrate (substitution /site/year)	95% HPD interval	Most recent common ancestor	tMRCA§	95% HPD interval	Posterior probability
			XY3				November 2016	(March 2016, July 2017)	0.9997
			XY44						
			XY46						
			A1-2			Huzhou duck H7N7 strain	February 2016	(July 2015, July 2016)	0.3266
			SN3						
NS	0.7598	TN+F+G4	PY8	1.86E-03	1.463E-3, 2.2967E-3	Guangxi duck H6N2 strain	June 2014	(June 2013, March 2015)	0.9975
			XY3						
			XY44						
			XY46						
			A1-2			Ganzhou chicken H3N2 strain	May 2013	(February 2012, August 2014)	0.4275
			SN3			Guangxi environment H3N2 strain			

PB2, basic polymerase 2; PB1, basic polymerase 1; PA, acidic polymerase; HA, hemagglutinin; NP, nucleoprotein; NA, neuraminidase; M, matrix protein; NS, non-structural protein. HPD, highest posterior density. tMRCA, time of most recent common ancestor.

to growth in mammals. In the PB2 of CIV H3N2, 2006–2015, the main amino acid at position 251 was K; in the PB2 of CIV H3N2, 2016–2017, it was R. The frequency of 251R in PB2 in influenza virus A (H3N2) in humans and influenza A (H1N1) pdm09 virus is approximately 99%. 590S in PB2 is a known determinant of adaptation to growth in mammals. 590G in PB2 has been identified in CIV H3N2, 2006–2015, whereas 590S has been identified in CIV H3N2, 2016–2017; influenza virus A (H3N2) in humans and influenza A (H1N1) pdm09 virus. The six H3N2 viruses identified in this study had the 590G substitution in the PB2 protein (Lyu et al., 2019). Several substitutions in the PB2 protein of AIV, including L89V, E627K and D701N, have been demonstrated to increase virulence and host range, especially the L89V and E627K substitutions, which confer adaptation to mammalian hosts (Ge et al., 2018; Yang et al., 2021). In this study, the six viruses we isolated had the 89V mutation but not the 627K and 701N mutations in the PB2 protein. The PB2 L89V mutation, which is known to confer adaptation to mammalian hosts, was detected in all six strains.

To determine whether our six H3N2 viruses had the 563R mutation, which is associated with increased virulence and modulation of the host-antiviral IFN response, we analyzed the polymerase basic 1 (PB1) protein. We did not detect the substitution at position 563. The 622G mutation that emerged in PB1 is known to increase polymerase activity and virulence in mice (Feng et al., 2016). We found that all of the six H3N2 strains we isolated showed this mutation in the PB1 protein. The N66S mutation in PB1-F2 is associated with increased replication, virulence, and antiviral response in mice (Ge et al., 2017; Suttie et al., 2019; Pawestri et al., 2020). The six H3N2 stains identified in this study encoded the full-length PB1-F2 protein, but we did not find the 66S mutation in any of the strains.

The T97I substitution in the PA protein has been proven to enhance polymerase activity and virulence (Yang et al., 2019); however, we did not detect the 97I mutation in any of the six H3N2 strains. H9N2 AIV has been the dominant AIV and the dominant epidemic AIV in China for a long time, and the 195K mutation in PA-X amino acids has been proven to enhance the virulence of H9N2 AIV in mammals in previous studies (Sun et al., 2020; Trinh et al., 2020). All the identified strains in this study have this substitution.

Analysis of NP protein from the six H3N2 isolated strains revealed no presence of the 319K mutation, which has been reported to increase virulence to mice and mammalian cells (Na et al., 2021). In addition to having several mutations, including N30D and T215A in the M1 protein, which are known to increase virulence in mice and mammalian cells (Zhang et al., 2019; Na et al., 2021), we found that all six H3N2 strains have D (aspartic acid) and A (alanine) at positions 30 and 215, respectively. Notably, PY8/H3N2, XY3/H3N2, and XY46/H3N2 have the 31N mutation in the M2 protein, which indicates that these strains have amantadine resistance (Mei et al., 2019; Tuong et al., 2020; Zhang et al., 2021). Notably, all six H3N2 viruses have a P/A42S mutation in the NS1 protein, which is associated with increased virulence in mammalian hosts (Tuong et al., 2020). The M31I substitution in the NS2 protein is thought to be associated with increased virulence in mammals (Trinh et al., 2020). However, our isolates did not contain this mutation, which indicated that these strains might have low virulence in mammals.

DISCUSSION

The natural reservoir of influenza A virus is waterfowl. Normally, waterfowl viruses are not adapted to infect and spread in the

TABLE 3 | Molecular characterization of six isolates presented in this study.

Viral protein	A1-2	SN3	PY8	XY3	XY44	XY46	Comments[reference]
HA(H3 numbering)	PEKQTR↓GLF	PEKQTR↓GLF	PERQTR↓GLF	PEKQTR↓GLF	PEKQTR↓GLF	PEKQTR↓GLF	Multi-basic cleavage site
	138A[ÿ]	138A	138A	138A	138A	138A	A→S: contributes virulence from influenza virus to mammalian hosts (Le et al., 2019)
	155T	155T	155T	155T	155T	155T	I→T: increases affinity for the human-type receptor (Li et al., 2014; Guan et al., 2019)
	226Q	226Q	226Q	226Q	226Q	226Q	Q→L: increases binding to human-type influenza receptor (Ge et al., 2018; Guan et al., 2019; Shi et al., 2020)
	228G	228G	228G	228G	228G	228G	G→S: increases binding to human-type influenza receptor (Ge et al., 2018; Guan et al., 2019; Shi et al., 2020)
NA	–	–	Amino acid necklace deletion	–	–	–	63–65: Enhances virus lethality in mice (Sun et al., 2013b; Shi et al., 2020)
	116V	116V	116V	116V	116V	116V	V→A: Resistance to neuraminidase inhibitors (Boltz et al., 2010)
	117T	117T	117T	117T	117T	117T	I→T: Reduces susceptibility to oseltamivir and zanamivir (Kode et al., 2019b)
	119E	119E	119E	119E	119E	119E	E→G: resistance to neuraminidase inhibitors (Shi et al., 2020)
	136Q	136Q	136Q	136Q	136Q	136Q	Q→L: Resistance to neuraminidase inhibitors (Hurt et al., 2010)
	152R	152R	152R	152R	152R	152R	R→K: Resistance to neuraminidase inhibitors (Gubareva et al., 2017; Shi et al., 2020)
	274H	274H	274H	274H	274H	274H	H→Y: Resistance to neuraminidase inhibitors (Gubareva et al., 2017; Shi et al., 2020)
	292R	292R	292R	292R	292R	292R	R→K: Resistance to neuraminidase inhibitors (Gubareva et al., 2017; Shi et al., 2020)
PB2	89V	89V	89V	89V	89V	89V	L→V: Adaptation to mammalian host (Ge et al., 2018)
	627E	627E	627E	627E	627E	627E	E→K: Adaptation to mammalian host (Ge et al., 2018)
	701D	701D	701D	701D	701D	701D	D→N: Increases virulence and host range (Yang et al., 2021)
PB1	622G	622G	622G	622G	622G	622G	D→G: Increases polymerase activity and virulence in mice (Feng et al., 2016)
PB1-F2	66N	66N	66N	66N	66N	66N	N→S: Increases replication, virulence and antiviral response in mice (Ge et al., 2017; Suttie et al., 2019; Pawestri et al., 2020)
PA	97T	97T	97T	97T	97T	97T	T→I: Enhances polymerase and virulence (Yang et al., 2019)
PA-X	195K	195K	195K	195K	195K	195K	R?K: Enhances the virulence in mammals (Sun et al., 2020; Trinh et al., 2020)
NP	319N	319N	319N	319N	319N	319N	N→K: Increases virulence in mice and mammalian cells (Na et al., 2021)
M1	30D	30D	30D	30D	30D	30D	N→D: Increases virulence in mice and mammalian cells (Li et al., 2014; Zhang et al., 2019)
	215A	215A	215A	215A	215A	215A	T→A:Increases virulence in mice and mammalian cells (Zhang et al., 2019; Na et al., 2021)
M2	31S	31S	31N	31N	31S	31N	S→N: Amantadine resistance (Mei et al., 2019; Tuong et al., 2020; Zhang et al., 2021)
NS1	42S	42S	42S	42S	42S	42S	P/A→S: Increases virulence in mammals (Tuong et al., 2020)
NEP/NS2	31M	31M	31M	31M	31M	31M	M→I: Increases virulence in mammals (Trinh et al., 2020)

[ÿ]Amino acid position. A, alanine; D, aspartic acid; E, glutamic acid; G, glycine; H, histidine; I, isoleucine; K, lysine; L, leucine; M, methionine; N, asparagine; P, proline; Q, glutamine; R, arginine; S, serine; T, threonine; V, valine; S, serine; Y, tyrosine.

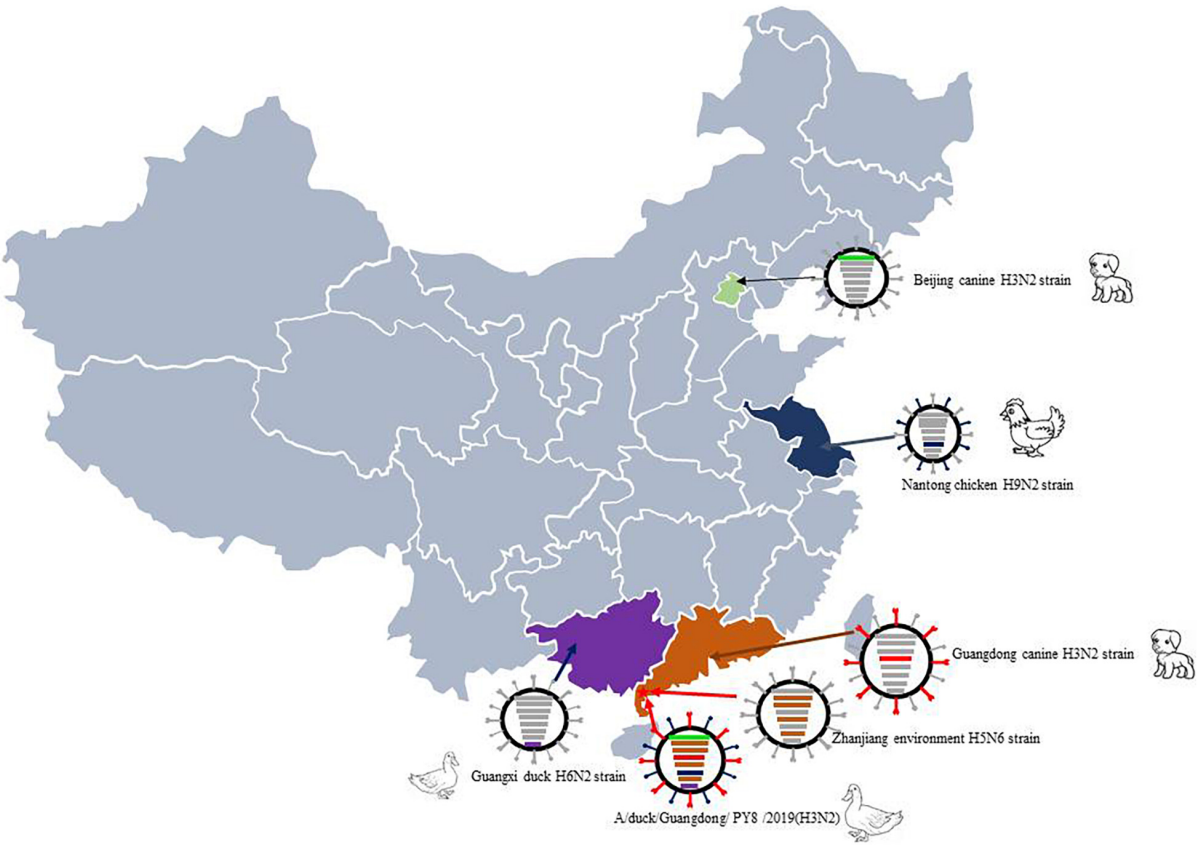

FIGURE 4 | Sampling point and the proposed reassortment and transmission of H3N2. The sampling point is marked with a red star, and the location of the case of canine infection with influenza A subtype H3N2 virus is marked in yellow. Guangdong-origin segments are colored in red, Guangxi-origin segments are colored in purple, and Jiangsu-origin segments are colored in blue.

human population. Sometimes, through reassortment or whole host-shift events, genetic material from waterfowl viruses is introduced into the human population and causes a worldwide pandemic. AIV poses a threat to both humans and animals. Humans were infected by the H5N1 and H9N2 subtypes of AIV in Southeast Asia in 1997 and the H5N6 subtype of AIV in China, revealing that AIVs can traverse the species barrier from birds to humans (Zou et al., 2020).

The H3N2 virus in chickens from live poultry markets (LPMs) was first detected in Central China in 2001 (Liu et al., 2003). Since 2009, H3N2 AIVs have been regularly reported in China (Zhou et al., 2011). As of September 12, 2021, there were 104255 H3N2 influenza virus strains in the GISAID database, of which only 5,546, including 154 avian-originated strains, were isolated from animals. H3N2 AIVs are LPAIVs, and infectious poultry generally have mild symptoms and lack control and prevention. However, H3N2 AIVs can donate their gene segments to HPAIVs and thereby cause accelerated recombination or mutation, potentially causing the next pandemic and threatening public health. Here, we extensively characterized 6 avian H3N2 viruses that were isolated from duck farms on the Leizhou Peninsula, China, and found that the H3N2 viruses circulating in avian species in nature have undergone frequent reassortment and formed complicated genotypes. Viral reassortment is the source of emergence of deadly HPAI viruses that are transmissible to mammals and are prone to adaptive evolution in their new hosts (Guo et al., 2019). It is still disputed whether the infamous 1918 Spanish flu pandemic was caused by a reassortant strain evolved in mammals or an entirely avian-like virus that adapted to humans (Taubenberger et al., 2005).

Exchange of gene segments through reassortment is a major feature of influenza A virus evolution and frequently contributes to the emergence of novel epidemic, pandemic, and zoonotic strains. In particular, some gene segments, such as the HA segment of PY8/H3N2, include surface genes from canines. Therefore, it has been reported that H3N2 CIV originated from avians. Our analyses suggested that the genes can circulate among different hosts and be transmitted from avians to mammals and vice versa. In addition, the tMRCA data indicated that the reassortment leading to the emergence of this H3N2 virus might have occurred in 2017. Importantly, the PB1, PA, NP and M genes of the novel PY8/H3N2 isolate show the highest nucleotide similarities to those of the avian H5N6 strains. The PB2 gene originated from canine virus isolated in Beijing, and the NA and NS genes originated from avian in Jiangsu and Guangxi. These

findings suggest that reassortment occurred in wild birds and/or domestic poultry (**Figure 4**).

The findings suggest a threat of these viruses with respect to influenza virus-acquired ability of transmission across species. During routine monitoring, we found that duck farms were located in remote locations far from residential areas, with little chance of outside contact. However, every duck farm had one or more dogs as guard dogs. We speculate that the viruses with canine-originated gene segments emerged because of long-term close contact between ducks and guard dogs. Additionally, whether dogs, as the closest companions of humans, could facilitate the transmission of CIV to humans needs further investigation. However, we found evidence that canines may have donated canine-origin gene segments to avian influenza viruses that lead to gene reassortment.

Some of the H3 AIV isolates had gene segments (PB2 and N2 genes) similar to those of not only LPAIVs (H3 and H9 AIVs) but also H5 and H7 HPAIVs. This result is consistent with reports that genetic reassortment involving H3 AIV and H5N6 HPAIV appeared in poultry in China. The origin analysis of the six H3N2 viruses isolated in this study indicated that most of the gene segments originated from different subtypes of influenza viruses previously detected in chickens and ducks, suggesting that different influenza viruses circulate together and that gene reassortment occurs frequently among these avian species.

The analysis of the protein sequences of surface and inner genes of the six H3N2 AIVs in this study suggest that circulating AIVs may have the potential to bind the human-type receptor and that antiviral drugs and amantadine may be ineffective for treating poultry infected with these AIVs. All six viruses have the ability to adapt to mammalian hosts and enhance virulence, thus posing severe threats to both public health and poultry markets.

CONCLUSION

In conclusion, the analysis of the six strains of AIVs we isolated proved that their genomes have undergone reassortment with the H1N3, H3N8, H5N6, H6N2, H7N7, and H9N2 subtypes of AIV. Our study has thus revealed the risks to human health posed by H3N2 avian viruses and emphasizes the importance of continuous monitoring and evaluation of H3N2 influenza viruses circulating in poultry.

DATA AVAILABILITY STATEMENT

The datasets presented in this study can be found in online repositories. The names of the repository/repositories and accession number(s) can be found in the article/supplementary material.

AUTHOR CONTRIBUTIONS

YG and ZZ were supported the fund. YG performed the data analysis. QuY and WM did the experiment. YL did the evolution analysis. MZ did the part the experiment. QaY revised the manuscript. CH supported the sampling. All authors contributed to the article and approved the submitted version.

FUNDING

This work was supported by the Innovation and Strengthening Project of Guangdong Ocean University (230419067), the Innovative Strong School Engineering Key Platform Projects by the Department of Education in Guangdong Province (Q2018302) and a Ph.D. start-up grant (No. 521202292). This study was also supported by the National Natural Science Foundation of China (No. 30972085) and the College Student Innovation and Entrepreneurship Training Program (No. 580520074).

REFERENCES

Boltz, D. A., Douangngeun, B., Phommachanh, P., Sinthasak, S., Mondry, R., Obert, C., et al. (2010). Emergence of H5N1 avian influenza viruses with reduced sensitivity to neuraminidase inhibitors and novel reassortants in Lao People's Democratic Republic. *J. Gen. Virol.* 91(Pt 4), 949–959. doi: 10.1099/vir.0.017459-0

Cui, H., Shi, Y., Ruan, T., Li, X., Teng, Q., Chen, H., et al. (2016). Phylogenetic analysis and pathogenicity of H3 subtype avian influenza viruses isolated from live poultry markets in China. *Sci. Rep.* 6:27360. doi: 10.1038/srep27360

Feng, X., Wang, Z., Shi, J., Deng, G., Kong, H., Tao, S., et al. (2016). Glycine at position 622 in PB1 contributes to the virulence of H5N1 avian influenza virus in mice. *J. Virol.* 90, 1872–1879. doi: 10.1128/JVI.02387-15

Ge, Y., Chai, H., Fan, Z., Wang, X., Yao, Q., Ma, J., et al. (2017). New H6 influenza virus reassortment strains isolated from Anser fabalis in Anhui Province, China. *Virol. J.* 14:36. doi: 10.1186/s12985-017-0680-1

Ge, Y., Yao, Q., Chai, H., Hua, Y., Deng, G., and Chen, H. (2018). A 627K variant in the PB2 protein of H9 subtype influenza virus in wild birds. *Influenza Other Respiratory Viruses* 12, 728–741. doi: 10.1111/irv.12592

Guan, L., Shi, J., Kong, X., Ma, S., Zhang, Y., Yin, X., et al. (2019). H3N2 avian influenza viruses detected in live poultry markets in China bind to human-type receptors and transmit in guinea pigs and ferrets. *Emerg. Microbes Infect.* 8, 1280–1290. doi: 10.1080/22221751.2019.1660590

Gubareva, L. V., Sleeman, K., Guo, Z., Yang, H., Hodges, E., Davis, C. T., et al. (2017). Drug susceptibility evaluation of an influenza A(H7N9) virus by analyzing recombinant neuraminidase proteins. *J. Infect. Dis.* 216(Suppl. 4), S566–S574. doi: 10.1093/infdis/jiw625

Guo, F., Li, Y., Yu, S., Liu, L., Luo, T., Pu, Z., et al. (2019). Adaptive evolution of human-isolated H5Nx avian influenza a viruses. *Front. Microbiol.* 10:1328. doi: 10.3389/fmicb.2019.01328

Hurt, A. C., Lowther, S., Middleton, D., and Barr, I. G. (2010). Assessing the development of oseltamivir and zanamivir resistance in A(H5N1) influenza viruses using a ferret model. *Antiviral Res.* 87, 361–366. doi: 10.1016/j.antiviral.2010.06.009

Kalyaanamoorthy, S., Minh, B. Q., Wong, T. K. F., von Haeseler, A., and Jermiin, L. S. (2017). ModelFinder: fast model selection for accurate phylogenetic estimates. *Nat. Methods* 14, 587–589. doi: 10.1038/nmeth.4285

Kode, S. S., Pawar, S. D., Cherian, S. S., Tare, D. S., Bhoye, D., Keng, S. S., et al. (2019a). Selection of avian influenza A (H9N2) virus with reduced susceptibility to neuraminidase inhibitors oseltamivir and zanamivir. *Virus Res.* 265, 122–126. doi: 10.1016/j.virusres.2019.03.019

Kode, S. S., Pawar, S. D., Tare, D. S., Keng, S. S., Hurt, A. C., and Mullick, J. (2019b). A novel I117T substitution in neuraminidase of highly pathogenic avian influenza H5N1 virus conferring reduced susceptibility to oseltamivir and zanamivir. *Vet. Microbiol.* 235, 21–24. doi: 10.1016/j.vetmic.2019.06.005

Le, T. B., Kim, H. K., Le, H. Y., Jeong, M. C., Kim, I. K., Jeong, D. G., et al. (2019). Complete genome sequence of a novel reassortant H3N3 avian influenza virus. *Arch. Virol.* 164, 2881–2885. doi: 10.1007/s00705-019-04386-8

Li, X., Shi, J., Guo, J., Deng, G., Zhang, Q., Wang, J., et al. (2014). Genetics, receptor binding property, and transmissibility in mammals of naturally isolated H9N2 Avian Influenza viruses. *PLoS Pathogens* 10:e1004508. doi: 10.1371/journal.ppat.1004508

Li, X., Yang, J., Liu, B., Jia, Y., Guo, J., Gao, X., et al. (2016). Co-circulation of H5N6, H3N2, H3N8, and emergence of novel reassortant H3N6 in a local community in hunan province in China. *Sci. Rep.* 6:25549. doi: 10.1038/srep25549

Lin, Y., Zhao, Y. B., Zeng, X. J., Lu, C. P., and Liu, Y. J. (2012). Complete genome sequence of an H3N2 canine influenza virus from dogs in Jiangsu, China. *J. Virol.* 86:11402. doi: 10.1128/JVI.01946-12

Liu, M., He, S., Walker, D., Zhou, N., Perez, D. R., Mo, B., et al. (2003). The influenza virus gene pool in a poultry market in South central china. *Virology* 305, 267–275. doi: 10.1006/viro.2002.1762

Lycett, S. J., Duchatel, F., and Digard, P. (2019). A brief history of bird flu. *Philos. Trans. R. Soc. Lond. Ser. B Biol. Sci.* 374:20180257. doi: 10.1098/rstb.2018.0257

Lyu, Y., Song, S., Zhou, L., Bing, G., Wang, Q., Sun, H., et al. (2019). Canine influenza virus A(H3N2) clade with antigenic variation, China, 2016-2017. *Emerg. Infect. Dis.* 25, 161–165. doi: 10.3201/eid2501.171878

Mei, K., Guo, Y., Zhu, X., Qu, N., Huang, J., Chen, Z., et al. (2019). Different pathogenicity and transmissibility of goose-origin H5N6 avian influenza viruses in chickens. *Viruses* 11:612. doi: 10.3390/v11070612

Na, E. J., Kim, Y. S., Lee, S. Y., Kim, Y. J., Park, J. S., and Oem, J. K. (2021). Genetic characteristics of avian influenza virus isolated from wild birds in South Korea, 2019-2020. *Viruses* 13:381. doi: 10.3390/v13030381

Parrish, C. R., Murcia, P. R., and Holmes, E. C. (2015). Influenza virus reservoirs and intermediate hosts: dogs, horses, and new possibilities for influenza virus exposure of humans. *J. Virol.* 89, 2990–2994. doi: 10.1128/JVI.03146-14

Pawestri, H. A., Nugraha, A. A., Han, A. X., Pratiwi, E., Parker, E., Richard, M., et al. (2020). Genetic and antigenic characterization of influenza A/H5N1 viruses isolated from patients in Indonesia, 2008-2015. *Virus Genes* 56, 417–429. doi: 10.1007/s11262-020-01765-1

Peng, Y., Xie, Z. X., Liu, J. B., Pang, Y. S., Deng, X. W., Xie, Z. Q., et al. (2013). Epidemiological surveillance of low pathogenic avian influenza virus (LPAIV) from poultry in Guangxi Province, Southern China. *PLoS One* 8:e77132. doi: 10.1371/journal.pone.0077132

Shi, J., Deng, G., Ma, S., Zeng, X., Yin, X., Li, M., et al. (2018). Rapid evolution of H7N9 highly pathogenic viruses that emerged in China in 2017. *Cell Host Microbe.* 24, 558–568.e7. doi: 10.1016/j.chom.2018.08.006

Shi, L., Yao, Q., Gao, Y., Yu, B., Yang, B., Yao, W., et al. (2020). Molecular evolution and amino acid characteristics of newly isolated H9N2 avian influenza viruses from Liaoning Province, China. *J. Vet. Med. Sci.* 82, 101–108. doi: 10.1292/jvms.19-0421

Song, D., Kang, B., Lee, C., Jung, K., Ha, G., Kang, D., et al. (2008). Transmission of avian influenza virus (H3N2) to dogs. *Emerg. Infect. Dis.* 14, 741–746. doi: 10.3201/eid1405.071471

Sun, W., Li, J., Hu, J., Jiang, D., Ge, Z., Xing, C., et al. (2017). Novel reassortant H3N2 avian influenza virus isolated from domestic ducks in eastern China in 2016. *Genome Announcements* 5, e1237–e1217. doi: 10.1128/genomeA.01237-17

Sun, Y., Hu, Z., Zhang, X., Chen, M., Wang, Z., Xu, G., et al. (2020). An R195K Mutation in the PA-X protein increases the virulence and transmission of influenza A virus in mammalian hosts. *J. Virol.* 94, e1817–e1819. doi: 10.1128/JVI.01817-19

Sun, Y., Sun, S., Ma, J., Tan, Y., Du, L., Shen, Y., et al. (2013a). Identification and characterization of avian-origin H3N2 canine influenza viruses in northern China during 2009-2010. *Virology* 435, 301–307. doi: 10.1016/j.virol.2012.09.037

Sun, Y., Tan, Y., Wei, K., Sun, H., Shi, Y., Pu, J., et al. (2013b). Amino acid 316 of hemagglutinin and the neuraminidase stalk length influence virulence of H9N2 influenza virus in chickens and mice. *J. Virol.* 87, 2963–2968. doi: 10.1128/JVI.02688-12

Suttie, A., Deng, Y. M., Greenhill, A. R., Dussart, P., Horwood, P. F., and Karlsson, E. A. (2019). Inventory of molecular markers affecting biological characteristics of avian influenza A viruses. *Virus Genes* 55, 739–768. doi: 10.1007/s11262-019-01700-z

Taubenberger, J. K., Reid, A. H., Lourens, R. M., Wang, R., Jin, G., and Fanning, T. G. (2005). Characterization of the 1918 influenza virus polymerase genes. *Nature* 437, 889–893. doi: 10.1038/nature04230

Trinh, T. T., Duong, B. T., Nguyen, A. T. V., Tuong, H. T., Hoang, V. T., Than, D. D., et al. (2020). Emergence of novel reassortant H1N1 avian influenza viruses in korean wild ducks in 2018 and 2019. *Viruses* 13:30. doi: 10.3390/v13010030

Tuong, H. T., Nguyen, N. M., Sung, H. W., Park, H., and Yeo, S. J. (2020). Genetic characterization of avian influenza A (H11N9) virus isolated from mandarin ducks in South Korea in 2018. *Viruses* 12:203. doi: 10.3390/v12020203

Webster, R. G. (1998). Influenza: an emerging disease. *Emerg. Infect. Dis.* 4, 436–441. doi: 10.3201/eid0403.980325

Yang, D., Liu, J., Ju, H., Ge, F., Wang, J., Li, X., et al. (2015). Genetic analysis of H3N2 avian influenza viruses isolated from live poultry markets and poultry slaughterhouses in Shanghai, China in 2013. *Virus Genes* 51, 25–32. doi: 10.1007/s11262-015-1198-5

Yang, F., Xiao, Y., Liu, F., Yao, H., Wu, N., and Wu, H. (2021). Isolation and characterization of two novel reassortant H5N6 avian influenza viruses from waterfowl in eastern China. *Arch. Virol.* 166, 1197–1201. doi: 10.1007/s00705-021-04995-2

Yang, J., Wang, Z., Du, Y., Jia, Y., Wang, L., Xu, S., et al. (2019). Clade 2.3.2.1 H5N1 avian influenza viruses circulate at the interface of migratory and domestic birds around Qinghai Lake in China. *Vet. Microbiol.* 235, 234–242. doi: 10.1016/j.vetmic.2019.07.009

Zhang, S., Yu, J. L., He, L., Gong, L., Hou, S., Zhu, M., et al. (2021). Molecular characteristics of the H9N2 avian influenza viruses in live poultry markets in Anhui Province, China, 2013 to 2018. *Health Sci. Rep.* 4:e230. doi: 10.1002/hsr2.230

Zhang, Y., Dong, J., Bo, H., Dong, L., Zou, S., Li, X., et al. (2019). Genetic and biological characteristics of avian influenza virus subtype H1N8 in environments related to live poultry markets in China. *BMC Infect. Dis.* 19:458. doi: 10.1186/s12879-019-4079-z

Zhang, Z. W., Liu, T., Zeng, J., Chen, Y. E., Yuan, M., Zhang, D. W., et al. (2015). Prediction of the next highly pathogenic avian influenza pandemic that can cause illness in humans. *Infect. Dis. Poverty* 4:50. doi: 10.1186/s40249-015-0083-8

Zhou, H., Zhang, A., Chen, H., and Jin, M. (2011). Emergence of novel reassortant H3N2 influenza viruses among ducks in China. *Arch. Virol.* 156, 1045–1048. doi: 10.1007/s00705-011-0940-0

Zhu, H., Hughes, J., and Murcia, P. R. (2015). Origins and evolutionary dynamics of H3N2 canine influenza virus. *J. Virol.* 89, 5406–5418. doi: 10.1128/JVI.03395-14

Zou, S., Tang, J., Zhang, Y., Liu, L., Li, X., Meng, Y., et al. (2020). Molecular characterization of H3 subtype avian influenza viruses based on poultry-related environmental surveillance in China between 2014 and 2017. *Virology* 542, 8–19.

Conflict of Interest: The authors declare that the research was conducted in the absence of any commercial or financial relationships that could be construed as a potential conflict of interest.

Publisher's Note: All claims expressed in this article are solely those of the authors and do not necessarily represent those of their affiliated organizations, or those of the publisher, the editors and the reviewers. Any product that may be evaluated in this article, or claim that may be made by its manufacturer, is not guaranteed or endorsed by the publisher.

frontiers | Frontiers in Microbiology

ORIGINAL RESEARCH
published: 11 April 2022
doi: 10.3389/fmicb.2022.863725

A One-Health Approach to Investigating an Outbreak of Alimentary Tick-Borne Encephalitis in a Non-endemic Area in France (Ain, Eastern France): A Longitudinal Serological Study in Livestock, Detection in Ticks, and the First Tick-Borne Encephalitis Virus Isolation and Molecular Characterisation

Gaëlle Gonzalez[1]‡, Laure Bournez[2]*‡, Rayane Amaral Moraes[1], Dumarest Marine[1], Clémence Galon[3], Fabien Vorimore[4], Maxime Cochin[5], Antoine Nougairède[5], Catherine Hennechart-Collette[6], Sylvie Perelle[6], Isabelle Leparc-Goffart[5,7], Guillaume André Durand[5,7], Gilda Grard[5,7], Thomas Bénet[8], Nathalie Danjou[9], Martine Blanchin[9], Sandrine A. Lacour[1], Boué Franck[2], Guillaume Chenut[10], Catherine Mainguet[10], Catherine Simon[10], Laurence Brémont[10], Stephan Zientara[1], Sara Moutailler[3], Sandra Martin-Latil[6], Nolwenn M. Dheilly[1‡], Cécile Beck[1‡] and Sylvie Lecollinet[1†‡]*

[1] ANSES, INRAE, Ecole Nationale Vétérinaire d'Alfort, UMR VIROLOGIE, Laboratoire de Santé Animale, Maisons-Alfort, France, [2] ANSES, Nancy Laboratory for Rabies and Wildlife, Malzéville, France, [3] ANSES, INRAE, Ecole Nationale Vétérinaire d'Alfort, UMR BIPAR, Laboratoire de Santé Animale, Maisons-Alfort, France, [4] Bacterial Zoonosis Unit, Laboratory for Animal Health, ANSES Maisons-Alfort, Paris-Est University, Paris, France, [5] Unité des Virus Émergents (UVE), Aix-Marseille Univ-IRD 190-Inserm 1207-IHU Méditerranée Infection, Marseille, France, [6] ANSES Laboratory for Food Safety, Université Paris-Est, Maisons-Alfort, France, [7] French National Reference Centre for Arbovirus, Armed Forces Biomedical Research Institute, Marseille, France, [8] Santé Publique France, French Public Health Agency, Auvergne-Rhône-Alpes Regional Office, Lyon, France, [9] Regional Health Agency (Agence Régionale de Santé), Auvergne-Rhône-Alpes, Lyon, France, [10] Local Health Authority, Direction Départementale de la Protection de la Population de l'Ain, Bourg-en-Bresse, France

Tick-borne encephalitis virus' (TBEV) geographic range and the human incidence are increasing throughout Europe, putting a number of non-endemic regions and countries at risk of outbreaks. In spring 2020, there was an outbreak of tick-born encephalitis (TBE) in Ain, Eastern France, where the virus had never been detected before. All patients but one had consumed traditional unpasteurised raw goat cheese from a local producer. We conducted an investigation in the suspected farm using an integrative One Health approach. Our methodology included (i) the detection of virus in cheese and milk products, (ii) serological testing of all animals in the suspected farm and surrounding farms, (iii) an analysis of the landscape and localisation of wooded area, (iv) the capture

OPEN ACCESS

Edited by:
Quan Liu,
Foshan University, China

Reviewed by:
Franz X. Heinz,
Medical University of Vienna, Austria
Peter Norberg,
University of Gothenburg, Sweden
Ashild Kristine Andreassen,
Norwegian Institute of Public Health (NIPH), Norway

***Correspondence:**
Gaëlle Gonzalez
gaelle.gonzalez@anses.fr
Laure Bournez
laure.bournez@anses.fr

†Present addresses
Sylvie Lecollinet,
CIRAD, UMR ASTRE, Petit Bourg, France;
ASTRE, CIRAD, INRAE, Univ. Montpellier, Montpellier, France

‡These authors have contributed equally to this work

Specialty section:
This article was submitted to Infectious Agents and Disease, a section of the journal Frontiers in Microbiology

Received: *27 January 2022*
Accepted: *04 March 2022*
Published: *11 April 2022*

of questing ticks and small mammals for virus detection and estimating enzootic hazard, and (v) virus isolation and genome sequencing. This approach allowed us to confirm the alimentary origin of the TBE outbreak and witness in real-time the seroconversion of recently exposed individuals and excretion of virus in goat milk. In addition, we identified a wooded focus area where and around which there is a risk of TBEV exposure. We provide the first TBEV isolate responsible for the first alimentary-transmitted TBE in France, obtained its full-length genome sequence, and found that it belongs to the European subtype of TBEV. TBEV is now a notifiable human disease in France, which should facilitate surveillance of its incidence and distribution throughout France.

Keywords: tick-borne encephalitis virus, one health, alimentary route, outbreak, environmental investigation

INTRODUCTION

Tick-borne encephalitis (TBE), caused by the tick-borne encephalitis virus (TBEV), is the most important tick-borne zoonotic disease in Europe and Asia from a medical perspective (Süss, 2011). Indeed, even though TBEV infection in humans often causes unspecific febrile symptoms and remain unnoticed, it can result in severe neurological diseases, including encephalitis, meningitis, and meningoencephalitis, with frequent incomplete recovery and, though rarely, death (Bogovic et al., 2010; Kohlmaier et al., 2021). TBEV is a positive-sense, single-stranded RNA virus of the genus *Flavivirus*, family *Flaviviridae* that circulates preferably among ticks of the genus *Ixodes* and small mammals, but large mammals and migrating birds also contribute to the virus geographic distribution and dispersion (Labuda et al., 1997; Randolph et al., 1999; Waldenström et al., 2007; Lindquist and Vapalahti, 2008; Gunnar et al., 2009; Jaenson et al., 2012; Tonteri et al., 2016; Paulsen et al., 2019). TBE most often results from tick bites, however, cases can also result from consumption of unpasteurised milk or dairy products from infected cows, goats, and ewes (Gresíková et al., 1975; Holzmann et al., 2009; Balogh et al., 2010; Cisak et al., 2010; Caini et al., 2012; Hudopisk et al., 2013; Markovinović et al., 2016; Brockmann et al., 2018; Dorko et al., 2018; Ilic et al., 2020; Chitimia-Dobler et al., 2021). Indeed, ruminants are also infected when bitten by an infected tick. Even if they remain asymptomatic, virus excretion in milk has been reported for cows, sheep, and goats (Gresíková et al., 1975; Balogh et al., 2010; Cisak et al., 2010; Caini et al., 2012). Pasteurisation prevents TBEV transmission through inactivation of virus infectivity (Rónai and Egyed, 2020). The increasing geographic range of TBEV and its patchy distribution around local foci puts an increasing number of countries at risk of sporadic occurrence of TBEV infections that can both be difficult to diagnose and prevent (Blaskovic, 1967; Deviatkin et al., 2020).

Tick-borne encephalitis virus (TBEV) is endemic throughout Central and Eastern Europe and has so far been detected in twenty-seven European countries. In the past decades, TBE human incidence has been increasing in several European countries (ECDC, 2012, 2018), with new foci detected in the United Kingdom (Holding et al., 2020) and Netherlands (Jahfari et al., 2017), expanding into previously unaffected areas (Daniel et al., 2004; Lukan et al., 2010; Donoso Mantke et al., 2011; Martello et al., 2014; Brabec et al., 2017; Rieille et al., 2017; Hellenbrand et al., 2019; Alfano et al., 2020). These observations, associated with evidence of a recent increase in TBEV diversity in Europe, suggest that TBEV may be regarded as an emerging disease (Deviatkin et al., 2020). France is located on the border of the known distribution of TBEV in Europe, and very few human cases are usually diagnosed annually, mainly in the Alsace region (about 10–30 cases per year, 0.5/100,000 inhabitants) based on suspect clinical presentation and the detection of TBEV-specific antibodies (Hansmann et al., 2006; Herpe et al., 2007; Donoso Mantke et al., 2011; Velay et al., 2018).

Herein, we report the first outbreak of alimentary TBEV in France and describe the investigation that was conducted within the suspected farm and surrounding area. In April 2020, an outbreak of encephalitis and meningoencephalitis occurred in the Ain department (Eastern France) where TBEV had never been detected. Consequently, a sanitary alert was decreed on May 10. Within a month, epidemiological investigation evidenced that 43 patients with encephalitis, meningoencephalitis, or flu-like symptoms, except for one, had consumed fresh goat cheese made of raw milk named "faisselle" coming from a single local producer. Immediately, the suspected goat flocks were confined into stall, unpasteurised goat cheese production was stopped, raw cheese produced before the alert was withdrawn from commercial markets, and an investigation was conducted within the farm. We confirmed the alimentary transmission by demonstrating the presence of TBEV in a batch of cheese and goat milk. We also monitored the serological status and virus excretion in milk of the animals after control measures had been established and demonstrated their efficacy since no TBEV infection has been reported later than early June. We assessed enzootic hazard for animal exposure through tick bites measured as the density of infected ticks in the pasture and in the neighbour woodland. The full-length virus genome sequence was obtained from milk, cheese, and tick samples, allowing the virus molecular characterisation, and an isolate was obtained. Finally, we assessed TBEV seroprevalence in surrounding farms to evaluate whether TBEV had been silently established in the area or not.

MATERIALS AND METHODS

An overview of the timeline of sampling collections is provided in **Figure 1**.

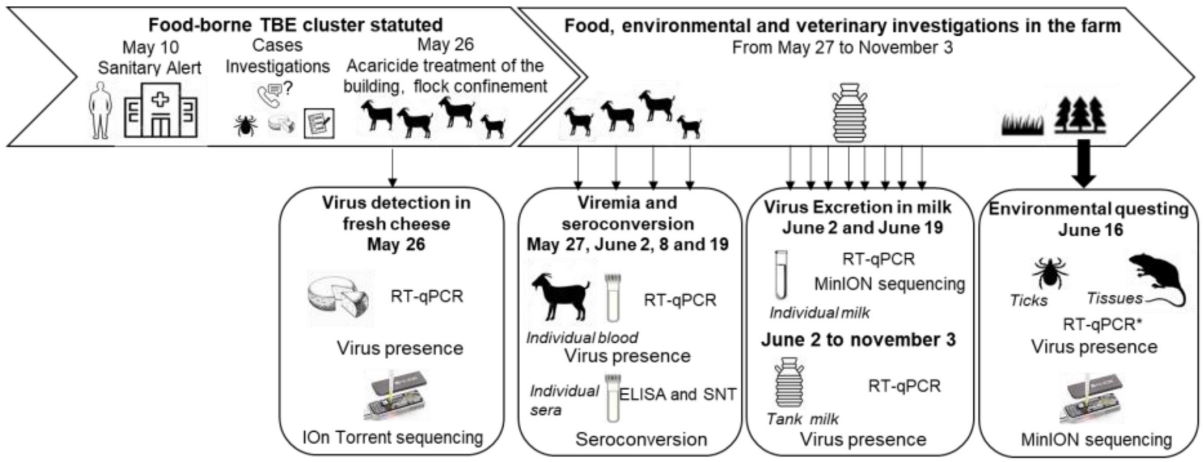

FIGURE 1 | Timeline of the food, environmental and veterinary investigations, and sampling scheme from April to November 2020.

Cheese Sampling

Case investigations performed by the French public health agency pointed out that one case still had cheese from the suspected farm at home at the time of the investigation. This fresh cheese was produced on April 28. The Ain local authorities recalled cheese produced at the suspected farm. Five samples from the batch produced on April 28 and 74 from other batches were sent to the National Reference Centre (NRC) for Arboviruses for screening of the TBE genome. Confirmation was conducted at the Food-safety national reference laboratory, ANSES, Maisons-Alfort.

Serum, Blood, Milk, and Tick Sampling

From Animals at the Suspected Farm

The farm suspected to be the source of the infection included 56 dairy goats, three dairy cows, and four suckling cows grazing on the same pasture.

The goats had grazed in only one pasture adjacent to the dairy cow farm. Half of the goat pasture was a wooded area, which was in continuity of a large mixed deciduous and coniferous forest dominated by beech trees. Goats that were found TBEV-antibody positive in the suspected and surrounding farms were aged between 2 and 10 years old, while cows sampled in the suspected and surrounding farms were aged between 1 and 10 years old.

When the epidemiological investigation led to determine that this farm was strongly suspected to be the source of the human contamination, all goats and dairy cows were confined into the stall, and cows were treated against ticks on May 26, 2020. Acaricide treatment of the flock buildings was also carried out. Serum and blood samples were collected as follows (**Figure 1**). On May 27, serum samples were collected from 30 goats. On June 2, 8, and 19, serum and blood samples were collected from all 56 goats from the farms. Serum samples were collected on the three dairy cows on June 2 and on the four suckling cows between July and August 2020. In addition, tank milk samples from goats and dairy cows were collected every week from June 2 to November 3. Individual milk samples were collected from the 55 lactating goats on June 8 and 19. In March 2021, a follow-up serological study was carried out on the entire goat herd among which 35 individuals were identical to 2020. Milk and sera were stored at 4°C, and blood samples were stored at −20°C until use.

From Animals in Surrounding Farms

To characterise the geographic distribution of the TBEV infections among the surrounding farms, one hundred and forty-two animals from five farms – two goat farms, one dairy cow farm, and two suckling cow farms – from which the animals have grazed in pastures located less than 2 km away from the infected farm's pasture were investigated for the presence of TBEV antibodies. Serum samples of all animals available at the time of sampling were collected between June and August 2020.

Collect of Questing Ticks

Questing ticks were counted and collected from 10 a.m. to 6 p.m. on June 16, 2020 by dragging a 1-m^2 white blanket. The pasture was divided into five geographic areas in which a total of 29 sub-areas were defined according to the habitat types: wooded areas (three sub-areas), wooded edge of the meadow (meadow-forest or meadow-wood ecotones, five sub-areas), hedgerows along the edge of the pasture or within the pasture (seven sub-areas), a meadow between 3 and 10 m away from the forest edge (four sub-areas) and from the hedgerows (four sub-areas), and a meadow more than 10 m from the edge (six sub-areas). The adjacent forest was divided into three sub-areas. The sampling scheme differed according to the sub-areas, with more effort made in wooded areas to collect more ticks for TBEV analysis. A total of twenty-eight 10-m-long transects were carried-out in either forest (18 transects) and wood (10 transects) sub-areas. In addition, the edges of the meadow and hedgerows were continuously checked for tick presence, and individuals were collected every 20-m-long transects. Within the meadow, five 20-m-long transects were realised. Because the dragging method is more appropriate for estimating the density of questing nymphs than those of larvae and adults, only the density of questing nymph per sub-area was estimated by evaluating the number of ticks collected per 100 m^2 and its mean per habitat type was calculated.

We calculated that, for an estimated virus prevalence in nymphs of 0.2%, it would be necessary to collect and test for TBEV presence in a minimum of 1,000 nymphs to have a 95% chance to detect the virus (Cannon, 2001). Given that previous estimates of TBEV prevalence in the French endemic region (Alsace) ranged from 0.03 to 0.3% in nymphs and from 0.6 to 0.8% in adults (Perez-Eid et al., 1992; Bestehorn et al., 2018; Bournez et al., 2020), we conducted an additional collect of ticks in the forest to reach that critical minimum number. Back in the laboratory, ticks were identified to the genus level based on their morphology (Pérez-Eid, 2007). All questing nymphs and adults were washed in 70% ethanol, rinsed twice in distilled water, dried, and stored at −80°C until use for TBEV detection.

Small Mammal Trapping and Sampling of Feeding Ticks

For three consecutive nights from June 15 to 18, 2020, two hundred small mammal live-traps (14 × 14 Ugglan special no. 3, Grahnab, Sweden) were set up every 10 m along the pasture and within the wooded area of the pasture. Traps were baited with carrots and sunflower seeds. Caught animals were euthanised and identified at the genus level. The spleen and brain of small mammals were collected and put in nitrogen containers until storage at −80°C in the laboratory.

Ticks feeding on trapped animals were removed and identified to the genus level based on their morphology (Pérez-Eid, 2007). Potential undetected ticks were collected by removing the skin of the animals and storing them in individual bags for 48 h to let the ticks detach.

Laboratory Analyses

Serological Tests

Antibodies against flaviviruses were detected using a multi-species commercial competitive enzyme-linked immunosorbent assay (cELISA; ID Screen® West Nile Competition, ID Vet, Montpellier, France) based on purified whole West Nile Virus (WNV) antigen for the detection of antibodies directed against the envelope E protein common to all flaviviruses. Although this ELISA test is designed for WNV detection, it can be used for the detection of TBEV antibodies because of the high cross-reactivity among flaviviruses (Rushton et al., 2013; Beck et al., 2015, 2016; Bournez et al., 2019; Reusken et al., 2019). The test was performed according to the manufacturer's instructions. The interpretation was modified for sera close to the doubtful and negative thresholds, with an extension of the doubtful interval, to ascertain the detection of sera with low-TBEV antibody levels by ELISA and then increase sensitivity. The sample was considered positive if <40%, doubtful between 40 and 72%, and negative if >72%.

In-house IgM-capture enzyme immunoassay (MAC-ELISA) with whole inactivated TBEV was performed as previously described (Peyrefitte et al., 2005) on all 30 goat sera sampled on May 27, 2020. MAC-ELISA was performed using rabbit anti-goat IgM antibodies (Bethyl Laboratories, Inc., Montgomery, United States).

Samples with positive and doubtful results in ELISA were then tested for the presence of specific neutralising antibodies against TBEV by micro virus neutralisation tests (MNTs, strain Hypr, Genbank ID U39292.1) as described in Beck et al. (2015). A serum sample was considered positive for TBEV if cells were protected at least at the serum dilution of 1:20.

RNA Extraction and Real-Time Tick-Borne Encephalitis Virus QRT-PCR

QRT-PCR Tests on Fresh Cheese

Cheese suspected to be infected with TBEV were stored at −80°C until analysis. The NRC for Arboviruses carried out TBEV genome screening following the protocol below. Dissolution of nearly 5 g of fresh or drier cheese was performed in phosphate buffer saline (PBS). Homogenisation steps were achieved to complete the process. RNA extraction was carried out using the QIAmp Viral RNA Mini Kit (Qiagen, Paris, France) according to manufacturer's instructions. Five microlitres of the eluted RNA were used to execute a quantitative RT-PCR with primers and probe targetting TBEV genome (sequences available on request) using the SuperScript™ III Platinum™ One-Step qRT-PCR amplification kit (Thermofischer, Paris, France) on LightCycler® 2.0 Instrument (Roche Life Science, Mannheim, Baden-Wurttemberg, Germany).

Confirmation of TBEV-infected cheese was conducted at the food-safety national reference laboratory, ANSES, Maisons-Alfort. The method used to recover TBEV from fresh cheese was based on the use of proteinase K as previously described in Hennechart-Collette et al. (2017). After enzymatic digestion, total nucleic acid extraction was carried out using the NucliSENS® easyMAG™ platform according to the manufacturer's instructions (bioMérieux). The primers and probe used to detect TBEV by RT-qPCR have been already described in the literature by Gondard et al. (2018).

QRT-PCR Tests on Goats, Cows, and Small Mammal Samples

Goat and dairy cow tank milks, goat individual milk samples, goat or cows ethylenediaminetetraacetic acid (EDTA) blood, and the spleen and brain of small mammals suspected to be infected with TBEV were stored at 4°C (milk), −20°C (EDTA blood), or −80°C (organs) until analysis. RNA extraction was performed using the MagVet™ Universal Isolation kit (Lifetechnologies, Saint-Aubin, France) on the King Fisher automat (ThermoFisher Scientific, Paris, France). Five microlitres of each RNA extract were subjected to qRT-PCR with primers and probe targetting the NS5 gene described in Gondard et al. (2018) using the AgPath-ID™One-Step RT-PCR Reagents kit (Lifetechnologies, Saint-Aubin, France) and cycling conditions as follows: reverse transcription for 10 min at 45°C; denaturation of cDNA 10 min at 95°C and 45 cycles of 15 s at 95°C, and 1 min at 60°C. The detection limit of the qRT-PCR, which is the lowest number of copy genome detected for a known dilution in 95% of cases, performed on goat milk samples was estimated at 1.10e4 TCID50/ml corresponding to a Ct value of 34.

QRT-PCR Tests on Questing Ticks and Descriptive Analysis of Tick-Borne Encephalitis Virus Infection in Ticks

Questing ticks were analysed to detect TBEV RNA. Adult ticks were individually analysed and nymphal ticks were analysed in

pools of 30 ticks maximum per sub-area. RNA was extracted using the Nucleospin RNA II extract kit (Macherey-Nagel, Düren, Germany) as described in Bournez et al. (2020) and were screened for TBEV by qRT-PCR targetting the NS5 as described in Gondard et al. (2018). Because TBEV infection prevalence in ticks is lower than 1% in endemic regions of France, the prevalence in nymphs was expressed as the minimum infection rate per 100 tested (MIR) based on the assumption that a single tick was positive within a positive pool. We calculated the overall MIR of TBEV in nymphs (the number of positive pools divided by the overall number of nymphs tested × 100) and TBEV prevalence infection in adults (the number of positive adult ticks by the overall number of adult ticks tested ×100). Their 95% CIs were calculated following a binomial distribution. We estimated the density of infected nymphs per habitat by multiplying the% MIR by the mean density of questing nymphs per habitat.

Virus Isolation From Contaminated Milk and Infected Ticks

Contaminated milk (500 μl) or tick grindings (100 μl/homogenates) positive for TBEV were diluted in serum-free Dulbeccos' Modified Eagle Medium (DMEM) culture, inoculated in a T25 flask seeded with Vero NK cells (ATCC: CCL81^{TM}) 24 h earlier, and washed with DMEM before inoculation. Following an incubation time of 1 h 30 at 37°C with 5% CO_2, cells were washed twice with PBS, and a complete medium (DMEM + 1% penicillin- streptomycin + 1% sodium pyruvate + 5% fetal calf serum) was added. The cells were observed every day from day 3 to day 7 post-infection (pi). As soon as cytopathic effects (CPE) were detected, the supernatant was collected, clarified, and stored at -80°C. RNA extraction was performed using the MagVet^{TM} Universal Isolation kit (Lifetechnologies, Saint-Aubin, France) on the King Fisher automat (ThermoFisher Scientific, Paris, France). RNA extracts were subjected to TBEV RT-qPCR as described above to confirm TBEV detection.

Full-Length Tick-Borne Encephalitis Virus Genome Assembly Performed From Contaminated Milk and Infected Ticks

Full-length virus genome sequencing was conducted on cDNA obtained from contaminated milk and infected ticks. Multiplex primers were designed using a Primal scheme[1] with default parameters. A multifasta file with reference genomes NC_001672.1, KF151173.1, MG589938.1, KC835596.1, MK801808.1, MK801803.1, MG210948.1, KX966399.1, and KP716974.1 was used to generate primers. Their sequences are listed in **Table 1** (**Supplementary Data**) (scheme.primer.tsv). A multiplex PCR method for targetted enrichment was adapted for library preparation and MinION sequencing of TBEV genome as previously described for Zika (WHO Control Reference 11474/16) and Chikungunya viruses (PEI N11602) in Quick et al. (2017).

Sample barcoding was performed with 14 barcodes (NB01 to 14) with the native barcoding genomic DNA protocol using the ligation sequencing kit SQK-LSK109 (Oxford Nanopore Technologies, Oxford, United Kingdom) and the Native barcoding expansion kits EXP-NBD104 and EXP-NBD114 (Oxford Nanopore Technologies, Oxford, United Kingdom). Two barcodes were assigned per sample depending on the pool of primers used (either pool 1 or 2) (**Supplementary Table 2**). A Flongle flow cell FLO-FLG001 was used for sequencing (Oxford Nanopore Technologies, Oxford, United Kingdom).

FAST5 reads were base called offline using guppy_basecaller v5.0.7. from Oxford Nanopore.[2] Subsequent FASTQ files were demultiplexed using guppy_barcoder using the –trim-barcodes flag. Twenty-five nucleotides were trimmed at both 5′ and 3′ ends in resulting FASTQ files to remove primers with a maximum length of 700 bp using NanoFilt v2.6. The sequences obtained with the two barcodes corresponding to a unique sample were concatenated into one FASTQ file. Each file was mapped to the reference NC_001672.1 using minimap2 v2.20 (Li, 2018). Consensus FASTA files were generated after four error correction steps, including three polishing steps of racon v1.4.20[3] and one polishing step with medaka v1.4.3.[4] Trimmed reads were mapped back to the assembly using minimap2, and coverage statistics were calculated on the sorted BAM file using SAMtools v1.12 (Li and Durbin, 2009). Multiple alignments of the nucleotide sequences were performed using the ClustalW algorithm to extract a high-quality full-length genome sequence.

Full-Length Tick-Borne Encephalitis Virus Genome Assembly Performed From Contaminated Cheese

Full-length virus genome sequencing was conducted on cDNA obtained from contaminated cheese using the ProtoScript® II Reverse Transcriptase kit (New England Biolabs, MA, United States) with 50 μM random hexamers (Invitrogen) (7:1 ratio) for 5 min at 65°C (Bournez et al., 2020). The full-length genome was amplified (multiplex PCR) with Q5® High-Fidelity 2X Master Mix kit (New England Biolabs, MA, United States) and a set of primers designed using the "Primal Scheme" program (see text footnote 1; Quick et al., 2017). The list of primers used for sequencing is presented in **Supplementary Table 3**. Sequencing analysis was performed using the S5 Ion torrent technology v5.12 (ThermoFisher Scientific, Paris, France) as previously described (Driouich et al., 2019). The consensus sequence was obtained after a trimming step of reads (reads with quality score < 0.99, and length < 100 bp were removed, and the thirty first and thirty last nucleotides were removed from the reads). Mapping of reads to a reference (determined following blast of *De Novo* contigs) was realised using CLC genomics workbench software v.20 (Qiagen, Hilden, Germany). A *de novo* contig was also generated to ensure that the consensus sequence was not impaired by the reference sequence. For genomic regions for which no sequence was obtained using this approach, cDNA was also generated and amplified using^{TM} the SuperScript IV One-Step RT-PCR System kit following the supplier's recommendations (Invitrogen). PCR mixes (final volume 50 μl) contained 3 μl of cDNA, 2.5 μl of each primer (final concentration of 0.5 μM), and 25 μl of 2X Platinum^{TM} SuperFi^{TM} RT-PCR Master Mix. Amplification was performed with the following conditions: 50 s at 50°C, 2 min

[1]http://primal.zibraproject.org

[2]https://nanoporetech.com

[3]https://github.com/isovic/racon

[4]https://github.com/nanoporetech/medaka

TABLE 1 | Summary of the test results carried out on serum and milk samples collected from the goats of the suspected farm.

Date	Serum tested by serological tests			Individual milk tested by qRT-PCR			Tank milk tested by RT-PCR	
	No.	No. TBEV positive	% TBEV-positive	No	No. TBEV positive	% TBEV-positive	Yes/no	Ct value
27/05	30	6	20	0			No	
02/06	56	11	20	0			Yes	35
09/06	56	13*	23	55	3	5.5	Yes	Neg
23/06	56	13*	23	55	0	0	Yes	Neg
07/07	0			0			Yes	Neg
15/07	0			0			Yes	Neg
28/07	0			0			Yes	Neg
04/08	0			0			Yes	Neg
11/08-03/11	0			0			Yes	Neg
2021	53	8	15	0			No	

Serum samples were initially tested by a competitive ELISA. Then, positive and doubtful ELISA samples were tested by specific-TBEV virus micro-neutralisation tests (MNT). A serum sample was considered TBEV-seropositive when MNT was positive.

**Two goats were MNT negative at one of these two dates but considered TBEV positive as these were clearly positive by MNT on 2020/06/02. Moreover, both of them excreted TBEV in the milk.*

at 98°C, then 40 cycles of amplification (10 s at 98°C, 10 s at 66°C, and 30 s at 72°C), and a final extension of 5 min at 72°C. PCR products were verified by gel electrophoresis and pooled. Sequencing analysis was performed as described above. The consensus sequence was obtained using the reads from both runs as described above.

Phylogenetic Analyses

The novel reference genome sequence was aligned against the known TBEV viral diversity. Nucleotide and protein percentage of identity were calculated with Clustal Omega (Madeira et al., 2019). Phylogenetic analyses were conducted on the full-length open reading frame. Phylogenetic trees were then inferred using the maximum likelihood method implemented in PhyML (version 3.0) (Lefort et al., 2017) using the best-fit model and best of nearest neighbor interchanges (NNI) and Subtree Pruning and Regrafting (SPR) branch swapping. Support for nodes on the trees was assessed using an approximate likelihood ratio test (aLRT) with the Shimodaira-Hasegawa-like procedure. Trees generated using the Neighbour–Joining and Maximum Likelihood methods implemented in MEGAX gave identical results.

RESULTS

Tick-Borne Encephalitis Virus Detection in Fresh Cheese Produced in the Suspected Farm

On June 2, the NRC Arbovirus detected one cheese that is tested positive for TBEV among seventeen. This cheese, produced on April 28, was collected on May 26 in a patient home during the investigation time. The local authorities suspected a food-born source of contamination as patients developed meningoencephalitis after consuming goat cheese produced on the same farm. The presence of TBEV genome was confirmed by the ANSES food-safety laboratory (Maisons-Alfort). The food-borne origin of TBEV contamination was therefore confirmed. On July 10, seventy-four cheese given by the producer were analysed and virus genome was detected in six of them.

Tick-Borne Encephalitis Virus Infection and Exposure in Suspected Farm Livestock

IgG and IgM antibodies against TBEV were detected using the ELISA tests (Igs competition and IgM capture) and MNT. On May 27, six goats out of thirty were TBEV-seropositive as assessed with competition ELISA and MNT. One of them had anti-TBEV IgM antibodies. The following weeks, after their placement in a stable to prevent further tick bites, all 56 goats were tested for a complete assessment of the TBEV exposure rate. Eleven goats were TBEV-seropositive on June 2 (20%) (with one seroconversion in the 30 goats collected on May 27) and 13 (23%) on June 9 (with two more seroconversions) (**Figure 2**). Goat seroconversions were confirmed by MNT (**Figure 2**, **Table 1**, and **Supplementary Data**). Overall, the ELISA results were confirmed by MNT with the exception of a single individual that appeared positive based on ELISA competition but did not develop neutralising antibodies (**Figure 2**). The seroconversion of three goats between May 27 and June 9 indicates that infection occurred very recently. Yet, none of the animals had high viremia given that all qRT-PCRs conducted on blood samples were negative (collected on June 2, 9, and 19). ELISA competition conducted in 2021, about 1 year after the initial infection, showed a decrease in IgG levels for most seropositive individuals (10/13), but the level of neutralising antibodies remained high. Two individuals that were TBEV-seropositive in 2020 turned negative based on competition ELISA in 2021, and one of those had no remaining neutralising antibodies according to MNT

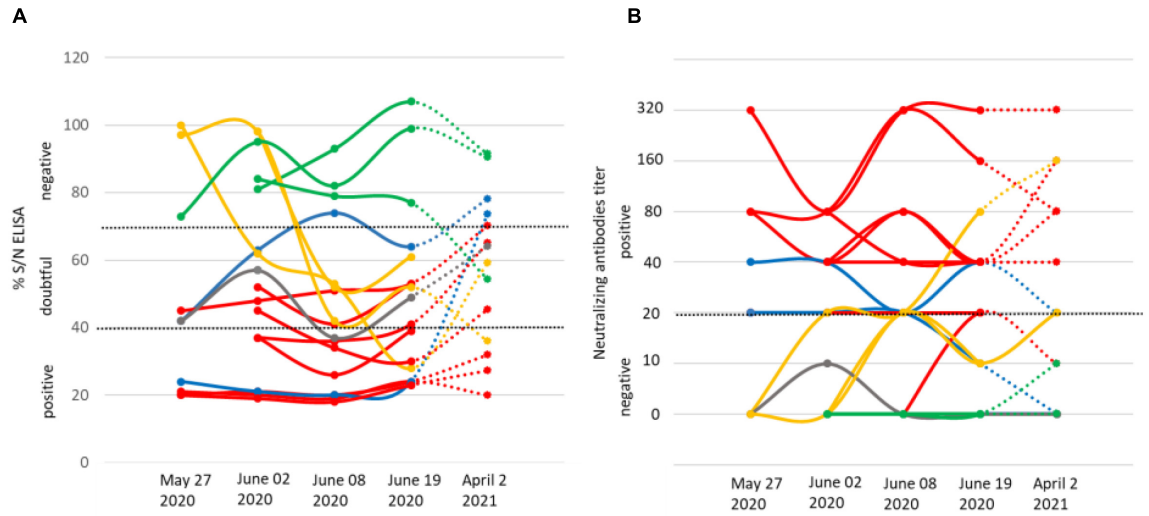

FIGURE 2 | IgG levels **(A)** and micro-neutralisation antibody levels **(B)** in goats on four dates in 2020 (May 27, June 2, June 8, and June 19) and on April 2, 2021. The threshold levels applied are indicated as dashed lines. We provide examples of seronegative individuals (green) and show results for the individual that returned seropositive *via* ELISA competition, but returned negative in neutralising antibody titre (grey), the three individuals that seroconverted after May 27 (yellow), the eight seropositive individuals (red), and the two individuals that returned negative IgG competition results in 2021 (blue), one of which maintains neutralising antibodies.

(**Figure 2**). Within the same farm, one of the three dairy cows and two of the four suckling cows which had grazed in the same or in the adjacent pasture as the goats were TBEV seropositive. No virus genome was detected in the blood of these animals.

Tick-Borne Encephalitis Virus Detection in Goat Milk at the Suspected Farm

The presence of the TBEV genome was detected in the tank of goat milk collected on June 2, but it was absent in the tank of cow milk (**Table 1**). The virus was not detected in either tank thereafter (between June 8 and November 3). The presence of TBEV was tested in the milk of individual goats collected on June 8 and 19. TBEV genome was detected in the milk of three goats on June 8 (23% of the thirteen seropositive animals), indicating that they continued excreting viruses 14 days after their confinement. Meanwhile, two individuals were TBEV-seropositive on May 27 and one seroconverted between June 2 and 8. On June 19, all individual milk samples returned negative results (**Table 1**).

Seroprevalence Survey in Surrounding Farms

Within a couple of kilometers away from the suspected farm, five farms that were hosting cows and goats were identified, and sera from all individuals were collected and processed as above. Few seropositive animals were found in three of the five farms, with one to five seropositive animals and a TBEV seroprevalence ranging from 5.5 to 25% (**Figure 2** and **Table 2**). Animals from the suspected farm and from farms #1 and #3 within which seropositive animals were found have all grazed in meadows located in close proximity to the same forest (**Figure 3**). On farm #4, a single 10-year-old cow was TBEV-seropositive, but it was not possible to trace back where the cow had grazed in the past.

Tick-Borne Encephalitis Virus Presence in Ticks and Rodents Within and Around the Pasture

The goats have grazed in only one pasture adjacent to the dairy cow farm. Half of the goat pasture was a wooded area which was in continuity of a large mixed deciduous and coniferous forest dominated by beech trees.

Detection of Tick-Borne Encephalitis Virus in Ticks

A total of 120 larvae, 907 nymphs, 27 females, and 31 males of questing *Ixodes* spp. and 1 female of *Dermacentor reticulatus* were collected within the pasture and in the adjacent forest. Within the pasture, ticks were only found in the wooded area, particularly along the wooded edge and hedgerow and in the meadow situated less than 10 m away from the forest edge. The density of questing *Ixodes* spp. nymphs was the highest in the forest with a mean of 71.5 nymphs/100 m^2, then in the wooded areas, in the wooded edge of the pasture with a mean of 24–32 nymphs/100 m^2, and, finally, in the meadow with a mean of 4.5 nymphs/100 m^2 (**Table 2**).

Two pool of nymphs - from the forest and from the meadow located between the wooded area of the pasture and the forest - and one male from the forest were subsequently tested positive for TBEV RNA. Overall, the MIR was 0.22% ($IC_{95\%}$: 0.03–0.80%) in nymphs, and the infection rate was 1.8% ($IC_{95\%}$: 0.1–9.9%) in adults. The estimated density of infected nymphs was the highest in the forest with 0.15 infected nymphs/100 m^2, then in the wooded area and in the wooded edge of the pasture with 0.05–0.06 infected nymphs/100 m^2.

TABLE 2 | Number of questing ticks collected and mean density per habitat.

Habitat	No. sub-areas	Sampled surface (m^2)	No. nymphs	No. female	No. male	Density of nymphs (/100 m^2)	
						mean	Range
Forest	3	540	382	10	20	71.5	64.2–81.3
Additional collection	/	/	*285*	*7*	*5*	/	/
Pasture							
Wooded area	3	300	105	6	3	31.7	20.0–50.0
Wooded edge	5	400	94	2	2	24.0	5–56.7
Hedgerows	7	870	4	0	0	0.3	0–1.1
Meadow between 3 and 10 m from the wooded edge	4	530	35	2	1	4.5	0–8.8
Meadow between 3 and 10 m from the hedgerow	4	400	2	0	0	0.3	0–1.1
Meadow > 10 m from the edge	6	600	0	0	0	0	0

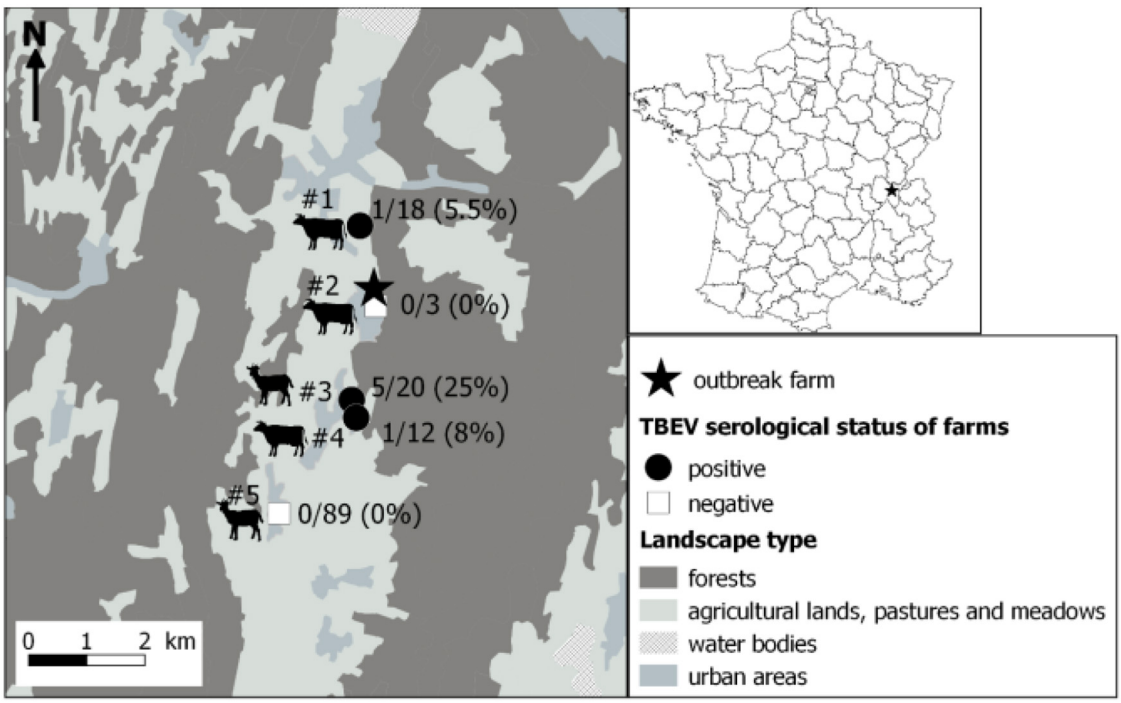

FIGURE 3 | Localisation of the farm responsible for the tick-borne encephalitis cluster through alimentary route (star) and results of the serological survey conducted in surrounding farms. Serum samples were first tested by a competitive ELISA. Then, positive and doubtful ELISA samples were tested by specific tick-borne encephalitis virus (TBEV) micro-neutralisation tests (MNT). A serum sample was considered TBEV-seropositive when MNT was positive. Dairy cows, suckling cows, goats, suckling cows, and goats were found in farms #1 to #5, respectively.

Absence of Tick-Borne Encephalitis Virus in Captured Small Mammals

In addition, small mammals were caught around the pasture to assess TBEV presence. In total, ten small mammals were captured: nine shrews (*Sorex* spp.) and one bank vole (*Myodes glareolus*). Only the bank vole was captured at the edge of the forest. Larvae of *Ixodes ricinus* were, respectively, observed on the bank vole (five larvae) and on two shrews (two larvae). All animal organs (spleen and brain) were negative to TBEV as assessed by qRT-PCR.

Phylogenetic Analysis

Three RNA samples were extracted from two TBEV-positive pools of nymphs and one TBEV-positive male tick, and RNA samples obtained from three individual infected-goat milk were subjected to sequencing. Our amplicon-based sequencing protocol allowed us to successfully sequence the TBEV genome from RNA extracted from milk and ticks (**Figure 4**). The full-length genome sequence obtained from milk and ticks was similar to the full-length genome obtained from the contaminated cheese collected during the investigation led by a local authority

agency. Sequences obtained from the milk sample, and the virus isolate obtained from ticks were 100% identical except for single nucleotide insertions and deletions that are most likely due to sequencing errors.

The full-length genome of the new viral strain was sequenced and compared to previously characterised TBEV genome sequences. The TBEV_Ain_France_2020 had limited homology (98.4% identity) to the partial NS5 of the TBEV from the Alsace region (AF0910) (**Supplementary Data**). The nucleotide sequence presents a 98.8% identity to the same partial NS5 and between 98 and 98.07% identity to the full-length genomes of TBEV isolates detected in Russia, Germany, Austria, Czech Republic, and the Netherlands with the most ancient isolate dating from 1951 in Russia. The polyprotein sequence presented up to 99.30 and 99.24% identity to MK922616 and MK922617 isolated from ticks collected in the German federal state of Lower Saxony in 2018. Our phylogenetic analyses confirmed that TBEV_Ain_2020 (OL441148) belongs to the European subtype (TBEV-Eu3) and is most closely related to TBEV strains recently isolated in bordering countries and Eastern Europe (**Figure 5**).

DISCUSSION

Food-borne TBE outbreaks had been reported in several endemic countries in Central Europe at a regular frequency, particularly in countries where the consumption of traditional raw milk products is popular (Kerlik et al., 2018). France is on the border of the TBEV geographic range, and cases resulting from tick bites are reported very occasionally. The first occurrence of TBE-food-borne outbreak in France in 2020 has led to an unexpected high number of cases. Forty-three patients have developed clinical symptoms compatible with TBE, and all but one had consumed raw goat milk and/or cheese products originating from a single producer, while 41 cases could be confirmed by detection of TBEV-specific antibodies in sera and/or in cerebrospinal fluid. A health alert was triggered within a month after the first patient showed symptoms, and an in-depth investigation of TBEV presence was conducted in the farm suspected to be the source of contamination and in animals in surrounding farms. We applied a "one health" approach, combining environmental, veterinary, virology, and food microbiology approaches to identify the origin of infection and provide a range of epidemiological information of significance to public health decision-makers. We characterised the TBEV strain circulating in Ain, detected viral genome presence in a batch of cheese, goat milk, and in questing ticks, demonstrated recent infection of goats, assessed the enzootic hazard for TBEV exposure, and identified a wooded TBEV-focus area. This integrative investigation provides information that would allow the farmer and authorities to assess the risk of infection and develop control measures.

The initial investigation of seroprevalence (23%) in goat flocks at the suspected farm reveals that the animals had been moderately exposed to the virus these past few years. In neighboring areas where TBEV is endemic, such as Switzerland and Germany, seroprevalence varies from 1 to 80% with median range value of 10–20% (calculated from Klaus et al., 2012; Klaus et al., 2014; Rieille et al., 2017; Casati Pagani et al., 2019). Seroconversion results, presence of IgM antibodies, and detection of the virus genome in milk indicate that infection was very recent for half of the animals that had been exposed to the virus (6 animals over 13). IgM was detected in one individual. Three individuals seroconverted after entering the stable, indicating that TBEV infection occurred a few days before they entered the stable. Indeed, seroconversion in goats and sheep occurs in 6–10 days (Van Tongeren, 1955; Klaus et al., 2014; Paulsen et al., 2019). One of these individuals and two others excreted viruses in milk 14 days after entering the stable. These results also support a recent infection given that virus excretion in goat and sheep milk is detected from 2 to 23 days after infection (Gresikova, 1958; Gresíková et al., 1975; Balogh et al., 2010, 2012). So far, information is relatively scarce on the infection dynamics in ruminants, especially in naturally infected animals. Our investigation confirmed a long-lasting excretion of the virus in milk in naturally infected goats since three individuals excreted the virus into milk for over 14 days post-infection. The date of the seroconversion of the additional seven TBEV-seropositive goats and two cows from the same farm is unclear. Previous studies suggest that TBEV-antibodies may persist up to 6 years, but the level of IgG produced decreases over time (Klaus et al., 2014, 2019). In agreement, even though the level of neutralising antibodies remain high a year later, we observed a decrease in the level of IgG detected by ELISA. Thus, the high level of IgG, as measured by ELISA competition, indicates that the remaining animals have been likely infected or re-infected by the virus in 2020. Since no virus excretion has been observed in five experimentally pre-immunised goats (Balogh et al., 2012), only naïve individuals would have excreted TBEV in milk. The high recent infection rate among naïve individuals of the flock would explain the high virus load detected in tank milk in June. Milk and cheese viral load were determined using a genome quantification assay, whereby milk sample concentration was estimated based on cycle threshold (Ct) values derived from measurements of serial dilutions of infectious TBE viral particles with known concentrations (from 10^8 to 10^3 TCID50/ml). We evaluated a minimal detection of infectious viral particles at 10^4 TCID50/ml of milk and 10^5 TCID50/ml after dissolution of 2.5 g of cheese. In ticks, the mean viral copy number lies between 2×10^2 and 4.8×10^3 RNA copies per sample (Liebig et al., 2020, 2021). Our data confirmed the high virus load detected in tank milk. Moreover, the virus was detected in seven cheese (over 91 tested). Among them, one contaminated cheese was produced on April 28. This is outstanding, especially when we consider that cheese was kept for several days at 1–5°C by consumers or producers before being analysed, which may have reduced the persistence of TBEV load and hence its detection.

The high recent infection rate of the goat flock suggests regular contact between TBE-infected ticks and goats in spring 2020, when ticks started to be active. We found infected questing nymphs and adults in the wooded edge of the pasture (in the meadow between the pasture wood and the forest) and in the forest nearby. With an MIR of 0.22% ($IC_{95\%}$: 0.03–0.80%) in nymphs and an infection rate of 1.8% ($IC_{95\%}$: 0.1–9.9%) in adults, it appears that TBEV is well established in the forest near the

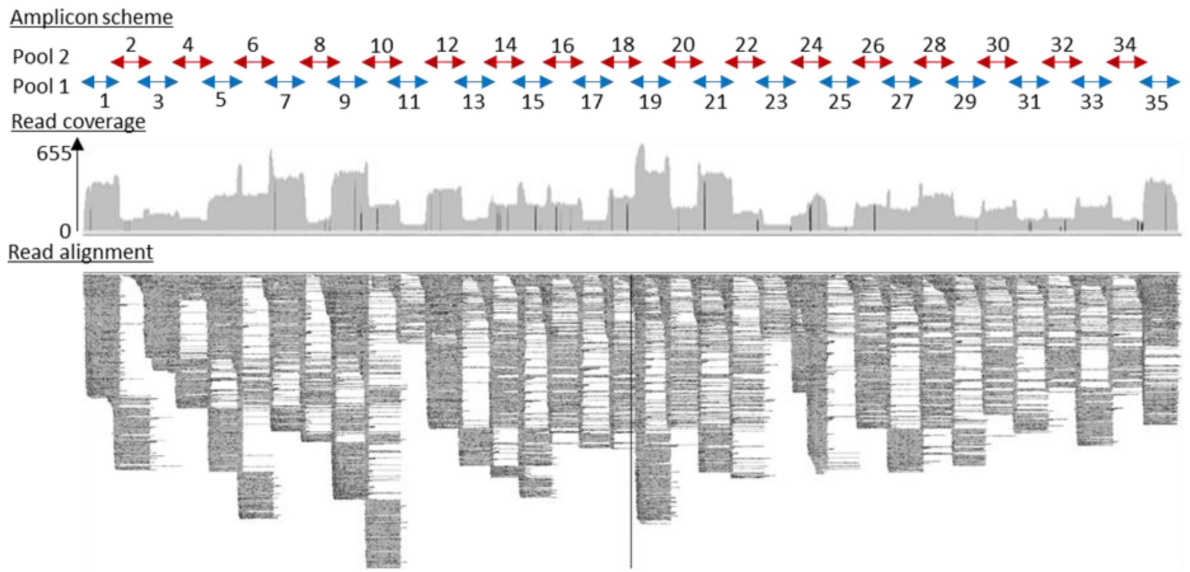

FIGURE 4 | Full-length TBEV genome sequence (GenBank accession number: OL441148) was obtained from sequencing 35 overlapping amplicons in two multiplex reactions. Read coverage varied along the sequence length, but a full-length genome sequence was successfully recovered.

pasture. Indeed, while the densities and prevalence of infected questing ticks may not be deemed exceptionally high compared to what is seen in endemic countries (Süss, 2011), it is similar to the highest values observed in an endemic foci in Alsace region, East France (Bournez et al., 2020). Since we captured a few adult ticks (probably because the dragging method is not well suited to capture this stage), the density of infected adults was estimated with a low precision and hence might be higher than those observed in Alsace. We did not detect TBEV RNA in small mammals trapped in the pasture, but we probably missed infected individuals since we only trapped a few rodents. Indeed, the year 2020 was probably a low phase of the usual yearly fluctuating rodent population. Overall, the results suggest that the presence of a large wooded area within the pasture frequently used by goats as a shelter as well as of a long pasture-forest edge where tick densities are relatively high have likely favoured the contacts between goats and TBEV-infected ticks. The forest may also represent a source of frequent introduction of infected ticks into the pasture through the movements of tick-feeding hosts.

This cluster was surprising by its location. It occurred in the Ain department in France where TBEV human cases had never been reported. Our investigation in surrounding farms also revealed that TBEV was also present in various pastures surrounding the same single forest where we found infected ticks over at least 2 km. In three of these farms, seroprevalence varied between 5.5 and 25%. With the exception of one individual (for which it was not possible to track back the pasture in which it had grazed), all seropositive animals had likely grazed within a pasture adjacent to the same forest. These results indicate that the virus is well established in the area and, probably, in a larger extent in the Ain department. Because of the absence of an active TBEV surveillance system assessing its distribution in France and potential misleading of TBE diagnosis, it is impossible to conclude whether the presence of TBEV in the department is ancient or whether it was recently introduced. In addition, diagnosis of human TBE cases was initially delayed as TBE serology was not systematically researched among patients presenting with meningitis or meningoencephalitis. Similarly, the presence of TBEV in centre France, in Loire, and Haute-Loire departments detected for the first time in 2017 and 2018 (Herpe et al., 2007; Velay et al., 2018) is impossible to date. Given that the life cycle of ticks involves generally one meal per stage per year, we can presume that TBEV-infected ticks have been present in the environment for at least 1 or 2 years before the occurrence of human cases. Evidence suggest that the geographic range of TBEV is currently expanding in Europe, especially in Western and Northern Europe (Csángó et al., 2004; Donoso Mantke et al., 2011; Rieille et al., 2017; Andersen et al., 2019; Casati Pagani et al., 2019; Smura et al., 2019; Alfano et al., 2020; Ullrich et al., 2021). This expansion also have occurred in France. For instance, in a recent expansion of TBEV in higher altitudes, other previously unaffected areas or ancient affected areas have been observed in several France's neighbouring endemic countries, including Germany (Dobler et al., 2019; Hellenbrand et al., 2019), Switzerland (Rieille et al., 2017; Casati Pagani et al., 2019; Desgrandchamps et al., 2019), and Italy (Alfano et al., 2020). The virus was also detected for the first time in the United Kingdom in 2018 (Holding et al., 2020) and in the Netherlands in 2015 (Jahfari et al., 2017). TBEV expansion is believed to be driven by climate, landscape, and anthropogenic changes (Randolph, 2010; Jaenson et al., 2012; Holding et al., 2020). Moreover, the first occurrence of TBEV in new areas in France since 2017 might be the results of exceptional high densities of infected ticks these past 5 years in endemic areas, which may have led to higher dispersal rates of infected ticks into new areas. Indeed, although TBE human incidence

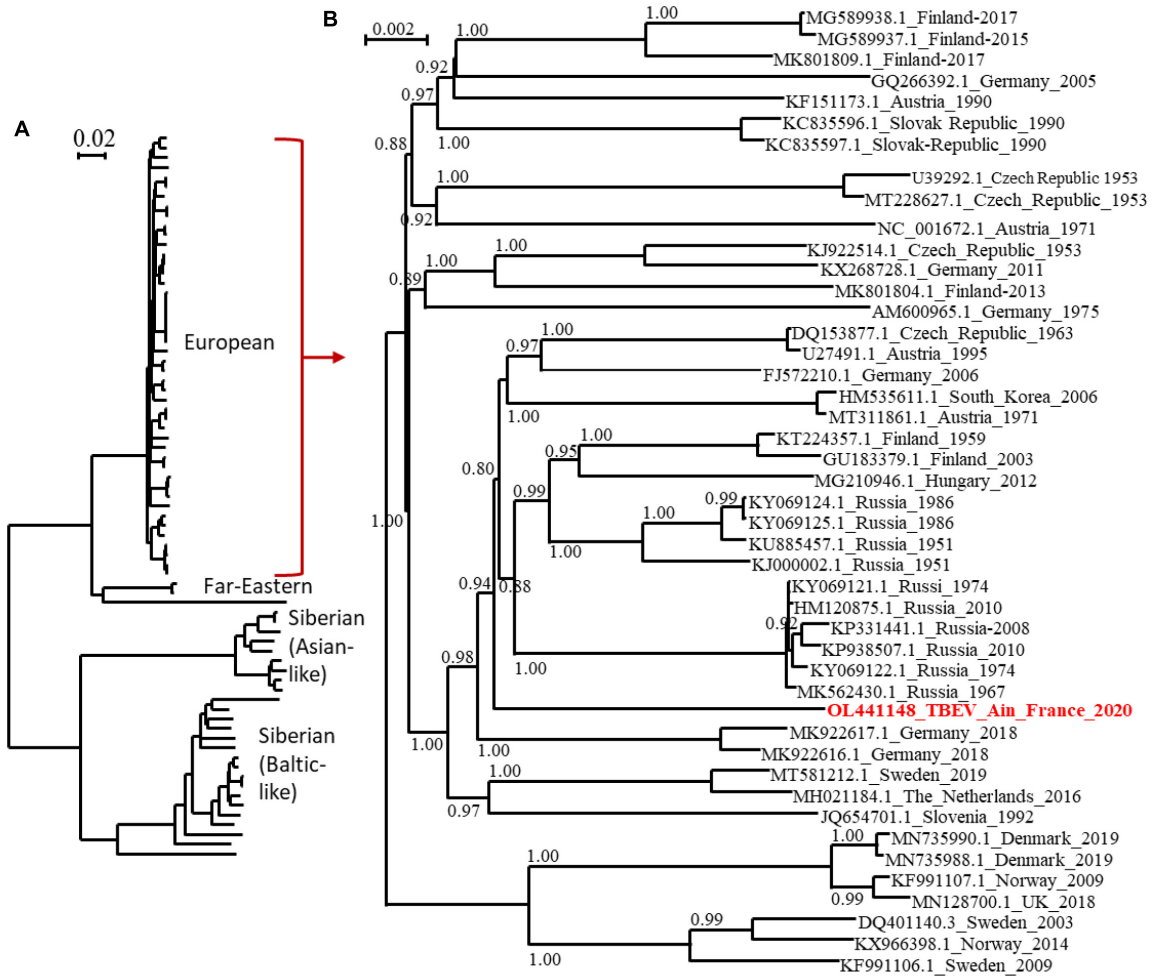

FIGURE 5 | Phylogenetic tree of TBEV complete open reading frames that were available in GenBank and the TBEV-Ain-France-2020 obtained in the present study (marked red) using all sequences **(A)** or those corresponding to the European subtype only **(B)**. The two trees were inferred in PhyML using the Le Gascuel (LG) substitution model. Branch points indicate that results of Shimodaira-Hasgawa branch test > 0.8. Scale bar shows the number of nucleotide changes. Virus isolate names are given as follows: accession number from NCBI_ country to name_year.

usually exhibits significant oscillations over time, in 2016–2020, it was persistently high in numerous endemic countries of Western and Central Europe (Germany, Switzerland, Czech Republic, Slovakia, and Italy), including France (Dobler et al., 2019). This may partly be caused by high densities of infected ticks during those years. A high density of infected ticks during several years in endemic areas may increase the frequency of medium or long-distance movements of infected ticks on their host (birds, cervids) and led to a more successful introduction of the virus into new areas. Alternatively, it is also possible that TBEV has been circulating in Ain department undetected for decades, and the 2020 outbreak could be the result of suitable conditions for its detection. Indeed, TBE cases are likely underdiagnosed in France given that human clinical cases are rare and local clinicians are unfamiliar with the disease (infection often asymptomatic, not yet notifiable disease in April 2020, low virus circulation, few TBEV foci, few human visits in infected areas) (Dollat et al., 2021). The year of 2020 was exceptional with a very high human incidence observed in numerous endemic European countries. In Switzerland and Germany, the notable increase of TBE cases observed in spring 2020 was partly associated with higher recreational activities in risky endemic areas around people's homes during the COVID-19 containment measures (Steffen et al., 2020; Ullrich et al., 2021). In France, the COVID-19 containment measures may have also indirectly increased the consumption of local products. Hence, the emergence of a cluster of food-borne TBE cases in a restricted geographical area that was easier to detect. However, this was not the sole factor as an upsurge of infected tick densities in 2020 likely contributed to the rise of human incidence. Indeed, models forecasting the human TBE incidence based on demographic parameters, large-scale atmospheric circulation patterns, the fructification of the European beech (*Fagus sylvatica*) 2 years prior, and the national TBE vaccination coverage already predicted an increase in TBE incidence in 2020 in Germany, Switzerland, and Austria (Rubel and Brugger, 2020, 2021). In Germany, an unusually high density

of infected adult ticks has also been observed in 2020 in some places (PROMED, 2020).

We provide the first TBEV isolate responsible for a source of dietary contamination in France, which will facilitate experimental studies. The genome sequences obtained were used to conduct phylogenetic analyses using the complete open reading frame. We revealed that the TBEV_Ain_France_2020 belonged to the European TBEV subtype, but do not cluster with the strain circulating in the Alsace region and to other isolates from Europe, with the closest relatives being isolates from Germany, Austria, Czech Republic, The Netherlands, and Russia. In all actuality, we do not know enough about the distribution of TBEV in France and the genetic diversity of the TBEV genome in Europe. The distinct genome of the French isolate would tend to indicate that this isolate has not recently spread to France but has remained undetected and evolved locally for some time. Further studies in the department and neighbouring regions are needed and are being set up to further characterise the focus-specific genetic diversity of TBEV and to confirm or disprove the ancient origin and geographical extension of this isolate.

In conclusion, the cluster of TBE alimentary cases in Ain was unexpected. It surprised clinicians and local health authorities given the number of infected patients. The high recent infection rate of the goat flock probably led to a high virus load in tank milk in April and May and facilitated infection by consumption of raw cheese. In addition, the COVID-19 containment measures in spring 2020 may have also indirectly increased the consumption of local products and, hence, the risk of food-borne TBE cases. The Ain outbreak also highlighted the need for improving surveillance, detection, and prevention of TBE in France. Clearly, a better understanding of TBEV distribution in France, of local virus dynamic, and of food-borne contamination with better identification of raw milk products being at risk is needed to better adapt surveillance and prevention measures. This is all more important as France produces each year 40,000 tonnes of raw milk-products and cheese. In addition, the local production and consumption of traditional delicacies is increasing. TBEV is now a notifiable disease in France, facilitating the systematic report of human cases and sensitising medical communities for diagnosis of humans showing encephalitis in France. In endemic regions and those surrounding affected areas, patients with meningitis and encephalitis in the absence of another etiological diagnosis should be more systemically screened for TBEV infection (Herpe et al., 2007; Velay et al., 2018; Botelho-Nevers et al., 2019; Blanchon et al., 2020). Surveillance could also include serological testing for anti-TBEV antibodies in animal blood or in milk tanks to allow early detection of virus foci (Imhoff et al., 2015; Rieille et al., 2017; Wallenhammar et al., 2020; Bauer et al., 2021). Finally, in focus areas, TBE vaccination could provide protection from disease caused by infections from tick bites or consumption of virus-contaminated dairy products (Chernokhaeva et al., 2018; Kubinski et al., 2020; Chitimia-Dobler et al., 2021).

DATA AVAILABILITY STATEMENT

The datasets presented in this study can be found in online repositories. The names of the repository/repositories and accession number(s) can be found in the article/**Supplementary Material**.

ETHICS STATEMENT

Ethical review and approval was not required for the animal study because the species captured during this study are neither protected in France nor included in the International Union for Conservation Nature Red List of threatened species and, therefore, no special authorisation was needed for trapping, according to French law. Animal trapping took place with permission from the landowners. All efforts were made to minimise animal suffering. The traps that we used are designed not to stress or harm the animals. Small mammals were euthanised by authorised experimenters according to French law and to the European guidelines (AVMA Guidelines for the euthanasia of Animals: 2020 editions). Written informed consent was obtained from the owners for the participation of their animals in this study.

AUTHOR CONTRIBUTIONS

All authors contributed to the article and approved the submitted version.

ACKNOWLEDGMENTS

We would like to thank the clinicians of Bourg-en-Bresse and Oyonnax hospitals, Beaufils, Canu, Decouchon, and Decroix in particular, who were involved in patient care and initiated the health alert.

SUPPLEMENTARY MATERIAL

The Supplementary Material for this article can be found online at: https://www.frontiersin.org/articles/10.3389/fmicb.2022.863725/full#supplementary-material

REFERENCES

Alfano, N., Tagliapietra, V., Rosso, F., Ziegler, U., Arnoldi, D., and Rizzoli, A. (2020). Tick-borne encephalitis foci in northeast Italy revealed by combined virus detection in ticks, serosurvey on goats and human cases. *Emerg. Microbes Infect.* 9, 474–484. doi: 10.1080/22221751.2020.1730246

Andersen, N. S., Larsen, S. L., Olesen, C. R., Stiasny, K., Kolmos, H. J., Jensen, P. M., et al. (2019). Continued expansion of tick-borne pathogens: tick-borne encephalitis virus complex and *Anaplasma phagocytophilum* in Denmark. *Ticks Tick-borne Dis.* 10, 115–123. doi: 10.1016/j.ttbdis.2018.09.007

Balogh, Z., Egyed, L., Ferenczi, E., Bán, E., Szomor, K. N., Takács, M., et al. (2012). Experimental infection of goats with tick-borne encephalitis virus and the

possibilities to prevent virus transmission by raw goat milk. *Intervirology* 55, 194–200. doi: 10.1159/000324023

Balogh, Z., Ferenczi, E., Szeles, K., Stefanoff, P., Gut, W., Szomor, K. N., et al. (2010). Tick-borne encephalitis outbreak in Hungary due to consumption of raw goat milk. *J. Virol. Methods* 163, 481–485. doi: 10.1016/j.jviromet.2009.10.003

Bauer, B. U., Könenkamp, L., Stöter, M., Wolf, A., Ganter, M., Steffen, I., et al. (2021). Increasing awareness for tick-borne encephalitis virus using small ruminants as suitable sentinels: Preliminary observations. *One Health* 12:100227. doi: 10.1016/j.onehlt.2021.100227

Beck, C., Desprès, P., Paulous, S., Vanhomwegen, J., Lowenski, S., Nowotny, N., et al. (2015). A high-performance multiplex immunoassay for serodiagnosis of flavivirus-associated neurological diseases in horses. *BioMed. Res. Int.* 2015:678084. . doi: 10.1155/2015/678084

Beck, Y., Fritz, R., Orlinger, K., Kiermayr, S., Ilk, R., Portsmouth, D., et al. (2016). Molecular basis of the divergent immunogenicity of two pediatric tick-borne encephalitis virus vaccines. *J. Virol.* 90, 1964–1972. doi: 10.1128/JVI.02985-15

Bestehorn, M., Weigold, S., Kern, W. V., Chitimia-Dobler, L., Mackenstedt, U., Dobler, G., et al. (2018). Phylogenetics of tick-borne encephalitis virus in endemic foci in the upper rhine region in France and Germany. *PLoS One* 13:e0204790. doi: 10.1371/journal.pone.0204790

Blanchon, T., Boulanger, N., Camus, D., Cazorla, C., Hansmann, Y., Leparc-Goffart, I., et al. (2020). *Avis Relatif à L'inscription de L'encéphalite à Tiques sur la Liste des Maladies à Déclaration Obligatoire*. Paris: Haut conseil de Santé Publique. 1–22.

Blaskovic, D. (1967). The public health importance of tick-borne encephalitis in Europe. *Bull. World Health Organ.* 36(Suppl.), 5–13.

Bogovic, P., Lotric-Furlan, S., and Strle, F. (2010). What tick-borne encephalitis may look like: clinical signs and symptoms. *Travel Med. Infect. Dis.* 8, 246–250. doi: 10.1016/j.tmaid.2010.05.011

Botelho-Nevers, E., Gagneux-Brunon, A., Velay, A., Guerbois-Galla, M., Grard, G., Bretagne, C., et al. (2019). Tick-Borne Encephalitis in Auvergne-Rhône-Alpes Region. France, 2017-2018. *Emerg. Infect. Dis.* 25, 1944–1948. doi: 10.3201/eid2510.181923

Bournez, L., Umhang, G., Faure, E., Boucher, J. M., Boué, F., Jourdain, E., et al. (2019). Exposure of wild ungulates to the usutu and tick-borne encephalitis viruses in France in 2009-2014: evidence of undetected flavivirus circulation a decade ago. *Viruses* 12:10. doi: 10.3390/v12010010

Bournez, L., Umhang, G., Moinet, M., Richomme, C., Demerson, J.-M., Caillot, C., et al. (2020). Tick-Borne encephalitis virus: seasonal and annual variation of epidemiological parameters related to nymph-to-larva transmission and exposure of small mammals. *Pathogens*. 9:518. doi: 10.3390/pathogens9070518

Brabec, M., Daniel, M., Malý, M., Danielová, V., Kříž, B., and Kott, I. (2017). Analysis of meteorological effects on the incidence of tick-borne encephalitis in the czech republic over a thirty-year period. *Virol. Res. Rev.* 2017, 1–8.

Brockmann, S. O., Oehme, R., Buckenmaier, T., Beer, M., Jeffery-Smith, A., Spannenkrebs, M., et al. (2018). A cluster of two human cases of tick-borne encephalitis (TBE) transmitted by unpasteurised goat milk and cheese in Germany. May 2016. *Euro. Surveill.* 23:17–0036. doi: 10.2807/1560-7917.ES.2018.23.15.17-00336

Caini, S., Szomor, K., Ferenczi, E., Szekelyne Gaspar, A., Csohan, A., Krisztalovics, K., et al. (2012). Tick-borne encephalitis transmitted by unpasteurised cow milk in western hungary. september to October 2011. *Euro. Surveill.* 17: 20128.

Cannon, R. M. (2001). Sense and sensitivity–designing surveys based on an imperfect test. *Prev. Vet. Med.* 49, 141–163. doi: 10.1016/s0167-5877(01)00184-2

Casati Pagani, S., Frigerio Malossa, S., Klaus, C., Hoffmann, D., Beretta, O., Bomio-Pacciorini, N., et al. (2019). First detection of TBE virus in ticks and sero-reactivity in goats in a non-endemic region in the southern part of Switzerland (Canton of Ticino). *Ticks Tick Borne Dis.* 10, 868–874. doi: 10.1016/j.ttbdis.2019.04.006

Chernokhaeva, L. L., Rogova, Y. V., Kozlovskaya, L. I., Romanova, L. I., Osolodkin, D. I., Vorovitch, M. F., et al. (2018). Experimental evaluation of the protective efficacy of tick-borne encephalitis (TBE) vaccines based on european and far-eastern TBEV strains in mice and in vitro. *Front. Microbiol* 9:1487. doi: 10.3389/fmicb.2018.01487

Chitimia-Dobler, L., Lindau, A., Oehme, R., Bestehorn-Willmann, M., Antwerpen, M., Drehmann, M., et al. (2021). Tick-borne encephalitis vaccination protects from alimentary TBE infection: results from an alimentary outbreak. *Microorganisms* 9:889. doi: 10.3390/microorganisms9050889

Cisak, E., Wójcik-Fatla, A., Zając, V., Sroka, J., Buczek, A., and Dutkiewicz, J. (2010). Prevalence of tick-borne encephalitis virus (TBEV) in samples of raw milk taken randomly from cows, goats and sheep in eastern Poland. *Ann. Agric. Environ. Med.* 17, 283–286.

Csángó, P. A., Blakstad, E., Kirtz, G. C., Pedersen, J. E., and Czettel, B. (2004). Tick-borne encephalitis in southern Norway. *Emerg. Infect. Dis.* 10, 533–534. doi: 10.3201/eid1003.020734

Daniel, M., Danielová, V., Kriz, B., and Kott, I. (2004). An attempt to elucidate the increased incidence of tick-borne encephalitis and its spread to higher altitudes in the Czech Republic. *Int. J. Med. Microbiol.* 293(Suppl. 37), 55–62. doi: 10.1016/s1433-1128(04)80009-3

Desgrandchamps, D., Posfay-Barbe, K. M., and Schmitt, H. J. (2019). "Chapter 12b – A: TBE in Switzerland and Liechtenstein," in *The TBE Book*, 2nd Edn. eds G. Dobler, W. Erber, M. Bröker, and H. J. Schmitt (Singapore: Global Health Press), 342–347.

Deviatkin, A. A., Kholodilov, I. S., Vakulenko, Y. A., Karganova, G. G., and Lukashev, A. N. (2020). Tick-borne encephalitis virus: an emerging ancient zoonosis? *Viruses* 12:247. doi: 10.3390/v12020247

Dobler, P. D. G., Erber, W., Bröker, M., and Schmit, P. D. H. J. (2019). *The TBE Book*, IInd Edn. Singapore: Global Health Press Pte Limited.

Dollat, M., Bellanger, A.-P., Millon, L., Chirouze, C., Lepiller, Q., and Marguet, P. (2021). Knowledge and vaccination practices among family physicians in northeastern France regarding tick-borne encephalitis virus. *Ticks and Tick-borne Dis.* 12:101774. doi: 10.1016/j.ttbdis.2021.101774

Donoso Mantke O, Escadafal, C., Niedrig, M., Pfeffer, M., and Working Group for Tick-Borne Encephalitis Virus , C. (2011). Tick-borne encephalitis in Europe, 2007 to 2009. *Euro. Surveill.* 16, 19976. doi: 10.2807/ese.16.39.19976-en

Dorko, E., Hockicko, J., Rimárová, K., Bušová, A., Popaď ák, P., Popaďáková, J., et al. (2018). Milk outbreaks of tick-borne encephalitis in Slovakia, 2012-2016. *Eur. J. Public Health* 26(Suppl.), S47–S50. doi: 10.21101/cejph.a5272

Driouich, J. S., Moureau, G., De Lamballerie, X., and Nougairède, A. (2019). Reverse Genetics of RNA viruses: ISA-based approach to control viral population diversity without modifying virus phenotype. *Viruses* 11:666. doi: 10.3390/v11070666

ECDC. (2012). *Epidemiological Situation of tick-Borne Encephalitis in the European Union and European free trade association countries*. Stockholm: European Centre for Disease Prevention and Control.

ECDC. (2018). *Tick-Borne Encephalitis: Epidemiological Report for 2016*. Stockholm: European Centre for Disease Prevention and Control, 1–7.

Gondard, M., Michelet, L., Nisavanh, A., Devillers, E., Delannoy, S., Fach, P., et al. (2018). Prevalence of tick-borne viruses in *Ixodes ricinus* assessed by high-throughput real-time PCR. *Pathog. Dis.* 2018:76. doi: 10.1093/femspd/fty083

Gresikova, M. (1958). Recovery of the tick-borne encephalitis virus from the blood and milk of subcutaneously infected sheep. *Acta. Virol.* 2, 113–119.

Gresíková, M., Sekeyová, M., Stúpalová, S., and Necas, S. (1975). Sheep milk-borne epidemic of tick-borne encephalitis in Slovakia. *Intervirology* 5, 57–61. doi: 10.1159/000149880

Gunnar, H., Gunnar, B., Erik, E., Christer, J., Bjørn, L., Jan Erik, R., et al. (2009). Transport of Ticks by Migratory Passerine Birds to Norway. *J. Parasitol.* 95, 1342–1351. doi: 10.1645/GE-2146.1

Hansmann, Y., Pierre Gut, J., Remy, V., Martinot, M., Allard Witz, M., and Christmann, D. (2006). Tick-borne encephalitis in eastern France. *Scand. J. Infect. Dis.* 38, 520–526.

Hellenbrand, W., Kreusch, T., Böhmer, M. M., Wagner-Wiening, C., Dobler, G., Wichmann, O., et al. (2019). Epidemiology of Tick-borne encephalitis (TBE) in Germany, 2001?2018. *Pathogens* 8:42. doi: 10.3390/pathogens8020042

Hennechart-Collette, C., Martin-Latil, S., Fraisse, A., and Perelle, S. (2017). Comparison of three extraction methods to detect noroviruses in dairy products. *Food Microbiol.* 61, 113–119. doi: 10.1016/j.fm.2016.09.001

Herpe, B., Schuffenecker, I., Pillot, J., Malvy, D., Clouzeau, B., Bui, N., et al. (2007). Tickborne encephalitis, southwestern France. *Emerg. Infect. Dis.* 13, 1114–1116. doi: 10.3201/eid1307.070041

Holding, M., Dowall, S. D., Medlock, J. M., Carter, D. P., Pullan, S. T., Lewis, J., et al. (2020). Tick-Borne Encephalitis Virus. United Kingdom. *Emerg. Infect. Dis.* 26, 90–96.

Holzmann, H., Aberle, S. W., Stiasny, K., Werner, P., Mischak, A., Zainer, B., et al. (2009). Tick-borne encephalitis from eating goat cheese in a mountain region of Austria. *Emerg. Infect. Dis.* 15, 1671–1673. doi: 10.3201/eid1510.090743

Hudopisk, N., Korva, M., Janet, E., Simetinger, M., Grgič-Vitek, M., Gubenšek, J., et al. (2013). Tick-borne encephalitis associated with consumption of raw goat milk. Slovenia, 2012. *Emerg. Infect. Dis.* 19, 806–808.

Ilic, M., Barbic, L., Bogdanic, M., Tabain, I., Savic, V., Kosanovic Licina, M. L., et al. (2020). Tick-borne encephalitis outbreak following raw goat milk consumption in a new micro-location. Croatia, June 2019. *Ticks Tick borne Dis.* 11:101513. doi: 10.1016/j.ttbdis.2020.101513

Imhoff, M., Hagedorn, P., Schulze, Y., Hellenbrand, W., Pfeffer, M., and Niedrig, M. (2015). Review: Sentinels of tick-borne encephalitis risk. *Ticks Tick Borne Dis.* 6, 592–600. doi: 10.1016/j.ttbdis.2015.05.001

Jaenson, T. G., Hjertqvist, M., Bergström, T., and Lundkvist, A. (2012). Why is tick-borne encephalitis increasing? A review of the key factors causing the increasing incidence of human TBE in Sweden. *Parasit Vectors* 5:184. doi: 10.1186/1756-3305-5-184

Jahfari, S., De Vries, A., Rijks, J. M., Van Gucht, S., Vennema, H., Sprong, H., et al. (2017). Tick-Borne encephalitis virus in ticks and roe deer, the Netherlands. *Emerg. Infect. Dis.* 23, 1028–1030. doi: 10.3201/eid2306.161247

Kerlik, J., Avdičová, M., Štefkovičová, M., Tarkovská, V., Pántiková Valachová, M., Molčányi, T., et al. (2018). Slovakia reports highest occurrence of alimentary tick-borne encephalitis in Europe: Analysis of tick-borne encephalitis outbreaks in Slovakia during 2007–2016. *Travel Med. Infect. Dis.* 26, 37–42. doi: 10.1016/j.tmaid.2018.07.001

Klaus, C., Beer, M., Saier, R., Schau, U., Moog, U., Hoffmann, B., et al. (2012). Goats and sheep as sentinels for tick-borne encephalitis (TBE) virus – Epidemiological studies in areas endemic and non-endemic for TBE virus in Germany. *Ticks Tick-borne Dis.* 3, 27–37. doi: 10.1016/j.ttbdis.2011.09.011

Klaus, C., Ziegler, U., Hoffmann, D., Press, F., Fast, C., and Beer, M. (2019). Tick-borne encephalitis virus (TBEV) antibodies in animal sera - occurrence in goat flocks in Germany, longevity and ability to recall immunological information after more than six years. *BMC Vet. Res.* 15:399. doi: 10.1186/s12917-019-2157-5

Klaus, C., Ziegler, U., Kalthoff, D., Hoffmann, B., and Beer, M. (2014). Tick-borne encephalitis virus (TBEV) – findings on cross reactivity and longevity of TBEV antibodies in animal sera. *BMC Vet. Res.* 10:78. doi: 10.1186/1746-6148-10-78

Kohlmaier, B., Schweintzger, N. A., Sagmeister, M. G., Švendová, V., Kohlfürst, D. S., Sonnleitner, A., et al. (2021). Clinical characteristics of patients with tick-borne encephalitis (TBE): a european multicentre study from 2010 to 2017. *Microorganisms* 9:1420. doi: 10.3390/microorganisms9071420

Kubinski, M., Beicht, J., Gerlach, T., Volz, A., Sutter, G., and Rimmelzwaan, G. F. (2020). Tick-borne encephalitis virus: a quest for better vaccines against a virus on the rise. *Vaccines* 8:451. doi: 10.3390/vaccines8030451

Labuda, M., Kozuch, O., Zuffová, E., Elecková, E., Hails, R. S., and Nuttall, P. A. (1997). Tick-borne encephalitis virus transmission between ticks cofeeding on specific immune natural rodent hosts. *Virology* 235, 138–143. doi: 10.1006/viro.1997.8622

Lefort, V., Longueville, J.-E., and Gascuel, O. (2017). SMS: smart model selection in PhyML. *Mol. Biol Evol.* 34, 2422–2424. doi: 10.1093/molbev/msx149

Li, H. (2018). Minimap2: pairwise alignment for nucleotide sequences. *Bioinformatics* 34, 3094–3100. doi: 10.1093/bioinformatics/bty191

Li, H., and Durbin, R. (2009). Fast and accurate short read alignment with burrows-wheeler transform. *Bioinformatics* 25, 1754–1760. doi: 10.1093/bioinformatics/btp324

Liebig, K., Boelke, M., Grund, D., Schicht, S., Bestehorn-Willmann, M., Chitimia-Dobler, L., et al. (2021). The Stable Matching Problem in TBEV enzootic circulation: how important is the perfect tick-virus match? *Microorganisms* 9:196. doi: 10.3390/microorganisms9010196

Liebig, K., Boelke, M., Grund, D., Schicht, S., Springer, A., Strube, C., et al. (2020). Tick populations from endemic and non-endemic areas in Germany show differential susceptibility to TBEV. *Sci. Rep.* 10:15478. doi: 10.1038/s41598-020-71920-z

Lindquist, L., and Vapalahti, O. (2008). Tick-borne encephalitis. *Lancet* 371, 1861–1871.

Lukan, M., Bullova, E., and Petko, B. (2010). Climate warming and tick-borne encephalitis. Slovakia. *Emerg Infect. Dis.* 16, 524–526. doi: 10.3201/eid1603.081364

Madeira, F., Park, Y. M., Lee, J., Buso, N., Gur, T., Madhusoodanan, N., et al. (2019). The EMBL-EBI search and sequence analysis tools APIs in 2019. *Nucleic. Acids Res.* 47, W636–W641. doi: 10.1093/nar/gkz268

Markovinović, L., Kosanović Ličina, M. L., Tešić, V., Vojvodić, D., Vladušić Lucić, I., Kniewald, T., et al. (2016). An outbreak of tick-borne encephalitis associated with raw goat milk and cheese consumption. Croatia, 2015. *Infection* 44, 661–665. doi: 10.1007/s15010-016-0917-8

Martello, E., Mannelli, A., Ragagli, C., Ambrogi, C., Selmi, M., Ceballos, L. A., et al. (2014). Range expansion of Ixodes ricinus to higher altitude, and co-infestation of small rodents with Dermacentor marginatus in the Northern Apennines. Italy. *Ticks Tick Borne Dis.* 5, 970–974. doi: 10.1016/j.ttbdis.2014.07.021

Paulsen, K. M., Stuen, S., Das, Neves C. G, Suhel, F., Gurung, D., Soleng, A., et al. (2019). Tick-borne encephalitis virus in cows and unpasteurized cow milk from Norway. *Zoonoses Public Health* 66, 216–222. doi: 10.1111/zph.12554

Perez-Eid, C., Hannoun, C., and Rodhain, F. (1992). The Alsatian tick-borne encephalitis focus: presence of the virus among ticks and small mammals. *Eur. J. Epidemiol.* 8, 178–186. doi: 10.1007/BF00144797

Pérez-Eid, C. (2007). *Les Tiques: Identification, Biologie, Importance Médicale et Vétérinaire., Monographies de Microbiologie*. Paris: TEC and DOC Lavoisier.

Peyrefitte, C. N., Pastorino, B. A., Bessaud, M., Gravier, P., Tock, F., Couissinier-Paris, P., et al. (2005). Dengue type 3 virus, saint Martin, 2003-2004. *Emerg. Infect. Dis.* 11, 757–761. doi: 10.3201/eid1105.040959

PROMED. (2020). *Tick-Borne Encephalitis – Germany (02). Archive Number: 20200907.7755195*. Boston, MA: Promed Post.

Quick, J., Grubaugh, N. D., Pullan, S. T., Claro, I. M., Smith, A. D., Gangavarapu, K., et al. (2017). Multiplex PCR method for minion and illumina sequencing of zika and other virus genomes directly from clinical samples. *Nat. Protoc.* 12, 1261–1276. doi: 10.1038/nprot.2017.066

Randolph, S. E. (2010). To what extent has climate change contributed to the recent epidemiology of tick-borne diseases? *Vet. Parasitol.* 167, 92–94. doi: 10.1016/j.vetpar.2009.09.011

Randolph, S. E., Miklisová, D., Lysy, J., Rogers, D. J., and Labuda, M. (1999). Incidence from coincidence: patterns of tick infestations on rodents facilitate transmission of tick-borne encephalitis virus. *Parasitology* 118(Pt 2), 177–186. doi: 10.1017/s0031182098003643

Reusken, C., Boonstra, M., Rugebregt, S., Scherbeijn, S., Chandler, F., Avšič-Županc, T., et al. (2019). An evaluation of serological methods to diagnose tick-borne encephalitis from serum and cerebrospinal fluid. *J.Clin. Virol.* 120, 78–83. doi: 10.1016/j.jcv.2019.09.009

Rieille, N., Klaus, C., Hoffmann, D., Péter, O., and Voordouw, M. J. (2017). Goats as sentinel hosts for the detection of tick-borne encephalitis risk areas in the Canton of Valais, Switzerland. *BMC Vet. Res.* 13:217. doi: 10.1186/s12917-017-1136-y

Rónai, Z., and Egyed, L. (2020). Survival of tick-borne encephalitis virus in goat cheese and milk. *Food Environ. Virol.* 12, 264–268. doi: 10.1007/s12560-020-09427-z

Rubel, F., and Brugger, K. (2020). Tick-borne encephalitis incidence forecasts for Austria. Germany, and Switzerland. *Ticks Tick-borne Dis.* 11:101437. doi: 10.1016/j.ttbdis.2020.101437

Rubel, F., and Brugger, K. (2021). Operational TBE incidence forecasts for Austria. Germany, and Switzerland 2019-2021. *Ticks Tick Borne Dis.* 12:101579. doi: 10.1016/j.ttbdis.2020.101579

Rushton, J. O., Lecollinet, S., Hubálek, Z., Svobodová, P., Lussy, H., and Nowotny, N. (2013). Tick-borne encephalitis virus in horses. Austria, 2011. *Emerg. Infect. Dis.* 19, 635–637.

Smura, T., Tonteri, E., Jääskeläinen, A., Von Troil, G., Kuivanen, S., Huitu, O., et al. (2019). Recent establishment of tick-borne encephalitis foci with distinct viral lineages in the Helsinki area. Finland. *Emerg. Microbes Infect.* 8, 675–683. doi: 10.1080/22221751.2019.1612279

Steffen, R., Lautenschlager, S., and Fehr, J. (2020). Travel restrictions and lockdown during the COVID-19 pandemic-impact on notified infectious diseases in Switzerland. *J. Travel Med.* 27, 180. doi: 10.1093/jtm/taaa180

Süss, J. (2011). Tick-borne encephalitis 2010: epidemiology, risk areas, and virus strains in Europe and Asia—An overview. *Ticks and Tick-borne Dis.* 2, 2–15. doi: 10.1016/j.ttbdis.2010.10.007

Tonteri, E., Jokelainen, P., Matala, J., Pusenius, J., and Vapalahti, O. (2016). Serological evidence of tick-borne encephalitis virus infection in moose and deer in Finland: sentinels for virus circulation. *Parasit. Vect.* 9:54. doi: 10.1186/s13071-016-1335-6

Ullrich, A., Schranz, M., Rexroth, U., Hamouda, O., Schaade, L., Diercke, M., et al. (2021). Impact of the COVID-19 pandemic and associated non-pharmaceutical interventions on other notifiable infectious diseases in Germany: An analysis of national surveillance data during week 1–2016 – week 32–2020. *Lancet Reg. Health Eur.* 6:100103. doi: 10.1016/j.lanepe.2021.100103

Van Tongeren, H. A. (1955). Encephalitis in Austria. IV. Excretion of virus by milk of the experimentally infected goat. *Arch. Gesamte Virusforsch.* 6, 158–162. doi: 10.1007/bf01247065

Velay, A., Solis, M., Kack-Kack, W., Gantner, P., Maquart, M., Martinot, M., et al. (2018). A new hot spot for tick-borne encephalitis (TBE): a marked increase of TBE cases in France in 2016. *Ticks Tick Borne Dis.* 9, 120–125. doi: 10.1016/j.ttbdis.2017.09.015

Waldenström, J., Lundkvist, A., Falk, K. I., Garpmo, U., Bergström, S., Lindegren, G., et al. (2007). Migrating birds and tickborne encephalitis virus. *Emerg. Infect. Dis.* 13, 1215–1218. doi: 10.3201/eid1308.061416

Wallenhammar, A., Lindqvist, R., Asghar, N., Gunaltay, S., Fredlund, H., Davidsson, Å, et al. (2020). Revealing new tick-borne encephalitis virus foci by screening antibodies in sheep milk. *Parasit. Vect.* 13:185. doi: 10.1186/s13071-020-04030-4

Conflict of Interest: The authors declare that the research was conducted in the absence of any commercial or financial relationships that could be construed as a potential conflict of interest.

Citation: Gonzalez G, Bournez L, Moraes RA, Marine D, Galon C, Vorimore F, Cochin M, Nougairède A, Hennechart-Collette C, Perelle S, Leparc-Goffart I, Durand GA, Grard G, Bénet T, Danjou N, Blanchin M, Lacour SA, Franck B, Chenut G, Mainguet C, Simon C, Brémont L, Zientara S, Moutailler S, Martin-Latil S, Dheilly NM, Beck C and Lecollinet S (2022) A One-Health Approach to Investigating an Outbreak of Alimentary Tick-Borne Encephalitis in a Non-endemic Area in France (Ain, Eastern France): A Longitudinal Serological Study in Livestock, Detection in Ticks, and the First Tick-Borne Encephalitis Virus Isolation and Molecular Characterisation. Front. Microbiol. 13:863725. doi: 10.3389/fmicb.2022.863725

frontiers | Frontiers in Microbiology

ORIGINAL RESEARCH
published: 27 April 2022
doi: 10.3389/fmicb.2022.893253

Comparative Antigenicity and Pathogenicity of Two Distinct Genotypes of Highly Pathogenic Avian Influenza Viruses (H5N8) From Wild Birds in China, 2020–2021

*Wenming Jiang[1†], Shuo Liu[1†], Xin Yin[1†], Zhixin Li[2], Zouran Lan[3], Luosong Xire[4], Zhongbing Wang[5], Yinqian Xie[6], Cheng Peng[1], Jinping Li[1], Guangyu Hou[1], Xiaohui Yu[1], Rongzhao Sun[1] and Hualei Liu[1]**

[1]China Animal Health and Epidemiology Center, Qingdao, China, [2]Ningxia Hui Autonomous Region Animal Disease Prevention and Control Center, Yinchuan, China, [3]Shandong Provincial Center for Animal Disease Control, Jinan, China, [4]Tibet Autonomous Region Veterinary Biological Pharmaceuticals Factory, Lhasa, China, [5]Shanxi Animal Disease Prevention and Control Center, Taiyuan, China, [6]Shaanxi Animal Disease Prevention and Control Center, Xi'an, China

OPEN ACCESS

Edited by:
Hongliang Chai,
Northeast Forestry University, China

Reviewed by:
Daxin Peng,
Yangzhou University, China
Chengjun Li,
Harbin Veterinary Research Institute (CAAS), China

***Correspondence:**
Hualei Liu
liuhualei@cahec.cn

[†]These authors have contributed equally to this work

Specialty section:
This article was submitted to Infectious Agents and Disease, a section of the journal Frontiers in Microbiology

Received: *10 March 2022*
Accepted: *07 April 2022*
Published: *27 April 2022*

Citation:
Jiang W, Liu S, Yin X, Li Z, Lan Z, Xire L, Wang Z, Xie Y, Peng C, Li J, Hou G, Yu X, Sun R and Liu H (2022) Comparative Antigenicity and Pathogenicity of Two Distinct Genotypes of Highly Pathogenic Avian Influenza Viruses (H5N8) From Wild Birds in China, 2020–2021. Front. Microbiol. 13:893253. doi: 10.3389/fmicb.2022.893253

To date, there have been three epidemic waves of H5N8 avian influenza worldwide. The current third epidemic wave began in October 2020 and has expanded to at least 46 countries. Active and passive surveillance were conducted to monitor H5N8 viruses from wild birds in China. Genetic analysis of 10 H5N8 viruses isolated from wild birds identified two different genotypes. Animal challenge experiments indicated that the H5N8 isolates are highly pathogenic in chickens, mildly pathogenic in ducks, while pathogenicity varied in BALB/c mice. Moreover, there were significant differences in antigenicity as compared to Re-11 vaccine strain and vaccinated chickens were not completely protected against challenge with the high dose of H5N8 virus. With the use of the new matched vaccine and increased poultry immune density, surveillance should be intensified to monitor the emergence of mutant strains and potential worldwide spread *via* wild birds.

Keywords: H5N8, highly pathogenic avian influenza, wild birds, genetic, pathogenicity, antigenicity

INTRODUCTION

The highly pathogenic H5N1 avian influenza virus (A/goose/Guangdong/1/1996(H5N1); clade 0) emerged from China in 1996 (Xu et al., 1999) and has spread throughout Eurasia and Africa possibly *via* migratory bird paths and have evolved into various genetic and antigenic clades and subclades since 2003 (WHO/OIE/FAO H5N1 Evolution Working Group, 2012; Li et al., 2020). These viruses have caused huge economic losses to the poultry industry and pose a substantial threat to human health. Since 2010, clade 2.3.4 H5 viruses have evolved and have gradually become dominant globally.

H5N8 avian influenza virus (AIV) clade 2.3.4 was first detected from a domestic duck in China, in 2010 (Wu et al., 2014; Li et al., 2016). To date, there have been three epidemic waves of H5N8 viruses worldwide. The first epidemic wave of H5N8 began in early 2014 in domestic and wild birds in South Korea and Japan and spread to Russia, several European

countries, and the United States by 2015 (Lee et al., 2014, 2015, 2016; Wu et al., 2014; Saito et al., 2015; The Global Consortium for H5N8 and Related Influenza Viruses, 2016). Additionally, an H5N2 virus containing gene segments related to H5N8 was identified in Canada in late 2014 (Pasick et al., 2015). Bayesian phylogenetic analysis revealed that H5Ny lineages were introduced into North America from Eurasia and into South Korea from Europe likely through migratory waterfowl (The Global Consortium for H5N8 and Related Influenza Viruses, 2016; Baek et al., 2021).

The second epidemic wave started in late 2016 and lasted until early 2017 (Beerens et al., 2017; Fusaro et al., 2017; Kim et al., 2017; Pohlmann et al., 2017; Selim et al., 2017; Wade et al., 2018; Yehia et al., 2018). H5N8 AIVs belonging to clade 2.3.4.4 reemerged in Europe, Asia, and Africa, suggesting that clade 2.3.4 H5 AIVs, particularly the H5N8 subtype, have a propensity for rapid global spread in migratory birds (Li et al., 2017; Napp et al., 2018).

The current third epidemic wave began in October 2020 and had the highest number of outbreaks. Outbreaks of H5N8 in poultry and wild birds have been reported in several European countries, including Denmark, Germany, Ireland, the Netherlands, and the United Kingdom (Lewis et al., 2021). Meanwhile, H5N8 outbreaks have been reported in poultry and wild birds in the Middle East (Israel) and East Asia (Japan, South Korea, and China), and have expanded to at least 46 countries (Isoda et al., 2020; Baek et al., 2021; Li et al., 2021; Sakuma et al., 2021). The third wave is more serious than the second in terms of the number of cases and extent of spread. To date, more than 20 million poultry have been slaughtered in South Korea and Japan due to infection with AIVs belonging to clade 2.3.4.4b, as determined by phylogenetic analysis (Twabela et al., 2020).

H5 viruses are known to infect humans. To date, 863 laboratory-confirmed human cases of H5N1 infection have been reported to the World Health Organization, which resulted in 456 (52.8%) deaths. Surprisingly, the first human cases of H5N8 infection were reported in Russia in December 2020 (Shi and Gao, 2021). Seven poultry farm workers who participated in a response operation to contain an outbreak of H5N8 tested positive, suggesting the potential for human infection.

From October 2020 to June 2021, several outbreaks of H5N8 in wild birds were reported in China. Therefore, the aim of the present study was to investigate the genetic, pathogenic, and antigenic characteristic of H5N8 by active and passive surveillance in China.

MATERIALS AND METHODS

Ethics Statements and Facility

The study protocol was approved by the Ethics Committee of China Animal Health and Epidemiology Center (Qingdao, China). All experiments with lethal H5 viruses were performed in a biosafety level 3 facility, and all animal experiments were performed in high-efficiency particulate air-filtered isolators at the China Animal Health and Epidemiology Center. All experimental animals were humanely handled in accordance with animal welfare.

Sampling

From September 2020 to June 2021, persistent surveillance of AIV infection in wild birds in China was conducted by collecting swab samples from the tracheae and cloacae of different species of wild birds and liver and lung tissue samples from dead birds. The swab samples were placed in transport medium (penicillin [2,000 IU/ml], streptomycin [2 mg/ml], amikacin [1,000 IU/ml], nystatin [2,000 IU/ml], and 10% glycerol [v/v] in sterile phosphate-buffered saline [pH 7.2]), transported to our laboratory at 4°C within 72 h, and stored at −70°C.

Virus Isolation and Identification

For virus isolation, the tissue samples were homogenated in transport medium followed by three freeze–thaw cycle. The homogenated tissue samples and swab samples were clarified by centrifugation at 10,000 × *g* for 5 min at 4°C, and the supernatants were inoculated into the allantoic cavity of 10-day-old specific-pathogen-free (SPF) chicken embryos, which were then incubated at 37°C for 4 days and checked daily. Dead embryos were removed and stored at 4°C. After the incubation period, live embryos were sacrificed at 4°C and the allantoic fluid was collected for testing with the hemagglutination assay.

RNA was extracted from the allantoic fluid of embryonated eggs with the QIAamp Viral RNA Mini Kit (Qiagen GmbH, Hilden, Germany) and the HA gene was amplified using the primer pair 5′-AGTGAARTGGAATATGGYMACTG-3′/5′-AACTGAGTGTTCATTTTGTCAAT-3′. Positive amplicons were confirmed by sequencing. H5 viruses grown in 10-day-old SPF embryonated eggs were purified by three rounds of the limited dilution method.

Subsequently, the complete genomes of purified H5 viruses were amplified using the PrimeScript One-step RT-PCR Kit (Takara Bio, Inc., Shiga, Japan) as described previously (Hoffmann et al., 2001; Jiang et al., 2017). The PCR products were purified with the QIAquick PCR purification kit (Qiagen GmbH) and sequenced using the ABI 3730xl DNA Analyzer (Applied Biosystems, Carlsbad, CA, United States). The nucleotide sequences were edited using the SeqMan module of the DNASTAR® Lasergene® package (DNASTAR, Inc., Madison, WI, United States). Phylogenetic analyses were conducted with Molecular Evolutionary Genetics Analysis (MEGA) software ver. 5.10[1] and aligned using the ClustalW algorithm.[2] Phylogenetic trees were constructed using the neighbor-joining method with a bootstrap value of 1,000; 96% sequence identity cutoffs were used to categorize the groups of each gene segment in the phylogenetic trees. The bioinformatics data were also analyzed based on the genome sequences.

Studies in Chickens

Two isolates with different genotypes (SX1/2020 and NX18/2020) were selected for pathogenicity studies in chickens, ducks, and mice.

[1]http://www.megasoftware.net
[2]http://www.clustal.org/

To assess the pathogenicity of the SX1/2020 and NX18/2020 viruses in chickens, the intravenous pathogenicity index (IVPI) was determined in accordance with the recommendations of the World Organization for Animal Health. Six-week-old SPF chickens ($n = 10$/group) were intravenously inoculated with 0.1 ml of a 1/10 dilution of bacteria-free fresh infectious allantoic fluid containing the challenge virus (HA titer > 16). 10 chickens were inoculated with 0.01 M phosphate-buffered saline as a control group. The chickens were then examined daily for 10 days for signs of disease or death. At each observation, each chicken was scored based on a 4-point scale (0, normal, 1, sick; 2, severely sick; or 3, dead). The IVPI was calculated as the mean score of each chicken at each observation point over the 10-day period.

10 additional chickens were inoculated intranasally with 10^6 50% egg infective dose (EID_{50}) of each virus in a 0.1-mL volume. At 3 days post-infection (dpi), the chickens were subjected to euthanasia and necropsy. The brain, heart, liver, spleen, lungs, intestine, and kidneys were collected for detection of viral RNA. Tracheal and cloacal swabs were collected from all birds for detection of virus shedding.

Studies in Ducks

To assess the pathogenicity of the SX1/2020 and NX18/2020 viruses in ducks, 3-week-old SPF ducks ($n = 10$/group) were intranasally inoculated with 0.1 ml of allantoic fluid containing 10^6 EID_{50} of the tested virus. The ducks were then observed for signs of disease or death until 14 dpi. At necropsy (3 dpi), the brain, heart, liver, spleen, lungs, intestine, and kidneys of five ducks were collected for detection of viral RNA. Tracheal and cloacal swabs were collected from the remaining birds at 3 dpi for detection of virus shedding. At the end of the experiment, the animals were subjected to blood collection for assessment of seroconversion, followed by euthanasia.

Studies in Mice

To assess the pathogenicity of the SX1/2020 and NX18/2020 viruses in a mammalian host, 6-week-old female Balb/c mice (Charles River Laboratories, Beijing, China; $n = 14$/group) were lightly anesthetized with CO_2 and inoculated intranasally with 10^6 EID_{50} of each virus in a volume of 50 µl. Nine of the 14 mice were euthanized at 3, 4, and 5 dpi for virus titration of the nasal turbinate, lungs, spleen, brain, and liver. The remaining five mice were monitored daily for weight loss and mortality until 14 dpi. At the endpoints of the experiment, the mice were anesthetized and sacrificed humanely.

Antigenic Analyses

Antigenic analyses were performed using cross-hemagglutination inhibition (HI) tests with polyclonal antisera against the indicated viruses. To generate the antisera, 21-day-old SPF chickens were injected with 1 ml of oil emulsion-inactivated vaccines derived from the selected viruses and sera samples were collected at 21 dpi. Antibodies to HI were tested with 0.5% (v/v) chicken erythrocytes.

Generation of Recombinant Viruses

A recombinant virus (rSD18) was generated with a reverse-genetics method using eight bidirectional pHW2000 plasmids. Human embryonic kidney 293 T cells were co-transfected with 0.8 µg of each of the six bidirectional pHW plasmids (corresponding to PB2, PB1, PA, NP, M, and NS) as well as the HA and NA genes of the SD18/2020 virus. The pHW plasmids expressing six internal genes were all derived from the A/PR/8/34(H1N1) virus with Lipofectamine 3,000 transfection reagent (Life Technologies, Carlsbad, CA, United States). The HA sequence of the SD18/2020 virus was attenuated from PLREKRRKRG to PLRETRG by deletion of the multibasic amino acid motif at the HA cleavage site. After 24 h, the cells were treated with L-(tosylamido-2-phenyl) ethyl chloromethyl ketone-treated trypsin (Sigma–Aldrich Corporation, St. Louis, MO, United States) at a final concentration of 2 µg/ml. After 72 h, the supernatants of transfected cells were collected and used to inoculate 10-day-old SPF chicken embryos, which were then incubated at 37°C for 72 h. Vaccine batches were produced in SPF chicken embryos after five egg passages of recombinants.

Vaccination and Challenge Study in Chickens

Two oil-adjuvant whole-virus inactivated vaccines were prepared from Re-11 [the HA and NA gene donor (A/duck/Guizhou/S4184/2017, H5N6), HA gene clade (clade 2.3.4.4 h)] (Zeng et al., 2020) and rSD18 (the inactivated virus mixed with mineral oil adjuvant at 1:2 (v/v) and then emulsified) by Qingdao Yebio Bioengineering Co., Ltd. (Qingdao, China). Groups of three-week-old SPF chickens were vaccinated with the Re-11 and rSD18 vaccines. 3 weeks later, the chickens were intranasally challenged with 10^6 EID_{50} of the tested viruses. Tracheal and cloacal swabs were collected from the chickens for virus titration at 3 and 5 dpi, and clinical signs were monitored daily until 10 dpi. In addition, two groups of 10 chickens were used as challenge controls. At the end of the experiment, the animals were anesthetized and sacrificed humanely.

RESULTS

Molecular and Phylogenetic Analysis

During September 2020 to June 2021, 10 viruses were isolated from eight kinds of wild birds in Shanxi, Ningxia, Shandong, Tibet, and Shaanxi provinces (**Figure 1**). The information of the strains is shown in **Supplementary Table S1**.

Phylogenetic analysis of HA genes showed that all 10 viruses isolated from wild birds in this study belonged to clade 2.3.4.4b during September 2020 to June 2021 (**Figure 2**). Furthermore, on the basis of their genomic similarity and phylogenetic analysis of genome sequences (**Supplementary Figures S1–S7**), the 10 H5N8 HPAIVs in this study were divided into two genotypes: seven strains belong to the genotype 1 and three strains formed a different genotype 2.

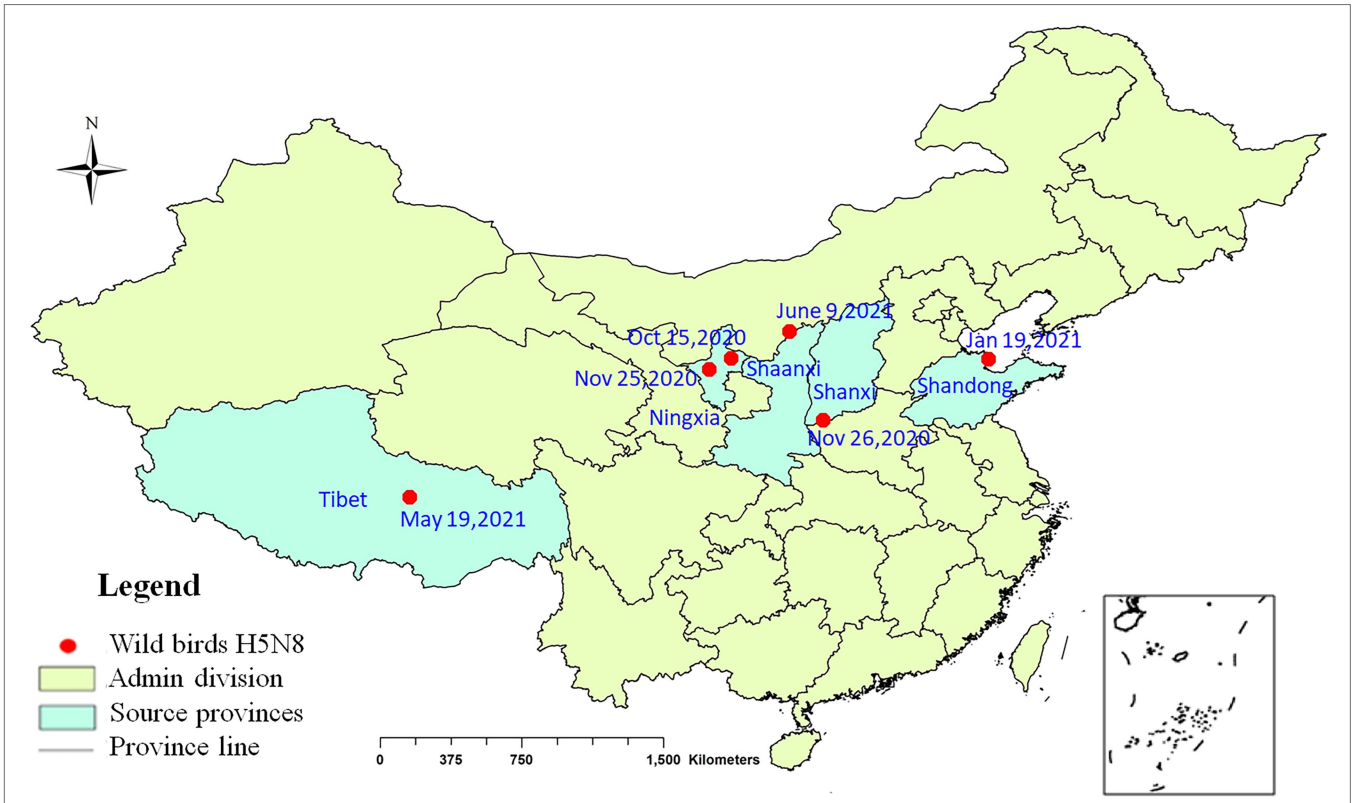

FIGURE 1 | Geographical distribution of H5N8 avian influenza viruses detected in wild birds in China, 2020–2021. Red dot indicates sampling sites. Dates refer to the day of initial H5N8 virus isolated in wild birds in each site.

The HA genes of clade 2.3.4.4b viruses contained a series of basic amino acids (PLREKRRKR/G) at the cleavage sites, a signature of highly pathogenic avian influenza virus The receptor binding sites of the viral HA genes possessed the residues Q226 and G228 (H3 numbering), suggesting preferential binding to avian-like receptors (Tharakaraman et al., 2013). However, the receptor binding site mutations A137, N158, A160, N186, I192, Q222, and R227 (H3 numbering) could increase binding to SAα-2,6Gal human-like receptors (Yang et al., 2007; Gao et al., 2009; Wang et al., 2010; Guo et al., 2017).

Bioinformatics analysis identified many mutations that would increase virulence in mice, such as R114 and I115 (H3 numbering) of the HA gene (Wessels et al., 2018); D30, M43, and A215 of the M1 gene (Fan et al., 2009; Nao et al., 2015); S42, E55, E66 (SX1/2020, Y173/2020, and Y175/2020), M106, and F138 (except SX1/2020, Y173/2020, and Y175/2020) of the NS1 gene (Jiao et al., 2008; Ayllon et al., 2014; Li et al., 2018); the NS1 C-terminal ESEV motif of the PDZ domain at position aa227–230 (Jackson et al., 2008; Soubies et al., 2010; Zielecki et al., 2010); combination of V89, D309, K339, G477, V495, E627, and T676 of the PB2 gene (Li et al., 2009); V3 (except NQ1/2021) and G622 of the PB1 gene (Feng et al., 2016; Elgendy et al., 2017); and D383 of the PA gene (Song et al., 2015; Suttie et al., 2019).

Pathogenicity in Chickens

To assess pathogenicity in chickens, 6-week-old SPF chickens were inoculated with viruses to determine the IVPI. Both SX1/2020 and NX18/2020 viruses caused 100% mortality within 1 day, conferring an IVPI of 3.00 and indicating that both were highly pathogenic in chickens (**Table 1**).

All chickens infected intranasally with 10^6 EID_{50} of the SX1/2020 and NX18/2020 viruses died within 5 dpi. Both viruses were detected in the heart, liver, spleen, lungs, kidneys, intestine, and brain samples collected during necropsy of inoculated chickens at 3 dpi. Virus shedding was detected from the tracheal and cloacal swabs of all dead chickens inoculated with the SX1/2020 and NX18/2020 viruses at 3 dpi (**Table 1**).

Pathogenicity in Ducks

To assess pathogenicity in ducks, 3-week-old SPF ducks were inoculated with the SX1/2020 and NX18/2020 viruses, which caused 20%—40% mortality within 14 dpi, indicating that both were moderately pathogenic in ducks.

To investigate the replication of these viruses in ducks, five ducks from each group were euthanized at 3 dpi to assess the viral load in the heart, liver, spleen, lungs, kidneys, intestine, and brain. The remaining five ducks in each group were assessed for seroconversion (**Table 1**).

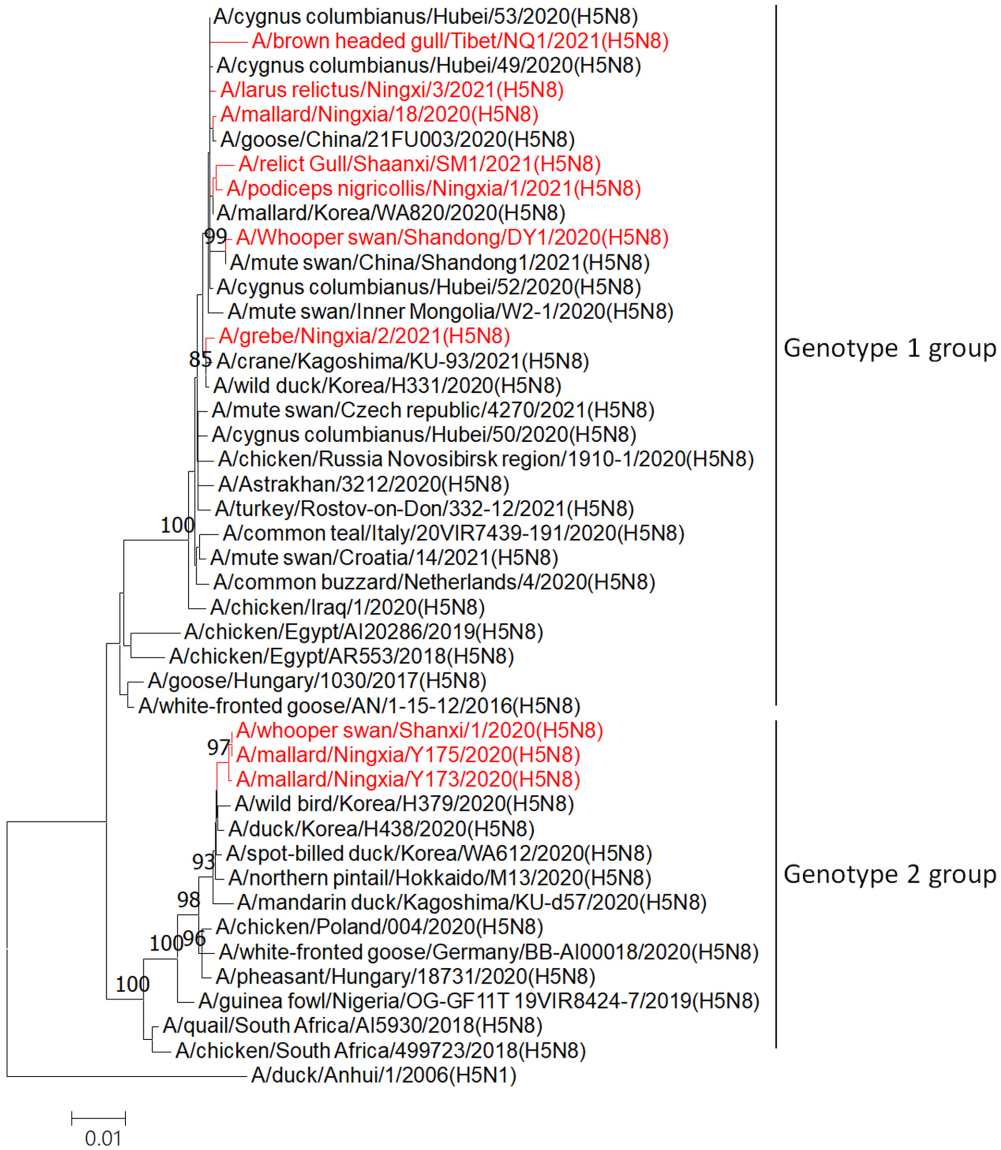

FIGURE 2 | Phylogenetic analyses of the HA genes of H5N8 highly pathogenic AIVs. Phylogenetic trees were constructed with MEGA (ver. 5.10) software using the neighbor-joining method. Bootstrap analysis was performed with 1,000 replications. The viruses sequenced in this study are shown in red in the phylogenetic trees. Scale bars indicate nucleotide substitutions per site.

Both viruses were detected in the heart, liver, spleen, lungs, kidneys, intestine, and brain samples collected during necropsy of inoculated ducks at 3 dpi. All ducks inoculated with the SX1/2020 and NX18/2020 viruses exhibited virus shedding and seroconversion (**Table 1**). The results indicated that both viruses were moderately pathogenic in ducks.

Replication and Pathogenicity in Mice

To assess the replication and virulence of the SX1/2020 and NX18/2020 viruses in a mammalian host, 6-weeks-old Balb/c mice ($n = 14$/group) were inoculated intranasally with 10^6 EID_{50} of each virus. On 3, 4, and 5 dpi, three mice from each group were euthanized to measure the viral load in nasal turbinate, lungs, spleen, brain, and liver, while the other five were observed for body weight changes and death until 14 dpi.

At 3, 4, and 5 dpi, mice infected with the NX18/2020 virus had high titers in the nasal turbinate, lungs, spleen, and brain, but not the liver (**Table 2**). The mice exhibited progressive signs of infection, such as inactivity, ruffled fur, lack of appetite, hunched backs, and labored breathing. The body weights of mock-infected mice gradually increased from 1 to 14 dpi. In contrast, the infected mice experienced dramatic weight loss of more than 25% and all died within 8 dpi (**Figure 3**). These results suggest that the NX18/2020 virus not only effectively replicated in the nasal turbinate, lung, spleen, and brain without preadaptation, but was also lethal.

TABLE 1 | Replication and virulence of 2.3.4.4b H5N8 viruses in chickens and ducks.

Avian species	Viruses	IVPI	Virus shedding on day 3 post inoculation: positive/total		Virus replication in organs on day 3 p.i.: positive/total					Death/Total	Sero-conversion: positive/total
			Pharynx	Cloacae	Lung	Intestine	Liver	Spleen	Kidney	Brain		
Chicken	SX1/2020	3.00	10/10	10/10	10/10	10/10	10/10	10/10	10/10	10/10	10/10	/
	NX18/2020	3.00	10/10	10/10	10/10	10/10	10/10	10/10	10/10	10/10	10/10	/
Duck	SX1/2020	/	10/10	10/10	5/5	5/5	4/5	3/5	5/5	3/5	1/5	4/4
	NX18/2020	/	10/10	10/10	5/5	5/5	4/5	4/5	5/5	4/5	2/5	3/3

The intravenous pathogenicity index (IVPI) test was carried out according to the OIE (World Organisation for Animal Health) manual. In brief, ten 6-week-old SPF chickens were intravenously inoculated with 0.1 ml of a 1/10 dilution of the fresh infectious allantoic fluid (HA titer > 16) and ten chickens were inoculated with 0.01 M PBS as a control group. All of the chickens were examined daily for 10 days. At each observation, each chicken was scored based on the condition: 0 (normal), 1 (sick), 2 (severely sick), and 3 (dead). IVPI was the mean score per chicken per observation over the ten-day period. Groups of 15 three-week-old specific-pathogen-free ducks were inoculated i.n. with 10^6 EID_{50} of each virus in a 0.1-ml volume. Pharyngeal and cloacal swabs were collected from all birds on Day 3 p.i., and then five birds in each group were euthanized, and their organs were detected for H5N8 viruses by RT-PCR. The remaining ten ducks in each group were observed for two weeks.

TABLE 2 | Replication level of SX1/2020 and NX18/2020 strains in organs of experimentally infected Balb/c mice.

Strains	Virus titers in organs of experimentally infected mice (log_{10} EID_{50}/g)[a]			
	Tissue	3 day	4 day	5 day
SX1/2020	Nasal turbinate	3.86 ± 0.32	3.83 ± 0.28	4.12 ± 0.45
	Lung	3.67 ± 0.36	3.82 ± 0.37	4.03 ± 0.42
	Liver	–	–	–
	Spleen	–	–	–
	Brain	–	–	–
NX18/2020	Nasal turbinate	4.45 ± 0.33	4.78 ± 0.32	5.32 ± 0.46
	Lung	4.27 ± 0.38	4.56 ± 0.38	5.18 ± 0.45
	Liver	–	–	–
	Spleen	3.07 ± 0.30	3.16 ± 0.31	3.46 ± 0.33
	Brain	2.23 ± 0.22	2.92 ± 0.26	3.26 ± 0.35

[a]*Groups of fourteen female Balb/c mice were intranasally inoculated with a 10^6 EID_{50} of each virus. On 3, 4, and 5 dpi, three mice of each group were euthanized after anesthetization, and the nasal turbinates, brains, lungs, livers, and spleens of the mice of each group were pooled separately and homogenized in L-15 medium containing antibiotics to make a 10% w/v tissue homogenate for virus titration in embryonated chicken eggs. Values are mean ± SD. –, virus titer lower than the detection limit.*

In contrast, the SX1/2020 virus replicated poorly and was only detected in the nasal turbinate and lungs of mice and was not fatal (**Figure 3**), indicating that H5N8 viruses circulating in nature have different pathotypes in mice.

Antigenic Analyses

Since December 2018, the inactivated reassortant vaccine Re-11 has been extensively used to control the spread of clade 2.3.4.4 viruses in China. To determine whether antigenic drift had occurred, antigenicity of the H5N8 viruses was evaluated with the cross-HI assay.

The results showed that the H5N8 isolates weakly reacted with Re-11 antisera (**Supplementary Table S2**). The cross-reactive HI titers of the Re-11 antiserum against the H5N8 isolates were 32- to 128-fold lower than that against the homologous Re-11 antigen (9 log2). In contrast, the cross-reactive HI titers of the antiserum against the Re-11 antigen from the H5N8 viruses were also 32- to 128-fold lower than that against the homologous H5N8 isolates. The amino acid homology between these isolates and Re-11 was 91.2–91.7%. These results indicate that the H5N8 viruses exhibited severe antigenic drift as compared to the more established H5 vaccine strains.

Protective Efficacy of the Vaccines

To determine whether these isolates reduce the protective effect of commercially available vaccines *in vivo*, the protection efficacies of the inactivated reassortant H5N1/PR8 vaccine Re-11 and rSD18 vaccine were evaluated.

During the 10-day observation period, birds vaccinated with the Re-11 vaccine displayed no clinical signs and all survived. In addition, the tracheal and cloacal swabs from only 10.0–20.0% of the experimental chickens exhibited virus shedding at 3 and 5 dpi. The rSD18-vaccinated birds all survived and displayed no clinical signs of infection. In addition, no virus shedding

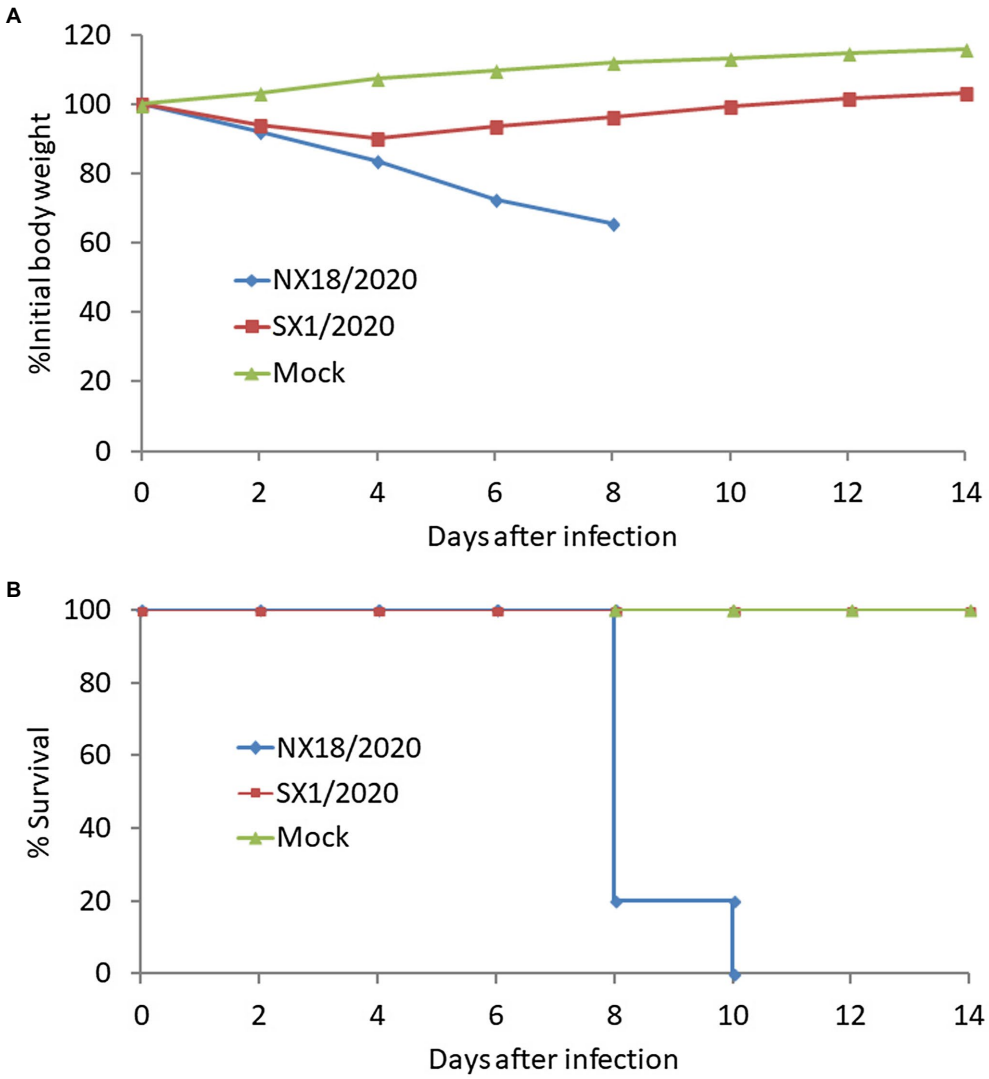

FIGURE 3 | Virulence of the H5N8 viruses in Balb/c mice intranasally inoculated with a 10^6 EID_{50} of virus. Body weight changes **(A)** and mortality **(B)** of Balb/c mice were monitored daily for 14 days.

was detected in tracheal or cloacal swabs from any of the experimental chickens at 3 and 5 dpi (**Table 3**). These results suggest that the Re-11 vaccine did not provide complete protection against the high dose of antigenically distinct highly pathogenic H5N8 AIV.

DISCUSSION

Since 2014, there have been three global waves of the H5N8 pandemic in wild birds and poultry. The spread of H5N8 viruses in many countries in Asia, Europe, Africa, and North America has resulted in numerous outbreaks in domestic poultry (Lee et al., 2014, 2015, 2016; Wu et al., 2014; Saito et al., 2015; The Global Consortium for H5N8 and Related Influenza Viruses, 2016). During the first and second epidemic waves, H5N8 strains were occasionally detected from wild birds, ducks, and geese in China, although the damage caused by these viruses was limited (Cui et al., 2020). However, the current third epidemic wave of H5N8 viruses has spread with a vengeance, resulting in heavy losses to the poultry industry worldwide.

In this study, positive and passive surveillance was conducted to monitor the invasion and spread of H5N8 viruses in China. The H5N8 viruses were first detected in two healthy mallards in Ningxia Province in October 2020 and dead whooper swans found in Shanxi Province in November 2020. Afterward, these viruses have been detected in seven other varieties of wild birds in several provinces. Genetic analysis revealed that two distinct genotypes of H5N8 viruses were circulating in wild birds in China, with wide spread of genotype 1. The results of the present study are consistent with those of previous reports (Baek et al., 2021; Cui et al., 2021). Interestingly,

TABLE 3 | Protection efficacy of H5 Re-11 vaccine against SX1/2020 and NX18/2020 in chickens[a].

Group	Vaccine	HI titer ± SD, log2		Challenge test results, by swab type, no. positive birds/no.tested (mean titer ± SD)[b]				No.surviving
				3 dpi		5 dpi		
		Re-11	Isolate	Tracheal	Cloacal	Tracheal	Cloacal	birds/total no.
SX1/2020	Re-11	10.6 ± 0.42	5.2 ± 0.25	1/10 (3.52)	1/10 (3.62)	1/10 (3.46)	1/10 (3.85)	10/10
	rSD18	5.6 ± 0.30	10.3 ± 0.37	0/10	0/10	0/10	0/10	10/10
	Mock	ND	ND	4/4 (3.98 ± 1.03)	4/4 (4.12 ± 1.35)	ND	ND	0/10
NX18/2020	Re-11	10.6 ± 0.38	5.2 ± 0.22	2/10 (3.65 ± 1.06)	2/10 (3.78 ± 1.14)	2/10 (3.58 ± 1.06)	2/10 (3.87 ± 1.25)	10/10
	rSD18	5.1 ± 0.32	10.2 ± 0.39	0/10	0/10	0/10	0/10	10/10
	Mock	ND	ND	4/4 (3.87 ± 1.15)	4/4 (4.25 ± 1.35)	ND	ND	0/10

[a]*Chickens were immunized with the Re-11 vaccine, and HI antibody titers were determined on day 21 post-vaccination. HI, Hemagglutination inhibition assay; dpi, days post-infection; ND, not done.*

[b]*Chickens were challenged with 10^6 50% egg infectious dose (EID_{50}) of SX1/2020 or NX18/2020 virus; virus titers are expressed as log10 EID_{50}/0.1 ml.*

virusesw isolated from different individuals at the same site may be of different genotypes, which illustrates the complexity of viruses in China.

Animal studies have shown that H5N8 viruses are highly pathogenic in chickens, but cause relatively mild disease in ducks. In previous studies, some H5N8 strains could kill nearly 100 percent of the challenged ducks (Dinev et al., 2020; Koethe et al., 2020). The pathogenicity of the virus may depend on the strain and duck species. In practice, even with the adoption of biosecurity measures, the production of ducks has been poorer than that of chickens and other pathogens, such as *Escherichia coli* and *Riemerella anatipestiferis*, which cause higher mortality rates in ducks. Furthermore, there is a clear antigenic difference between H5N8 viruses and the H5N1 vaccine strain Re-11 used in China against 2.3.4.4 viruses, as vaccinated chickens are not completely protected against challenge with the high dose of H5N8 viruses. The results were inconsistent with those of Cui et al., which may be related to bird species and immune background where the layer chickens and ducks in the field were immunized with two or more doses of the H5/H7 AI inactivated vaccine (Cui et al., 2021). As we known, under field conditions, birds unlikely to get sustained high levels of antibody and would more likely be susceptible to infection and virus shedding. Normally, when HI titer to the challenge virus of H5 subtype is above 4 log2, the vaccinated chickens were completely protected without virus shedding. However, in this study, vaccinated chickens with HI antibody titers of 5.2 log2 still shed viruses after challenge. It is highly likely that the reduced immune protection is caused by the high dose of challenge virus. The 10^6EID_{50} dose of the challenged H5N8 virus in this study is tenfold higher than the normal dose (10^5EID_{50}).

Animal studies have shown that the virulence of H5N8 viruses in mice varies among strains, as a highly pathogenic virus was lethal in mice without preadaptation and effectively replicated in several organs, while replication of a less pathogenic virus was limited in some organs. The H5N8 virus isolated in 2013 showed similar results (Wu et al., 2014).

In 2004 and 2005, an epidemic of the H5N1 virus occurred in China (Chen, 2009). Thus, the Chinese government adopted comprehensive prevention and control measures, including surveillance, culling, and mass vaccination, which achieved great success. For example, replacement of the Re-4 vaccine with the Re-7 vaccine in 2014 completely eliminated infection of a clade 7.2 virus (Liu et al., 2016). In 2017, the use of the H7N9-Re1 vaccine successfully controlled H7N9 infection in humans and highly pathogenic viruses in chickens (Shi et al., 2018; Jiang et al., 2019). However, vaccines were less effective in controlling other clades of the H5 virus, such as clade 2.3.4, which is found in chickens and especially waterfowl, while clade 7.2 and H7N9 viruses are found mainly in chickens and less often in waterfowl. In China, the number of waterfowl is huge and many are raised in open environments in contact with wild birds. Clade 2.3.4.4b viruses circulate in wild birds and spread easily to waterfowl and, thus, are more difficult to control. In addition, the immune density of waterfowl is much lower than that of chickens, which causes waterfowl to

become more susceptible to infection and further spread of the virus. Due to continuous mutation and reassortment, antigenic drift of avian influenza viruses occurs frequently. Timely updating the vaccine seeds could maintain the effectiveness of the vaccine in control and elimination of the target avian influenza virus. Although the Re-11 vaccine strain was updated by antigenically matched Re-14 vaccine to prevent and control clade 2.3.4.4b viruses since 2022, many challenges remain. With the use of new matched vaccines and increased poultry immune density, surveillance should be strengthened to early detect the emergence of mutant strains and worldwide spread *via* wild birds.

DATA AVAILABILITY STATEMENT

The datasets presented in this study can be found in online repositories. The names of the repository/repositories and accession number(s) can be found in the article/**Supplementary Material**.

ETHICS STATEMENT

The animal study was reviewed and approved by Ethics Committee of China Animal Health and Epidemiology Center.

AUTHOR CONTRIBUTIONS

WJ and HL: conceptualization and methodology. ZhL, ZoL, LX, ZW, and YX: sample collection. SL, XY, and CP: genetic analysis. WJ, HL, ZhL, ZoL, LX, ZW, and YX: investigation. XnY, XaY, and RS: data curation. WJ: writing—original draft preparation. HL: writing—review and editing. GH and JL: animal experiment. All authors contributed to the article and approved the submitted version.

FUNDING

This work was supported by National Key Research and Development Program (2021YFD1800201), Natural Science Foundation of Ningxia Hui Autonomous Region (2022AAC02071), and Shandong Provincial Key Research and Development Program (2022CXGC010606).

SUPPLEMENTARY MATERIAL

The Supplementary Material for this article can be found online at: https://www.frontiersin.org/articles/10.3389/fmicb.2022.893253/full#supplementary-material

REFERENCES

Ayllon, J., Domingues, P., Rajsbaum, R., Miorin, L., Schmolke, M., Hale, B. G., et al. (2014). A single amino acid substitution in the novel H7N9 influenza A virus NS1 protein increases CPSF30 binding and virulence. *J. Virol.* 88, 12146–12151. doi: 10.1128/JVI.01567-14

Baek, Y. G., Lee, Y. N., Lee, D. H., Shin, J. I., Lee, J. H., Chung, D. H., et al. (2021). Multiple Reassortants of H5N8 Clade 2.3.4.4b Highly Pathogenic Avian Influenza Viruses Detected in South Korea during the Winter of 2020-2021. *Viruses* 13:490. doi: 10.3390/v13030490

Beerens, N., Heutink, R., Bergervoet, S. A., Harders, F., Bossers, A., and Koch, G. (2017). Multiple Reassorted viruses as cause of highly pathogenic avian Influenza A(H5N8) virus epidemic, the Netherlands, 2016. *Emerg. Infect. Dis.* 23, 1974–1981. doi: 10.3201/eid2312.171062

Chen, H. (2009). H5N1 avian influenza in China. Science in China. *Series C, Life sci.* 52, 419–427. doi: 10.1007/s11427-009-0068-6

Cui, Y., Li, Y., Li, M., Zhao, L., Wang, D., Tian, J., et al. (2020). Evolution and extensive reassortment of H5 influenza viruses isolated from wild birds in China over the past decade. *Emerg. Micr. Infec.* 9, 1793–1803. doi: 10.1080/22221751.2020.1797542

Cui, P., Zeng, X., Li, X., Li, Y., Shi, J., Zhao, C., et al. (2021). Genetic and biological characteristics of the globally circulating H5N8 avian influenza viruses and the protective efficacy offered by the poultry vaccine currently used in china. *Sci. China Life Sci.* 65, 795–808. doi: 10.1007/s11427-021-2025-y

Dinev, I., Zarkov, I., Goujgoulova, G. V., Stoimenov, G. M., Georgiev, G., and Kanakov, D. (2020). Pathologic evaluation of Influenza A H5N8 infection outbreaks in mule ducks in Bulgaria. *Avian Dis.* 64, 203–209. doi: 10.1637/0005-2086-64.2.203

Elgendy, E. M., Arai, Y., Kawashita, N., Daidoji, T., Takagi, T., Ibrahim, M. S., et al. (2017). Identification of polymerase gene mutations that affect viral replication in H5N1 influenza viruses isolated from pigeons. *J. Gen. Virol.* 98, 6–17. doi: 10.1099/jgv.0.000674

Fan, S., Deng, G., Song, J., Tian, G., Suo, Y., Jiang, Y., et al. (2009). Two amino acid residues in the matrix protein M1 contribute to the virulence difference of H5N1 avian influenza viruses in mice. *Virology* 384, 28–32. doi: 10.1016/j.virol.2008.11.044

Feng, X., Wang, Z., Shi, J., Deng, G., Kong, H., Tao, S., et al. (2016). Glycine at position 622 in PB1 contributes to the virulence of H5N1 avian Influenza virus in mice. *J. Virol.* 90, 1872–1879. doi: 10.1128/JVI.02387-15

Fusaro, A., Monne, I., Mulatti, P., Zecchin, B., Bonfanti, L., Ormelli, S., et al. (2017). Genetic diversity of highly pathogenic avian Influenza A(H5N8/H5N5) viruses in Italy, 2016-17. *Emerg. Infect. Dis.* 23, 1543–1547. doi: 10.3201/eid2309.170539

Gao, Y., Zhang, Y., Shinya, K., Deng, G., Jiang, Y., Li, Z., et al. (2009). Identification of amino acids in HA and PB2 critical for the transmission of H5N1 avian influenza viruses in a mammalian host. *PLoS Pathog.* 5:e1000709. doi: 10.1371/journal.ppat.1000709

Guo, H., de Vries, E., McBride, R., Dekkers, J., Peng, W., Bouwman, K. M., et al. (2017). Highly pathogenic Influenza A(H5Nx) viruses with altered H5 receptor-binding specificity. *Emerg. Infect. Dis.* 23, 220–231. doi: 10.3201/eid2302.161072

Hoffmann, E., Stech, J., Guan, Y., Webster, R. G., and Perez, D. R. (2001). Universal primer set for the full-length amplification of all influenza A viruses. *Arch. Virol.* 146, 2275–2289. doi: 10.1007/s007050170002

Isoda, N., Twabela, A. T., Bazarragchaa, E., Ogasawara, K., Hayashi, H., Wang, Z. J., et al. (2020). Re-invasion of H5N8 high pathogenicity avian Influenza virus clade 2.3.4.4b in Hokkaido, Japan, 2020. *Viruses* 12:439. doi: 10.3390/v12121439

Jackson, D., Hossain, M. J., Hickman, D., Perez, D. R., and Lamb, R. A. (2008). A new influenza virus virulence determinant: the NS1 protein four C-terminal residues modulate pathogenicity. *Proc. Natl. Acad. Sci. U. S. A.* 105, 4381–4386. doi: 10.1073/pnas.0800482105

Jiang, W., Hou, G., Li, J., Peng, C., Wang, S., Liu, S., et al. (2019). Prevalence of H7N9 subtype avian influenza viruses in poultry in China, 2013-2018. *Transbound. Emerg. Dis.* 66, 1758–1761. doi: 10.1111/tbed.13183

Jiang, W., Wang, S., Zhang, C., Li, J., Hou, G., Peng, C., et al. (2017). Characterization of H5N1 highly pathogenic mink influenza viruses in eastern China. *Vet. Microbiol.* 201, 225–230. doi: 10.1016/j.vetmic.2017.01.028

Jiao, P., Tian, G., Li, Y., Deng, G., Jiang, Y., Liu, C., et al. (2008). A single-amino-acid substitution in the NS1 protein changes the pathogenicity of H5N1 avian influenza viruses in mice. *J. Virol.* 82, 1146–1154. doi: 10.1128/JVI.01698-07

Kim, Y. I., Park, S. J., Kwon, H. I., Kim, E. H., Si, Y. J., Jeong, J. H., et al. (2017). Genetic and phylogenetic characterizations of a novel genotype of highly pathogenic avian influenza (HPAI) H5N8 viruses in 2016/2017 in South Korea. *Infection, genetics and Evolution* 53, 56–67. doi: 10.1016/j.meegid.2017.05.001

Koethe, S., Ulrich, L., Ulrich, R., Amler, S., Graaf, A., Harder, T. C., et al. (2020). Modulation of lethal HPAIV H5N8 clade 2.3.4.4B infection in AIV pre-exposed mallards. *Emerg. Micr.Iinfec.* 9, 180–193. doi: 10.1080/22221751.2020.1713706

Lee, D. H., Bahl, J., Torchetti, M. K., Killian, M. L., Ip, H. S., DeLiberto, T. J., et al. (2016). Highly pathogenic avian Influenza viruses and generation of novel Reassortants, United States, 2014-2015. *Emerg. Infect. Dis.* 22, 1283–1285. doi: 10.3201/eid2207.160048

Lee, Y. J., Kang, H. M., Lee, E. K., Song, B. M., Jeong, J., Kwon, Y. K., et al. (2014). Novel reassortant influenza A(H5N8) viruses, South Korea, 2014. *Emerg. Infect. Dis.* 20, 1087–1089. doi: 10.3201/eid2006.140233

Lee, D. H., Torchetti, M. K., Winker, K., Ip, H. S., Song, C. S., and Swayne, D. E. (2015). Intercontinental spread of Asian-origin H5N8 to North America through Beringia by migratory birds. *J. Virol.* 89, 6521–6524. doi: 10.1128/JVI.00728-15

Lewis, N. S., Banyard, A. C., Whittard, E., Karibayev, T., Al Kafagi, T., Chvala, I., et al. (2021). Emergence and spread of novel H5N8, H5N5 and H5N1 clade 2.3.4.4 highly pathogenic avian influenza in 2020. *Emerg. Micr.Iinfec.* 10, 148–151. doi: 10.1080/22221751.2021.1872355

Li, J., Gu, M., Liu, D., Liu, B., Jiang, K., Zhong, L., et al. (2016). Phylogenetic and biological characterization of three K1203 (H5N8)-like avian influenza A virus reassortants in China in 2014. *Arch. Virol.* 161, 289–302. doi: 10.1007/s00705-015-2661-2

Li, J., Ishaq, M., Prudence, M., Xi, X., Hu, T., Liu, Q., et al. (2009). Single mutation at the amino acid position 627 of PB2 that leads to increased virulence of an H5N1 avian influenza virus during adaptation in mice can be compensated by multiple mutations at other sites of PB2. *Virus Res.* 144, 123–129. doi: 10.1016/j.virusres.2009.04.008

Li, Y., Li, M., Li, Y., Tian, J., Bai, X., Yang, C., et al. (2020). Outbreaks of highly pathogenic avian Influenza (H5N6) virus subclade 2.3.4.4h in swans, Xinjiang, Western China, 2020. *Emerg. Infect. Dis.* 26, 2956–2960. doi: 10.3201/eid2612.201201

Li, M., Liu, H., Bi, Y., Sun, J., Wong, G., Liu, D., et al. (2017). Highly pathogenic avian Influenza A(H5N8) virus in wild migratory birds, Qinghai Lake, China. *Emerg. Infect. Dis.* 23, 637–641. doi: 10.3201/eid2304.161866

Li, X., Lv, X., Li, Y., Peng, P., Zhou, R., Qin, S., et al. (2021). Highly pathogenic avian Influenza A(H5N8) virus in swans, China, 2020. *Emerg. Infect. Dis.* 27, 1732–1734. doi: 10.3201/eid2706.204727

Li, J., Zhang, K., Chen, Q., Zhang, X., Sun, Y., Bi, Y., et al. (2018). Three amino acid substitutions in the NS1 protein change the virus replication of H5N1 influenza virus in human cells. *Virology* 519, 64–73. doi: 10.1016/j.virol.2018.04.004

Liu, L., Zeng, X., Chen, P., Deng, G., Li, Y., Shi, J., et al. (2016). Characterization of clade 7.2 H5 avian Influenza viruses That continue to circulate in chickens in China. *J. Virol.* 90, 9797–9805. doi: 10.1128/JVI.00855-16

The Global Consortium for H5N8 and Related Influenza Viruses (2016). Role for migratory wild birds in the global spread of avian influenza H5N8. *Science* 354, 213–217. doi: 10.1126/science.aaf8852

WHO/OIE/FAO H5N1 Evolution Working Group (2012). Continued evolution of highly pathogenic avian influenza A (H5N1): updated nomenclature. *Influenza Other Respir. Viruses* 6, 1–5. doi: 10.1111/j.1750-2659.2011.00298.x

Nao, N., Kajihara, M., Manzoor, R., Maruyama, J., Yoshida, R., Muramatsu, M., et al. (2015). A single amino acid in the M1 protein responsible for the different pathogenic potentials of H5N1 highly pathogenic avian Influenza virus strains. *PLoS One* 10:e0137989. doi: 10.1371/journal.pone.0137989

Napp, S., Majo, N., Sanchez-Gonzalez, R., and Vergara-Alert, J. (2018). Emergence and spread of highly pathogenic avian influenza A(H5N8) in Europe in 2016-2017. *Transbound. Emerg. Dis.* 65, 1217–1226. doi: 10.1111/tbed.12861

Pasick, J., Berhane, Y., Joseph, T., Bowes, V., Hisanaga, T., Handel, K., et al. (2015). Reassortant highly pathogenic influenza A H5N2 virus containing gene segments related to Eurasian H5N8 in British Columbia, Canada, 2014. *Sci. Rep.* 5:9484. doi: 10.1038/srep09484

Pohlmann, A., Starick, E., Harder, T., Grund, C., Hoper, D., Globig, A., et al. (2017). Outbreaks among wild birds and domestic poultry caused by Reassorted Influenza A(H5N8) clade 2.3.4.4 viruses, Germany, 2016. *Emerg. Infect. Dis.* 23, 633–636. doi: 10.3201/eid2304.161949

Saito, T., Tanikawa, T., Uchida, Y., Takemae, N., Kanehira, K., and Tsunekuni, R. (2015). Intracontinental and intercontinental dissemination of Asian H5 highly pathogenic avian influenza virus (clade 2.3.4.4) in the winter of 2014-2015. *Rev. Med. Virol.* 25, 388–405. doi: 10.1002/rmv.1857

Sakuma, S., Uchida, Y., Kajita, M., Tanikawa, T., Mine, J., Tsunekuni, R., et al. (2021). First outbreak of an H5N8 highly pathogenic avian Influenza virus on a chicken farm in Japan in 2020. *Viruses* 13:489. doi: 10.3390/v13030489

Selim, A. A., Erfan, A. M., Hagag, N., Zanaty, A., Samir, A. H., Samy, M., et al. (2017). Highly pathogenic avian Influenza virus (H5N8) clade 2.3.4.4 infection in migratory birds. *Egypt. Emerg. infect. Dis.* 23, 1048–1051. doi: 10.3201/eid2306.162056

Shi, J., Deng, G., Ma, S., Zeng, X., Yin, X., Li, M., et al. (2018). Rapid evolution of H7N9 highly pathogenic viruses that emerged in China in 2017. *Cell Host Microbe* 24, 558.e7–568.e7. doi: 10.1016/j.chom.2018.08.006

Shi, W., and Gao, G. F. (2021). Emerging H5N8 avian influenza viruses. *Science* 372, 784–786. doi: 10.1126/science.abg6302

Song, J., Xu, J., Shi, J., Li, Y., and Chen, H. (2015). Synergistic effect of S224P and N383D substitutions in the PA of H5N1 avian Influenza virus contributes to mammalian adaptation. *Sci. Rep.* 5:10510. doi: 10.1038/srep10510

Soubies, S. M., Volmer, C., Croville, G., Loupias, J., Peralta, B., Costes, P., et al. (2010). Species-specific contribution of the four C-terminal amino acids of influenza A virus NS1 protein to virulence. *J. Virol.* 84, 6733–6747. doi: 10.1128/JVI.02427-09

Suttie, A., Deng, Y. M., Greenhill, A. R., Dussart, P., Horwood, P. F., and Karlsson, E. A. (2019). Inventory of molecular markers affecting biological characteristics of avian influenza A viruses. *Virus Genes* 55, 739–768. doi: 10.1007/s11262-019-01700-z

Tharakaraman, K., Raman, R., Viswanathan, K., Stebbins, N. W., Jayaraman, A., Krishnan, A., et al. (2013). Structural determinants for naturally evolving H5N1 hemagglutinin to switch its receptor specificity. *Cell* 153, 1475–1485. doi: 10.1016/j.cell.2013.05.035

Twabela, A., Okamatsu, M., Matsuno, K., Isoda, N., and Sakoda, Y. (2020). Evaluation of Baloxavir Marboxil and Peramivir for the treatment of high pathogenicity avian Influenza in chickens. *Viruses* 12:1407. doi: 10.3390/v12121407

Wade, A., Jumbo, S. D., Zecchin, B., Fusaro, A., Taiga, T., Bianco, A., et al. (2018). Highly pathogenic avian Influenza A(H5N8) virus, Cameroon, 2017. *Emerg. Infect. Dis.* 24, 1367–1370. doi: 10.3201/eid2407.172120

Wang, W., Lu, B., Zhou, H., Suguitan, A. L. Jr., Cheng, X., Subbarao, K., et al. (2010). Glycosylation at 158N of the hemagglutinin protein and receptor binding specificity synergistically affect the antigenicity and immunogenicity of a live attenuated H5N1 A/Vietnam/1203/2004 vaccine virus in ferrets. *J. Virol.* 84, 6570–6577. doi: 10.1128/JVI.00221-10

Wessels, U., Abdelwhab, E. M., Veits, J., Hoffmann, D., Mamerow, S., Stech, O., et al. (2018). A dual motif in the Hemagglutinin of H5N1 goose/Guangdong-Like highly pathogenic avian Influenza virus strains is conserved from their early evolution and increases both membrane fusion pH and virulence. *J. Virol.* 92:18. doi: 10.1128/JVI.00778-18

Wu, H., Peng, X., Xu, L., Jin, C., Cheng, L., Lu, X., et al. (2014). Novel reassortant influenza A(H5N8) viruses in domestic ducks, eastern China. *Emerg. Infect. Dis.* 20, 1315–1318. doi: 10.3201/eid2008.140339

Xu, X., Subbarao, C., Cox, N. J., and Guo, Y. (1999). Genetic characterization of the pathogenic influenza A/goose/Guangdong/1/96 (H5N1) virus: similarity of its hemagglutinin gene to those of H5N1 viruses from the 1997 outbreaks in Hong Kong. *Virology* 261, 15–19. doi: 10.1006/viro.1999.9820

Yang, Z. Y., Wei, C. J., Kong, W. P., Wu, L., Xu, L., Smith, D. F., et al. (2007). Immunization by avian H5 influenza hemagglutinin mutants with altered receptor binding specificity. *Science* 317, 825–828. doi: 10.1126/science.1135165

Yehia, N., Naguib, M. M., Li, R., Hagag, N., El-Husseiny, M., Mosaad, Z., et al. (2018). Multiple introductions of reassorted highly pathogenic avian influenza viruses (H5N8) clade 2.3.4.4b causing outbreaks in wild birds and poultry in Egypt. *Infec. Gene. Evo.* 58, 56–65. doi: 10.1016/j.meegid.2017.12.011

Zeng, X. Y., Chen, X. H., Ma, S. J., Wu, J. J., Bao, H. M., Pan, S. X., et al. (2020). Protective efficacy of an H5/H7 trivalent inactivated vaccine produced from re-11, re-12, and H7-Re2 strains against challenge with different H5 and H7 viruses in chickens. *J. Integr. Agric.* 19, 2294–2300. doi: 10.1016/S2095-3119(20)63301-9

Zielecki, F., Semmler, I., Kalthoff, D., Voss, D., Mauel, S., Gruber, A. D., et al. (2010). Virulence determinants of avian H5N1 influenza A virus in mammalian and avian hosts: role of the C-terminal ESEV motif in the viral NS1 protein. *J. Virol.* 84, 10708–10718. doi: 10.1128/JVI.00610-10

Conflict of Interest: The authors declare that the research was conducted in the absence of any commercial or financial relationships that could be construed as a potential conflict of interest.

Publisher's Note: All claims expressed in this article are solely those of the authors and do not necessarily represent those of their affiliated organizations, or those of the publisher, the editors and the reviewers. Any product that may be evaluated in this article, or claim that may be made by its manufacturer, is not guaranteed or endorsed by the publisher.

frontiers | Frontiers in Microbiology

ORIGINAL RESEARCH
published: 12 May 2022
doi: 10.3389/fmicb.2022.898184

Molecular Detection of Parvovirus in Captive Siberian Tigers and Lions in Northeastern China From 2019 to 2021

Shuping Huang[1†], Xiang Li[1†], Wei Xie[1], Lijun Guo[1], Dan You[1], Haitao Xu[2], Dan Liu[2], Yulong Wang[1], Zhijun Hou[1], Xiangwei Zeng[1], Siyuan Yang[3], Hongliang Chai[1]* and Yajun Wang[1]**

[1] College of Wildlife and Protected Area, Northeast Forestry University, Harbin, China, [2] Siberian Tiger Park, Harbin, China, [3] Heilongjiang Vocational College for Nationalities, Harbin, China

OPEN ACCESS

Edited by:
Svetlana Khaiboullina, University of Nevada, Reno, United States

Reviewed by:
Feng Na, Chinese Academy of Agricultural Sciences (CAAS), China
Julian Ruiz-Saenz, Cooperative University of Colombia, Colombia
Edward Ramsay, The University of Tennessee, Knoxville, United States

***Correspondence:**
Siyuan Yang
yangsiyuan0451@126.com
Hongliang Chai
Hongliang_Chai@hotmail.com
Yajun Wang
wangyajun@nefu.edu.cn

[†] These authors have contributed equally to this work

Specialty section:
This article was submitted to Infectious Agents and Disease, a section of the journal Frontiers in Microbiology

Received: 17 March 2022
Accepted: 19 April 2022
Published: 12 May 2022

Citation:
Huang S, Li X, Xie W, Guo L, You D, Xu H, Liu D, Wang Y, Hou Z, Zeng X, Yang S, Chai H and Wang Y (2022) Molecular Detection of Parvovirus in Captive Siberian Tigers and Lions in Northeastern China From 2019 to 2021. Front. Microbiol. 13:898184. doi: 10.3389/fmicb.2022.898184

The fact that wild felines are carriers of pernicious infectious viruses should be a major concern due to the potential cross-species transmission between the felines and human or domestic animals. However, studies on the virus in the captive wild felines, especially in tigers, are thin on the ground. In this study, we screened four infectious viruses, namely, feline parvovirus (FPV), feline coronavirus (FCoV), canine distemper virus (CDV), and influenza A virus (IAV), in the blood samples of 285 captive Siberian tigers (*Panthera tigris altaica*) and in the spleen samples of two deceased lions (*Panthera leo*), which were collected from 2019 to 2021 in three Siberian Tiger Parks from the northeast of China. Nucleic acids isolated from the blood samples collected from tigers and the spleen samples collected from two deceased lions were positive for FPV by PCR, and the positive rate was 4.6% (13/285) in tigers. Furthermore, the VP2 gene of FPV was amplified by nested PCR, and the sequences of the VP2 gene from these six FPV positive strains shared 98.3–99.9% homology with the reference. The key amino acid sites of VP2 protein were consistent with that of FPV reference strains. Phylogenetic analysis based on the VP2 gene showed that in this study, FPV-positive strains were grouped within the FPV clade and closely related to the Asian strains clade. The results of this study showed that FPV circulated in the captive Siberian tigers and lions in northeastern China and provided valuable information for the study of FPV epidemiology in wild felines. Therefore, we suggest that regular antibody monitoring and booster immunization for tigers should be performed.

Keywords: Siberian tigers, lion, FPV, VP2 gene, nested PCR, real-time PCR

INTRODUCTION

The captive breeding mode of feline species increases the possibility of cross-species transmission between the species and humans (Foley et al., 2013; Carver et al., 2016), which can potentially impact the survival of wildlife populations. For example, feline parvovirus (FPV), feline coronavirus (FCoV), canine distemper virus (CDV), and influenza A virus (IAV) are widespread in wild felines (Duarte et al., 2012; Candela et al., 2019; McCauley et al., 2021). FPV is a pathogen that causes

panleukopenia in felines, the symptoms of which include high fever, vomiting, severe leukopenia, and enteritis (Stuetzer and Hartmann, 2014). It is closely related to blue fox parvovirus (BFPV), mink enteritis virus (MEV), raccoon dog parvovirus (RDPV), and canine parvovirus (CPV) in gene, structure, and antigen. FPV affects cats of all ages and has a wide range of hosts, affecting all members of the family felines (Allison et al., 2013). Goodrich et al. (2012) found that the antibody-positive rate of FPV among Siberian tigers in eastern Russia was 68% (n = 44). In addition, FPV exposure or infection has been reported in captive Siberian tigers in Guangzhou and Jilin, China (Wang et al., 2017, 2019). CDV is a multi-host pathogen with various clinical outcomes of interspecies and cross-species transmission. PCR and antibody detection of CDV infection have been reported in wolves, tigers, lions, ferrets, minks, red foxes, giant pandas, and genets (Feng et al., 2016; Loots et al., 2017; Weckworth et al., 2020). FCoV infects domestic cats and wild felines; although FCoV tends to cause mild or inconspicuous illness, a small percentage of felines die from the fatal systemic disease feline infectious peritonitis (FIP) (Stout et al., 2021). IAV infects a variety of vertebrates, including birds, humans, and other mammals (Driskell et al., 2013). Although felines were previously considered to be resistant to IAV infection, the H5N1 subtype virus is wreaking havoc in many countries and has caused fatal infection in domestic cats, leopards, and tigers (Driskell et al., 2013; He et al., 2015).

To investigate the prevalence of FPV, FCoV, CDV, and IAV in Siberian tigers and lions in northeastern China, and to enrich the epidemiological data of tigers, FPV, FCoV, CDV, and IAV were detected by PCR, and the key amino acid site mutation and phylogenetic analysis of VP2 gene were performed.

MATERIALS AND METHODS

Samples Collection

A total of 285 blood samples of captive Siberian tigers were randomly collected from the Siberian Tiger Parks in three cities: Harbin (n = 190, 200–300 tiger/km^2), Hailin (n = 55, 1,300–1,400 tiger/km^2), and Shenyang (n = 40, 600–700 tiger/km^2) in northeastern China (41–46°N, 122–130°E), from January 2019 to March 2021. The samples used in this study are the same as our previous studies, but after the detection of four viruses [i.e., feline herpesvirus 1 (FHV-1), feline calicivirus (FCV), feline immunodeficiency virus (FIV), and feline leukemia virus (FeLV)] and persistent organic pollutants, some samples have been run out, so the sample size in this study is 285, smaller than the sample size of 324 last time (Liu et al., 2021a,b; Huang et al., 2022). All tigers fasted for 1 day before the blood sample collection, and the tigers were anesthetized with a dart containing 10 mg/kg of ketamine (Jiangsu Zhongmu Beikang Pharmaceutical Co., Ltd., China). In addition, spleen samples were collected from two dead lions in the Siberian Tiger Park of Harbin, and all samples were stored at −80°C for later use. All tigers were dewormed once a year (Hailechong, Zhejiang Hai Zheng Animal Health Products Co., Ltd., China) and were vaccinated twice. The first immunization was taken after birth and the second was 1 month later (Fel-O-Vax PCT, Zoetis, United States). No animals were killed for investigative purposes, and all samples were collected by the veterinarian of Siberian Tiger Park, which was approved by the Northeast Forestry University Institutional Review Board of Ethics and Administration of Experimental Animals (NEFU-IRBEA) (Liu et al., 2022).

Virus Detection by PCR

The viral nucleotide extraction from the blood of tigers and the spleen of deceased lions was performed by the Baypure^{TM} Universal Magnetic Bead Viral DNA/RNA Rapid Extraction Kit (BayBio, Guangzhou, China), and reverse transcription was performed to get the cDNA of FCoV. The extracted DNA, RNA, and cDNA were stored at −80°C.

Feline parvovirus, CDV, and IAV were detected by real-time PCR, and FCoV was detected by nested PCR, as previously described (Herrewegh et al., 1995; Meli et al., 2009; Streck et al., 2013); the PCR primers are shown in **Supplementary Table 1**. VP2 gene of FPV was amplified by nested PCR (Mochizuki et al., 1996; Steinel et al., 2000; Battilani et al., 2001; Sacristán et al., 2021). FPV and FCoV positive controls were cat samples with the corresponding disease, which were collected in pet hospitals. CDV positive control is the CDV live attenuated vaccine. Birds infected with IAV are used as positive controls for testing IAV. To avoid contamination of samples, RNase-free water was used as a negative control for each assay.

Phylogenetic Analysis

Multiple sequence alignments were conducted using the MegAlign program of DNAStar 11 software and were translated into putative amino acid sequences using the MEGA 7.0 software.[1] Reference sequences were selected based on the VP2 gene of panleukopenia viruses from the GenBank database.[2] The phylogenetic tree was established in MEGA 7.0 software. The neighbor-joining method with 1,000 bootstrap replications was used with the Kimura 2-parameter model to analyze the relationship between the partial VP2 sequences in this study and other reference sequences.

RESULTS

In this study, only parvovirus infection was detected in the tigers (13/285; 4.6%) and two deceased lions (2/2; 100%) from Harbin, but no FCoV-, CDV-, and IAV-positive samples were found. FPV-positive samples were detected only in the Harbin area, and there is no much difference in the positive rate between male (4.9%) and female (4.3%) animals. However, the positive rate of young tigers (5.5%) was higher than that of adult tigers (3.8%) (**Table 1**).

In this study, we have got six partial VP2 gene sequences and approximately 800 bp fragments from five positive strains (i.e., HB1807, HB1752, HB1765, HB1819, and LWL) and 1,683 bp from the HB1811 strain. Multiple sequences alignment based on the nucleotide (nt) of the VP2 gene showed that six positive

[1] http://www.megasoftware.net/

[2] https://www.ncbi.nlm.nih.gov/nucleotide/

TABLE 1 | Information of FPV positive samples, including the number and positive rate by species, sex, age, and region.

Species	Sex/positive samples (rate)	Age/positive samples (rate)	Region/positive samples (rate)
Siberian tiger (*Panthera tigris altaica*) (*n* = 285)	male (*n* = 144)/7 (4.9%) female (*n* = 141)/6 (4.3%)	young (*n* = 128)/7 (5.5%) adult (*n* = 157)/6 (3.8%)	Harbin (*n* = 190)/13 (6.8%) Hailin (*n* = 55)/0 Shenyang (*n* = 40)/0
Lion (*Panthera leo*) (*n* = 2)	male (*n* = 1)/1 (100%) female (*n* = 1)/1 (100%)	young (*n* = 1)/1 (100%) adult (*n* = 1)/1 (100%)	Harbin (*n* = 2)/2 (100%)

TABLE 2 | Amino acid residues characteristic and pairwise identity of VP2 in this study compared with other related parvovirus strains.

Strain	The main amino acid sites												Nucleotide identity (%)	Antigenic type
	80	87	93	101	103	297	300	305	323	426	564	568		
HB1807*	K	M	K	T	V	S	A	D	D	N	–	–	99.3–100%	TPV
HB1752*	–	–	–	–	–	–	–	D	D	N	N	–		TPV
HB1765*	–	–	–	–	–	S	A	D	D	N	N	–		TPV
HB1819*	K	M	K	T	V	S	A	D	D	–	–	–		TPV
HB1811*	K	M	K	T	V	S	A	D	D	N	–	–		TPV
LWL*	–	–	–	–	–	–	–	–	D	N	N	A		FPV
AB054227	K	M	K	T	V	S	A	D	D	N	N	A	99.4–99.9%	TPV
FJ405225	K	M	K	T	V	S	A	D	D	N	N	A	99.3–99.6%	TPV
EU697384	K	M	K	T	V	S	A	D	D	N	N	A	99.3–99.6%	TPV
M38246	K	M	K	I	V	S	A	D	D	N	N	A	99.4–99.6%	FPV
EU498680#	K	M	K	I	V	S	A	D	D	N	N	A	99.3–99.6%	FPV
EU498681#	K	M	K	T	V	S	A	D	D	N	N	A	99.3–99.6%	FPV
M38245	R	M	N	I	A	S	A	D	N	N	S	G	98.9–99.9%	CPV-2
M24003	R	L	N	T	A	S	G	Y	N	D	S	G	98.7–98.9%	CPV-2a
AF306444	R	L	N	T	A	A	G	Y	N	D	S	G	98.3–98.9%	CPV-2b
KP682519	R	L	N	T	A	A	G	Y	N	E	S	G	98.4–98.7%	CPV-2c

"–" represents sequencing failure; "" represents the positive strains in this study. The first five samples are tiger samples, and LWL sample is lion sample. "#" represents vaccine strains. EU498680: Purevax Merial vaccine, EU498681: Felocell Pfizer vaccine.*

strains shared 99.3–99.9% homology with FPV isolates and 98.3–98.9% homology with CPV isolates. The amino acids at 80, 93, 103, 323, 564, and 568 of the VP2 gene were the key sites to distinguish FPV and CPV antigen types (Yi et al., 2021). To further analyze the mutation of positive strains, the amino acid sequences of VP2 are compared in **Table 2**. The result showed that the amino acid mutation sites of six VP2 proteins were identical with FPV reference strains. However, due to the quality of samples or primers, the full-length sequence of the VP2 gene was not successfully amplified.

A phylogenetic tree about the VP2 nucleotide sequences was constructed based on the positive strain sequences in this study and 37 reference sequences from Europe, America, and Asia (**Supplementary Table 2**). The phylogenetic analysis indicated that all the parvoviruses can be grouped into two large branches: the FPV branch and the CPV branch (**Figure 1**). FPV branch comprised TPV (The feline parvovirus isolated from tigers was named TPV), FPV, MEV, and BFPV. In the FPV branch, 26 strains from China, Korea, Japan, India, United States, and Italy formed a cluster, and four sequences from Portugal (EF418568, EF418569, EU221279, JF422105) formed a different clade. All positive strains in this study belong to the FPV strains branch and were closely related to the Asia-isolated strains, but they were distant from the Portugal-isolated strains. The Asian isolates were mainly divided into two differentiated clades, and HB1811 strain was closely related to a tiger strain isolated in China (MN908257), but was not in the same clade as other strains in this study.

DISCUSSION

Wild felines are susceptible to virus infection due to cross-species transmission potentially by domestic cats or dogs (Canuti et al., 2020). Early detection of viral shedding in asymptomatic or symptomatic felines may help inspect the health status of wild felines and are critical for early treatment and prevention plans for animal diseases. In this study, the positive rate of FPV in captive Siberian tigers was 4.6%, higher than previous results of FPV in Malaysian tigers was 2.7% (Nur-Farahiyah et al., 2021), and the positive rate of the virus in Italian red foxes was 2.8% (Ndiana et al., 2021). The tigers in this study are captive, and such a large sample size may be the main reason for this result. Furthermore, there are no coinfection among FPV and the other four viruses (i.e., FHV-1, FCV, FIV, and FeLV) (Huang et al., 2022).

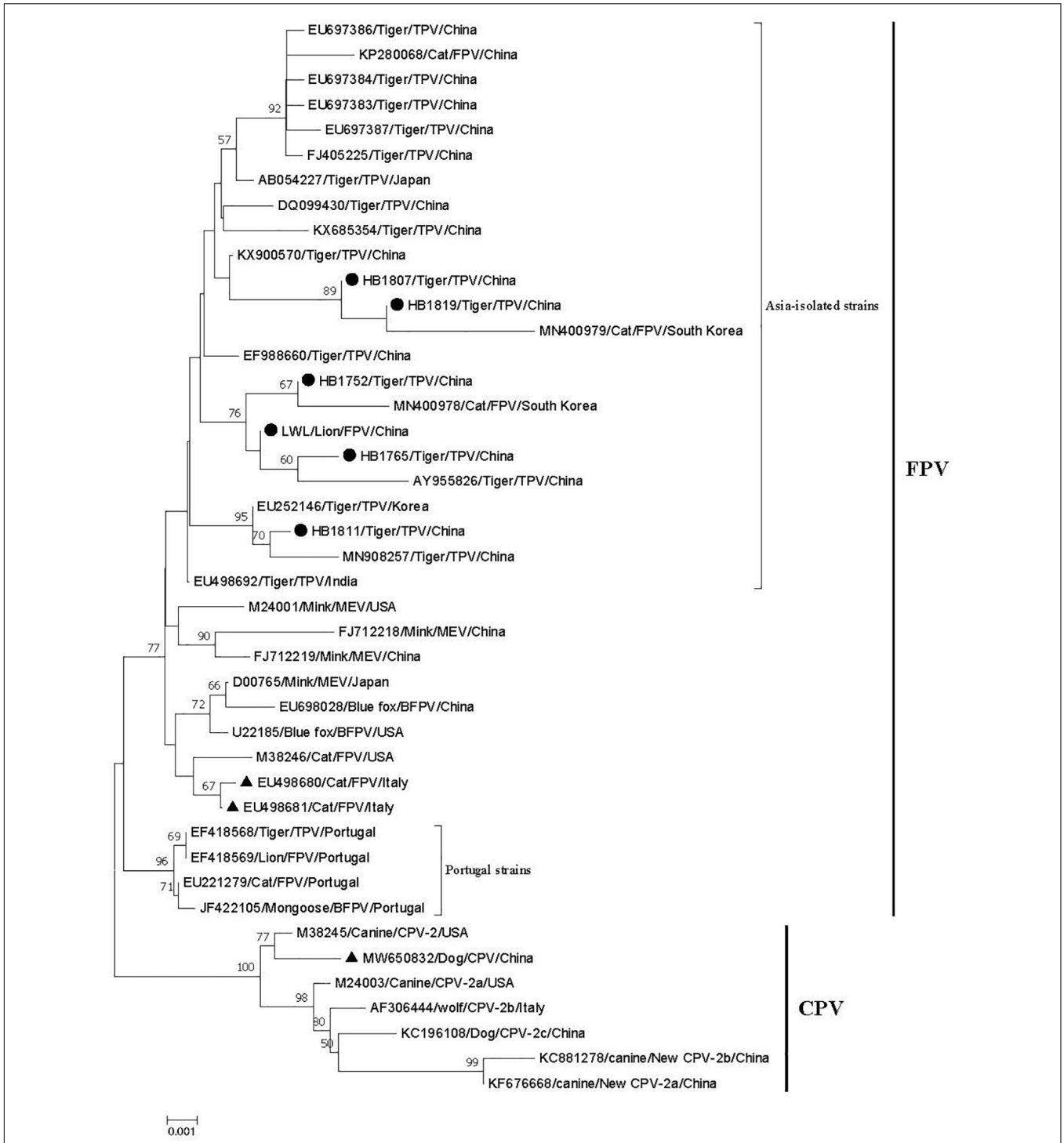

FIGURE 1 | Phylogenetic tree of six FPV partial VP2 genes compared with other references of parvovirus strains obtained from GenBank. The tree was generated using the neighbor-joining method in MEGA 7.0 using the Kimura 2-parameter model with 1,000 bootstrap values. Bootstrap values ≥ 50 at the nodes of the tree. "●" represents the strains in this study; "▲" represents vaccine strains; EU498680 and EU498681 are the FPV vaccine strain; MW650832 is the CPV vaccine strain. The length of the six VP2 genes is as follows: HB1807: 973 bp; HB1752: 790 bp; HB1765: 984 bp; HB1819 bp: 973; HB1811: 1683 bp; LWL: 825 bp.

Real-time PCR detection of FPV in the two dead deceased lions was also positive. The two deceased lions showed depressed spirit, lost appetite with shame and tears, dry nose, dark red vomit, bloody stool, dehydration, a body temperature of 39.5°C, and leukocyte elevation during the paroxysm of symptoms. The pathological changes after autopsy mainly

included gastric bleeding, bile reflux, severe intestinal bleeding, hemorrhagic enteritis, mesenteric lymphadenitis enlargement, and hemorrhage, so we believe that FPV infection may be the main reason for the death of lions. These results suggest that FPV has a certain prevalence in captive Siberian tigers and lions in northeastern China. However, we have not found FCoV, CDV, and IAV in any of these samples, which showed that there was no epidemic of FCoV, CDV, and IAV in the three Siberian Tiger parks.

Feline parvovirus was first discovered in 1928, and canine parvovirus type 2 (CPV-2) was discovered in 1978. CPV-2 originated from FPV or an FPV-like parvovirus in carnivores. In 1979, CPV-2a mutated away from the original type 2 in five amino acids (aa) in VP2 that alter relevant biological properties between the strains. Another antigenic variant, CPV-2b, with a single additional substitution (Asn426Asp) in the VP2 protein appeared in 1984 and spread globally (Parrish et al., 1985; Parrish, 1991). Since then, many new CPV variants throughout the world have been detected, such as the "new CPV-2a" and "new CPV-2b" with an additional 297-Ala mutation, CPV-2c with an additional 300-Asp mutation, and 426-Glu mutation (Buonavoglia et al., 2001; Decaro and Buonavoglia, 2012). In this study, due to the sample's quality and DNA concentration reasons, such as samples stored for a long time, repeated freezing, and thawing, we only got six positive sample sequences, and we failed to amplify the entire VP2 gene. The main amino acid mutation sites obtained in this study were identical to FPV (**Table 2**).

The viruses are named after the host from which they are isolated, such as FPV, TPV, MEV, BFPV, and CPV. In this study, five TPV strains from tigers and one FPV (LWL) of lion strain are identified. We selected 37 parvovirus VP2 genes from GenBank for phylogenetic analysis, and all six positive strains in this study belong to the Asia-isolated FPV strains but had a distant relationship to the Portugal-isolated FPV strains. These results suggest that the spreading and prevalence of FPV are related to the geographical location of the animals. The relationship between positive strains and commercial FPV vaccine strains (i.e., EU498680 and EU498681) is also distant. Inactivated vaccines (Fel-O-Vax PCT, Zoetis, United States), which combine FCV, FHV, and FPV strains, are used to prevent disease in tigers. However, tigers and lions are still infected with FPV; the reason for this result may be the low antibody level and short antibody duration of the FPV-inactivated vaccine (Bergmann et al., 2019). In the FPV clade, both the tigers and lion strains in this study belong to the same evolutionary clade, and in this clade, the tiger and lion strains are closely related to the reference strains from tigers and cats. The Siberian tigers in these three regions were all fenced with wire mesh that prevents the tigers from escaping but does not restrict domestic cat movement, and the staffs often see the stray cats pass in and out of the Siberian Tiger Park freely, which allows for the possibility of contact, and therefore transmission, between the stray cats and tigers or lions (Liu et al., 2022). Considering the widespread infection of FPV (Franzo et al., 2017) and the captive environment, FPV might be transmitted from the stray cats to tigers and lions. Previous studies have confirmed the possibility of cross-species transmission of FPV in domestic cats and other felines (Wang et al., 2017; Shetty et al., 2019). Furthermore, human participation in the landscape is an important factor affecting the spread of pathogens across species (Carver et al., 2016).

Combined with our previous study (Huang et al., 2022), FHV-1, FCV, FIV, and FPV have certain prevalence rates in the Siberian Tiger Park of northeastern China, and interspecies and cross-species transmission may happen. This study not only provides new data on the prevalence of FPV among tigers and lions but also contributes to improving the management of captive felines.

DATA AVAILABILITY STATEMENT

The data presented in the study are deposited in the NCBI repository, accession numbers OM810192, OM810193, OM810194, OM810195, and OM810196.

ETHICS STATEMENT

The authors confirm that the ethical policy has been followed as noted on the author guidelines page of the journal, and all blood samples and swabs of the Siberian tigers were collected by the Siberian Tiger Park, which was approved by the Northeast Forestry University Institutional Review Board of Ethics and Administration of Experimental Animals (NEFU-IRBEA).

AUTHOR CONTRIBUTIONS

All authors of this research manuscript have directly participated in the planning, execution, and analysis of the study.

FUNDING

This work was supported by the Surveillance of Wildlife Diseases Project from the National Forestry and Grassland Administration of China.

ACKNOWLEDGMENTS

We thank the financial support from the Surveillance of Wildlife Diseases Project from the National Forestry and Grassland Administration, China. We are also very grateful to the Siberian Tiger Park for providing us with the Siberian tiger samples.

SUPPLEMENTARY MATERIAL

The Supplementary Material for this article can be found online at: https://www.frontiersin.org/articles/10.3389/fmicb.2022.898184/full#supplementary-material

REFERENCES

Allison, A. B., Kohler, D. J., Fox, K. A., Brown, J. D., Gerhold, R. W., Shearn-Bochsler, V. I., et al. (2013). Frequent cross-species transmission of parvoviruses among diverse carnivore hosts. *J. Virol.* 87, 2342–2347. doi: 10.1128/JVI.02428-12

Battilani, M., Scagliarini, A., Tisato, E., Turilli, C., Jacoboni, I., Casadio, R., et al. (2001). Analysis of canine parvovirus sequences from wolves and dogs isolated in Italy. *J. Gen. Virol.* 82, 1555–1560. doi: 10.1099/0022-1317-82-7-1555

Bergmann, M., Schwertler, S., Speck, S., Truyen, U., Reese, S., and Hartmann, K. (2019). Faecal shedding of parvovirus deoxyribonucleic acid following modified live feline panleucopenia virus vaccination in healthy cats. *Vet. Rec.* 185:83. doi: 10.1136/vr.104661

Buonavoglia, C., Martella, V., Pratelli, A., Tempesta, M., Cavalli, A., Buonavoglia, D., et al. (2001). Evidence for evolution of canine parvovirus type 2 in Italy. *J. Gen. Virol.* 82, 3021–3025. doi: 10.1099/0022-1317-82-12-3021

Candela, M. G., Pardavila, X., Ortega, N., Lamosa, A., Mangas, J. G., and Martinez-Carrasco, C. (2019). Canine distemper virus may affect European wild cat populations in Central Spain. *Mamm. Biol.* 97, 9–12. doi: 10.1016/j.mambio.2019.04.006

Canuti, M., Todd, M., Monteiro, P., Van Osch, K., Weir, R., Schwantje, H., et al. (2020). Ecology and infection dynamics of multi-host amdoparvoviral and protoparvoviral carnivore pathogens. *Pathogens* 9:124. doi: 10.3390/pathogens9020124

Carver, S., Bevins, S. N., Lappin, M. R., Boydston, E. E., Lyren, L. M., Alldredge, M., et al. (2016). Pathogen exposure varies widely among sympatric populations of wild and domestic felids across the United States. *Ecol. Appl.* 26, 367–381. doi: 10.1890/15-0445

Decaro, N., and Buonavoglia, C. (2012). Canine parvovirus–a review of epidemiological and diagnostic aspects, with emphasis on type 2c. *Vet. Microbiol.* 155, 1–12. doi: 10.1016/j.vetmic.2011.09.007

Driskell, E. A., Jones, C. A., Berghaus, R. D., Stallknecht, D. E., Howerth, E. W., and Tompkins, S. M. (2013). Domestic cats are susceptible to infection with low pathogenic avian influenza viruses from shorebirds. *Vet. Pathol.* 50, 39–45. doi: 10.1177/0300985812452578

Duarte, A., Fernandes, M., Santos, N., and Tavares, L. (2012). Virological Survey in free-ranging wildcats (*Felis silvestris*) and feral domestic cats in Portugal. *Vet. Microbiol.* 158, 400–404. doi: 10.1016/j.vetmic.2012.02.033

Feng, N., Yu, Y., Wang, T., Wilker, P., Wang, J., Li, Y., et al. (2016). Fatal canine distemper virus infection of giant pandas in China. *Sci. Rep.* 6:27518. doi: 10.1038/srep27518

Foley, J. E., Swift, P., Fleer, K. A., Torres, S., Girard, Y. A., and Johnson, C. K. (2013). Risk factors for exposure to feline pathogens in California mountain lions (*Puma concolor*). *J. Wildl. Dis.* 49, 279–293. doi: 10.7589/2012-08-206

Franzo, G., Tucciarone, C. M., Cecchinato, M., and Drigo, M. (2017). *Canine parvovirus* type 2 (CPV-2) and *Feline panleukopenia* virus (FPV) codon bias analysis reveals a progressive adaptation to the new niche after the host jump. *Mol. Phylogenet. Evol.* 114, 82–92. doi: 10.1016/j.ympev.2017.05.019

Goodrich, J. M., Quigley, K. S., Lewis, J. C., Astafiev, A. A., Slabi, E. V., Miquelle, D. G., et al. (2012). Serosurvey of free-ranging Amur tigers in the Russian Far East. *J. Wildl. Dis.* 48, 186–189. doi: 10.7589/0090-3558-48.1.186

He, S., Shi, J., Qi, X., Huang, G., Chen, H., and Lu, C. (2015). Lethal infection by a novel reassortant H5N1 avian influenza a virus in a zoo-housed tiger. *Microbes Infect.* 17, 54–61. doi: 10.1016/j.micinf.2014.10.004

Herrewegh, A. A., de Groot, R. J., Cepica, A., Egberink, H. F., Horzinek, M. C., and Rottier, P. J. (1995). Detection of feline coronavirus RNA in feces, tissues, and body fluids of naturally infected cats by reverse transcriptase PCR. *J. Clin. Microbiol.* 33, 684–689. doi: 10.1128/jcm.33.3.684-689.1995

Huang, S., Li, X., Guo, L., You, D., Xie, W., Xu, H., et al. (2022). Prevalence of four viruses in captive siberian tigers from Northeastern China. *Transbound. Emerg. Dis* doi: 10.1111/tbed.14475

Liu, E., Ma, L., Huang, S., You, D., Guo, L., Li, X., et al. (2022). The first feline immunodeficiency virus from Siberian tigers (*Panthera tigris* altaica) in Northeastern China. *Arch. Virol.* 167, 545–551. doi: 10.1007/s00705-022-05370-5

Liu, E., Ma, L., You, D., Yang, C., Hu, Y., Xu, H., et al. (2021a). Haematological and biochemical parameters of captive Siberian Tigers (*Panthera tigris* altaica) from the Heilongjiang Province, China. *Vet. Med. Sci.* 7, 1015–1022. doi: 10.1002/vms3.395

Liu, H., Plancarte, M., Ball, E. E., Weiss, C. M., Gonzales-Viera, O., Holcomb, K., et al. (2021b). Respiratory tract explant infection dynamics of influenza a virus in California sea Lions, Northern Elephant Seals, and Rhesus Macaques. *J. Virol.* 95:e0040321. doi: 10.1128/JVI.00403-21

Loots, A. K., Mitchell, E., Dalton, D. L., Kotzé, A., and Venter, E. H. (2017). Advances in canine distemper virus pathogenesis research: a wildlife perspective. *J. Gen. Virol.* 98, 311–321. doi: 10.1099/jgv.0.000666

McCauley, D., Stout, V., Gairhe, K. P., Sadaula, A., Dubovi, E., Subedi, S., et al. (2021). Serologic survey of selected pathogens in free-ranging Bengal tigers (*Panthera tigris* tigris) in Nepal. *J. Wildl. Dis.* 57, 393–398. doi: 10.7589/JWD-D-20-00046

Meli, M. L., Cattori, V., Martinez, F., Lopez, G., Vargas, A., Simon, M. A., et al. (2009). Feline leukemia virus and other pathogens as important threats to the survival of the critically endangered Iberian lynx (*Lynx pardinus*). *PLoS One* 4:e4744. doi: 10.1371/journal.pone.0004744

Mochizuki, M., Horiuchi, M., Hiragi, H., San, G. M., Yasuda, N., and Uno, T. (1996). Isolation of canine parvovirus from a cat manifesting clinical signs of feline panleukopenia. *J. Clin. Microbiol.* 34, 2101–2105. doi: 10.1128/jcm.34.9.2101-2105.1996

Ndiana, L. A., Lanave, G., Desario, C., Berjaoui, S., Alfano, F., Puglia, I., et al. (2021). Circulation of diverse protoparvoviruses in wild carnivores, Italy. *Transbound. Emerg. Dis.* 68, 2489–2502. doi: 10.1111/tbed.13917

Nur-Farahiyah, A. N., Kumar, K., Yasmin, A. R., Omar, A. R., and Camalxaman, S. N. (2021). Isolation and genetic characterization of *Canine Parvovirus* in a Malayan tiger. *Front. Vet. Sci.* 8:660046. doi: 10.3389/fvets.2021.660046

Parrish, C. R. (1991). Mapping specific functions in the capsid structure of canine parvovirus and feline panleukopenia virus using infectious plasmid clones. *Virology* 183, 195–205. doi: 10.1016/0042-6822(91)90132-u

Parrish, C. R., O'Connell, P. H., Evermann, J. F., and Carmichael, L. E. (1985). Natural variation of canine parvovirus. *Science* 230, 1046–1048. doi: 10.1126/science.4059921

Sacristán, I., Esperón, F., Pérez, R., Acuña, F., Aguilar, E., García, S., et al. (2021). Epidemiology and molecular characterization of Carnivore protoparvovirus-1 infection in the wild felid *Leopardus guigna* in Chile. *Transbound. Emerg. Dis.* 68, 3335–3348. doi: 10.1111/tbed.13937

Shetty, B. D., Zachariah, A., Smith, B., Goldstein, T., and Mazet, J. A. K. (2019). Carnivore protorarvirus 1 (parvoviruses) at the domestic-wild carniovore interface in India. *J. Zoo Wildl. Med.* 50, 1016–1020. doi: 10.1638/2018-0166

Steinel, A., Munson, L., van Vuuren, M., and Truyen, U. (2000). Genetic characterization of feline parvovirus sequences from various carnivores. *J. Gen. Virol.* 81, 345–350. doi: 10.1099/0022-1317-81-2-345

Stout, A. E., Andre, N. M., and Whittaker, G. R. (2021). Feline coronavirus and FelineE infectious peritionitis in nondomestic felid species. *J. Zoo Wildlife Med.* 52, 14–27. doi: 10.1638/2020-0134

Streck, A. F., Ruster, D., Truyen, U., and Homeier, T. (2013). An updated TaqMan real-time PCR for canine and feline parvoviruses. *J. Virol. Methods* 193, 6–8. doi: 10.1016/j.jviromet.2013.04.025

Stuetzer, B., and Hartmann, K. (2014). Feline parvovirus infection and associated diseases. *Vet. J.* 201, 150–155. doi: 10.1016/j.tvjl.2014.05.027

Wang, K., Du, S., Wang, Y., Wang, S., Luo, X., Zhang, Y., et al. (2019). Isolation and identification of tiger parvovirus in captive siberian tigers and phylogenetic analysis of VP2 gene. *Infect. Genet. Evol.* 75:103957. doi: 10.1016/j.meegid.2019.103957

Wang, X., Li, T., Liu, H., Du, J., Zhou, F., Dong, Y., et al. (2017). Recombinant feline parvovirus infection of immunized tigers in central China. *Emerg Microbes Infect.* 6:e42. doi: 10.1038/emi.2017.25

Weckworth, J. K., Davis, B. W., Dubovi, E., Fountain-Jones, N., Packer, C., Cleaveland, S., et al. (2020). Cross-species transmission and evolutionary dynamics of canine distemper virus during a spillover in African lions of Serengeti National Park. *Mol. Ecol.* 29, 4308–4321. doi: 10.1111/mec.15449

Yi, S., Liu, S., Meng, X., Huang, P., Cao, Z., Jin, H., et al. (2021). Feline panleukopenia virus with G299E substitution in the VP2 protein first identified from a captive Giant Panda in China. *Front. Cell. Infect. Microbiol.* 11:820144. doi: 10.3389/fcimb.2021.820144

Conflict of Interest: The authors declare that the research was conducted in the absence of any commercial or financial relationships that could be construed as a potential conflict of interest.

Publisher's Note: All claims expressed in this article are solely those of the authors and do not necessarily represent those of their affiliated organizations, or those of the publisher, the editors and the reviewers. Any product that may be evaluated in this article, or claim that may be made by its manufacturer, is not guaranteed or endorsed by the publisher.

frontiers | Frontiers in Microbiology

ORIGINAL RESEARCH
published: 23 May 2022
doi: 10.3389/fmicb.2022.865233

Evaluation of Serum Ferritin, Procalcitonin, and C-Reactive Protein for the Prediction of Severity and Mortality in Hemorrhagic Fever With Renal Syndrome

*Lihe Che[1,2,3], Zedong Wang[1,2], Na Du[3], Liang Li[1], Yinghua Zhao[2], Kaiyu Zhang[3] and Quan Liu[1,2,4]**

[1] Changchun Veterinary Research Institute, Chinese Academy of Agricultural Sciences, Changchun, China, [2] Key Laboratory of Organ Regeneration and Transplantation of the Ministry of Education, Center for Pathogen Biology and Infectious Diseases, The First Hospital of Jilin University, Changchun, China, [3] Department of Infectious Diseases, The First Hospital of Jilin University, Changchun, China, [4] School of Life Sciences and Engineering, Foshan University, Foshan, China

OPEN ACCESS

Edited by:
Svetlana Khaiboullina, University of Nevada, Reno, United States

Reviewed by:
Silvia Spoto, Policlinico Universitario Campus Bio-Medico, Italy
Evdoxia Kyriazopoulou, National and Kapodistrian University of Athens, Greece

***Correspondence:**
Quan Liu
liuquan1973@hotmail.com

Specialty section:
This article was submitted to Infectious Agents and Disease, a section of the journal Frontiers in Microbiology

Received: 29 January 2022
Accepted: 08 March 2022
Published: 23 May 2022

Citation:
Che L, Wang Z, Du N, Li L, Zhao Y, Zhang K and Liu Q (2022) Evaluation of Serum Ferritin, Procalcitonin, and C-Reactive Protein for the Prediction of Severity and Mortality in Hemorrhagic Fever With Renal Syndrome. Front. Microbiol. 13:865233. doi: 10.3389/fmicb.2022.865233

This study aimed to analyze the clinical significance of serum ferritin, procalcitonin (PCT), and C-reactive protein (CRP) in patients with hemorrhagic fever with renal syndrome (HFRS). The demographical, clinical, and laboratory data of 373 patients with HFRS in northeastern China were retrospectively analyzed. The levels of serum ferritin and PCT in severe patients (n = 108) were significantly higher than those in mild patients (n = 265, $p < 0.001$) and associated with HFRS severity. The area under the receiver operating characteristic curve (AUC) values of serum ferritin and PCT for predicting the severity of HFRS were 0.732 (95% CI 0.678–0.786, $p < 0.001$) and 0.824 (95% CI 0.773–0.875, $p < 0.001$), respectively, showing sensitivity and specificity of 0.75 and 0.88 for serum ferritin, and 0.76 and 0.60 for PCT. The CRP level in HFRS with bacterial co-infection (n = 115) was higher than that without bacterial co-infection (n = 258, $p < 0.001$). The AUC value of CRP for predicting bacterial co-infection was 0.588 (95% CI 0.525–0.652, $p < 0.001$), showing sensitivity and specificity of 0.43 and 0.76, respectively. The serum ferritin level in non-survivors (n = 14) was significantly higher than in survivors (n = 359, $p < 0.001$). The AUC value of serum ferritin for predicting mortality was 0.853 (95% CI 0.774–0.933, $p < 0.001$), showing sensitivity and specificity of 0.933 and 0.739. Serum ferritin and PCT have a robust association with HFRS severity and mortality, which may be promising predictors, and CRP is an effective biomarker to assess bacterial co-infection in HFRS.

Keywords: hantaviruses, serum ferritin, hemorrhagic fever with renal syndrome, C-reactive protein, procalcitonin

INTRODUCTION

Hemorrhagic fever with renal syndrome (HFRS) is caused by Hantaviruses of the genus *Orthohantavirus* in the family *Hantaviridae* and is characterized by acute kidney injury, increased vascular permeability, and coagulation abnormalities. HFRS is an important rodent-associated zoonosis endemic in eastern Asia, especially in China, accounting for ∼90% of the cases globally

(Jonsson et al., 2010). Hantaan virus and Seoul virus are the major etiologies of HFRS in China that cause severe and mild forms of HFRS, respectively (Zhang et al., 2010). Although effective treatment and vaccination have greatly reduced the impact of HFRS in the past few decades in China, the number of infected patients still remains at a relatively high level, with ∼10,000 cases reported annually. Clinical parameters are necessary for improving the management of patients with HFRS, which may be used as clinical references for severity assessment and prognosis prediction (Du et al., 2014; Zhang et al., 2015).

Cytokine storm of excessive immune response plays a central role in the pathogenesis of HFRS, which can damage the vascular endothelial cell and accelerate platelet activation, leading to multi-organ dysfunction or failure (Wang et al., 2012). The pathophysiology of organ damage that occurs with hantavirus infection also motivates the increase in biomarkers, including ferritin, CRP, and PCT. Ferritin has been identified as an important molecule in the host immune system that can reflect the cellular defense against inflammatory response (Valero et al., 2019). Studies also have confirmed ferritin as a potential biomarker in the diagnosis of viral and bacterial infection, as well as macrophage-activation syndrome and hemophagocytic lymphohistiocytosis (Barut et al., 2010; Kyriazopoulou et al., 2017; Franco-Martinez et al., 2021; Zhou J. et al., 2021). Patients with HFRS appear to have a higher level of serum ferritin and PCT (Tjendra et al., 2020). Procalcitonin (PCT) is a precursor of calcitonin hormone secreted by different cells under inflammatory stimulation, which is increased and associated with disease severity, secondary bacterial infection, and mortality in patients with HFRS (Fan X. et al., 2018). C-reactive protein (CRP) is a sensitive biomarker of viral infection and inflammation (Shin et al., 2018). CRP and PCT can be used to evaluate disease severity and predict outcomes in patients with COVID-19 (Liu et al., 2020; Pan et al., 2020; Zhang et al., 2020, 2021; Zhou Y.Z. et al., 2021). In this study, we aimed to analyze the clinical significance of serum ferritin, procalcitonin (PCT), and C-reactive protein (CRP) in patients with HFRS.

MATERIALS AND METHODS

Study Design

We collected the demographical, laboratory, and clinical data of patients with HFRS who were admitted to The First Hospital of Jilin University during 2018–2019. Patients who were hantavirus (HV) serological IgM positive, had typical clinical manifestations of febrile, hemorrhage, renal injury, and travel history to HV epidemiology areas were diagnosed with HFRS and included in this study. Exclusion criteria included other infections similar to HFRS, hantaviruses IgM negative, or acute kidney injury due to other diseases (e.g., dehydration, hemorrhagic shock, glomerulonephritis, and acute intoxication).

To investigate the change of serum ferritin, PCT, and CRP associated with severity, bacterial co-infection, and death due to HFRS, we divided the patients into two groups according to the classification criteria (Escutenaire and Pastoret, 2000; Liu et al., 2008; Brocato and Hooper, 2019). The clinical types were categorized into four groups (mild, moderate, severe, and critical) according to the severity of hantavirus infection (**Table 1**). To understand the relationship between serum ferritin, PCT, CRP, and hantavirus infection more clearly, we divided the patients into two groups (mild group: mild and moderate type patients, and severe group: severe and critical type patients).

Clinical Diagnosis and Data Collection

The clinical information of HFRS included the patients' age, sex, admission days after fever, days in the hospital, primary disease or comorbidity, complication caused by HFRS, such as hemorrhage, bacterial co-infection, acute respiratory distress syndrome (ARDS), and multiple-organ dysfunction syndrome (MODS). Clinical symptoms, including hemoptysis, hematemesis, melena, hematuria, ecchymosis, and rupture or bleeding of internal organs of the body, were diagnosed with hemorrhage. The bacterial co-infection, including *Staphylococcus aureus*, methicillin-resistant *S. aureus, Streptococcus pneumoniae, Klebsiella pneumoniae, Pseudomonas aeruginosa*, and *Enterobacter aerogenes*, was confirmed by liquid culture assay (blood, urine, or feces) combined with higher levels of CRP, PCT, and/or radiological evidence. ARDS and MODS were diagnosed according to the criteria (Ramirez, 2013; Fan E. et al., 2018).

Serum ferritin, PCT, and CRP were detected at least three times at the same timepoint (hospital admission, the third day in hospital, and the day patients were discharged or bacterial co-infection was detected) from the first day of admission to the last day. Other laboratory results, such as white blood cell (WBC), platelet (PLT), alanine transaminase (ALT), aspartate aminotransferase (AST), lactate dehydrogenase (LDH), and α-hydroxybutyrate dehydrogenase (α-HBDH), were detected at least once at a different stage of HFRS. All the patients with HFRS received ribavirin and supportive treatment (maintaining fluid and electrolyte balance).

TABLE 1 | Standard for the classification of HFRS severity.

Clinical types	Manifestations*
Mild	$T < 39°C$; mild toxemic symptoms and renal damage; no bleeding except for hemorrhagic spots, no shock and oliguria
Medium	$T = 39°C \sim 40°C$; severe toxemic symptoms and obvious chemosis; The systolic Bp < 90 mmHg, or pulse pressure < 26 mmHg during the whole clinical course; Obvious hemorrhage and oliguria, urinary protein "+++"
Severe	$T > 40°C$; severe toxemic symptoms and effusion, some may have toxemic psychiatric symptoms; Shock; Severe ecchymoses on skin and cavity hemorrhage; Oliguria lasting for <5 days or anuresis less than 2 days
Critical	Combining one of the following on severe style: Refractory shock; Hemorrhage of important organs; Oliguria lasting for >5 days, or anuresis for >2 days or urea nitrogen >120 mg/dl (42.84 mmol/L); Heart failure or pulmonary edema; Central nervous system damage such as cerebral edema, brain hemorrhage and cerebral hernia; Severe secondary infections

**T, body temperature; BP, blood pressure.*

Statistical Analysis

Statistical analysis was performed using SAS 9.3 software. Categorical data were presented as numbers and percentages, and analyzed using Pearson's Chi-square test or Fisher's Exact. Distributed data were described using mean and standard deviation and analyzed using Student's *t*-test. Non-parametric data were analyzed using the Mann–Whitney *U* test, shown as median and interquartile range (IQR). Results with a value of $p < 0.05$ were deemed as statistically significant. To make data conform to normality and reduce the variability, we used log transformation, especially in data sets that included outlying observations. Predictive values of variables for disease severity, bacterial co-infection, or prognosis were tested with receiver operating characteristic (ROC) curves and quantified by calculating the area under the ROC curve (AUC) and the 95% confidence interval (CI) using SPSS 19.0 software (SPSS Inc., Chicago, IL, United States; Fan X. et al., 2018).

RESULTS

Clinical Information

The study included 373 patients with HFRS (286 men and 87 women) with a mean age of 45.38 ± 14.13 years; 108 patients were grouped into severe types (97 critical forms and 11 severe forms) and 265 patients were grouped into mild types (47 mild forms and 218 medium forms). Non-bacterial co-infections included 258 patients, while bacterial co-infections included 115 patients. Survivors included 359 patients and 14 died of HFRS. Patients who died of HFRS were all in the severe group ($p < 0.001$). The patients in the severe group had higher frequencies of complication of hemorrhage ($p < 0.001$), hepatic injury (ALT > 50 U/L and AST > 40 U/L) ($p < 0.001$), ARDS ($p < 0.001$), MODS ($p < 0.001$) than those of the mild group. Continuous renal replacement therapy (CRRT) and respirators were used in the severe group ($p < 0.001$). The patients in the severe group had a longer hospital stay than those in the mild group ($p < 0.001$), but there was no significant difference in incubation between the two groups. Higher WBC and lower PLT in the severe group were other characteristics ($p = 0.147$ and $p < 0.001$, respectively). The patients in the severe group had more severe hepatic and myocardial injury than those in the mild group.

TABLE 2 | Demographics and clinical and laboratory data at admission in the patients with HFRS of different clinical types*.

Variables	Mild (*n* = 265)	Severe (*n* = 108)	*P*-value
Male, n (%)	208 (78.5)	78 (72.2)	0.1975
Age, years	45 (32–54)	49.3 ± 12.6	0.0009
Time from symptom onset to hospital admission, days	5 (4–7)	5 (4–6)	0.0353
Hospital stay, days	7 (5–9)	9 (7–13)	<0.0001
Comorbidity			
Hypertension, n (%)	10 (3.8)	11 (10.2)	0.0148
Coronary heart disease, n (%)	2 (0.8)	2 (1.9)	0.7048
Diabetes, n (%)	8 (3.0)	10 (9.3)	0.0108
Complication			
Hemorrhage, n (%)	34 (12.8)	71 (65.7)	<0.0001
Hepatic injury, n (%)	169 (63.8)	90 (83.3)	0.0002
Myocardial damage, n (%)	80 (30.2)	76 (70.4)	<0.0001
Bacterial infection, n (%)	78 (29.4)	37 (34.3)	0.3600
ARDS, n (%)	0	19 (17.6)	<0.0001
MODS, n (%)	0	21 (19.4)	<0.0001
Respiratory support, n (%)	0	35 (32.4)	<0.0001
CRRT, n (%)	0	42 (38.9)	<0.0001
Number of death, n (%)	0	14 (13.0)	<0.0001
Parameters			
WBC, $\times 10^9$/L	8.4 (5.3–10.8)	9.6 (5.5–11.5)	0.1407
PLT, $\times 10^9$/L	109.0 (88.0–125.0)	39.0 (20.0–85.0)	<0.0001
AST, U/L	88.8 (56.0–155.6)	149.4 (77.5–297.4)	<0.0001
ALT, U/L	109.1 (68.9–187.0)	88.0 (67.9–173.2)	0.2602
LDH, U/L	415.0 (344.0–536.0)	655.0 (415.0–1011.0)	<0.0001
α-HBDH, U/L	303.0 (247.0–376.5)	515.0 (340.0–804.0)	<0.0001
PCT, ng/ml	1.3 (0.8–2.1)	3.8 (2.4–6.8)	<0.0001
Ferritin, ng/ml	2502.4 (1237.7–6670.5)	9930.5 (3604.3–17080.0)	<0.0001
CRP, mg/l	29.5 (16.4–53.2)	42.1 (25.8–69.4)	0.0006
Lg PCT	0.1 (−0.1 to 0.3)	0.6 (0.4–0.8)	<0.0001
Lg Ferritin	3.4 (3.1–3.8)	4.0 (3.6–4.2)	<0.0001
Lg CRP	1.5 ± 0.4	1.6 (1.4–1.8)	0.0006

**ARDS, acute respiratory distress syndrome; MODS, multiple organ dysfunction syndrome; CRRT, continuous renal replacement therapy; WBC, white blood cell count; PLT, platelet; ALT, alanine transaminase; AST, aspartate aminotransferase; LDH, lactate dehydrogenase; and α-HBDH, α-hydroxybutyrate dehydrogenase; Lg Ferritin, Lg PCT, and Lg CRP, Ferritin, procalcitonin, and CRP after log10 transformation.*

Serum Ferritin, Procalcitonin, and C-Reactive Protein Association With Severity of Virus Infection

In the 373 patients with HFRS, the median serum ferritin level was 3620.3 ng/ml, ranging from 70.1 to 117,500 ng/ml. The median serum ferritin level in the severe group was higher than that of the mild group ($p < 0.001$, **Table 2**). The median PCT and CRP levels in these patients with HFRS were 1.84 (0.02–82.92) ng/ml and 32 (1.25–212) mg/l, respectively, which were higher than the reference value of less than 0.5 ng/ml and 10 mg/l; both PCT and CRP in the severe group were higher than those of the mild group ($p < 0.001$; **Table 2**).

In 258 patients without bacterial co-infection (73 patients in the severe group and 185 patients in the mild group), the median serum ferritin level of the severe group [976 ng/ml (range 219–3,683.3 ng/ml)] was higher than that of mild [778.4 ng/ml (range 70.1–5,310 ng/ml)]. The median PCT level of the severe group [1.26 ng/ml (range 0.02–12.93 ng/ml)] was higher than that of the mild group [0.99 ng/ml (range 0.08–41.3 ng/ml)]. The median CRP level of the severe group [32.5 mg/l (range 3.11–509.9 mg/l)] was higher than that of the mild group [24.9 mg/l (range 1.25–167 mg/l)], although the difference was not statistically significant.

In the 21 patients with MODS (all in the severe group), the median levels of serum ferritin, PCT, and CRP were 33,070 ng/ml (range 20,691–99,800 ng/ml), 4.13 ng/ml (range 0.26–56 ng/ml), and 49.4 mg/l (range 8.78–127 mg/l), respectively; in the 19 patients with ARDS (all in the severe group), the median levels of serum ferritin, PCT, and CRP were 18,511 ng/ml (range 10,550–99,800 ng/ml), 5.0 ng/ml (range 0.02–82.92 ng/ml), and 55.89 mg/l (range 5.02–145 mg/l), respectively.

The AUC value of serum ferritin for predicting the severity of HFRS was 0.732 (95% CI 0.678–0.786, $p < 0.001$), while PCT and CRP for predicting the severity of HFRS were 0.824 (95% CI 0.773–0.875, $p < 0.001$) and 0.614 (95% CI 0.552–0.676, $p = 0.001$), respectively (**Figure 1** and **Table 3**), showing that PCT and ferritin may be potential biomarkers to predict the severity of HFRS.

Serum Ferritin, Procalcitonin, and C-Reactive Protein Association With Bacterial Co-infection

In 373 patients with HFRS, 115 patients combined bacterial co-infection (37 patients in severe group and 78 patients in mild group). The incidence of secondary bacterial co-infection of patients in the hospital was 30.8%, generally occurring on days 7–10 of the virus infection. The level of serum ferritin in patients with bacterial co-infection was significantly higher than that in patients with non-bacterial co-infection. The median serum ferritin level in 115 patients with bacterial co-infection [2,799.0 ng/ml (range 1,542.8–5,941.7 ng/ml)] was higher than that in 258 patients with non-bacterial co-infection [807.85 ng/ml (range 515.1–1,358.8 ng/ml)] ($p < 0.001$, **Table 3**). The AUC value of serum ferritin for predicting bacterial co-infection was 0.54 (95% CI 0.477–0.602, $p = 0.214$).

Procalcitonin and CRP in patients with bacterial co-infection were significantly higher than those in patients with non-bacterial co-infection (both $p < 0.001$, **Table 4**). The median PCT and CRP levels in 115 patients with bacterial co-infection [2.09 ng/ml (range 0.99–3.6 ng/ml) and 43.2 mg/l (range 20.5–75.3 mg/l)] were higher than those in 258 patients with non-bacterial co-infections [0.99 ng/ml (range 0.63–2.00 ng/ml) and 26.4 mg/l (range 14.2–46.3 mg/l), respectively, both $p < 0.001$] (**Table 4**). The AUC values of PCT and CRP for predicting bacterial co-infection were 0.527 (95% CI 0.464–0.589, $p = 0.401$) and 0.588 (95% CI 0.525–0.652, $p = 0.005$), respectively (**Figure 2** and **Table 5**). These results showed that CRP can be used as a potential biomarker to predict bacterial co-infection in patients with HFRS.

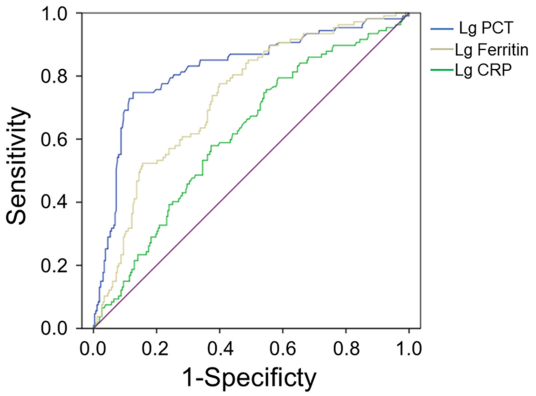

FIGURE 1 | Performance of serum ferritin, PCT, and CRP as predictors of severity by receiver operating characteristics curve analysis. The AUC of serum ferritin = 0.732, the AUC of PCT = 0.824, and the AUC of CRP = 0.614, all $p < 0.01$.

TABLE 3 | Predictive values of parameters for the severity of HFRS*.

Variables	AUC	*p* value	Cut-off value	Sensitivity	Specificity	95% CI for AUC	
						Lower	Upper
Lg PCT	0.824	<0.001	0.45	0.75	0.88	0.773	0.875
Lg CRP	0.614	0.001	1.41	0.76	0.45	0.552	0.676
Lg Ferritin	0.732	<0.001	3.55	0.76	0.60	0.678	0.786

**AUC, area under the receiver operating characteristic curve; CI, confidence interval; Lg PCT, procalcitonin after log10 transformation; Lg CRP, C-reactive protein after log10 transformation; Lg Ferritin, serum ferritin after log10 transformation.*

Serum Ferritin, Procalcitonin, and C-Reactive Protein Association With Patient Survival

Of the 373 patients, 14 patients died of HFRS with a mortality rate of 3.8%. All the non-survivors had a severe hemorrhage, hepatic injury, myocardial damage, and even MODS, and received CRRT treatment and/or respiratory support. The occurrence of ARDS and MODS in non-survivors was significantly higher than those of survivors (both $p < 0.001$, **Table 6**). Non-survivors had a significantly lower PLT, but higher LDH and α-HBDH ($p < 0.001$, **Table 6**).

The levels of serum ferritin, PCT, and CRP in non-survivors were significantly higher compared with survivors (all $p < 0.001$, **Table 6**). The median serum ferritin level of non-survivors [21,708.0 ng/ml (range 14,101.0–36,078.0 ng/ml)] was higher than that in 359 survivors [3,410.0 ng/ml (range 1,456.9–9,028.0 ng/ml)] ($p < 0.001$, **Table 6**). The median PCT [3.6 ng/ml (range 2.2–42.9 ng/ml)] and CRP [50.4 mg/l (range 29.5–100.5 mg/l)] levels of non-survivors was higher than those in 359 survivors [1.7 ng/ml (range 0.9–3.1 ng/ml) and 31.2 mg/l (range 17.6–60.1 mg/l)], respectively ($p < 0.001$, **Table 6**).

The AUC values of serum ferritin, PCT, and CRP for predicting mortality were 0.853 (95% CI 0.774–0.933, $p < 0.001$), 0.737 (95% CI 0.587–0.887, $p = 0.002$), and 0.703 (95% CI 0.577–0.828, $p = 0.008$), respectively (**Figure 3** and **Table 7**), showing that serum ferritin was the best marker to predict mortality of HFRS.

DISCUSSION

This study analyzed the changes of serum ferritin, PCT, and CRP in patients with HFRS and compared their

TABLE 4 | Demographics and clinical and laboratory data at admission in the patients with and without bacterial infection*.

Variables	Non-bacterial infection (*n* = 258)	Bacterial infection (*n* = 115)	*P*-value
Male, n (%)	199 (77.7)	87 (75.7)	0.7550
Age, years	46 (34–54)	48.1 ± 14.3	0.0143
Time from symptom onset to hospital admission, days	5 (4–7)	5 (4–7)	0.3315
Hospital stays, days	7 (5–9)	9 (6–12)	<0.0001
Comorbidity			
Hypertension, n (%)	9 (3.5)	12 (10.4)	0.0072
Coronary heart disease, n (%)	1 (0.4)	3 (2.6)	0.1679
Diabetes, n (%)	5 (1.9)	13 (11.3)	<0.0001
Complication			
Hemorrhage, n (%)	18 (7.0)	87 (75.7)	<0.0001
Hepatic injury, n (%)	171 (66.3)	88 (76.5)	0.0752
Myocardial damage, n (%)	104 (40.3)	52 (45.2)	0.4228
CNS damage	0	1 (0.9)	0.3351
ARDS, n (%)	2 (0.78)	17 (14.8)	<0.0001
MODS, n (%)	0	21 (18.3)	<0.0001
Respiratory support, n (%)	2 (0.8)	33 (28.7)	<0.0001
CRRT, n (%)	20 (7.8)	22 (19.1)	0.0013
Number of death, n (%)	0	14 (12.2)	<0.0001
Parameters			
WBC, × 10^9/L	8.9 (5.5–10.8)	8.3 (4.9–11.2)	0.9748
PLT, × 10^9/L	98.0 (54.0–121.0)	94.5 (50.0–120.0)	0.4762
AST, U/L	98.4 (58.6–183.9)	128.4 (72.1–212.6)	0.0273
ALT, U/L	104.6 (64.0–184.0)	108.0 (74.0–168.0)	0.5610
LDH, U/L	460 (345–657)	489.0 (380.0–765.5)	0.1093
α-HBDH, U/L	333.0 (259.0–496.0)	364.0 (289.0–556.0)	0.0295
PCT, ng/ml	0.99 (0.63–2.00)	2.09 (0.99–3.6)	0.0001
Ferritin, ng/ml	807.85 (515.1–1358.8)	2799.0 (1542.8–5941.7)	0.0001
CRP, mg/l	26.4 (14.2–46.3)	43.2 (20.5–75.3)	0.0001
Lg PCT	−0.004 (−0.2 to 0.3)	0.3 (−0.004 to 0.6)	0.0001
Lg Ferritin	2.9 ± 0.3	3.4 ± 0.4	0.0001
Lg CRP	1.4 ± 0.4	1.6 (1.3–1.9)	0.0001

**ARDS, acute respiratory distress syndrome; MODS, multiple organ dysfunction syndrome; CNS, central nervous system; CRRT, continuous renal replacement therapy; WBC, white blood cell count; PLT, platelet; ALT, alanine transaminase; AST, aspartate aminotransferase; LDH, lactate dehydrogenase; and α-HBDH, α-hydroxybutyrate dehydrogenase; Lg Ferritin, Lg PCT, and Lg CRP, Ferritin, procalcitonin, and CRP after log10 transformation.*

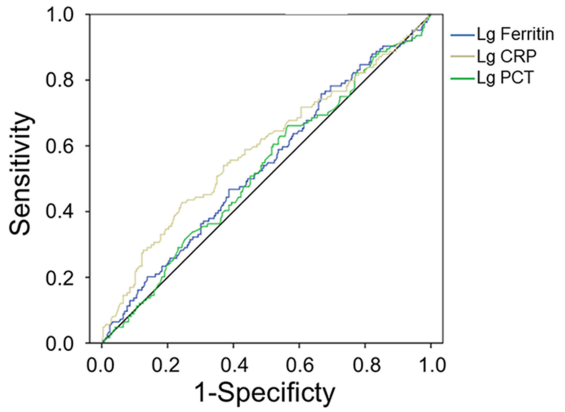

FIGURE 2 | Receiver operating characteristics curve showing the performance of serum ferritin as a predictor of bacterial co-infection. The AUC of serum ferritin = 0.540, the AUC of PCT = 0.527, and the AUC of CRP = 0.588, only $p_{CRP} < 0.01$.

TABLE 5 | Predictive values of parameters for the bacterial infection of HFRS*.

Variables	AUC	*p* value	Cut-off value	Sensitivity	Specificity	95% CI for AUC	
						Lower	Upper
Lg PCT	0.527	0.401	0.16	0.66	0.44	0.464	0.589
Lg CRP	0.588	0.005	1.73	0.43	0.76	0.525	0.652
Lg Ferritin	0.540	0.214	3.32	0.758	0.333	0.477	0.602

**AUC, area under the receiver operating characteristic (ROC) curve; CI, confidence interval; Lg PCT, procalcitonin after log10 transformation; Lg CRP, C-reactive protein after log10 transformation; Lg Ferritin, serum ferritin after log10 transformation.*

clinical significance for the prediction of severity and mortality in patients with HFRS. Results showed that serum ferritin and PCT concentrations have a robust association with severity and mortality of HFRS, which can be used as promising predictors of severity and mortality, and CRP may be an effective biomarker to assess bacterial co-infection in HFRS.

High levels of serum ferritin have been detected in patients of acute viral infections, such as Epstein-Barr virus, human immunodeficiency virus, and dengue virus, and it is associated with the severity and poor prognosis of virus infection (Riera et al., 1994; Mustafa et al., 2001; van de Veerdonk et al., 2012; Soundravally et al., 2015). Serum ferritin is associated with viremia and is significantly elevated in patients with hemorrhagic manifestation and the fatal outcome of the Ebola virus (McElroy et al., 2014; van der Ven et al., 2015). Recent studies have shown that serum ferritin is also a prognostic biomarker that contributes to therapeutic decision-making concerning patients with COVID-19 (Cooper et al., 2020; Kappert et al., 2020). Our results have demonstrated that serum ferritin is a potential biomarker to predict the severity of patients with HFRS, with the cutoff value of 3,548 ng/ml in serum concentration.

Procalcitonin and CRP are considered the most sensitive and effective biomarkers to assess the severity of bacterial co-infection or sepsis (Hu et al., 2017; Cui et al., 2019). Recently, PCT has been reported to be associated with the severity and prognosis of the hantavirus infection (Fan X. et al., 2018) and COVID-19 (Guan et al., 2020; Huang et al., 2020; Lu et al., 2020; Zhang et al., 2020). In the present study, we compared the clinical significance of serum ferritin, PCT, and CRP in patients with HFRS, and found

TABLE 6 | Demographics and clinical and laboratory data at admission in survivors and non-survivors of patients with HFRS*.

Variables	Survivors (n = 359)	Non-survivors (n = 14)	P-value
Male, n (%)	273 (76.0)	13 (92.9)	0.1445
Age, years	46 (35–56)	49 (43–55)	0.5351
Time from symptom onset to hospital admission, days	5 (4–7)	5 (4–7)	0.887
Hospital stays, days	7 (5–10)	13.7 ± 9.0	0.0066
Comorbidity			
Hypertension, n (%)	17 (4.7)	4 (28.6)	0.0047
Coronary heart disease, n (%)	1 (0.3)	3 (21.4)	<0.0001
Diabetes, n (%)	16 (4.5)	2 (14.3)	0.1173
Complication			
Hemorrhage, n (%)	91 (25.3)	14 (100.0)	<0.0001
Hepatic injury, n (%)	245 (68.2)	14 (100.0)	0.0114
Myocardial damage, n (%)	142 (39.6)	14 (100.0)	<0.0001
ARDS, n (%)	7 (1.9)	12 (85.7)	<0.0001
MODS, n (%)	7 (1.9)	14 (100.0)	<0.0001
Respiratory support, n (%)	27 (0.75)	8 (57.1)	<0.0001
CRRT, n (%)	28 (0.78)	14 (100.0)	<0.0001
Parameters			
WBC, × 10^9/L	8.9 (5.3–11.0)	8.3 (4.9–10.3)	0.6899
PLT, × 10^9/L	102 (65–121)	29 (10–60)	0.0001
AST, U/L	101.0 (67.9–182.5)	145.2 (72.7–275.0)	0.1812
ALT, U/L	99.7 (60.0–183.9)	172.0 (86.0–306.1)	0.0458
LDH, U/L	443.0 (348.0–623.0)	1343.1 ± 883.4	<0.0001
α-HBDH, U/L	328.0 (263.0–461.0)	698.0 (377.0–1114.0)	0.0001
PCT, ng/ml	1.7 (0.9–3.1)	3.6 (2.2–42.9)	0.0009
Ferritin, ng/ml	3410.0 (1456.9–9028.0)	21708.0 (14101.0–36078.0)	<0.0001
CRP, mg/l	31.2 (17.6–60.1)	65.0 ± 35.5	0.0055
Lg PCT	0.2 (−0.6 to 0.5)	0.8 ± 0.8	0.0009
Lg Ferritin	3.6 ± 0.6	4.3 ± 0.4	<0.0001
Lg CRP	1.5 (1.3–1.8)	1.7 ± 0.3	0.0054

**ARDS, acute respiratory distress syndrome; MODS, multiple organ dysfunction syndrome; CRRT, continuous renal replacement therapy; WBC, white blood cell count; PLT, platelet; ALT, alanine transaminase; AST, aspartate aminotransferase; LDH, lactate dehydrogenase; and α-HBDH, α-hydroxybutyrate dehydrogenase; Lg Ferritin, Lg PCT, and Lg CRP, Ferritin, procalcitonin, and CRP after log10 transformation.*

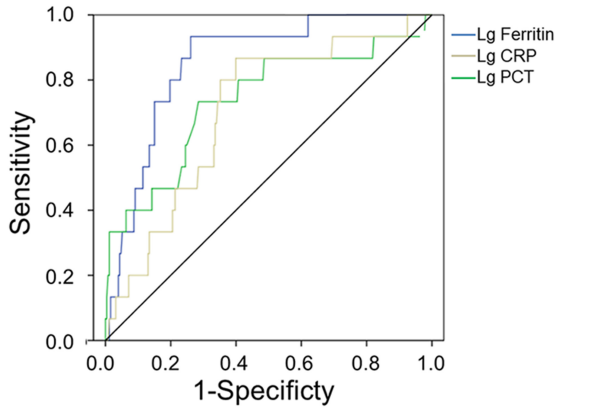

FIGURE 3 | Receiver operating characteristics curve showing the performance of serum ferritin, PCT, and CRP as predictors of mortality. The AUC of serum ferritin = 0.853, the AUC of PCT = 0.737, and the AUC of CRP = 0.703, only $p_{Serumferritin} < 0.001$.

TABLE 7 | Predictive values of parameters for the mortality of HFRS*.

Variables	AUC	p value	Cut-off value	Sensitivity	Specificity	95% CI for AUC	
						Lower	Upper
Lg PCT	0.737	0.002	0.50	0.733	0.715	0.587	0.887
Lg CRP	0.703	0.008	1.62	0.867	0.601	0.577	0.828
Lg Ferritin	0.853	<0.001	4.03	0.933	0.739	0.774	0.933

**AUC, area under the receiver operating characteristic (ROC) curve; CI, confidence interval; Lg PCT, procalcitonin after log10 transformation; Lg CRP, C-reactive protein after log10 transformation; Lg Ferritin, serum ferritin after log10 transformation.*

that they were all associated with mortality, but the serum ferritin had better performance than both PCT and CRP to predict the prognosis of HFRS.

Procalcitonin is also shown to be associated with the severity and prognosis of HFRS, as PCT greater than 2.8 ng/ml suggested a severe virus infection and more than 3.16 ng/ml indicated a very poor prognosis. In patients with HFRS with bacterial co-infection, PCT began to rise in the viremia stage, so PCT is unable to distinguish between viral and bacterial co-infections. In contrast, the level of CRP was normally or slightly elevated in hantavirus infection, but it was significantly increased in patients with HFRS with bacterial co-infection, which was related to the severity of infection and prognosis. Therefore, it can be used in the evaluation of bacterial co-infection and prognosis in patients with HFRS.

CONCLUSION

The study showed that serum ferritin and PCT have a robust association with the severity and mortality of HFRS, which can be used as a promising predictor of severity and mortality in rodent-borne disease. CRP may be an effective biomarker to assess bacterial co-infection in HFRS.

DATA AVAILABILITY STATEMENT

The original contributions presented in the study are included in the article/supplementary material, further inquiries can be directed to the corresponding author/s.

ETHICS STATEMENT

The studies involving human participants were reviewed and approved by the Ethics Committee of The First Hospital of

Jilin University. The patients/participants provided their written informed consent to participate in this study.

AUTHOR CONTRIBUTIONS

LC and QL conceived the project. LC planned the study. ND, LL, YZ, and KZ collected the data. LC, ZW, and QL analyzed the data and drafted the manuscript. All authors were involved in critically revising the manuscript and approving the final version.

FUNDING

This study was supported by the Science and Technology Innovation Project in Foshan, Guangdong Province, China (2020001000151).

REFERENCES

Barut, S., Dincer, F., Sahin, I., Ozyurt, H., Akkus, M., and Erkorkmaz, U. (2010). Increased serum ferritin levels in patients with Crimean-Congo hemorrhagic fever: can it be a new severity criterion? *Int. J. Infect. Dis.* 14, e50–e54. doi: 10.1016/j.ijid.2009.03.009

Brocato, R. L., and Hooper, J. W. (2019). Progress on the prevention and treatment of Hantavirus disease. *Viruses* 11:610. doi: 10.3390/v11070610

Cooper, I. D., Crofts, C. A. P., DiNicolantonio, J. J., Malhotra, A., Elliott, B., Kyriakidou, Y., et al. (2020). Relationships between hyperinsulinaemia, magnesium, vitamin D, thrombosis and COVID-19: rationale for clinical management. *Open Heart* 7:e001356. doi: 10.1136/openhrt-2020-001356

Cui, N., Zhang, H., Chen, Z., and Yu, Z. (2019). Prognostic significance of PCT and CRP evaluation for adult ICU patients with sepsis and septic shock: retrospective analysis of 59 cases. *J. Int. Med. Res.* 47, 1573–1579. doi: 10.1177/0300060518822404

Du, H., Wang, P. Z., Li, J., Bai, L., Li, H., Yu, H. T., et al. (2014). Clinical characteristics and outcomes in critical patients with hemorrhagic fever with renal syndrome. *BMC Infect. Dis.* 14:191. doi: 10.1186/1471-2334-14-191

Escutenaire, S., and Pastoret, P. P. (2000). Hantavirus infections. *Rev. Sci. Tech.* 19, 64–78. doi: 10.20506/rst.19.1.1209

Fan, E., Brodie, D., and Slutsky, A. S. (2018). Acute respiratory distress syndrome: advances in diagnosis and treatment. *JAMA* 319, 698–710. doi: 10.1001/jama.2017.21907

Fan, X., Deng, H., Sang, J., Li, N., Zhang, X., Han, Q., et al. (2018). High serum procalcitonin concentrations in patients with hemorrhagic fever with renal syndrome caused by Hantaan virus. *Front. Cell. Infect. Microbiol.* 8:129. doi: 10.3389/fcimb.2018.00129

Franco-Martinez, L., Ceron, J. J., Vicente-Romero, M. R., Bernal, E., Torres Cantero, A., Tecles, F., et al. (2021). Salivary ferritin changes in patients with COVID-19. *Int. J. Environ. Res. Public. Health.* 19:41. doi: 10.3390/ijerph19010041

Guan, W. J., Ni, Z. Y., Hu, Y., Liang, W. H., Ou, C. Q., He, J. X., et al. (2020). Clinical characteristics of Coronavirus disease 2019 in China. *N. Engl. J. Med.* 382, 1708–1720. doi: 10.1056/nejmoa2002032

Hu, L., Shi, Q., Shi, M., Liu, R., and Wang, C. (2017). Diagnostic value of PCT and CRP for detecting serious bacterial co-infections in patients with fever of unknown origin: a systematic review and meta-analysis. *Immunohistochem. Mol. Morphol.* 25, e61–e69. doi: 10.1097/PAI.0000000000000552

Huang, C., Wang, Y., Li, X., Ren, L., Zhao, J., Hu, Y., et al. (2020). Clinical features of patients infected with 2019 novel coronavirus in Wuhan, China. *Lancet* 395, 497–506. doi: 10.1016/S0140-6736(20)30183-5

Jonsson, C. B., Figueiredo, L. T., and Vapalahti, O. (2010). A global perspective on hantavirus ecology, epidemiology, and disease. *Clin. Microbiol. Rev.* 23, 412–441. doi: 10.1128/CMR.00062-09

Kappert, K., Jahic, A., and Tauber, R. (2020). Assessment of serum ferritin as a biomarker in COVID-19: bystander or participant? Insights by comparison with other infectious and non-infectious diseases. *Biomarkers.* 25, 616–625. doi: 10.1080/1354750X.2020.1797880

Kyriazopoulou, E., Leventogiannis, K., Norrby-Teglund, A., Dimopoulos, G., Pantazi, A., Orfanos, S. E., et al. (2017). Macrophage activation-like syndrome: an immunological entity associated with rapid progression to death in sepsis. *BMC Med.* 15:172. doi: 10.1186/s12916-017-0930-5

Liu, F., Li, L., Xu, M., Wu, J., Luo, D., Zhu, Y., et al. (2020). Prognostic value of interleukin-6, C-reactive protein, and procalcitonin in patients with COVID-19. *J. Clin. Virol.* 127:104370. doi: 10.1016/j.jcv.2020.104370

Liu, Z., Zhao, Q., Han, Q., Gao, M., and Zhang, N. (2008). Serum thrombospondin-1 is altered in patients with hemorrhagic fever with renal syndrome. *J. Med. Virol.* 80, 1799–1803. doi: 10.1002/jmv.21270

Lu, R., Zhao, X., Li, J., Niu, P., Yang, B., Wu, H., et al. (2020). Genomic characterisation and epidemiology of 2019 novel coronavirus: implications for virus origins and receptor binding. *Lancet.* 395, 565–574. doi: 10.1016/S0140-6736(20)30251-8

McElroy, A. K., Erickson, B. R., Flietstra, T. D., Rollin, P. E., Nichol, S. T., Towner, J. S., et al. (2014). Ebola hemorrhagic Fever: novel biomarker correlates of clinical outcome. *J. Infect. Dis.* 210, 558–566. doi: 10.1093/infdis/jiu088

Mustafa, A. S., Elbishbishi, E. A., Agarwal, R., and Chaturvedi, U. C. (2001). Elevated levels of interleukin-13 and IL-18 in patients with dengue hemorrhagic fever. *FEMS Immunol. Med. Microbiol.* 30, 229–233. doi: 10.1111/j.1574-695X.2001.tb01575.x

Pan, F., Yang, L., Li, Y., Liang, B., Li, L., Ye, T., et al. (2020). Factors associated with death outcome in patients with severe coronavirus disease-19 (COVID-19): a case-control study. *Int. J. Med. Sci.* 17, 1281–1292. doi: 10.7150/ijms.46614

Ramirez, M. (2013). Multiple organ dysfunction syndrome. *Curr. Probl. Pediatr. Adolesc. Health Care* 43, 273–277. doi: 10.1016/j.cppeds.2013.10.003

Riera, A., Gimferrer, E., Cadafalch, J., Remacha, A., and Martin, S. (1994). Prevalence of high serum and red cell ferritin levels in HIV-infected patients. *Haematologica.* 79, 165–167.

Shin, J. H., Yu, E., Kim, E. N., and Kim, C. J. (2018). C-reactive protein overexpression in the background liver of hepatitis B virus-associated hepatocellular carcinoma is a prognostic biomarker. *J. Pathol. Transl. Med.* 52, 267–274. doi: 10.4132/jptm.2018.07.14

Soundravally, R., Agieshkumar, B., Daisy, M., Sherin, J., and Cleetus, C. C. (2015). Ferritin levels predict severe dengue. *Infection.* 43, 13–19. doi: 10.1007/s15010-014-0683-4

Tjendra, Y., Al Mana, A. F., Espejo, A. P., Akgun, Y., Millan, N. C., Gomez-Fernandez, C., et al. (2020). Predicting disease severity and outcome in COVID-19 patients: a review of multiple biomarkers. *Arch. Pathol. Lab. Med.* 144, 1465–1474. doi: 10.5858/arpa.2020-0471-SA

Valero, N., Mosquera, J., Torres, M., Duran, A., Velastegui, M., Reyes, J., et al. (2019). Increased serum ferritin and interleukin-18 levels in children with dengue. *Braz. J. Microbiol.* 50, 649–656. doi: 10.1007/s42770-019-00105-2

van de Veerdonk, F. L., Wever, P. C., Hermans, M. H., Fijnheer, R., Joosten, L. A., van der Meer, J. W., et al. (2012). IL-18 serum concentration is markedly elevated in acute EBV infection and can serve as a marker for disease severity. *J. Infect. Dis.* 206, 197–201. doi: 10.1093/infdis/jis335

van der Ven, A. J., Netea, M. G., van der Meer, J. W., and de Mast, Q. (2015). Ebola virus disease has features of hemophagocytic lymphohistiocytosis syndrome. *Front. Med.* 2:4. doi: 10.3389/fmed.2015.00004

Wang, P. Z., Li, Z. D., Yu, H. T., Zhang, Y., Wang, W., Jiang, W., et al. (2012). Elevated serum concentrations of inflammatory cytokines and chemokines in patients with haemorrhagic fever with renal syndrome. *J. Int. Med. Res.* 40, 648–656. doi: 10.1177/147323001204000227

Zhang, J. J., Cao, Y. Y., Tan, G., Dong, X., Wang, B. C., Lin, J., et al. (2021). Clinical, radiological, and laboratory characteristics and risk factors for severity and mortality of 289 hospitalized COVID-19 patients. *Allergy.* 76, 533–550. doi: 10.1111/all.14496

Zhang, J. J., Dong, X., Cao, Y. Y., Yuan, Y. D., Yang, Y. B., Yan, Y. Q., et al. (2020). Clinical characteristics of 140 patients infected with SARS-CoV-2 in Wuhan, China. *Allergy* 75, 1730–1741. doi: 10.1111/all.14238

Zhang, Y., Ma, Y., Zhang, C., Zhang, Y., Zhuang, R., Liu, B., et al. (2015). Soluble scavenger receptor CD163 is associated with severe acute kidney injury in patients with Hantaan virus infection. *Viral. Immunol.* 28, 241–246. doi: 10.1089/vim.2014.0112

Zhang, Y. Z., Zou, Y., Fu, Z. F., and Plyusnin, A. (2010). Hantavirus infections in humans and animals, China. *Emerg. Infect. Dis.* 16, 1195–1203. doi: 10.3201/eid1608.090470

Zhou, J., Zhou, J., Wu, Z. Q., Goyal, H., and Xu, H. G. (2021). Ferritin index is a strong prognostic marker in adult hemophagocytic lymphohistiocytosis. *Int. J. Clin. Pract.* 75:e13704. doi: 10.1111/ijcp.13704

Zhou, Y. Z., Teng, X. B., Han, M. F., Shi, J. F., Li, C. X., Zhang, X. H., et al. (2021). The value of PCT, IL-6, and CRP in the early diagnosis and evaluation of COVID-19. *Eur. Rev. Med. Pharmacol. Sci.* 25, 1097–1100. doi: 10.26355/eurrev_202101_24680

Conflict of Interest: The authors declare that the research was conducted in the absence of any commercial or financial relationships that could be construed as a potential conflict of interest.

frontiers | Frontiers in Microbiology

ORIGINAL RESEARCH
published: 24 May 2022
doi: 10.3389/fmicb.2022.896965

Clinical Characteristics of Immune Response in Asymptomatic Carriers and Symptomatic Patients With COVID-19

Entao Li[1†], Shen Wang[1†], Wenwen He[1,2], Jun He[3], Luogeng Liu[2], Xiaotuan Zhang[2], Songtao Yang[1], Feihu Yan[1], Yuwei Gao[1*], Bin Liu[2*] and Xianzhu Xia[1]*

[1] Key Laboratory of Jilin Province for Zoonosis Prevention and Control, Changchun Veterinary Research Institute, Chinese Academy of Agricultural Sciences, Changchun, China, [2] Department of Laboratory Medicine, The Second Affiliated Hospital, University of South China, Hengyang, China, [3] Department of Laboratory Medicine, Nanhua Hospital, University of South China, Hengyang, China

OPEN ACCESS

Edited by:
Quan Liu,
Foshan University, China

Reviewed by:
Binod Rayamajhee,
University of New South Wales, Australia
Bochao Liu,
Guangzhou Blood Center, China

***Correspondence:**
Feihu Yan
yanfh1990@163.com
Yuwei Gao
yuwei0901@outlook.com
Bin Liu
llbb520@aliyun.com

[†] These authors have contributed equally to this work

Specialty section:
This article was submitted to Infectious Agents and Disease, a section of the journal Frontiers in Microbiology

Received: 15 March 2022
Accepted: 12 April 2022
Published: 24 May 2022

Citation:
Li E, Wang S, He W, He J, Liu L, Zhang X, Yang S, Yan F, Gao Y, Liu B and Xia X (2022) Clinical Characteristics of Immune Response in Asymptomatic Carriers and Symptomatic Patients With COVID-19. Front. Microbiol. 13:896965. doi: 10.3389/fmicb.2022.896965

The pandemic of coronavirus disease 2019 (COVID-19) has emerged as a major public health challenge worldwide. A comprehensive understanding of clinical characteristics and immune responses in asymptomatic carriers and symptomatic patients with COVID-19 is of great significance to the countermeasures of patients with COVID-19. Herein, we described the clinical information and laboratory findings of 43 individuals from Hunan Province, China, including 13 asymptomatic carriers and 10 symptomatic patients with COVID-19, as well as 20 healthy controls in the period from 25 January to 18 May 2020. The serum samples of these individuals were analyzed to measure the cytokine responses, receptor-binding domain (RBD), and nucleocapsid (N) protein-specific antibody titers, as well as SARS-CoV-2 neutralizing antibodies (nAbs). For cytokines, significantly higher Th1 cytokines including IL-2, IL-8, IL-12p70, IFN-γ, and TNF-α, as well as Th2 cytokines including IL-10 and IL-13 were observed in symptomatic patients compared with asymptomatic carriers. Compared with symptomatic patients, higher N-specific IgG4/IgG1 ratio and RBD-specific/N-specific IgG1 ratio were observed in asymptomatic carriers. Comparable nAbs were detected in both asymptomatic carriers and symptomatic patients with COVID-19. In the symptomatic group, nAbs in patients with underlying diseases were weaker than those of patients without underlying diseases. Our retrospective study will enrich and verify the clinical characteristics and serology diversities in asymptomatic carriers and symptomatic patients with COVID-19.

Keywords: COVID-19, SARS-CoV-2, asymptomatic carriers, serology, cytokine, antibody

INTRODUCTION

Over the past 20 years, there have been two waves of betacoronavirus emerging, including severe acute respiratory syndrome CoV (SARS-CoV) in 2003 (Peiris et al., 2003) and Middle East respiratory syndrome CoV (MERS-CoV) in 2012 (Zaki et al., 2012). In December 2019, another betacoronavirus causing human pneumonia emerged and soon was isolated (Zhu et al., 2020). The etiologic agent was renamed severe acute respiratory syndrome coronavirus 2 (SARS-CoV-2), and the infection was named coronavirus disease 2019 (COVID-19) by the [World Health Organization WHO (WHO, 2020)]. As of 25 February 2022, SARS-CoV-2 had spread to 212 countries and regions, causing over 428 million infected cases and more than 5.91 million deaths across the

globe (WHO, 2022a). The COVID-19 pandemic has seriously threatened public health safety and attacked the global economy.

Coronavirus disease 2019 is clinically characterized by fever, cough, acute respiratory distress syndrome (ARDS), and in some cases, death (Chen et al., 2020; Guan et al., 2020). Patients with COVID-19 present a broad spectrum of clinical presentation, including asymptomatic, mild, moderate, severe, and critical cases. According to a meta-analysis covering 29,776,306 individuals from January 2020 to February 2021, asymptomatic carriers account for 40.50% of all confirmed population (95% CI, 33.50–47.50%) (Ma et al., 2021). Besides, undergoing a mutate period from B.1.1.7 (Alpha), B.1.351 (Beta), P.1 (Gamma), and B.1.617.2 (Delta) to B.1.1.529 (Omicron), SARS-CoV-2 variants appeared to be more contagious and less pathogenicity, especially the currently global disseminated Omicron variant (Lewnard et al., 2022; WHO, 2022b). Compared with symptomatic patients with COVID-19, asymptomatic carriers exhibit a longer median length of viral shedding, weaker nAbs, and faster nAb decrease (Long et al., 2020). Moreover, transmission from asymptomatic carriers was estimated to account for more than half of all transmission, of which children and females are more likely to present as asymptomatic COVID-19 carriers (Johansson et al., 2021; Syangtan et al., 2021).

Some studies have attempted to elucidate the difference in immune response and other clinical characteristics between asymptomatic carriers and symptomatic patients with COVID-19 from different points of view (Liu et al., 2020, 2021; Long et al., 2020; Wang Y. et al., 2020; Wu et al., 2020; Zhou et al., 2020; Cai et al., 2021; Tutukina et al., 2021), including complete blood count, neutrophil-to-lymphocyte ratio, kidney function indicators, viral loads, and anti-RBD/anti-N antibody ratio, as well as other risk factors. Among them, an indicator of the neutralization potency of anti-RBD antibody quality has been established, and it revealed that high potency was a predictor of survival (Garcia-Beltran et al., 2021). Nevertheless, few consensuses have been achieved in terms of the intuitive and quantifiable indicators between asymptomatic carriers and symptomatic patients. Additional and specialized immunological analysis is required to better recognize the differences between these two groups.

In this study, we described the clinical characteristics and immune responses, including cytokine levels and SARS-CoV-2-specific antibodies, as well as nAbs in 13 asymptomatic carriers and 10 symptomatic patients with COVID-19. Longitudinal comparisons of immune response between asymptomatic carriers and symptomatic patients provide information and assist in the risk stratification and triage of patients with COVID-19, supporting the clinical diagnosing, prevention, and treatment of COVID-19.

MATERIALS AND METHODS

Study Subjects

From 25 January to 18 May 2020, 23 individuals were enrolled and admitted to The Second Affiliated Hospital of Nanhua University (Hengyang, China), including 13 asymptomatic carriers and 10 symptomatic patients with COVID-19, and the serum samples were harvested on admission. Besides, 20 healthy volunteers from physical examination centers were involved, and the sera were collected as healthy controls in the same period. Clinical pathological data on patients with COVID-19 were retrieved from the electronic medical records. Individuals who tested positive for SARS-CoV-2 nucleic acids but did not exhibit symptoms were identified as asymptomatic carriers. Symptomatic patients were defined as those who tested positive for SARS-CoV-2 nucleic acids and accompanied by symptoms including fever, cough, fatigue, chest discomfort, sore throat, hyposmia, and rhinobyon. All the test results of SARS-CoV-2 nucleic acids were negative for the healthy human controls. The study protocol was approved by the Ethics Committee in the hospital, with informed consent waived for public health outbreak investigations.

Laboratory and Chest Imaging Examination

Laboratory examination and chest CT imaging of 10 symptomatic patients with COVID-19 were involved in the previous study (Chung et al., 2020; Wang D. et al., 2020; Cai et al., 2021). The routine blood test was performed using Sysmex XN-3000, and detection panels include neutrophils, lymphocytes, monocytes, red blood cells (RBCs), hemoglobin, platelets (PLTs), and white blood cells (WBCs). The blood chemistry test was conducted with Cobas 8000, and liver function indexes include total bile acid (TBA), aspartate aminotransferase (AST), alanine aminotransferase (ALT), total bilirubin (TB), and direct bilirubin (DB); myocardial enzyme indexes include creatine kinase (CK), CK isoenzyme (CK-MB), and isozyme (MB); renal function indexes include blood urea nitrogen (BUN) and serum creatinine (SCr). Chest CT scans were performed by GE Discovery CT750 HD.

Cytokine Analyses

Serum samples from the 13 asymptomatic carriers and 10 symptomatic patients with COVID-19 were involved to detect the cytokine levels by the Meso Scale Discovery (MSD) detection technology according to the manufacturer's instruction as in the previous study (Cillo et al., 2021; Karaba et al., 2022). For the economy, 12 samples were randomly selected from 20 healthy controls for cytokine detection. Preparation of standard antigen is as follows: add 1 ml of diluent 2 to the standard antigen, shake and mix fully, place it at room temperature for 15–20 min, dilute it four times successively, and 7 standards and 1 blank sample should be prepared; preparation of antibody diluent is as follows: 60 μl of specific antibody was diluted to 3 ml with diluent 3; preparation of wash buffer is as follows: 1 × phosphate-buffered saline (PBS) (with 0.05% Tween-20); preparation of plate reading buffer is as follows: configure 2 × plate reading buffer; after three washes of the MSD plate with 150 μl wash buffer, 50 μl sample or standard antigen was added to each well, followed by incubation at room temperature for 2 h. After three washes, 25 μl detection antibodies were added and incubated at room temperature for 2 h. Finally, 150 μl of the plate reading buffer was added to each

well. Data were acquired on the MESO QuickPlex SQ 120. Sample concentrations for each marker were then calculated based on the respective standard curve.

SARS-CoV-2 Specific Antibody Detection

The SARS-CoV-2 specific antibody level of 13 asymptomatic carriers and 10 symptomatic patients with COVID-19 were detected. Binding antibodies against the SARS-CoV-2 RBD and N protein were detected using an enzyme-linked immunosorbent assay (ELISA).

Antibody Subtype Detection

Serum samples were subjected to an ELISA for N and RBD-specific IgE, IgM, IgG, IgG1, IgG2a, IgG3, and IgG4 antibody detection as in the previous study (Jiang et al., 2021; Yan et al., 2022). First, 96-well microtiter plates (Corning-Costar, Corning, NY, United States) were coated overnight at 4°C with recombinant SARS-CoV-2 N or RBD protein from SARS-CoV-2 Wuhan-Hu-1 strain (NCBI accession no. NC_045512.2) using baculovirus-insect cells (Sino Biological, Beijing, China) at 1 μg/ml. Following three PBST washes and blocking for 2 h at 37°C with PBS containing 3% bovine serum albumin (BSA), the plates were incubated with 1:200 dilutions of samples in PBS containing 0.5% (w/v) BSA at 37°C for 1 h. After another three washes with PBST, the plates were incubated at 37°C for 1 h with the following HRP-labeled goat antibodies: anti-human IgM (1:2,000; Southern Biotech, Birmingham, AL, United States) and anti-human IgG (1:5,000; Bioworld Technology, Inc., St. Louis Park, MN, United States); HRP-labeled mouse antibodies: anti-human IgE (1:5,000; Southern Biotech, Birmingham, AL, United States), anti-human IgG1 (1:5,000; Southern Biotech), anti-human IgG2 (1:5,000; Southern Biotech), anti-human IgG3 (1:5,000; Southern Biotech), and anti-human IgG4 (1:5,000; Southern Biotech). After the final three washes, 100 μl tetramethylbenzidine (TMB) substrate was added to each well, and the color development was stopped with 50 μl/well H_2SO_4 for plate reading at 450 nm (Bio-Rad, Hercules, CA, United States).

IgG Detection

Notably, 96-well microtiter plates (Corning-Costar, Corning, NY, United States) were coated overnight at 4°C with recombinant RBD protein at 1 μg/ml. Following three PBST washes and blocking for 2 h at 37°C with PBS containing 3% BSA, the plates were incubated with 1:80-1:163,840 dilutions of samples in PBS containing 0.5% (w/v) BSA at 37°C for 1 h. After another three PBST washes, the plates were incubated at 37°C for 1 h with the following HRP-labeled goat anti-human IgG antibodies (1:5,000; Bioworld Technology, Inc., St. Louis Park, MN, United States). After the final three washes, 100 μl TMB substrate was added to each well, and the color development was stopped with 50 μl/well H_2SO_4 for plate reading at 450 nm (Bio-Rad, Hercules, CA, United States).

Neutralizing Antibody Detection

The nAb test of 10 symptomatic patients with COVID-19, 13 asymptomatic carriers, and 20 healthy controls was detected following the method of our previous study (Yan et al., 2022). All sera were heat-inactivated at 56°C for 30 min, then diluted in 96-well plates with 2-fold serial dilutions (from 1:20 to 1:40,960), mixed with 100 $TCID_{50}$ of SARS-CoV-2 (Beta-Cov/Wuhan/AMMS01/2020), and incubated at 37°C, 5% CO_2 for 1 h. Vero E6 cells were mixed with the virus-serum mixture in a volume of 50 μl/well. The virus mixture without serum and blank cells served as the control. Plates were incubated at 37°C, 5% CO_2 for 48 h. The nAb titer of each sample was the reciprocal of the serum dilution that protected cells from cytopathic effect (CPE).

Statistical Analyses

GraphPad Prism 8.0 software (GraphPad Software Inc., San Diego, CA, United States) was used to analyze the data, which are expressed as the mean ± standard error of the mean (SEM). Significant differences between groups were determined using one-way ANOVA. $P < 0.05$ was considered statistically significant.

RESULTS

Basic Information and Clinical Manifestation

The gender, age, underlying diseases, clinical symptoms, and computed tomography (CT) imaging information of 10 symptomatic patients were summarized in **Figure 1**. In symptomatic patients, 70% (7/10) men and 30% (3/10) women were included. Elderly people (51–76 years old) account for 80% (8/10) of all symptomatic patients, while young people (21–50 years old) account for 20% (2/10), with a median age of 57.6 years (21–76 years old). Underlying diseases were recorded in 60% (6/10) individuals in symptomatic patients, including hypertension, chronic bronchitis, type 2 diabetes, and coronary disease. Patients with COVID-19 exhibited manifestations of viral pneumonia including fever (seen in 100% of patients), cough (seen in 100% of patients), and chest discomfort. Multiple ground glass shadows and interstitial lesions were frequently observed in lung lesions by CT. Typical CT imaging of symptomatic patients and asymptomatic carriers with COVID-19 is shown in **Figure 2**. The above results indicated that men and elderly people with underlying diseases are the main risk factors for patients with COVID-19; among them, cough, fever, and multiple ground glass shadows were predominant clinical characteristics of symptomatic patients with COVID-19.

Body Temperature and Hematology Parameters of Symptomatic Patients With COVID-19

Body temperature and hematology parameters of 10 symptomatic patients with COVID-19 were recorded. As shown in **Supplementary Figure 1**, a rise in body temperature was observed in 90% (9/10) of patients on admission. The temperature of all patients fluctuated and returned to the normal range after 7 days following hospitalization

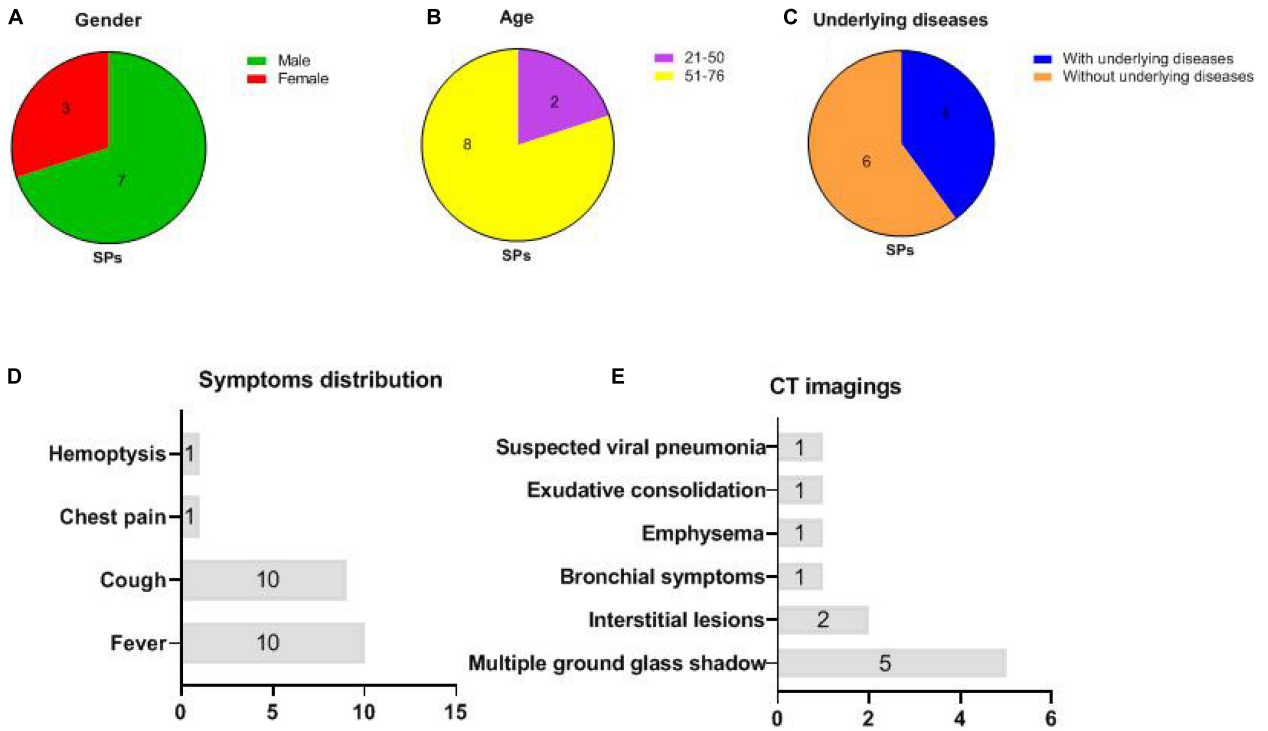

FIGURE 1 | Basic information and clinical manifestations of 10 symptomatic patients (SPs) (same abbreviations in subsequent figures). **(A)** Gender distributions of SPs: 3 women and 7 men. **(B)** Age distributions of SPs: 8 individuals were between 51 and 76 while 2 individuals were between 21 and 50 years old. **(C)** 4 SPs with underlying diseases, whereas 6 SPs without underlying disease were recorded. **(D)** Distributions of clinical symptoms in SPs: fever (10/10) and cough (10/10) were the most frequently recorded. **(E)** CT imaging: multiple ground glass shadows were seen in 50% (5/10) individuals; interstitial lesions, bronchial symptoms, emphysema, exudative consolidation, and suspected viral pneumonia were recorded.

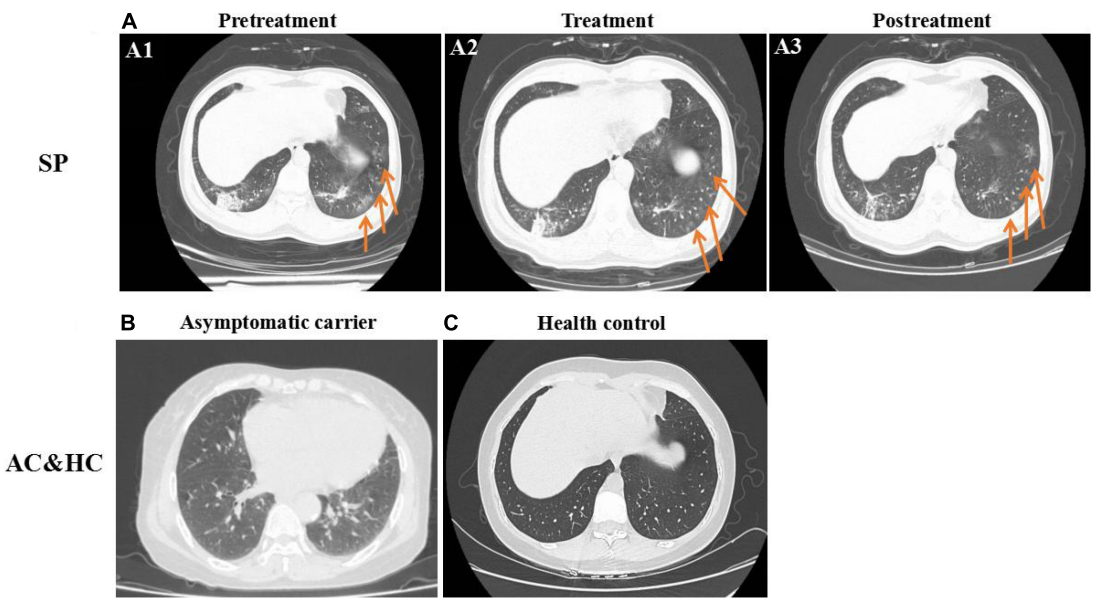

FIGURE 2 | Typical chest CT imaging in SPs, asymptomatic carriers (ACs), and healthy controls (HCs) (same abbreviations in subsequent figures). **(A)** CT imaging in SPs. **(A1)** Pretreatment. **(A2)** Treatment. **(A3)** Posttreatment. **(B)** CT imaging in ACs. **(C)** CT imaging in HCs. Bilateral pneumonia and multiple ground glass shadows were obvious in SPs and were marked with arrows **(A1–A3)**, whereas pulmonary lesions in ACs **(B)** were not obvious compared with the control **(C)**.

(**Supplementary Figure 1A**). On admission, 60% (6/10) of patients exhibited neutrophils above the normal range, which returned to normal after treatment (**Supplementary Figure 1B**). Lymphocytopenia was observed in 80% (8/10) of patients and returned to normal posttreatment (**Supplementary Figure 1C**). The patients with mononuclear cells above the normal range account for 20% (2/10) before treatment. During the treatment period, the monocytes of 30% (3/10) patients showed large fluctuations, but in the end, the monocytes of all patients returned to their normal range (**Supplementary Figure 1D**). The RBCs, hemoglobin, PLTs, and WBCs were relatively stable during the disease course (**Supplementary Figures 1E–H**). The above results indicated that increased neutrophil counts and lymphocytopenia are the most frequently observed parameters in symptomatic patients with COVID-19, accompanied by increased mononuclear cells.

Blood Biochemical of Symptomatic Patients With COVID-19

Blood biochemical indicators of 10 symptomatic patients with COVID-19 are summarized in **Supplementary Figure 2**. For liver function (**Supplementary Figure 2A**), elevated TBA, AST, ALT, and DB levels were observed in 10% (1/10), 10% (1/10), 20% (2/10), and 20% (2/10) patients, respectively (**Supplementary Figure 2A**). Abnormal TB was not observed. For renal function (**Supplementary Figure 2B**), Cre and BUN of all individuals were in the normal range. For heart function (**Supplementary Figure 2C**), 20% (2/10) of patients exhibited elevated MB. CK and CK-MB were in the normal range in all symptomatic patients. Consequently, elevated liver function indicators such as ALT and DB levels are more obvious in symptomatic patients with COVID-19.

Cytokine Measurement

Cytokine detection results of interleukin-1β (IL-1β), IL-2, IL-4, IL-6, IL-8, IL-10, IL-12p70, IL-13, interferon-gamma (IFN-γ), and tumor necrosis factor-alpha (TNF-α) in asymptomatic carriers, symptomatic patients, and healthy controls are summarized in **Figure 3**. Of which IL-1β, IL-2, IL-8, IL-12p70, IFN-γ, and TNF-α are Th1 cytokines, while IL-4, IL-6, IL-10, IL-13 are Th2 cytokines. For Th1 cytokines, significantly higher IL-2, IL-12p70 ($P < 0.01$) as well as IL-8, IFN-γ, and TNF-α ($P < 0.05$) levels were observed in symptomatic patients compared with asymptomatic carriers (**Figures 3B,E,G,I,J**). For Th2 cytokines, significantly higher IL-10 and IL-13 were observed in symptomatic patients compared with asymptomatic carriers ($P < 0.05$) (**Figures 3F,H**). No obvious difference was observed among the above-mentioned three groups regarding IL-1β, IL-4, and IL-6 levels (**Figures 3A,C,D**). The above results showed that the cytokine levels are much higher in symptomatic patients than those in asymptomatic carriers, relating to clinical symptoms.

Antibody Responses

To better understand the antibody responses in serum from symptomatic patients and asymptomatic carriers, the IgE, IgM, IgG, IgG1, IgG2, IgG3, and IgG4 antibody responses against the N and RBD proteins of SARS-CoV-2 were detected by ELISA (**Figure 4**). No significant differences in IgE antibody levels were observed among symptomatic patients, asymptomatic

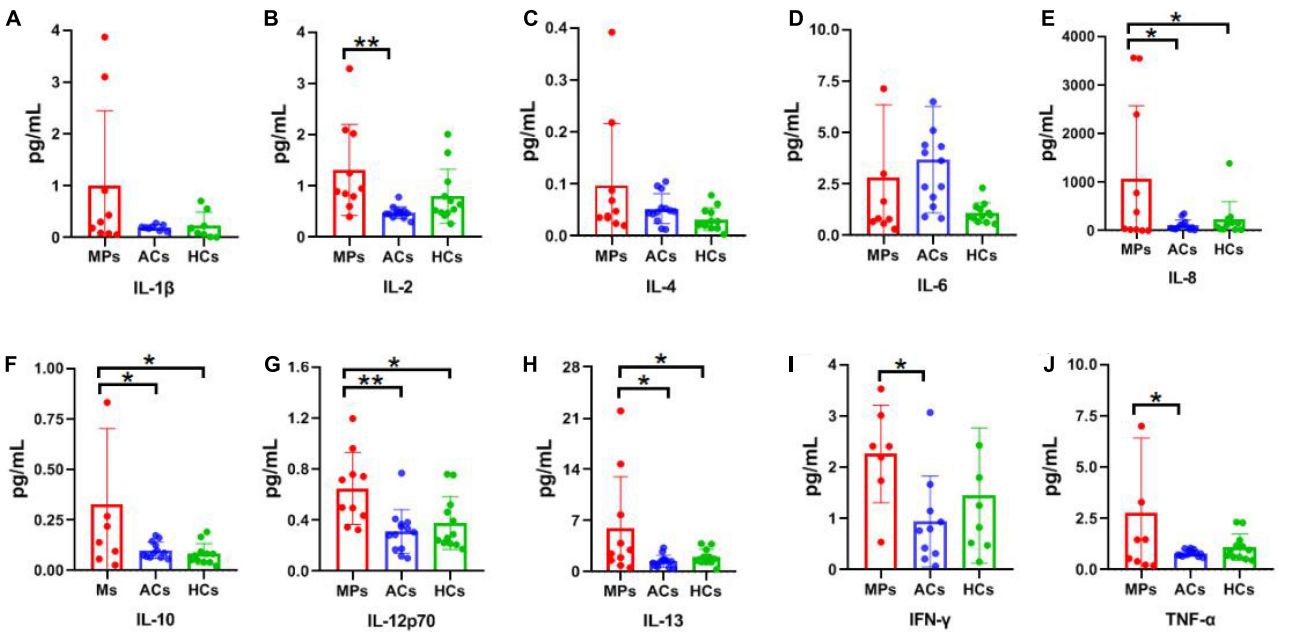

FIGURE 3 | Cytokine detection results of SPs, ACs, and HCs. Red, blue, and green columns refer to SPs (10 individuals), ACs (13 individuals), and HCs (12 individuals), respectively. Unit: pg/ml. **(A)** IL-1β. **(B)** IL-2. **(C)** IL-4. **(D)** IL-6. **(E)** IL-8. **(F)** IL-10. **(G)** IL-12p70. **(H)** IL-13. **(I)** IFN-γ. **(J)** TNF-α. Data are presented as means ± SEM. $^{*}P < 0.05$, $^{**}P < 0.01$.

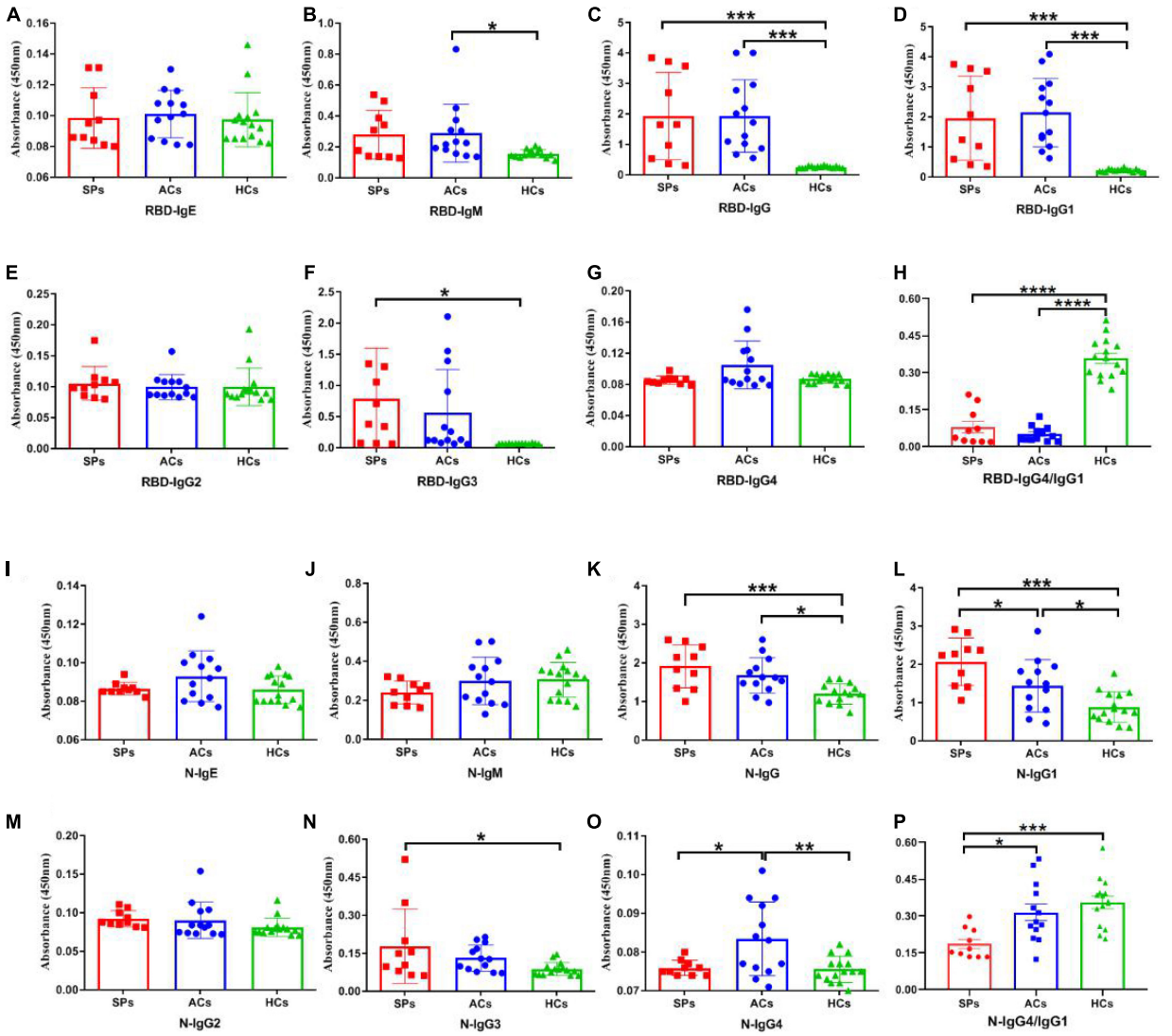

FIGURE 4 | SARS-CoV-2 RBD and N-specific binding antibodies in SPs, ACs, and HCs. IgE, IgM, IgG, IgG1, IgG2, IgG3, and IgG4 antibody RBD protein of SARS-CoV-2 were detected in sera **(A–G)**. IgE, IgM, IgG, IgG1, IgG2, IgG3, and IgG4 antibody against N protein of SARS-CoV-2 were detected in sera **(I–O)**. The ratio of IgG4/IgG1 against RBD and N protein of SARS-CoV-2 in SPs and ACs were summarized **(H,P)**. Data are presented as means ± SEM. *$P < 0.05$, **$P < 0.01$,***$P < 0.001$, ****$P < 0.0001$.

carriers, and healthy controls (**Figures 4A,I**). The RBD-targeting IgM antibody in symptomatic patients was significantly higher than that in asymptomatic carriers ($P < 0.05$) (**Figure 4B**). Significantly higher RBD-targeting IgG titers were observed in both symptomatic and asymptomatic groups compared with the healthy controls ($P < 0.001$), whereas more obvious increased N-targeting IgG was exhibited in the symptomatic group ($P < 0.001$) than that of the asymptomatic group ($P < 0.05$) (**Figures 4C,K**). Antibody subtype analysis indicated that virus-specific antibody was IgG1-biased, and IgG1 response was corresponded with IgG (**Figures 4C,D,K,L**). IgG3 in the symptomatic group was significantly higher than in healthy controls ($P < 0.05$) (**Figures 4F,N**). No obvious difference in IgG2 was observed (**Figures 4E,M**). Of interest, N-targeting IgG4 antibodies were more obvious in asymptomatic carriers ($P < 0.05$) (**Figure 4O**). Furthermore, the ratio of RBD and N-targeting IgG4/IgG1 was compared. The results indicated that the ratio of RBD-targeting IgG4/IgG1 was comparable between asymptomatic carriers and symptomatic patients with COVID-19 while a significantly lower N-targeting IgG4/IgG1 ratio was observed in symptomatic patients than that of asymptomatic carriers (**Figures 4H,P**). The above results suggested that the ratio of N-targeting IgG4/IgG1 may be served as a potential indicator of symptomatic patients.

Subsequently, the positive rate of IgG was compared between these groups. The OD_{450} of the serum ≥ cut-off was determined as positive. For RBD-targeting IgG, an 80% (8/10) positive rate was seen in symptomatic patients with COVID-19, and a

100% (13/13) positive rate was seen in asymptomatic carriers (**Figure 5A**). For N-targeting IgG, a 30% (3/10) positive rate was seen in symptomatic patients with COVID-19, and a 7.69% (1/13) positive rate was seen in asymptomatic carriers (**Figure 5B**). The above results indicated that RBD-specific IgG was more sensitive than that N-specific IgG antibody response in asymptomatic carriers. Furthermore, the ratio of RBD-specific/N-specific IgG and IgG1 was compared (**Figures 6A,B**). A trend of higher RBD-specific/N-specific IgG ratio was observed while the RBD-specific/N-specific IgG1 ratio was significantly higher in asymptomatic carriers compared with symptomatic patients ($P < 0.05$). The above results exhibited that the ratio of RBD-specific/N-specific IgG1 was a more sensitive indicator than RBD-specific/N-specific IgG.

As shown in **Figures 7A–C**, with the increase in serum dilution, the optical density value of asymptomatic carriers decreased more significantly compared with the symptomatic group, indicating that symptomatic patients acquired a stronger binding to SARS-CoV-2 RBD protein than asymptomatic carriers.

The nAb titers of the sera from the samples were detected with live SARS-CoV-2. The nAb titers could be detected in symptomatic patients and asymptomatic carriers, and no significant difference was observed between the two groups (**Figure 7D**). Furthermore, symptomatic patients with underlying diseases tended to produce significantly lower nAbs compared with their counterparts ($P < 0.05$) (**Figure 7E**). Overall, these results showed that potent human nAbs could be elicited by SARS-CoV-2 infection, and the nAb titers produced by patients with underlying diseases are much lower compared with their counterparts.

DISCUSSION

With the continuous efforts of scientists worldwide, people have got a better grasp of the clinical symptoms and hematological signs of symptomatic patients with COVID-19 (Terpos et al., 2020; WHO, 2020; Wu et al., 2020; Zhou et al., 2020; Zhu et al., 2020). Our study confirmed and presented several

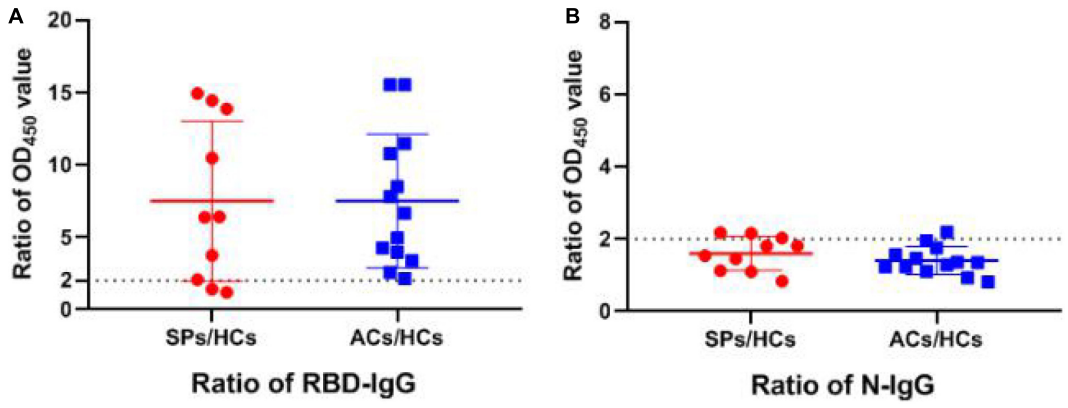

FIGURE 5 | The ratio of OD_{450} value of RBD and N-specific IgG between SPs and ACs and HCs. **(A)** The ratio of RBD-specific IgG OD_{450} value between experiment group and HCs. **(B)** The ratio of N-specific IgG OD_{450} value between experiment group and HCs. Data are presented as means ± SEM.

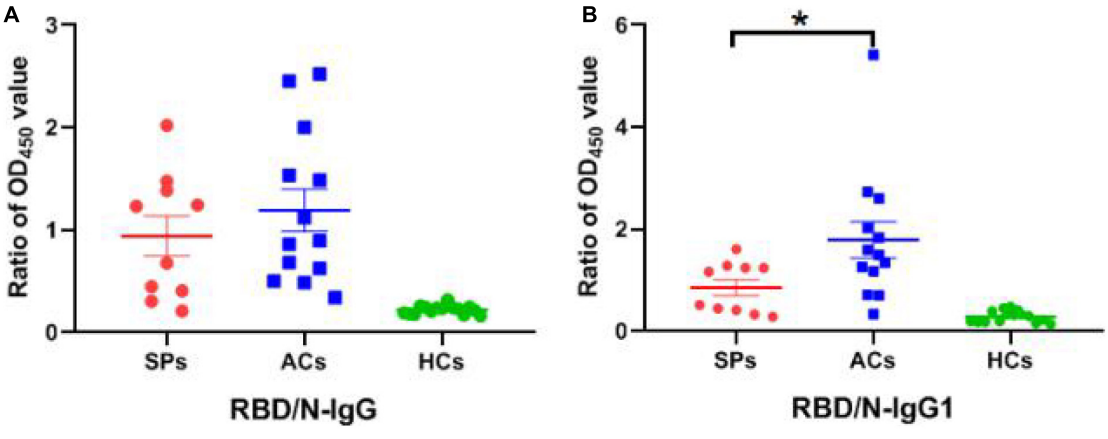

FIGURE 6 | The ratio of OD_{450} value between RBD-specific and N-specific IgG and IgG1 in SPs, ACs, and HCs. **(A)** The ratio of OD_{450} value between RBD-specific IgG and N-specific IgG. **(B)** The ratio of OD_{450} value between RBD-specific IgG1 and N-specific IgG1. *$P < 0.05$.

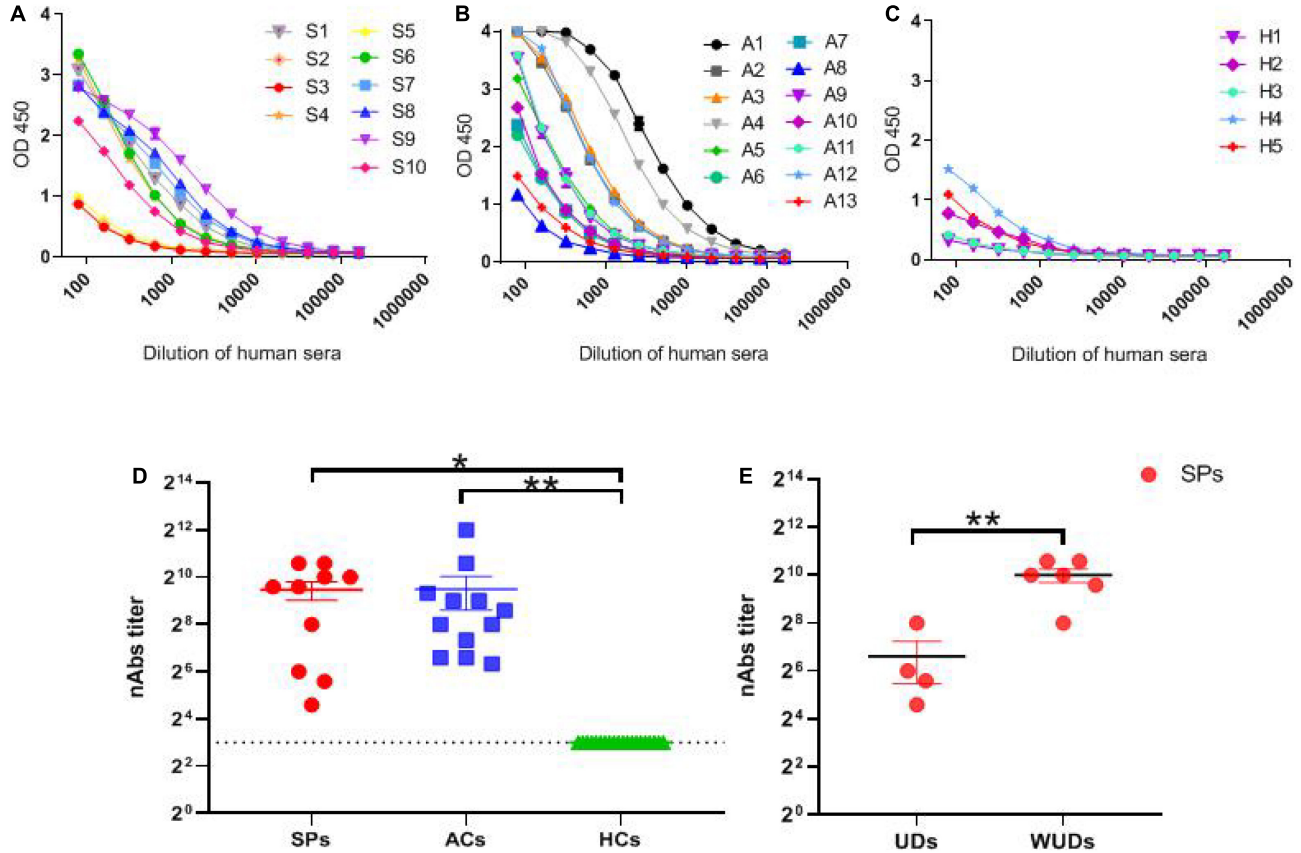

FIGURE 7 | SARS-CoV-2-specific IgG and nAb response in SPs, ACs, and HCs. **(A–C)** 1 μg/ml RBD coating, OD_{450} values with the dilution of human sera. **(A)** SPs. **(B)** ACs. **(C)** HCs. **(D)** Comparison of the level of nAbs in SPs, ACs, and HCs. **(E)** Comparison of the level of nAbs between patients with underlying diseases (UDs) and patients without underlying diseases (WUDs) in both SPs. Data are presented as means ± SEM. $^{*}P < 0.05$, $^{**}P < 0.01$.

aspects of COVID-19 clinical manifestations. Fever, cough, elevated neutrophils, lymphopenia, erythrocytosis, and multiple ground-glass opacity of lungs are the most frequently observed clinical characteristics of symptomatic patients with COVID-19. Meanwhile, serum liver function index (ALT and DB) abnormalities are common in symptomatic patients with COVID-19. In addition to the above, the neutrophil-to-lymphocyte (NLR) ratio >6.11 (Cai et al., 2021), elevated BUN (Liu et al., 2020), decreased blood uric acid level, D-dimer concentrations >1 μg/L, a greater sequential organ failure assessment (SOFA) score, high-sensitivity cardiac troponin I, and lactate dehydrogenase were correlated with increased risk of in-hospital death (Zhou et al., 2020). Interestingly, a scoring model has been developed to accurately and dynamically determine the death risk of hospitalized patients with COVID-19 based on blood routine examination indicators, namely, the PAWNN score (Liu et al., 2021). Using the Cox proportional hazard regression model, five risk factors were involved to construct the PAWNN score, including PLT counts, age, WBC counts, neutrophil counts, and neutrophil/lymphocyte ratio. The above-mentioned clinical manifestations and hematology information enrich our knowledge of COVID-19 and support auxiliary methods for the clinical diagnosis and prognosis of COVID-19.

"Cytokine Storm," a systemic hyper-inflammation that can cause rapid clinical deterioration and fatality, illustrates the immune system's inability to eradicate SARS-CoV-2, which contributes to the development of ARDS and multiple organ failure in COVID-19 cases (McGonagle et al., 2020; Merad and Martin, 2020; Ye et al., 2020). The dynamics of serum cytokine levels of patients with severe COVID-19 have been in-depth elucidated. IL-6, IL-8, IL-10, and TNF-α were increased in severe cases of COVID-19 while IFN-α, IL-1β, IL-4, and IL-15 were enriched in mild cases (Del Valle et al., 2020; Huang et al., 2020; Ruan et al., 2020; Garcia-Beltran et al., 2021). IL-2 and IL-7 were enriched in both severe and mild cases. The excessive inflammatory response characterized by the upregulated IL-6 and TNF-α is a typical immune disorder in patients with severe COVID-19 (Hadjadj et al., 2020). Our study focuses on cytokine diversity between symptomatic patients and asymptomatic carriers. Interestingly, obviously elevated IL-2, IL-8, IL-10, TNF-α, and IL-12p70 were observed in symptomatic patients with COVID-19 compared with asymptomatic carriers, which were consistent with the results in that of patients with COVID-19.

Antibodies are key indicators following SARS-CoV-2 infection. Several studies have attempted to elucidate antibody response in relation to COVID-19 severity. Severe patients

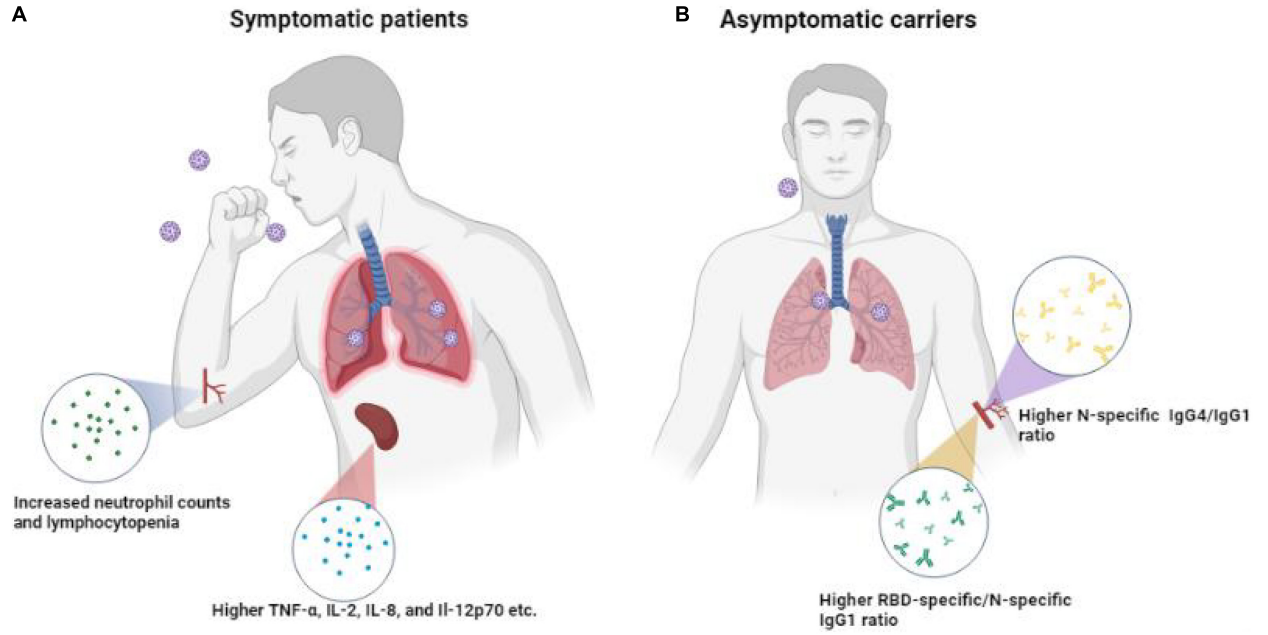

FIGURE 8 | Differences in immune response in SPs, ACs, and HCs. **(A)** Symptomatic patients exhibited higher anti-RBD/anti-N antibody ratios and higher TNF-α, IL-2, IL-8, and IL-12p70. **(B)** Asymptomatic carriers exhibited higher N-specific IgG4/IgG1 ratio antibodies.

are biased toward lower-than-predicted neutralization titers, suggesting that they harbor anti-RBD IgG antibodies that did not contribute to neutralization (Garcia-Beltran et al., 2021). Asymptomatic individuals are not equivalent to weaker immune responses. As has been described (Tutukina et al., 2021), a higher anti-RBD/anti-N IgG ratio reflects less severe symptoms. A higher anti-RBD/anti-N IgG ratio in asymptomatic carriers compared with symptomatic patients was confirmed in this study. Furthermore, we suggested that the higher anti-RBD/anti-N IgG1 ratio was more obvious in asymptomatic carriers. Particularly, in terms of higher IgG4 antibodies in asymptomatic carriers, we proposed for the first time that the higher N-specific IgG4/IgG1 ratio may be another sensitive indicator in asymptomatic carriers. The above sensitive indicators demand further larger-scale clinical investigations. Previous study showed that the asymptomatic group exhibited a more obvious decrease in nAbs levels compared with the symptomatic group. From the shedding of antigen to the level of antibody, subsequently the duration of antibody, the results varied among different research groups (Long et al., 2020; Wang Y. et al., 2020). We did not observe differences in the level of nAbs between asymptomatic carriers and symptomatic patients. Although the protective immunity of COVID-19 has yet been clearly elucidated, nAbs are thought to play a key role in the control of SARS-CoV-2 infection (Mercado et al., 2020; Yu et al., 2020; Dispinseri et al., 2021), which explained the relatively consistent but potent nAbs in both groups in this study.

This study has some limitations. It is a short-term case analysis in a specific district, so the samples size is relatively small. Besides, the dynamic characteristics of the immune response during SARS-CoV-2 infection were not assessed. Once the kinetics of virus shedding and changes in antibody titers during the progression of COVID-19 was obtained, a better grasp of the delicate difference between symptomatic patients and asymptomatic carriers with COVID-19 will be obtained.

To sum up, differences in immune response between asymptomatic carriers and symptomatic patients with COVID-19 are depicted in **Figure 8**. Asymptomatic carriers exhibited higher N-specific IgG4/IgG1 ratio and higher RBD-specific/N-specific IgG1 while symptomatic patients exhibited increased neutrophil counts and lymphocytopenia as well as higher TNF-α, IL-2, IL-8, and IL-12p70. Collectively, our study of clinical and serological manifestations revealed distinct immunity patterns of SARS-CoV-2 infection in symptomatic and asymptomatic patients. Our findings contribute to the understanding of the interaction of SARS-CoV-2 and host immune system, improving the risk stratification and management of patients with COVID-19.

DATA AVAILABILITY STATEMENT

The raw data supporting the conclusions of this article will be made available by the authors, without undue reservation.

ETHICS STATEMENT

The studies involving human participants were reviewed and approved by the Medical Ethics Committee of The

Second Affiliated Hospital of Nanhua University. The patients/participants provided their written informed consent to participate in this study. Written informed consent was obtained from the individual(s) for the publication of any potentially identifiable images or data included in this article.

AUTHOR CONTRIBUTIONS

YG and BL: conceptualization. FY: methodology and project administration. EL: software. EL and SW: formal analysis and writing original draft preparation. WH: investigation. JH: resources. LL: data curation. XZ: writing review and editing. XX and SY: supervision. BL: funding acquisition. All authors have read and agreed to the published version of the manuscript.

FUNDING

This research was funded by the Special Project for Basic Research of Hengyang Science and Technology Bureau (Grant No.202010031549), Key Research and Development Program of Hunan Province (Grant No. 2020SK3039), University of South China Novel Coronavirus Pneumonia Prevention and Control Emergency Special (Grant No. nk20200333), and Emergency Special Project of Epidemic Prevention and Control of COVID-19 Pneumonia in the University of South China (Grant No. 12).

SUPPLEMENTARY MATERIAL

The Supplementary Material for this article can be found online at: https://www.frontiersin.org/articles/10.3389/fmicb.2022.896965/full#supplementary-material

REFERENCES

Cai, J., Li, H., Zhang, C., Chen, Z., Liu, H., Lei, F., et al. (2021). The neutrophil-to-lymphocyte ratio determines clinical efficacy of corticosteroid therapy in patients with COVID-19. *Cell Metab.* 33, 258–269. doi: 10.1016/j.cmet.2021.01.002

Chen, N., Zhou, M., Dong, X., Qu, J., Gong, F., Han, Y., et al. (2020). Epidemiological and clinical characteristics of 99 cases of 2019 novel coronavirus pneumonia in Wuhan. *Lancet* 395, 507–513. doi: 10.1016/s0140-6736(20)30211-7

Chung, M., Bernheim, A., Mei, X., Zhang, N., Huang, M., Zeng, X., et al. (2020). CT Imaging Features of 2019 novel coronavirus (2019-nCoV). *Radiology* 295, 202–207. doi: 10.1148/radiol.2020200230

Cillo, A. R., Somasundaram, A., Shan, F., Cardello, C., Workman, C. J., Kitsios, G. D., et al. (2021). People critically ill with COVID-19 exhibit peripheral immune profiles predictive of mortality and reflective of SARS-CoV-2 lung viral burden. *Cell Rep. Med.* 2:100476. doi: 10.1016/j.xcrm.2021.100476

Del Valle, D. M., Kim-Schulze, S., Huang, H. H., Beckmann, N. D., Nirenberg, S., Wang, B., et al. (2020). An inflammatory cytokine signature predicts COVID-19 severity and survival. *Nat. Med.* 26, 1636–1643. doi: 10.1038/s41591-020-1051-9

Dispinseri, S., Secchi, M., Pirillo, M. F., Tolazzi, M., Borghi, M., Brigatti, C., et al. (2021). Neutralizing antibody responses to SARS-CoV-2 in symptomatic COVID-19 is persistent and critical for survival. *Nat. Commun.* 12:2670. doi: 10.1038/s41467-021-22958-8

Garcia-Beltran, W. F., Lam, E. C., Astudillo, M. G., Yang, D., Miller, T. E., Feldman, J., et al. (2021). COVID-19-neutralizing antibodies predict disease severity and survival. *Cell* 184, 476.e–488.e. doi: 10.1016/j.cell.2020.12.015

Guan, W., Ni, Z., Hu, Y., Liang, W., Ou, C., He, J., et al. (2020). Clinical characteristics of coronavirus disease 2019 in China. *New Engl. J. Med.* 382, 1708–1720. doi: 10.1056/NEJMoa2002032

Hadjadj, J., Yatim, N., Barnabei, L., Corneau, A., Boussier, J., Smith, N., et al. (2020). Impaired type I interferon activity and inflammatory responses in severe COVID-19 patients. *Science* 369, 718–724. doi: 10.1126/science.abc6027

Huang, C., Wang, Y., Li, X., Ren, L., Zhao, J., Hu, Y., et al. (2020). Clinical features of patients infected with 2019 novel coronavirus in Wuhan. *China. Lancet.* 395, 497–506. doi: 10.1016/S0140-6736(20)30183-5

Jiang, X. L., Wang, G. L., Zhao, X. N., Yan, F. H., Yao, L., Kou, Z. Q., et al. (2021). Lasting antibody and T cell responses to SARS-CoV-2 in COVID-19 patients three months after infection. *Nat. Commun.* 12:897. doi: 10.1038/s41467-021-21155-x

Johansson, M. A., Quandelacy, T. M., Kada, S., Prasad, P. V., Steele, M., Brooks, J. T., et al. (2021). SARS-CoV-2 Transmission From People Without COVID-19 Symptoms. *JAMA Netw. Open* 4:e2035057. doi: 10.1001/jamanetworkopen.2020.35057

Karaba, A. H., Zhu, X., Benner, S. E., Akinde, O., Eby, Y., Wang, K. H., et al. (2022). Higher proinflammatory cytokines are associated with increased antibody titer after a third dose of sars-cov-2 vaccine in solid organ transplant recipients. *Transplantation* 106, 835–841. doi: 10.1097/tp.0000000000004057

Lewnard, J. A., Hong, V. X., Patel, M. M., Kahn, R., Lipsitch, M., and Tartof, S. Y. (2022). Clinical outcomes among patients infected with Omicron (B.1.1.529) SARS-CoV-2 variant in southern California. *medRxiv* 2022,2001.2011.22269045. doi: 10.1101/2022.01.11.22269045

Liu, H., Chen, J., Yang, Q., Lei, F., Zhang, C., Qin, J.-J., et al. (2021). Development and validation of a risk score using complete blood count to predict in-hospital mortality in COVID-19 Patients. *Med* 2, 435–447. doi: 10.1016/j.medj.2020.12.013

Liu, Y.-M., Xie, J., Chen, M.-M., Zhang, X., Cheng, X., Li, H., et al. (2020). Kidney function indicators predict adverse outcomes of COVID-19. *Med* 2, 1–11. doi: 10.1016/j.medj.2020.09.001

Long, Q. X., Tang, X. J., Shi, Q. L., Li, Q., Deng, H. J., Yuan, J., et al. (2020). Clinical and immunological assessment of asymptomatic SARS-CoV-2 infections. *Nat. Med.* 26, 1200–1204. doi: 10.1038/s41591-020-0965-6

Ma, Q., Liu, J., Liu, Q., Kang, L., Liu, R., Jing, W., et al. (2021). Global percentage of asymptomatic SARS-CoV-2 infections among the tested population and individuals with confirmed COVID-19 diagnosis: a systematic review and meta-analysis. *JAMA Netw. Open* 4, e2137257–e2137257. doi: 10.1001/jamanetworkopen.2021.37257

McGonagle, D., Sharif, K., O'Regan, A., and Bridgewood, C. (2020). The role of cytokines including interleukin-6 in COVID-19 induced Pneumonia and macrophage activation syndrome-like disease. *Autoimmun. Rev.* 19:102537. doi: 10.1016/j.autrev.2020.102537

Merad, M., and Martin, J. C. (2020). Pathological inflammation in patients with COVID-19: a key role for monocytes and macrophages. *Nat. Rev. Immunol.* 20, 355–362. doi: 10.1038/s41577-020-0331-4

Mercado, N. B., Zahn, R., Wegmann, F., Loos, C., Chandrashekar, A., Yu, J., et al. (2020). Single-shot Ad26 vaccine protects against SARS-CoV-2 in rhesus macaques. *Nature* 590:E25. doi: 10.1038/s41586-020-2607-z

Peiris, J. S. M., Yuen, K. Y., Osterhaus, A. D. M. E., and Stöhr, K. (2003). The Severe Acute Respiratory Syndrome. *New Engl. J. Med.* 349, 2431–2441. doi: 10.1056/NEJMra032498

Ruan, Q., Yang, K., Wang, W., Jiang, L., and Song, J. (2020). Clinical predictors of mortality due to COVID-19 based on an analysis of data of 150 patients

from Wuhan. *China. Intensive Care Med.* 46, 846–848. doi: 10.1007/s00134-020-05991-x

Syangtan, G., Bista, S., Dawadi, P., Rayamajhee, B., and Joshi, D. R. (2021). Asymptomatic SARS-CoV-2 Carriers: a systematic review and meta-analysis. *Front. Public Health* 8:587374. doi: 10.3389/fpubh.2020.587374

Terpos, E., Ntanasis-Stathopoulos, I., Elalamy, I., Kastritis, E., Sergentanis, T. N., Politou, M., et al. (2020). Hematological findings and complications of COVID-19. *Am. J. Hematol.* 95, 834–847. doi: 10.1002/ajh.25829

Tutukina, M., Kaznadzey, A., Kireeva, M., and Mazo, I. (2021). IGG antibodies develop to spike but not to the nucleocapsid viral protein in many asymptomatic and light COVID-19 Cases. *Viruses* 13:1945. doi: 10.3390/v13101945

Wang, D., Hu, B., Hu, C., Zhu, F., Liu, X., Zhang, J., et al. (2020). Clinical characteristics of 138 hospitalized patients with 2019 novel coronavirus-infected pneumonia in Wuhan. *China. Jama* 323, 1061–1069. doi: 10.1001/jama.2020.1585

Wang, Y., Zhang, L., Sang, L., Ye, F., Ruan, S., Zhong, B., et al. (2020). Kinetics of viral load and antibody response in relation to COVID-19 severity. *J. Clin. Invest.* 130, 5235–5244. doi: 10.1172/JCI138759

WHO. (2020). *Director-General's Remarks At The Media Briefing On 2019-nCoV on 11 February 2020*. Geneva: World Health Organization.

WHO. (2022a). *Coronavirus (COVID-19) Dashboard*. Available online at https://covid19.who.int/?gclid=Cj0KCQiA-OeBBhDiARIsADyBcE7PVve11fZgyLj_kI8swygsjyQf8sMt-rAkiRRBbPgHo0VpON9KyPMaAkgfEALw_wcB [Accessed March 27 2022].

WHO. (2022b). *Update on Omicron*. Available online at https://www.who.int/news/item/28-11-2021-update-on-omicron [Accessed Febuary 21 2022]

Wu, C., Chen, X., Cai, Y., Xia, J.a, Zhou, X., Xu, S., et al. (2020). Risk factors associated with acute respiratory distress syndrome and death in patients with coronavirus disease 2019 Pneumonia in Wuhan, China. *JAMA Int. Med.* 180, 934–943. doi: 10.1001/jamainternmed.2020.0994

Yan, F., Li, E., Wang, T., Li, Y., Liu, J., Wang, W., et al. (2022). Characterization of two heterogeneous lethal mouse-adapted sars-cov-2 variants recapitulating representative aspects of human COVID-19. *Front. Immunol.* 13:821664. doi: 10.3389/fimmu.2022.821664

Ye, Q., Wang, B., and Mao, J. (2020). The pathogenesis and treatment of the 'Cytokine Storm' in COVID-19. *J. Infect.* 80, 607–613. doi: 10.1016/j.jinf.2020.03.037

Yu, J., Tostanoski, L. H., Peter, L., Mercado, N. B., McMahan, K., Mahrokhian, S. H., et al. (2020). DNA vaccine protection against SARS-CoV-2 in rhesus macaques. *Science* 369, 806–811. doi: 10.1126/science.abc6284

Zaki, A. M., van Boheemen, S., Bestebroer, T. M., Osterhaus, A. D. M. E., and Fouchier, R. A. M. (2012). Isolation of a novel coronavirus from a man with pneumonia in saudi Arabia. *New Engl. J. Med.* 367, 1814–1820. doi: 10.1056/NEJMoa1211721

Zhou, F., Yu, T., Du, R., Fan, G., Liu, Y., Liu, Z., et al. (2020). Clinical course and risk factors for mortality of adult inpatients with COVID-19 in Wuhan, China: a retrospective cohort study. *Lancet* 395, 1054–1062. doi: 10.1016/s0140-6736(20)30566-3

Zhu, N., Zhang, D., Wang, W., Li, X., Yang, B., Song, J., et al. (2020). A Novel coronavirus from patients with pneumonia in China, 2019. *New Engl. J. Med.* 382, 727–733. doi: 10.1056/NEJMoa2001017

Conflict of Interest: The authors declare that the research was conducted in the absence of any commercial or financial relationships that could be construed as a potential conflict of interest.

Publisher's Note: All claims expressed in this article are solely those of the authors and do not necessarily represent those of their affiliated organizations, or those of the publisher, the editors and the reviewers. Any product that may be evaluated in this article, or claim that may be made by its manufacturer, is not guaranteed or endorsed by the publisher.

frontiers | Frontiers in Microbiology

REVIEW
published: 02 June 2022
doi: 10.3389/fmicb.2022.889643

A Tale of Three Recent Pandemics: Influenza, HIV and SARS-CoV-2

Mafalda N. S. Miranda[1], Marta Pingarilho[1], Victor Pimentel[1], Andrea Torneri[2], Sofia G. Seabra[1], Pieter J. K. Libin[2,3,4†] and Ana B. Abecasis[1†]*

[1]Global Health and Tropical Medicine (GHTM), Instituto de Higiene e Medicina Tropical/Universidade Nova de Lisboa (IHMT/UNL), Lisboa, Portugal, [2]Artificial Intelligence Lab, Department of Computer Science, Vrije Universiteit Brussel, Brussels, Belgium, [3]Interuniversity Institute of Biostatistics and Statistical Bioinformatics, Data Science Institute, Hasselt University, Hasselt, Belgium, [4]Department of Microbiology and Immunology, Rega Institute for Medical Research, KU Leuven, University of Leuven, Leuven, Belgium

OPEN ACCESS

Edited by:
Hongliang Chai, Northeast Forestry University, China

Reviewed by:
Silvia Spoto, Policlinico Universitario Campus Bio-Medico, Italy
Julià Blanco, IrsiCaixa, Spain

***Correspondence:**
Mafalda N. S. Miranda
a21000919@ihmt.unl.pt

[†]These authors have contributed equally to this work

Specialty section:
This article was submitted to Infectious Agents and Disease, a section of the journal Frontiers in Microbiology

Received: *04 March 2022*
Accepted: *06 May 2022*
Published: *02 June 2022*

Citation:
Miranda MNS, Pingarilho M, Pimentel V, Torneri A, Seabra SG, Libin PJK and Abecasis AB (2022) A Tale of Three Recent Pandemics: Influenza, HIV and SARS-CoV-2. Front. Microbiol. 13:889643. doi: 10.3389/fmicb.2022.889643

Emerging infectious diseases are one of the main threats to public health, with the potential to cause a pandemic when the infectious agent manages to spread globally. The first major pandemic to appear in the 20th century was the influenza pandemic of 1918, caused by the influenza A H1N1 strain that is characterized by a high fatality rate. Another major pandemic was caused by the human immunodeficiency virus (HIV), that started early in the 20th century and remained undetected until 1981. The ongoing HIV pandemic demonstrated a high mortality and morbidity rate, with discrepant impacts in different regions around the globe. The most recent major pandemic event, is the ongoing pandemic of COVID-19, caused by the severe acute respiratory syndrome coronavirus 2 (SARS-CoV-2), which has caused over 5.7 million deaths since its emergence, 2 years ago. The aim of this work is to highlight the main determinants of the emergence, epidemic response and available countermeasures of these three pandemics, as we argue that such knowledge is paramount to prepare for the next pandemic. We analyse these pandemics' historical and epidemiological contexts and the determinants of their emergence. Furthermore, we compare pharmaceutical and non-pharmaceutical interventions that have been used to slow down these three pandemics and zoom in on the technological advances that were made in the progress. Finally, we discuss the evolution of epidemiological modelling, that has become an essential tool to support public health policy making and discuss it in the context of these three pandemics. While these pandemics are caused by distinct viruses, that ignited in different time periods and in different regions of the globe, our work shows that many of the determinants of their emergence and countermeasures used to halt transmission were common. Therefore, it is important to further improve and optimize such approaches and adapt it to future threatening emerging infectious diseases.

Keywords: pandemics, infectious diseases, HIV-1, influenza, SARS-CoV-2

INTRODUCTION

A pandemic is caused by a newly emerging pathogen that spreads rapidly among naive human hosts, thereby affecting a great number of individuals globally (Kelly, 2011). In the last century, the most noteworthy pandemic events originated from three distinct pathogens: HIV, influenza, and SARS-CoV-2. In this review, we discuss these three pandemics from a historical, epidemiological and virological perspective, with the aim to highlight the main determinants of its emergence, epidemic response and available countermeasures. Understanding the differences and similarities between these pandemics is paramount to know where to focus on, when preparing for the next pandemic. To this end, we compare technological advances, adopted preventive measures and policy making decisions, across the distinct pandemic eras. The three pandemics discussed in this work present ideal candidates for this perspective, as they cover different time periods and correspond to different types of respiratory pathogens (i.e. influenza and SARS-CoV-2) and a sexually transmissible pathogen (i.e. HIV), which exhibit distinct virological and epidemiological characteristics. Our review demonstrates the importance of an intimate understanding of the transmission networks through which epidemics are perpetuated, and the evolution in research and technology that enable pandemic preparedness and response. Additionally, we compare the evolutionary and virological specificities of these pathogens and the impact this has on the global spread and developments of its pandemics. Furthermore, we discuss different pharmaceutical interventions, examine the revolutionary developments that took place during the HIV and SARS-CoV-2 pandemics, and project this to evaluate our preparedness for the next pandemic. Finally, we detail the importance of epidemiological models to understand the pathogen, host, and its environment, and how such models can be used to evaluate mitigation policies *in silico*. The organization of this manuscript deviates from the chronological ordering of pathogens by date of emergence, to group the respiratory pathogens (i.e. influenza and SARS-CoV-2) and to allow for a back-to-back comparison of these pathogens.

HISTORICAL PERSPECTIVE ON THE EMERGENCE OF THREE RECENT PANDEMICS

In 1981, the first cases concerning young homosexual men with depleted T-lymphocytes were reported in the United States (Greene, 2007). This depletion rendered these men susceptible to opportunistic infections, eventually resulting in death. This condition would later be known as the Acquired Immunodeficiency Syndrome (AIDS; Greene, 2007). In 1983, the cause of AIDS was yet to be identified and the number of people with AIDS in the US continued to grow (De Cock et al., 2012). It was clear that transmission occurred between individuals and the diversity of the affected individuals implied that the infectious agent could spread *via* distinct transmission routes, including sexual, vertical and blood-borne transmission (i.e. intravenous drug use and blood products; De Cock et al., 2012). To figure out which pathogen was responsible for this syndrome, scientists studied the immune response of individuals that exhibited AIDS-related symptoms, which led to the identification of a new human retrovirus in 1983, by scientists of the Pasteur institute. This retrovirus was dubbed lymphadenopathy-associated virus (LAV), as it was isolated from a patient that was diagnosed with generalized lymphadenopathy (Montagnier et al., 1984). This virus was confirmed as the cause of AIDS and was later renamed to human immunodeficiency virus (HIV; Gallo and Montagnier, 2003). By then, the HIV pandemic had already unfolded, with high numbers of infections worldwide, resulting in high morbidity and mortality in the affected patients across different age groups until recent years as shown in **Figure 1A**.

The 1918 Influenza pandemic, colloquially referred to as the 'Spanish flu', was one of the most devastating pandemics of the 20th century. During this pandemic, three waves were recorded, with the first cases reported in March 1918, as show in **Figure 2**. The pandemic caused infections in one third of the world population and it is estimated that it caused between 50 and 100 million deaths worldwide (Morens and Fauci, 2007; Spreeuwenberg et al., 2018). The virus was first reported in Kansas (United States of America) and was spread from there throughout Europe and the rest of the world by American military personnel (Martini et al., 2019). This pathogen induced illness in all age groups, but healthy young adults accounted for half of the influenza-related deaths, which is quite atypical for influenza epidemics, and this gave the death rate versus age figure a unique W-shaped pattern as shown in **Figure 1B** (Taubenberger and Morens, 2006). In 1933, more than a decade after the end of this pandemic, the causative influenza virus was isolated (Barberis et al., 2016). After the 1918 pandemic, influenza viruses continued to circulate globally, with new and re-emerged strains, causing other pandemic outbreaks [including the 2009 influenza pandemic (Smith et al., 2009)] and contributing to seasonal flu epidemics (Liu et al., 2009; Nickol and Kindrachuk, 2019).

The *Coronaviridae* family receives its name after the virus' crown-like morphology. In 1965, a human coronavirus (strain B814) was isolated for the first time (Liu et al., 2021). It was generally believed that coronaviruses typically led to mild symptoms in humans (Liu et al., 2021). This however changed in 2003, when a new human coronavirus, identified as SARS-CoV, emerged in China and caused a pandemic (Weiss and Navas-Martin, 2005). This global epidemic ended through the eradication of SARS-CoV by the use of infection control measures, such as contact tracing and effective quarantine (Baric, 2008). In December 2019, an outbreak of pneumonia in Wuhan, Hubei Province in China was reported to WHO. The cause of the outbreak was identified to be a novel coronavirus related to SARS-CoV that was named SARS-CoV-2. This virus manifests in distinct clinical outcomes, ranging from asymptomatic infection to COVID-19 disease, with a mild to severe (and potentially fatal) progression (Wang et al., 2020). This virus caused a pandemic that is

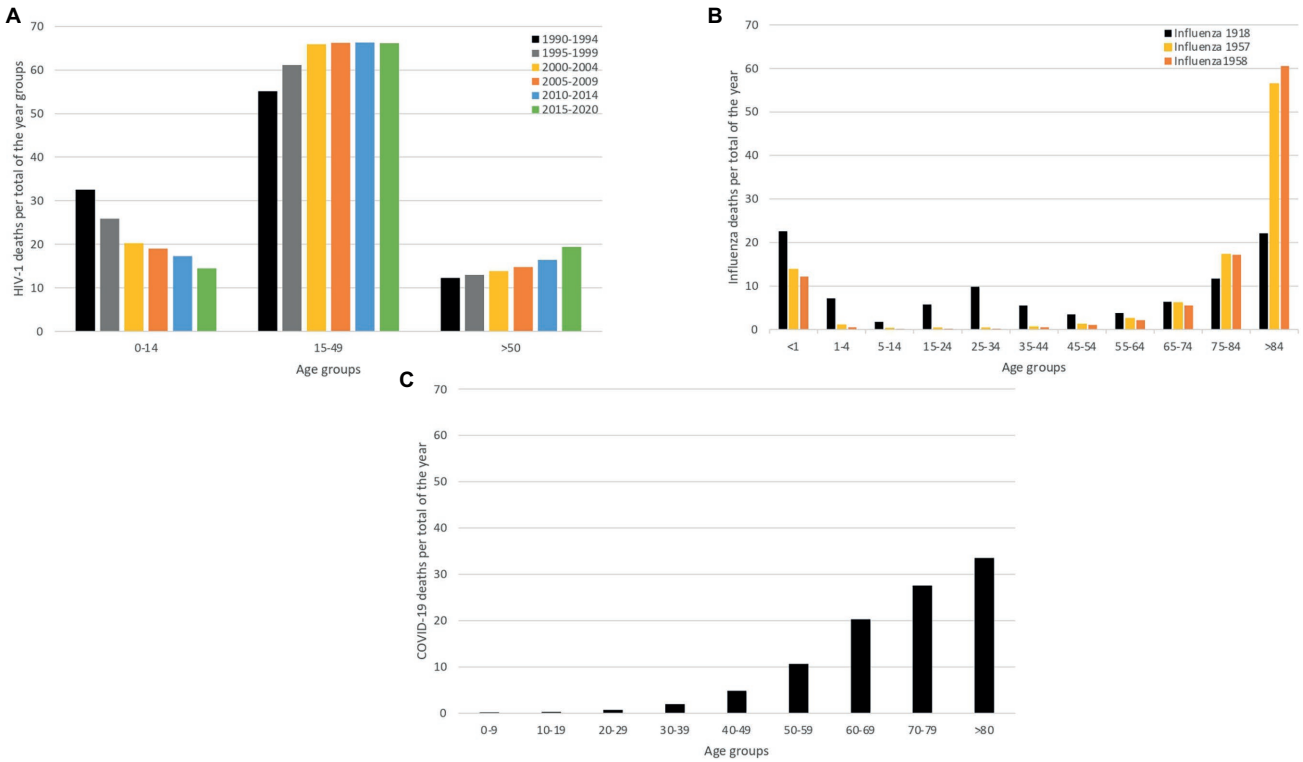

FIGURE 1 | Mortality caused by HIV-1, Influenza and COVID-19. We compare mortality between two acute infectious diseases (SARS-CoV-2 and influenza pandemic) and a chronic infectious disease (HIV), to demonstrate that their impact on mortality is inherently different. For all the infectious diseases, we show deaths proportional to age (panels **A–C**). **(A)** Age-proportional deaths divided into six time-periods grouped by 4 years (1990–1994; 1995–1999; 2000–2004; 2005–2009; 2010–2014 and 2015–2020), to show the age-specific mortality evolution over the years (UNAIDS, 2022). **(B)** Influenza age-proportional deaths for three major influenza pandemics (1918, 1957 and 1958), to show age-specific mortality patterns over the different influenza pandemics (Luk et al., 2001). **(C)** Age-proportional COVID-19 deaths for the first year of the pandemic (2020), when only non-pharmaceutical interventions were available (Riffe et al., 2021). This panel demonstrates how COVID-19 deaths exponentially increase by age.

still ongoing, and by February 2022, there were 383 million recorded cases and 5 million deaths confirmed globally (WHO, 2022a). **Figure 1C** represents the year only the deaths of 2020.

These pandemics all contributed to the development of public health measures, in distinct scientific eras. The 1918 influenza pandemic took place at a time when knowledge about viruses and their transmission dynamics was scarce. The HIV pandemic started more recently when knowledge and investigation of viral diseases were growing. At that time, antiviral drugs aimed at controlling viral load in infected individuals were developed quite rapidly. For SARS-CoV-2, scientific insights were produced at an unseen pace. For example, the viral strain of the index case was isolated and sequenced as soon as 11 January 2020. Furthermore, the scientific process benefited from many useful tools for virus investigation such as molecular epidemiology and next generation sequencing (NGS), novel diagnostic tools, epidemiological models to evaluate preventive measures and an unprecedented race towards the development of vaccines and treatment options. While such advances are both impressive and encouraging, many of the preventive measures used at the start of the SARS-CoV-2 pandemic were similar to those used during the 1918 influenza pandemic, where the focus was predominantly on non-pharmaceutical interventions.

DETERMINANTS OF EMERGING DISEASES

We will discuss the major determinants of HIV, pandemic influenza, and SARS-CoV-2, focusing on the host, the infectious agent and the environment in which they interact.

The infectious agent is the focal point of any emerging disease. There are a variety of infectious agents, including viruses, fungi and bacteria. Such agents cause infectious diseases by infecting hosts and the agents' properties will determine their potential to adapt to new hosts and environments. For a virus, these properties include the mutation rate, the cell tropism, the virus' antigenic immunodominance and the virus' ability to escape innate immune responses (Morens and Fauci, 2020). Such properties will determine the virulence and infectiousness, which might evolve whilst an epidemic unfolds (Morens and Fauci, 2020).

The host constitutes the organism that is susceptible to infection by the infectious agent; in this work, we consider

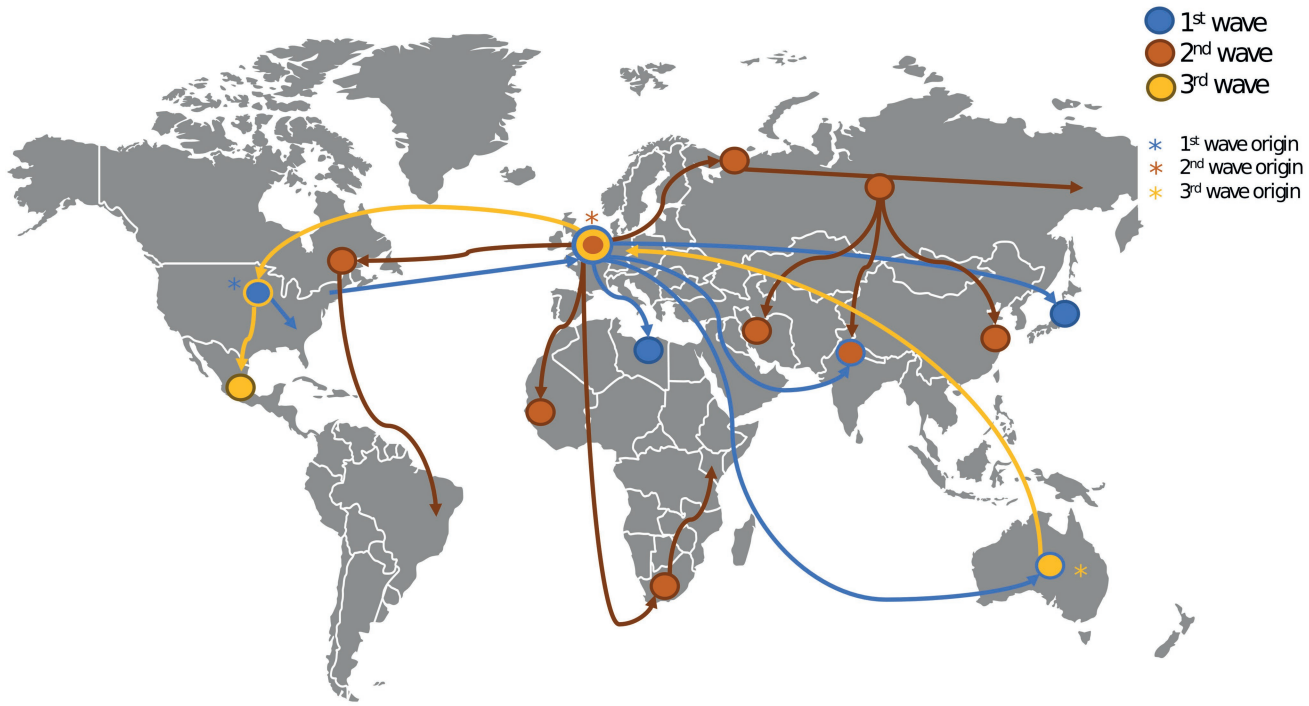

FIGURE 2 | Geospatial spread of influenza during the 1918 pandemic. This figure shows the origin (marked with asterisks) and spread (marked with edges) of the three waves of the 1918 influenza pandemic (Earth.Org, 2022). The first wave originated in the United States (US). and spread throughout Europe and the rest of the world. The second wave originated in Europe and spread through the US, Europe, Asia and Africa. The third wave originated in Australia and spread through Europe and the US.

viruses that can infect animals and humans. Once the host becomes exposed to a pathogen, viral replication can be initiated if the host is capable of expressing surface proteins or cellular receptors to which the virus can bind to (McArthur, 2019). In order to facilitate the ability for viruses to infect new host species, the virus needs to adapt to this new host, which is referred to as a host-switching event or zoonotic jump (Morens and Fauci, 2020). Transmission and pathogenesis can also be impacted by behavioural factors of the host and therefore transmission routes, clinical outcomes and symptoms can be altered in the new host species (McArthur, 2019; Morens and Fauci, 2020).

The environment constitutes the external conditions that affect the host that enable the emergence and persistence of a pathogen. Examples of such conditions are exposure to wildlife, environmental degradation, malnourishment and atmospheric conditions (Chen et al., 2021). Next to the impact on emergence, environmental factors can also impact the further spread of viruses.

We will now discuss how these determinants acted specifically for the emergence of the viruses discussed in this work: HIV, pandemic influenza, and SARS-CoV-2.

Simian immunodeficiency viruses (SIV) were transmitted from non-human primates to humans leading to the development of the human immunodeficiency virus (HIV). In **Figure 3A**, we show how these zoonotic events led to the HIV pandemic. HIV is a single stranded RNA virus that is part of the *Retroviridae* family and Lentivirus genus (Requejo, 2006). In the early 20th century, at least four independent zoonotic transmission events, originating from these primates, led to the origin of the four currently described HIV-1 groups. Group M, responsible for the global HIV-1 pandemic, directly originated from the chimpanzee *Pan troglodytes troglodytes* (Korber et al., 2000), as show in **Figure 4A**. The scientific consensus on the genesis of HIV-1 group M is that the zoonotic transmission event took place in Central Africa, possibly through hunting chimpanzees for bushmeat. The epidemic ignition, on the other hand, occurred in Kinshasa (Democratic Republic of Congo) likely due to increasing mobility of populations that occurred in that area during the first half of the 20th century (Faria et al., 2014). From there it spread to other regions in Africa and subsequently different strains were exported regions throughout the world (Korber et al., 2000), as visualised in **Figure 5**.

HIV-1 group M exhibits a great amount of natural diversity, with an evolutionary process that is driven both by within-host and between-host dynamics (Theys et al., 2018). This virus can generate 9×10^{-5} mutations per nucleotide per virus replication cycle (Hemelaar, 2012), and is prone to recombination events. The resulting viral diversity can be classified in nine subtypes and a set of Circulating Recombinant Forms (CRFs; Burke, 1997; Hemelaar, 2012). The genetic diversity that is exhibited by HIV, resulted in numerous sub-epidemics, heterogeneous in nature, and

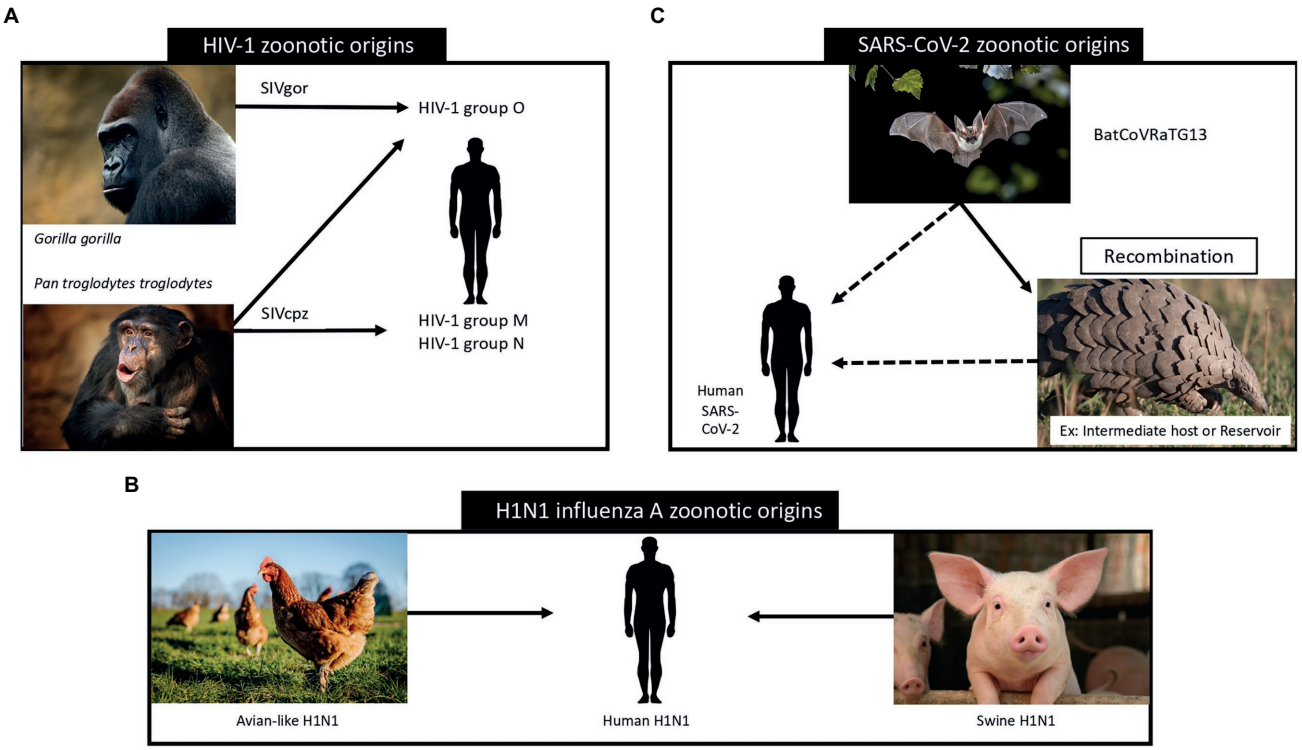

FIGURE 3 | Zoonotic origins of HIV-1 (panel **A**; Tebit and Arts, 2011), influenza (panel **B**; Taubenberger and Morens, 2006) and SARS-CoV-2 (panel **C**; Konda et al., 2020) viruses and their relation to human transmission. In panel **A** we show the zoonotic transmission of Simian immunodeficiency viruses (SIV) from non-human primates to humans, leading to the development of the human immunodeficiency virus. Panel **B** depicts the main zoonotic origins of influenza A H1N1 viruses and their transmission to human hosts. In panel **C** we visualize the assumed zoonotic origin of SARS-CoV-2 virus.

influenced by patterns of human migration and globalization (Vandamme et al., 2011; Pimentel et al., 2020). While the HIV-1 pandemic progressed, the extraction of genetic sequences became more accessible, resulting in the availability of a large collection of HIV-1 strains (Stoesser et al., 2004). Using these sequences, the subtype and CRF nomenclature enable the studying of this global spread (Alcantara et al., 2009; Pineda-Peña et al., 2013; Hemelaar et al., 2019). Furthermore, we note that these subtypes are associated with differences regarding transmissibility (Alcantara et al., 2009), susceptibility to antiretroviral drugs (Ngcapu et al., 2017), pathogenicity (Hemelaar et al., 2019) and preferred route of transmission (van Harmelen et al., 1997). HIV viruses are typically transmitted through the exchange of bodily fluids, such as blood, pre-ejaculate, semen and vaginal fluids. Once an infection has been established, the HIV virus induces a chronic infection that can be broadly categorized in three stages (Enger et al., 1996). First, about 2–4 weeks post HIV infection, the individual will experience an acute stage that is associated with flu-like symptoms. While this acute stage typically only lasts a few weeks, due to the high viral load (and infectiousness) that is associated with this phase, infected individuals have the potential to generate many new infections, depending on their behavioural context (HIV.gov, 2021). This highlights the importance of frequent testing of high-risk individuals and raising awareness of flu-like symptoms in the context of an early HIV infection. Second, the infected individual enters a stage where the viral load drops steeply, and the virus will multiply at a lower rate. At this point, infected individuals will typically no longer experience any symptoms. When the infection progresses without antiretroviral treatment, this stage can last between 10 and 15 years. During this stage, the individual's infectiousness is lower and depends on the patients' set-point viral load. Due to the long period during which individuals are not aware of their infection state, there is the potential to generate a large number of infections inadvertently (HIV.gov, 2021; CDC, 2021a). Therefore, shortening the time-to-diagnosis is key to reduce HIV incidence (CDC, 2021a). Furthermore, early diagnosis decreases the onward transmission of the virus and increases the chances of treatment success (Miranda et al., 2021). Over this period, the individual will slowly progress into the third stage, at which the viral load will rise again, resulting in a rapid decline in CD4 count, which preludes the third and final stage, that is, the AIDS stage. During this phase, the immune system of the patient is weakened, which results in a wide range of opportunistic diseases, eventually resulting in death (HIV.gov, 2021; CDC, 2021a). By 2020, 36.3 million people had died from AIDS-related disease worldwide, since the start of the pandemic (UNAIDS, 2021).

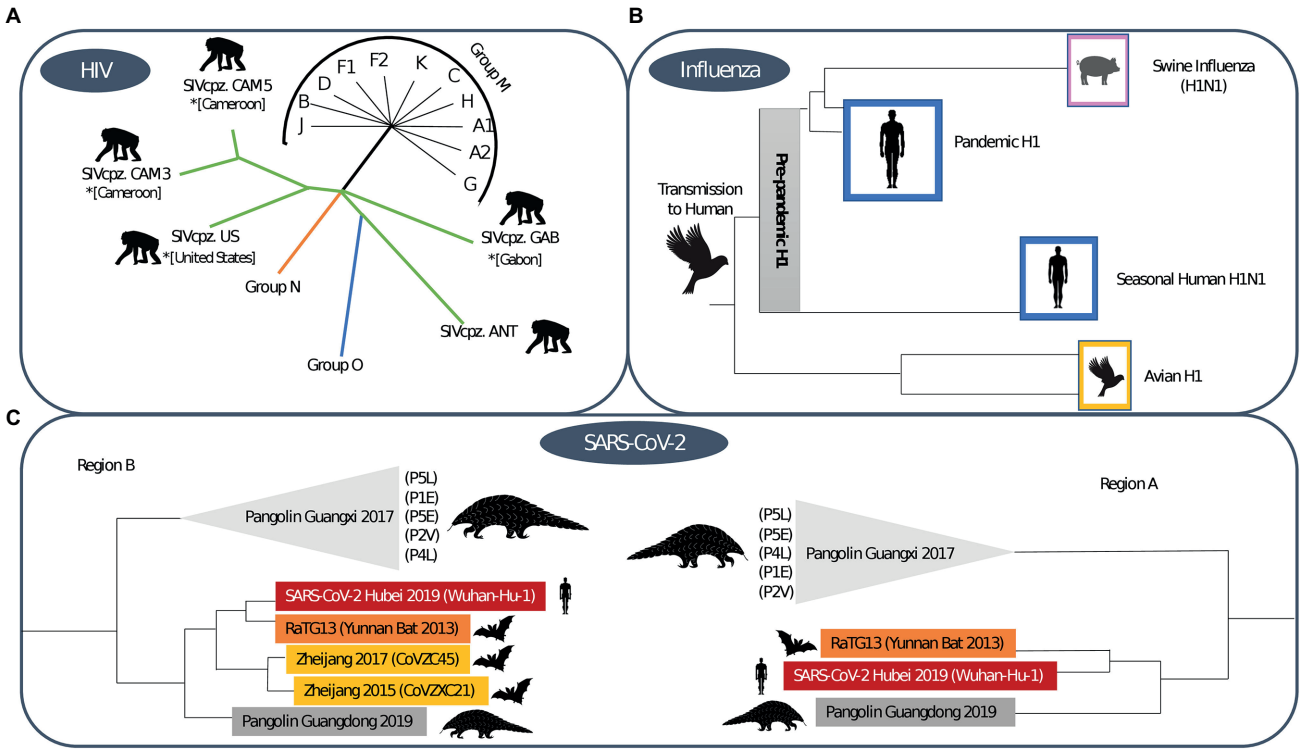

FIGURE 4 | Phylogenetic trees for **(A)** HIV-1, **(B)** Influenza and **(C)** SARS-CoV-2. The HIV-1 phylogenetic tree shows sequences that demonstrate the zoonotic jump of the distinct HIV-1 groups (Thomson et al., 2002). The influenza phylogenetic tree was based on the H1 subtype, the initial origin of the 1918 pandemic and the post-pandemic spread through human and animal species (Xu et al., 2008). The SARS-CoV-2 phylogenetic tree shows the origin of sarbecovirus and is based on distinct regions, where region A is shorter due to the potential of recombination of the genome region and region B is wider (Boni et al., 2020).

HIV is transmitted *via* different routes, the most common being sexual contacts, both *via* vaginal and anal intercourse (Moir et al., 2011). Another major route of transmission is *via* intravenous drug use, blood products and vertical transmission (Moir et al., 2011). The probability for a transmission to take place depends both on the transmission route and on the viral load in the exchanged body fluids (Galvin and Cohen, 2004). Furthermore, the occurrence of other sexually transmitted diseases are associated with an increase in the risk of sexual transmission of HIV (Galvin and Cohen, 2004). The transmission route of HIV in different regions of the globe is dynamically influenced by cultural and societal factors. For example, while in Africa, the main route of transmission is *via* unprotected heterosexual contact followed by mother-to-child transmission (Fettig et al., 2014), in Latin and Central America new cases are predominantly generated between homosexual men (MSM) and *via* the sharing of needles by intravenous drug users (IDU; Fettig et al., 2014). In North America and Western Europe, the main transmission route is sexual, where MSM are most at risk (Van De Vijver and Boucher, 2018). In Eastern Europe and Central Asia, the most prevalent mode of transmission remains *via* IDU (Fettig et al., 2014; Paraschiv et al., 2017).

Influenza viruses are part of the *Orthomyxoviridae* family and *Alpha influenza* virus genus (Taubenberger et al., 2019) and have been circulating among humans since time immemorial (Nickol and Kindrachuk, 2019). Influenza viruses constitute a group of single-stranded RNA viruses, of which currently, there are four types circulating, with type A being the most widespread. They are divided into subtypes according to the type of proteins that exist on their surface, considering both the type of hemagglutinin (H) and neuraminidase (N; Xu et al., 2008). The virus that caused the 1918 pandemic originated through recombination between the H1 and N1 subtype, and is thus referred to as Influenza A (H1N1; Humphreys, 2018). We visualise the phylogenetic tree that supports this zoonotic origin in **Figure 4B**.

The 1918 pandemic was caused by an influenza A virus, which originated from natural reservoirs of birds, specifically waterfowls and shorebirds (Taubenberger et al., 2019), as shown schematically in **Figure 3B**. An important catalyst of the 1918 influenza was the first world war and its aftermath, forcing individuals to live close to each other, and thus facilitating the spread of this respiratory virus (Humphreys, 2018).

For the 1918 influenza virus, it was shown that there was a significant variability in transmissibility (Fraser et al., 2011). While there was no certainty on transmission routes during the 1918 pandemic (Taubenberger and Morens, 2020), later the main respiratory transmission pathway of influenza (i.e. *via* droplets or aerosols) was demonstrated in animals (Mermel, 2018), in combination with physical contact and fomite contact

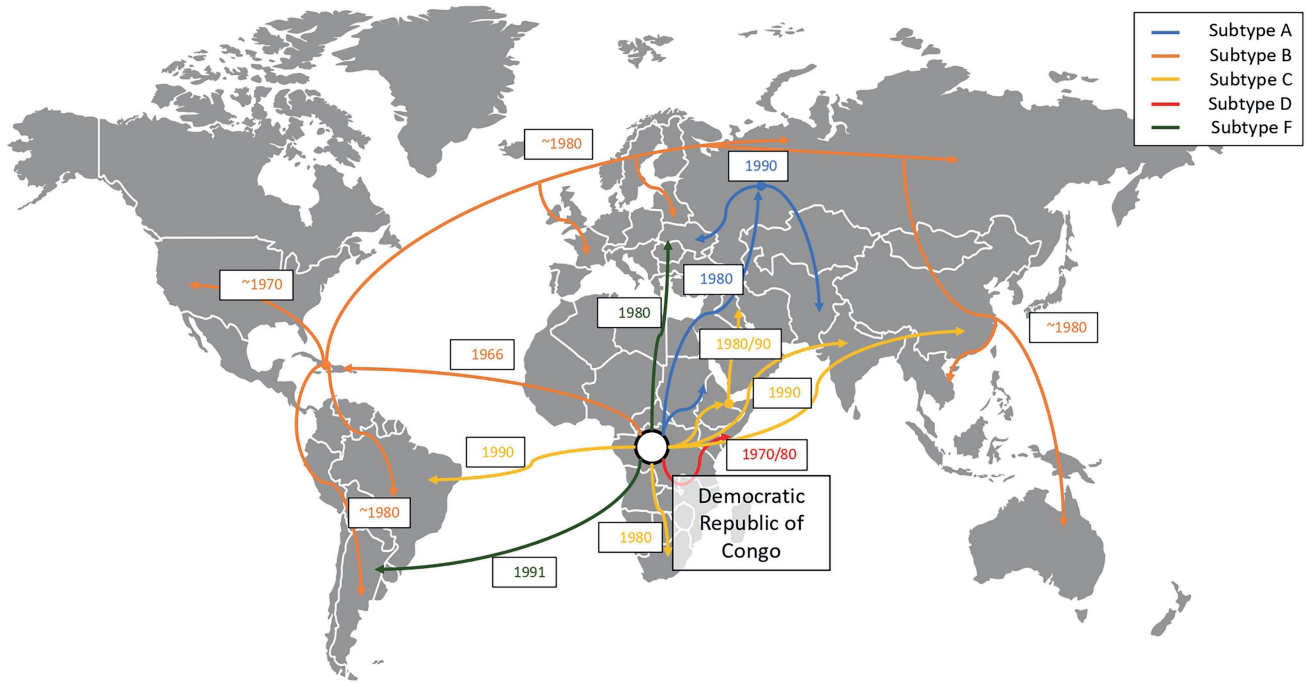

FIGURE 5 | Global evolution and chronology of events of spread of the HIV-1 group M subtypes (Tebit and Arts, 2011). We show how HIV-1 group M disseminated from its original epidemic location (Kinshasa, Democratic Republic of Congo) to other regions of the globe. The figure depicts how subtype B is the most widely spread subtype, subtype A spread mostly to the east regions of Africa, Europe and Asia and subtype C spread mostly through Brazil, South Africa and Southeast Asia.

(Brankston et al., 2007). Certain factors were considered to delay or enhance the transmission of the virus As with HIV, the increasing mobility of populations had an important role in the dissemination of the pandemics: as an example, the migration of soldiers from war fronts in crowded trains likely enhanced the spread of the virus (Martini et al., 2019). With respect to the transmission dynamics, it was reported that individuals were infectious prior to symptoms onset (Mills et al., 2004).

Coronaviruses (CoV), a kind of single-stranded RNA viruses, have been circulating in animals, such as birds and mammals, since the dawn of time and make up the *Coronaviridae* family of the *Betacoronavirus* genus (Malik, 2020). Bats are assumed to be a major CoV reservoir and phylogenetic analyses indicate that the origin of SARS-CoV also lies in this reservoir (Konda et al., 2020). It remains unclear whether SARS-CoV emerged due to a zoonotic event involving bats, as racoon dogs, pangolins and ferret badgers were also identified as intermediate hosts, as depicted in **Figure 3C** (Konda et al., 2020). In 2012, the Middle East Respiratory Syndrome coronavirus (MERS-CoV) emerged in Saudi Arabia (Umakanthan et al., 2020), and it is also believed that MERS-CoV also finds its origin in bat reservoirs (WHO, 2021a). For MERS-CoV goats, sheep and cows and the Arabian dromedary were identified as intermediate hosts (Umakanthan et al., 2020). In 2019, SARS-CoV-2 was identified and shown to be phylogenetically related to SARS-CoV (Umakanthan et al., 2020). SARS-CoV-2 is thought to have originated through recombination between a bat CoV and a CoV of unknown origin (Umakanthan et al., 2020). We show the phylogenetic tree that supports this origin hypothesis in **Figure 4C**.

While SARS-CoV-2 is the causative agent of COVID-19, a disease that can be mild or severe, many infected individuals remain asymptomatic. As the risk of developing severe disease grows exponentially with age, as shown in **Figure 1C**, we note that children are likely to be asymptomatic (Palmer et al., 2021). When suffering from severe COVID-19, the respiratory and immune system are fragile and the development of opportunistic diseases like pneumonia can occur (WHO, 2021b). Furthermore, severe COVID-19 can induce acute respiratory distress syndrome (ARDS) and other potentially fatal complications (Xu et al., 2020). Besides severe COVID-19, in some patients the virus can cause long-term illness, commonly referred to as Long-COVID, where individuals continue to experience symptoms for several months after being infected (Harrison et al., 2020). The large proportion of SARS-CoV-2 cases that results in an asymptomatic or very mild progression (Sekine et al., 2020; comparative to the common cold), that complicates contact tracing efforts, and facilitates the rapid spread of the virus (Davis et al., 2021). Furthermore, pre-symptomatic infection is an important driver of SARS-CoV-2 transmission, which renders a symptom-based isolation approach less effective. SARS-CoV-2's main transmission route is *via* respiratory droplets (Umakanthan et al., 2020) and the virus is also considered capable of airborne transmission in ill-ventilated environments (Prather et al., 2020). At the start

of the pandemic fomite contacts were hypothesized to play an important role in the transmission of SARS-CoV-2, however, recent studies indicate that transmission *via* contact surfaces is limited (Lotfi et al., 2020; Umakanthan et al., 2020). The infectiousness of SARS-CoV-2 has been shown to be highly heterogeneous indicating that the effects of superspreading should be carefully considered when drafting control measures, usually these control measure are based on local measures where it is easier to control the SARS-CoV-2 spread (Sneppen et al., 2021). While a pandemic is inherently a global process, containment strategies are to be implemented in a local setting. Therefore, understanding local transmission dynamics is vital to optimize epidemic control, which is demonstrated in the spatial analysis of SARS-CoV-2 spread in New York City (Dellicour et al., 2021).

SARS-CoV-2 has been circulating since the end of 2019 and over the course of the pandemic new variants evolved. Individuals can be diagnosed *via* polymerase chain reaction PCR or lateral flow antigen (Ag) testing (Peto et al., 2021). To monitor the evolution of SARS-CoV-2, a proportion of positive samples can be rapidly sequenced using next-generation sequencing technologies (Chiara et al., 2021). Through these sequences, and with the development of computational tools to process such large amounts of sequences (Hufsky et al., 2021), the evolution of SARS-CoV-2 was monitored in real time (Oude Munnink et al., 2021). To propose a system to classify SARS-CoV-2 lineages, the nomenclature implemented in the Pangolin COVID-19 lineage assigner[1] was introduced (O'Toole et al., 2021). The first mutation to be detected was D614G, which increased transmissibility and infectiousness and replaced the original SARS-CoV-2 strain becoming the dominant form of the virus circulating worldwide (Zhou et al., 2021). This event was followed by the emergence of a series of variants of concern (VoC) and a variant of interest (VOI) as listed in **Table 1**. The Omicron variant is the most recent VoC (WHO, 2021c).

While the 1918 influenza pandemic and SARS-CoV-2 pandemic emerged in different eras, both epidemics had to rely on similar non-pharmaceutical measures. Nonetheless, through technological advances, antiviral drugs have been developed at an unprecedented pace, both for HIV and SARS-CoV-2. Furthermore, the introduction of novel vaccine platforms, such as mRNA and vector-based vaccines, have led to an unprecedented race towards vaccines in the SARS-CoV-2 pandemic.

One major similarity between these three viruses is that transmission from asymptomatic patients plays a major role in viral dispersion. As such, asymptomatic individuals continue to spread the viruses inadvertently, as they are unaware of their infection status. In that context, early diagnosis through testing is an important strategy to contain transmission. We therefore stress the importance of the availability of efficient diagnostics, such that infected individuals can take the appropriate precautions is vital to control an epidemic. PCR and Ag rapid testing strategies grown unprecedently in the context of the COVID-19 pandemic. We believe that this will be an important venue to prepare for future outbreaks.

Furthermore, all these three pandemics, as most others find their origin on zoonotic events, indicating that monitoring zoonotic spill over events is another crucial research field (Allen et al., 2017). In this context, finding potentially threatening Emerging Infectious Diseases implies intensifying research in a One Health perspective and not only at the human level (McArthur, 2019). The movement and expansion of zoonotic reservoirs throughout different territories, due to the quick environmental evolution, for example due to climate change or urbanization, also warrant special attention (Baker et al., 2021).

PHARMACEUTICAL AND NON-PHARMACEUTICAL INTERVENTIONS

Non-pharmaceutical Interventions

The prevention strategies for HIV-1 have historically changed and evolved over the last 40 years of the pandemic. These have included sexual abstinence, condom use, promoting the use of sterilized needles for intravenous drug users (IDUs), and improved protocols to decrease the diagnosis delay for newly infected individuals (Alnwick et al., 2007). In low-income countries, the use of male circumcision has also shown to be an effective prevention strategy (Williams et al., 2006). In recent years, treatment as prevention (TasP) has become a crucial prevention approach to halt the HIV-1 pandemic, either through pre-exposure prophylaxis (PrEP), post-exposure prophylaxis (PEP) or through treatment for all.

When implementing prevention strategies it is vital to target vulnerable populations, but due to stigma and discrimination, this remains challenging (Alnwick et al., 2007). Furthermore, due to particularities in the cultural and societal context of the affected region (Wegbreit et al., 2006), prevention strategies need to be tailored to the relevant context (Wegbreit et al., 2006; Pineda-Peña et al., 2019).

When the H1N1 pandemic erupted in 1918, non-pharmaceutical interventions were the only available resources to control the epidemic. These interventions include the notification of suspected cases to authorities, the isolation of infected individuals and a mandated quarantine for the contacts of infected individuals (Markel et al., 2007; Martini et al., 2019). Furthermore, the use of face masks, surveillance of communities, closure of meeting venues and hygienic measures were implemented to reduce transmissions (Markel et al., 2007; Humphreys, 2018; Martini et al., 2019).

For SARS-CoV-2, individuals are isolated at home when they experience any COVID-19-related symptoms, until they obtain a negative test or recover from the infection (Pradhan et al., 2020). Furthermore, as individuals are highly infectious prior to developing symptoms and as many infected individuals stay asymptomatic or with very mild symptoms that can be easily mistaken for a common cold, additional prevention measures are necessary (Pradhan et al., 2020). Such prevention measures

[1]https://pangolin.cog-uk.io

TABLE 1 | Description of variants of concern and variant of interest (CDC, 2021d; WHO, 2021c,d; European Centre for Disease Prevention and Control, 2022).

Pangolin nomenclature	WHO nomenclature	Spike mutations of interest	Main properties	Country of first detection	Date classified as VOC/VOI	Date classified as previous VOC/VOI
VOC B.1.1.7	Alpha (VOC)	N501Y, D614G, P681H	➔ Increased transmissibility and severity	United Kingdom	December 2020	March 2022
VOC B.1.351	Beta (VOC)	K417N, E484K, N501Y, D614G, A701V	➔ Increased transmissibility and severity, immune escape	South Africa	December 2020	March 2022
P.1	Gamma (VOC)	K417T, E484K, N501Y, D614G, H655Y	➔ Increased transmissibility and severity, immune escape	Japan	January 2021	March 2022
B.1.617.2	Delta (VOC)	L452R, T478K, D614G, P681R	➔ Increased transmissibility and severity, immune escape	India	May 2021	
B.1.1.529	Omicron (VOC)	A67V, Δ69-70, T95I, G142D, Δ143-145, N211I, Δ212, ins215EPE, G339D, S371L, S373P, S375F, K417N, N440K, G446S, S477N, T478K, E484A, Q493R, G496S, Q498R, N501Y, Y505H, T547K, D614G, H655Y, N679K, P681H, N764K, D796Y, N856K, Q954H, N969K, L981F	➔ Large number of mutations; ➔ Increased transmissibility, reduced severity, immune escape	South Africa	November 2021	
B.1.621	Mu (VOI)	R346K, E484K, N501Y, D614G, P681H	➔ Increased impact on transmissibility ➔ Increased impact on immunity	Colombia	August 2021	March 2022

include early screening or self-testing and diagnosis (through testing and contact tracing), isolation, social distancing, facial masks and hygienic measures (e.g. hand washing, alcohol-based sanitizer, cleaning surface environments; Pradhan et al., 2020). Given that SARS-CoV-2 is transmitted *via* the respiratory tract (i.e. droplets or aerosols), the use of masks and ventilation is particularly important (Peeples, 2021). However, different surges globally have demonstrated that these measures can easily fail when social distancing measures are released and the use of mass testing has been suggested to control the epidemic (Burki, 2020).

Antiviral Drugs for Treatment and Prevention

As a cure for HIV remains elusive to date, highly active antiretroviral therapy (HAART) is the only option to improve the quality of life of an HIV patient (Cohen et al., 2008). Upon HAART, patients achieve viral suppression to increase the CD4 cell count and recover the immune system function, which improves the clinical status of the patient (Pau and George, 2014). Furthermore, contemporary HAART regimens decrease viral load to undetectable levels, thereby significantly reducing the infectiousness of the treated individual (Pau and George, 2014). This observation led to the use of antiviral therapy to prevent individuals from getting infected, so-called Pre-exposure prophylaxis (PrEP), which is mostly used in people at increased risk of contracting HIV. PrEP has been demonstrated effective in reducing the risk of HIV-1 infection (Alnwick et al., 2007; Cohen et al., 2008; Fonner et al., 2016).

The development of HAART introduced a revolutionary improvement for HIV patients. However, due to the fast evolutionary rate of HIV and the selective pressure that is induced by HAART, resistance mutations to antiretroviral drugs can emerge and impede viral suppression (Pingarilho et al., 2020). The resistance to antiretroviral drugs can manifest in two ways, as a result of selective pressure of antiretrovirals in treated individuals (i.e. acquired drug resistance) and as a result of an infection with a virus strain that carries drug resistance mutations (i.e. transmitted drug resistance; Baesi et al., 2014; Clutter et al., 2016). Drug resistance testing is a necessary tool to detect transmitted drug resistance in newly diagnosed patients in order to guide the selection of antiretroviral therapy, to minimize the risks of virological failure (Charles and Hicks, 2008). Resistance to antiretroviral therapy, that could be related to poor treatment adherence, is still a global reality and a major barrier to end HIV/AIDS pandemic (Kim et al., 2018). A new approach that can minimize problems of adherence is the use of injectable long-acting HIV medication, which has been shown to be well accepted and effective (Simoni et al., 2020). Also, it is important to mention that contemporary antiretrovirals have a higher genetic barrier, meaning that the virus is less likely to escape from selective pressure (Theys et al., 2019).

For influenza, the use of antiviral drugs can be used to reduce morbidity and mortality, and as a prophylactic agent to reduce individual susceptibility. Nonetheless, when a novel

influenza strain emerges, it remains unclear whether resistance mutations could hinder the antiviral activity of the current generation of antiviral drugs (Lipsitch et al., 2007; Wang et al., 2013; Hussain et al., 2017; Lee and Hurt, 2018). There are three groups of therapeutic drugs for influenza: the neuraminidase inhibitors, the M2 inhibitors and the polymerase inhibitors (De Clercq, 2006). The neuraminidase inhibitors include oseltamivir, which is the most used and its efficacy is proved to prevent transmission and outbreaks within households (Welliver et al., 2001), zanamivir and peramivir (Lee and Hurt, 2018; Chow et al., 2019). The class of M2 inhibitors includes amantadine and rimantadine (De Clercq, 2006; Keshavarz et al., 2020). A novel therapeutic for influenza virus is Baloxavir marboxil: a cap-dependent endonuclease inhibitor that inhibits viral mRNA synthesis (Du et al., 2020; Lampejo, 2020). The most common resistance to influenza antivirals is towards M2 inhibitors, which is the major reason why this class is no longer widely used (Wang et al., 2013). Resistance to neuraminidase inhibitors have also been reported and further monitoring is warranted (Lee and Hurt, 2018).

For SARS-CoV-2, besides vaccines, the use of monoclonal antibodies, interferon-based preventive therapies and antiviral agents have been considered (Lotfi et al., 2020). Interferon-α and interferon-β were previously approved for, respectively, hepatitis B and for chronic obstructive pulmonary disorder. These interferons are now under investigation for SARS-CoV-2 prevention (Ahsan et al., 2020). Currently, different studies for the use of monoclonal antibodies are ongoing (Valle et al., 2020; Malani and Golub, 2021; Starr et al., 2021), yet the potential development of resistance mutations poses a threat to the efficacy of such therapeutics. Different antiviral agents have been considered, both as prophylactic and therapeutic agents, including drugs previously targeted at HIV-1 (Andreani et al., 2020; Lotfi et al., 2020) or Ebola (i.e. remdesivir; Kumar et al., 2020). However, these regimens were disappointing in clinical trials, and only recently a set of antiviral drugs has shown promise. As of December 2021, the United States Food and Drug Administration approved Paxlovid (a combination of nirmatrelvir and ritonavir) for the treatment of mild-to-moderate COVID-19 disease (U.S. Food and Drug Administration, 2022), although other antiviral drugs are currently being considered for approval, i.e. molnupiravir and an orally active 3CL protease inhibitor (Boras et al., 2021; GOV.UK, 2021).

Vaccines

Currently, there is no vaccine for HIV-1, with many trials rendering unsatisfying results (Tebas et al., 2012; Pollard et al., 2014; Ensoli et al., 2015; Dinges et al., 2016; Macatangay et al., 2016; Jacobson et al., 2016a,b; Brekke et al., 2017), which is often attributed to the extensive genetic diversity that is exhibited by HIV-1. Recent work investigates the use of mRNA-based vaccines that incorporate multiple HIV subtypes, in order to cover a larger genetic diversity (Aidsmap, 2021).

Since 1918, there has been immense progress with respect to influenza vaccine development, and these technologies have been used to control more recent influenza pandemics and seasonal influenza epidemics (Wu et al., 2010; Huddleston et al., 2020). Vaccines have shown to decrease hospitalizations, susceptibility and infectiousness (Koszalka et al., 2017; Robson et al., 2019). Yet, in case of a pandemic emergency, it will take time in order to produce vaccines for a novel influenza strain, rendering the use of non-pharmaceutical intervention measures necessary until the vaccine becomes widely available (WHO, 2004).

For Influenza A there are two types of vaccine platforms available, the inactivated influenza vaccines and the life attenuated influenza vaccines. The viruses for inactivated vaccines can be grown in eggs, cell culture or using recombinant technology (WHO/Europe, 2021; CDC, 2021b). The life attenuated influenza vaccine consists of a nasal spray vaccine (WHO/Europe, 2021; CDC, 2021b). Also, studies are ongoing to use mRNA technology as a new platform for influenza vaccines (Moderna, Inc., 2021).

For SARS-CoV-2, vaccines were developed at an unprecedented pace. A large number of vaccine platforms has been studied in the context of SARS-CoV-2, but the class of mRNA vaccines and vector-based vaccines were the first to show promising results (Bettini and Locci, 2021; FDA, 2021; CDC, 2021c). The most common class of vaccines, available since late 1800s, are the inactivated vaccines derived from killed virus, which also have been produced for COVID-19. However, this type of vaccine had a time and complexity of production higher when compared to mRNA and vector-based vaccines (Plotkin, 2014; Park et al., 2021; Zhang et al., 2022). These latter two vaccine classes were most widely used during the COVID-19 pandemic. The mRNA vaccine uses a piece of mRNA to instruct the production of a specific protein that will be recognized by the human immune system. While the development of mRNA vaccines has been active for at least 30 years (Dolgin, 2021), this class of vaccines has been approved for human use for the first time during the COVID-19 pandemic (WHO, 2022b). The vector-based vaccines, studied since 1982 (Ura et al., 2014) and first approved in 2019 to prevent Ebola virus (Vrba et al., 2020), aim to trigger an immune response by delivering a specific protein of the pathogen (Creech et al., 2021; WHO, 2022b).

When these vaccines were first released, they were welcomed with great optimism given their high effectiveness, both regarding preventing symptomatic infection (VE_I) and severe disease (VE_S). This was the case for the vector-based vaccines, where a single dose of the Janssen vaccine showed a VE_I of 85% (Andreano and Rappuoli, 2021), while for the Vaxzevria vaccine (two doses) a VE_I of 73% was recorded (Lopez Bernal et al., 2021). Equally so for the mRNA-based vaccines, where the Pfizer-BioNtech vaccine (two doses) was reported a VE_I of 91.1% according to a study of safety and efficacy through 6 months (Thomas et al., 2021), while the Moderna vaccine (two doses) displayed a VE_I of 94.1% (WHO, 2022c). When new variants emerged, the VE_I was reduced, yet, for individuals that were administered a two-dose regimen, VE_S remained high (Tregoning et al., 2021). The wide distribution of vaccines therefore significantly reduced hospital loads, even after the emergence of the first variants (Lauring et al., 2022). For the most recent Omicron VoC, to this point the most infectious variant, the two-dose regimen shows a significant reduction in both VE_I and VE_S (Andrews et al., 2022). However, recent

research shows that a third vaccine dose boosts vaccine efficacy both against symptomatic infection and sever disease (Andrews et al., 2022; Nyberg et al., 2022).

Since December 2020, three vaccines have been approved by the United States Food and Drug Administration for emergency use, while one has been authorised by the European Medicines Agency (EMA) for use in the European Union (EU; **Table 2**; FDA, 2021; European Medicines Agency, 2022). The mRNA and vector-based vaccine platforms were used not only to rapidly develop vaccines, but also to produce it at an unprecedented pace. As vaccine production was previously a major limiting step for vaccine distribution and as these platforms facilitate a rapid response to novel pathogens, we argue that these constitute an important innovative means of pharmaceutical intervention to combat future pandemics.

MODELLING

Epidemiological models have become an increasingly ubiquitous tool to support public health policy making, regarding the mitigation of epidemics. The first mathematical formalization of an epidemiological process is commonly attributed to Kermack and Mckendrick (1991a,b,c). As this mathematical framework was published between 1927 and 1933, it clearly postdates the 1918 influenza pandemic. Yet, given the considerable advances with respect to research on model structures and the current computational capabilities, epidemiological models facilitate the investigation of epidemics in detail and aid epidemiologists to inform public health policy in the process.

To study the impact of mitigation policies, a pertinent epidemiological model structure needs to be defined, which depends on the pathogen, its routes of transmission, ecological aspects (e.g. vector ecology) and the character of the investigated mitigation policy. Furthermore, an important decision with respect to model structure is its granularity. Here we discuss the three main model structures: compartment models, individual-based models and meta-population models.

Compartment models divide the population into discrete homogeneous states (i.e. compartments) and describe the transition rates from one state to another, *via* which communication between the compartments occurs (Diekmann et al., 2013). For each pathogen, to which a patient can obtain immunity after being infected (e.g. pandemic influenza), we can partition the population in three groups: individuals that are susceptible to infection (i.e. susceptibles), individuals that are infected (i.e. infected), and individuals that recovered and obtained immunity (i.e. recovered; **Figure 6** panel **A**). This model, referred to as the SIR model (i.e. abbreviation of Susceptible-Infected-Recovered), was introduced by Kermack and Mckendrick (1991a,b,c). Compartment models can be formalized as a system of ordinary differential equations. While the SIR model is a basic model that assumes homogeneity in the population, it can be extended in various ways to accommodate more complex modelling inquiries.

While compartment models group individuals together based on common properties (e.g. infection or age group), an individual-based model will explicitly represent all individuals and their properties (Diekmann et al., 2013). In this model individuals are connected, either in a static or a dynamic fashion, and the spread of the epidemic is simulated among this network. The most fundamental individual-based model will thus represent each of the individuals and maintain their infection status, i.e. susceptible (S), infected (I), recovered (R). Given this

TABLE 2 | Comparison of the COVID-19 vaccines approved by FDA and EMA (FDA, 2021; CDC, 2021c; European Medicines Agency, 2022).

Vaccines	Pfizer-BioNTech	Moderna	Janssen	Vaxzevria (previously AstraZeneca)
Date of approval	11 December 2020 (FDA)	18 December 2020 (FDA)	27 February 2021 (FDA)	29 January 2021 (European Union)
Manufacturer	Pfizer, Inc. BioNTech	ModernaTX, Inc.	Janssen Pharmaceuticals Companies of Johnson & Johnson	AstraZeneca AB
Name	BNT162b2	mRNA-1,273	JNJ-78436735	EMEA/H/C/005675
Type of vaccine	mRNA	mRNA	Viral vector	Viral vector
Number of shots	2 shots, 21 days apart	2 shots, 28 days apart	1 shot	2 shots, 28–84 days apart
Authorized Use	Individuals 16yo and older	Individuals 18yo and older	Individuals 18yo and older	Individuals 18yo and older
Main side effects	Pain at the injection site Tiredness Headache Muscle pain Chills Joint pain Fever	Pain at the injection site Tiredness Headache Muscle pain Chills Joint pain Swollen lymph nodes in the same arm as the injection Nausea and vomiting Fever	Pain at the injection site Headache Fatigue Muscle aches Nausea	Tenderness Pain and bruising at the injection site Headache Tiredness Muscle pain General feeling of being unwell Chills Fever Joint pain Nausea

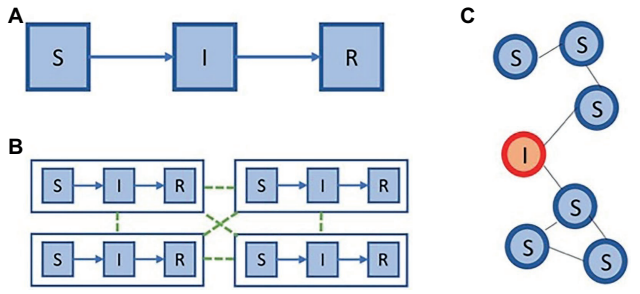

FIGURE 6 | Modelling impact on policy. Two extremes in model space: **(A)** an SIR compartment model, **(C)** and individual-based model. We show a meta population model **(B)**, that is situated between the models in **(A,C)**, in terms of complexity.

fundamental example, these individuals can be connected using a static network, for example, an Erdos–Rényi random graph, which has a binomial degree distribution. This example is depicted schematically in **Figure 6** panel **C**.

On the one hand, compartment models are computationally efficient to evaluate, yet they need to divide the population in coarse compartments. On the other hand, individual-based models allow for more fine-grained modelling, yet require a lot of computation. To balance between these trade-offs, meta-population models are frequently used, especially to enable the modelling of epidemic processes in a spatially explicit context. Meta-population models were first introduced in the context of ecology (Hanski, 1999), to model sub-populations that can be separated geographically. In **Figure 6** panel **B**, we show an example of a simple meta-population model with four patches, where each patch consists of an SIR model.

In between these extremes in model space, all kinds of meta-population models can be constructed, as shown in **Figure 6**. These distinct model structures are important to address different aspects of public health inquiries (Coletti et al., 2021).

While the 1918 influenza pandemic predates the advent of epidemiological models, epidemics of influenza have a predominant place in model literature. On the one hand, the historic 1918 pandemic has been studied extensively using mathematical models (Eggo et al., 2011), and on the other hand, the risk of future pandemics is often explored in an influenza context (Ferguson et al., 2006). The modelling of influenza culminated with the public health modelling efforts related to the 2009 influenza pandemic (Van Kerkhove et al., 2010). As the main body of research focuses on the average reduction in attack rate, in order to reduce the burden with respect to mortality and morbidity, compartment models have been used extensively (Eames et al., 2012). In such models, typically mitigation strategies that are targeted to particular groups of individuals are explored, such as school closures (Wu et al., 2010), antiviral drugs (Lipsitch et al., 2007) and vaccines (Medlock and Galvani, 2009). Furthermore, the spatial spread of the influenza virus and its impact on mitigation policies has been investigated using meta-population models (De et al., 2018) and important advances in the context of large-scale individual-based models have been achieved to study pandemic influenza mitigation (Germann et al., 2006; Chao et al., 2010).

For HIV, compartment models have been used early in the pandemic to understand and estimate the incidence based on observed diagnoses (Sweeting et al., 2005) and continue to be used to evaluate policy options (Kerr et al., 2015). Yet, due to the scale-free nature of the sexual transmission network that enables the transmission of HIV (Liljeros, 2011), and the importance to diagnose individuals early on in their infection (Farnham et al., 2013), interest to use individual-based models for HIV was raised. Through individual-based models, the particularities of scale free sexual networks were investigated (Bakker et al., 2000). Furthermore, they enable the explicit modelling of personal attributes such as partnership properties (Schmid and Kretzschmar, 2012), coinfections with other pathogens that modulate HIV infectiousness (Hendrickx et al., 2021), policies to implement PrEP (LeVasseur et al., 2018), testing and contact tracing strategies (Graw et al., 2012) and virus strains (i.e. HIV subtypes; Ferdinandy et al., 2015).

As a respiratory pathogen, SARS-CoV-2 shares the transmission network and many of the virological properties with influenza viruses. Thus, compartment models with a similar structure than influenza epidemiological models were used to project epidemiological trajectories at the start of the epidemic, to inform policy makers about the expected extent of the burden with respect to hospitalizations and deaths (Kucharski et al., 2020). Yet, early in the pandemic it became clear that the asymptomatic and presymptomatic nature of SARS-CoV-2 infections, combined with differences in disease outcome, needs to be captured in the epidemiological models (Willem et al., 2021).

From a compartment model perspective, this meant that traditional SEIR models (Eames et al., 2012; that is, models that consider four epidemiological states: susceptible, exposed, infected and recovered) required extensions to take into account this additional complexity (Abrams et al., 2021). Compartment models have thus been instrumental in the evaluation of population-wide strategies such as lockdowns, school closures, teleworking and more recently vaccination policies (Prem et al., 2020; Moore et al., 2021). However, in order to study prevention strategies that target the individual, such as contact tracing and mass testing policies, the use of individual-based models provide important insights (Willem et al., 2021). These individual-based models extend the ideas from influenza literature (Chao et al., 2010), but explore novel modelling approaches to respond to particular properties of SARS-CoV-2, including antivirals that modulate the viral load curve of infected individuals (Torneri et al., 2020), understanding the serial and generation intervals under control measures (Torneri et al., 2021), contact tracing telephone apps (Ferretti et al., 2020) and universal testing (Libin et al., 2021). Finally, to study the impact of mobility, meta-population models that were developed in the context of influenza (Dolgin, 2021), were adapted to the COVID-19 context (Coletti et al., 2020; Saldaña and Velasco-Hernández, 2021).

Epidemiological models thus facilitate a framework to make predictions and to study the effect of prevention strategies in

simulation. Nevertheless, the development of prevention strategies, which need to fulfil distinct criteria (i.e. prevalence, mortality, morbidity and cost), remains a challenging task. For this reason, the use of machine learning techniques to optimise prevention policies in an epidemiological model constitutes a promising venue for future research. In the context of influenza, the use of reinforcement learning has been shown to learn prevention policies in complex epidemiological models (Libin et al., 2018, 2020). From another perspective, Kerr et al. (2015) use mathematical optimization in combination with compartment models, to optimize HIV mitigation strategies. For COVID-19, both mathematical optimization and reinforcement learning techniques have been used to learn optimal mitigation strategies (Kompella et al., 2020; Richard et al., 2021).

This overview shows that epidemiological models contribute a great amount to the understanding of how pathogens spread, and what can be done to mitigate their spread. A significant part of the power of the public health response to COVID-19, builds on decades of modelling research, but this global emergency also demonstrated some weakness with respect to the state of the reproducibility and availability of the models' source code (Hazelbag et al., 2020). Therefore, we celebrate the availability of high-quality software code of many important models that are continued to be used to study the ongoing COVID-19 pandemic (Hinch et al., 2021; Kerr et al., 2021; Willem et al., 2021).

DISCUSSION

In this work, we cover three distinct pandemics and discuss their emergence, zoonotic origin and global spread. Alongside, we compare the public health measures implemented by health authorities to the distinct and similar properties of these pandemics and contextualize it across the eras in which they took place.

During these three pandemics, we witnessed major technical advances regarding the development of pharmaceutical interventions. For SARS-CoV-2, two novel vaccine delivery platforms (i.e. mRNA and vector-based platforms) were used to develop and produce vaccines at an unprecedented pace. These platforms facilitate a swift response to novel pathogens and will be of vital importance to combat future pandemics. The ease of use with which mRNA vaccines can be developed also triggered their use in the context of HIV, for which a vaccine is long due (Aidsmap, 2021). The vaccines targeted at SARS-CoV-2 were developed in less than a year, rendering it an impressive achievement. Nonetheless, it also shows that non-pharmaceutical interventions remain indispensable to react to a pandemic before treatment or vaccines become available. Therefore, studying optimal strategies for non-pharmaceutical interventions remains as crucial as it was for the 1918 influenza pandemic, and it deserves the appropriate attention to prepare for future epidemic calamities. An important concern in the face of the available vaccines, is the continuous evolution of variants, that may affect their effectiveness. This indicates the potential for pan-vaccines, that target a more conserved region in the genome, and could even offer protection for novel pathogens (Wei et al., 2020).

An important determinant in the spread of viruses, is the potential for pre-symptomatic transmission from the infected host to other individuals. This greatly impacts how a pathogen can be controlled, as individuals might be unaware of their infection status before symptoms appear. This is not only a concern for acute respiratory pathogens, such as SARS-CoV-2, but it also plays an important role in the spread of chronic infectious diseases such as HCV and HIV-1, where the presymptomatic phase can last many years. To control pathogens that can be transmitted prior to symptom onset, early diagnosis is key (Fraser et al., 2004).

Recognizing the need for early diagnosis, we could hope to control the next emerging pathogen by means of testing, tow swiftly control the local outbreak, to avoid it to become pandemic. For this to work, we would need to have the capabilities to scale up testing in a short time, to cope with the exponential growth of infections. This could be achieved by advancing diagnostic methods (Kerr et al., 2015) and by maintaining a stock of reagents and diagnostic material that can be flown into the epicentre of the virus outbreak, to enable mass testing to nip the epidemic in the bud.

Eventually, the origin of all novel pathogens lies in a zoonotic jump. Therefore, monitoring ecological niches from which such a jump might originate is of crucial importance. This is especially true for areas where forestial regions are connected to large urban areas. Furthermore, livestock farms remain at risk as farm animals come into close contact with human hosts and are often housed in shelters that facilitate the rapid spread of a novel pathogen. While undoubtedly challenging, we argue that the use of ecological models can be of great use to identify areas that are at risk and warrant close monitoring.

In this work, we address the significant advances related to epidemiological modelling. We are now at the point that flexible individual-based models can quickly be configured to simulate a novel emerging pathogen. Such models have a fine-grained resolution that makes them suitable to model prevention strategies that focus on individuals (i.e. contact tracing, antivirals and isolation) and are crucial during the initial phase of a pandemic. While powerful, such fine-grained models require a detailed understanding of human contacts and mobility. Therefore, we should invest in the collection of data on human contacts and mobility prior to the next epidemic emergency, and study how we can use such datasets to model the impact of social distancing measures on human behaviour. We note that this data is sensitive, and its collection can be prone to ethical and regulatory affairs, which requires the necessary attention. Next to factors that influence human behaviour, individual-based models also require detailed information on properties that are specific to the pathogen under investigation, i.e. the proportion of presymptomatic infection, age factors of the host that modulate virus traits (e.g. virulence, symptoms) and dispersion in infectiousness (i.e. superspreading). Figuring out these factors is challenging while a pandemic unfolds, and therefore, we should prepare by establishing protocols to collect the right data in an optimal way (i.e. transmission networks,

genomics, viral load profiles). Such protocols can be optimized by simulating what-if scenarios in individual-based models.

Finally, we note that during the SARS-CoV-2, an unprecedented number of virus sequences was published, *via* the use of next-generation sequencing (NGS) platforms. During the initial phase of an epidemic, sequencing a large proportion of cases can shed light on several virus properties such as the proportion of asymptomatic cases, superspreading effects and properties related to attributes of the host (e.g. age, gender, underlying conditions). In a later phase of the epidemic, sequencing virus genomes allows for monitoring viral diversity, for example, monitoring variants of concerns in the context of SARS-CoV-2. However, it remains to be investigated whether mass sequencing delivers a benefit to a more modest testing policy with a carefully calibrated sampling strategy.

To conclude, we witnessed many advances over this course of these three major pandemics. With all this knowledge, we now have the potential to better prepare for the next pandemic, and perhaps even stop a new pathogen in its tracks before it is able to become a pandemic.

AUTHOR CONTRIBUTIONS

MM, PL, and AA: conceptualization. MM and SS: software. MM, MP, AT, PL, and AA: validation and writing—review and editing. MM, VP, MP, SS, PL, and AA: formal analysis. MM, MP, VP, and PL: investigation. MM, SS, and PL: resources. MM, PL, AT, and AA: writing—original draft preparation. MM, MP, VP, PL, and AA: visualization. PL and AA: supervision. AA: project administration and funding acquisition. All authors contributed to the article and approved the submitted version.

FUNDING

This study was financed by FCT through the following projects: GHTM-UID/04413/2020, INTEGRIV (PTDC/SAU-INF/31990/2017) and the scholarship PD/BD/135714/2018 and MARVEL (PTDC/SAU-PUB/4018/2021). This project has received funding from the European Union's Horizon Europe Research and Innovation Programme under grant agreement No. 101046016. This work also received funding from the European Research Council (ERC) under the European Union's Horizon 2020 research and innovation program (PL and AT: grant number 101003688 – EpiPose project). PL gratefully acknowledges support from the Fonds voor Wetenschappelijk Onderzoek (FWO) *via* postdoctoral fellowship 1242021N and research project G0H0420N, and the Research council of the Vrije Universiteit Brussel (OZR-VUB) *via* grant number OZR3863BOF. This research acknowledges funding from the Flemish Government through the AI Research Program.

REFERENCES

Abrams, S., Wambua, J., Santermans, E., Willem, L., Kuylen, E., Coletti, P., et al. (2021). Modelling the early phase of the Belgian COVID-19 epidemic using a stochastic compartmental model and studying its implied future trajectories. *Epidemics* 35:100449. doi: 10.1016/j.epidem.2021.100449

Ahsan, W., Javed, S., Al, B. M., Alhazmi, H. A., and Najmi, A. (2020). Treatment of SARS-CoV-2: how far have we reached? *Drug Discov. Ther.* 14, 67–72. doi: 10.5582/ddt.2020.03008

Aidsmap (2021). mRNA vaccine protects monkeys against HIV-like virus | aidsmap [Internet]. Available at: https://www.aidsmap.com/news/mar-2021/mrna-vaccine-protects-monkeys-against-hiv-virus (Accessed July 29, 2021).

Alcantara, L. C. J., Cassol, S., Libin, P., Deforche, K., Pybus, O. G., Van Ranst, M., et al. (2009). A standardized framework for accurate, high-throughput genotyping of recombinant and non-recombinant viral sequences. *Nucleic Acids Res.* 37, W634–W642. doi: 10.1093/nar/gkp455

Allen, T., Murray, K. A., Zambrana-Torrelio, C., Morse, S. S., Rondinini, C., Di Marco, M., et al. (2017). Global hotspots and correlates of emerging zoonotic diseases. *Nat. Commun.* 8:1124. doi: 10.1038/s41467-017-00923-8

Alnwick, D., Altman, D., Kates, J., Rhodes, T., Kaiser, H. J., Foundation, F., et al. (2007). Bringing HIV Prevention to Scale: An Urgent Global Priority and Infectious Diseases.

Andreani, J., Le, M., Du, I., Jardot, P., Rolland, C., Lisi, L., et al. (2020). Remdesivir, lopinavir, emetine, and homoharringtonine inhibit SARS-CoV-2 replication in vitro. *Antivir. Res.* 178:104786. doi: 10.1016/j.antiviral.2020.104786

Andreano, E., and Rappuoli, R. (2021). SARS-CoV-2 escaped natural immunity, raising questions about vaccines and therapies. *Nat. Med.* 27, 759–761. doi: 10.1038/s41591-021-01347-0

Andrews, N., Stowe, J., Kirsebom, F., Toffa, S., Rickeard, T., Gallagher, E., et al. (2022). Covid-19 vaccine effectiveness against the omicron (B.1.1.529) variant. *N. Engl. J. Med.* 386, 1532–1546. doi: 10.1056/NEJMoa2119451

Baesi, K., Ravanshad, M., Ghanbarisafari, M., Saberfar, E., SeyedAlinaghi, S., and Volk, J. E. (2014). Antiretroviral drug resistance among antiretroviral-naïve and treatment experienced patients infected with HIV in Iran. *J. Med. Virol.* 86, 1093–1098. doi: 10.1002/jmv.23898

Baker, R. E., Mahmud, A. S., Miller, I. F., Rajeev, M., Rasambainarivo, F., Rice, B. L., et al. (2021). Infectious disease in an era of global change. *Nat. Rev. Microbiol.* 20, 193–205. doi: 10.1038/s41579-021-00639-z

Bakker, R., Korenromp, E., Meester, E., Van Der Ploeg, C., Voeten, H., Van Vliet, C., et al. (2000). STDSIM: a microsimulation model for decision support in the control of HIV and other STDs. *Sex. Transm. Dis.* 27:652. doi: 10.1097/00007435-200011000-00029

Barberis, I., Myles, P., Ault, S. K., Bragazzi, N. L., and Martini, M. (2016). History and evolution of influenza control through vaccination: from the first monovalent vaccine to universal vaccines. *J. Prev. Med. Hyg.* 57, E115–E120.

Baric, R. S. (2008). SARS-CoV: lessons for global health. *Virus Res.* 133, 1–3. doi: 10.1016/j.virusres.2007.03.024

Bettini, E., and Locci, M. (2021). SARS-CoV-2 mRNA vaccines: immunological mechanism and Beyond. *Vaccine* 9:147. doi: 10.3390/vaccines9020147

Boni, M. F., Lemey, P., Jiang, X., Lam, T. T.-Y., Perry, B. W., Castoe, T. A., et al. (2020). Evolutionary origins of the SARS-CoV-2 sarbecovirus lineage responsible for the COVID-19 pandemic. *Nat. Microbiol.* 5, 1408–1417. doi: 10.1038/s41564-020-0771-4

Boras, B., Jones, R. M., Anson, B. J., Arenson, D., Aschenbrenner, L., Bakowski, M. A., et al. (2021). Preclinical characterization of an intravenous coronavirus 3CL protease inhibitor for the potential treatment of COVID19. *Nat. Commun.* 12:6055. doi: 10.1038/s41467-021-26239-2

Brankston, G., Gitterman, L., Hirji, Z., Lemieux, C., and Gardam, M. (2007). Transmission of influenza A in human beings. *Lancet Infect. Dis.* 7, 257–265. doi: 10.1016/S1473-3099(07)70029-4

Brekke, K., Sommerfelt, M., Ökvist, M., Dyrhol-Riise, A. M., and Kvale, D. (2017). The therapeutic HIV Env C5/gp41 vaccine candidate Vacc-C5 induces

specific T cell regulation in a phase I/II clinical study. *BMC Infect. Dis.* 17:228. doi: 10.1186/s12879-017-2316-x

Burke, D. (1997). Recombination in HIV: an important viral evolutionary strategy. *Emerg. Infect. Dis.* 3, 253–259. doi: 10.3201/eid0303.970301

Burki, T. (2020). Mass testing for COVID-19. *Lancet Microbe* 1:e317. doi: 10.1016/S2666-5247(20)30205-6

CDC (2021a). About HIV/AIDS | HIV Basics | HIV/AIDS | CDC [Internet]. Available at: https://www.cdc.gov/hiv/basics/whatishiv.html (Accessed June 30, 2021).

CDC (2021b). Different Types of Flu Vaccines | CDC [Internet]. Available at: https://www.cdc.gov/flu/prevent/different-flu-vaccines.htm (Accessed June 30, 2021).

CDC (2021c). Different COVID-19 Vaccines | CDC [Internet]. Available at: https://www.cdc.gov/coronavirus/2019-ncov/vaccines/different-vaccines.html (Accessed March 16, 2021).

CDC (2021d). SARS-CoV-2 Variant Classifications and Definitions [Internet]. Available at: https://www.cdc.gov/coronavirus/2019-ncov/variants/variant-info.html#Interest (Accessed July 29, 2021).

Chao, D. L., Halloran, M. E., Obenchain, V. J., and Longini, I. M. (2010). FluTE, a publicly available stochastic influenza epidemic simulation model. *PLoS Comput. Biol.* 6:e1000656. doi: 10.1371/journal.pcbi.1000656

Charles, B., and Hicks, M. (2008). Antiretroviral Drug Resistance Testing – Updated Guidelines from the IAS–USA. NEJM J Watch 2008. Available at: https://www.jwatch.org/AC200807140000002/2008/07/14/antiretroviral-drug-resistance-testing-updated (Accessed March 12, 2021).

Chen, S., Prettner, K., Kuhn, M., Geldsetzer, P., Wang, C., Bärnighausen, T., et al. (2021). Climate and the spread of COVID-19. *Sci. Rep.* 11:9042. doi: 10.1038/s41598-021-87692-z

Chiara, M., D'Erchia, A. M., Gissi, C., Manzari, C., Parisi, A., Resta, N., et al. (2021). Next generation sequencing of SARS-CoV-2 genomes: challenges, applications and opportunities. *Brief. Bioinform.* 22, 616–630. doi: 10.1093/bib/bbaa297

Chow, E. J., Doyle, J. D., and Uyeki, T. M. (2019). Influenza virus-related critical illness: prevention, diagnosis, treatment. *Crit. Care* 23:214. doi: 10.1186/s13054-019-2491-9

Clutter, D. S., Jordan, M. R., Bertagnolio, S., and Shafer, R. W. (2016). HIV-1 drug resistance and resistance testing. *Infect. Genet. Evol.* 46, 292–307. doi: 10.1016/j.meegid.2016.08.031

Cohen, M. S., Hellmann, N., Levy, J. A., DeCock, K., and Lange, J. (2008). The spread, treatment, and prevention of HIV-1: evolution of a global pandemic. *J. Clin. Invest.* 118, 1244–1254. doi: 10.1172/JCI34706

Coletti, P., Libin, P., Petrof, O., Willem, L., Abrams, S., Herzog, S. A., et al. (2021). A data-driven metapopulation model for the Belgian COVID-19 epidemic: assessing the impact of lockdown and exit strategies. *BMC Infect. Dis.* 21:503. doi: 10.1186/s12879-021-06092-w

Coletti, P., Wambua, J., Gimma, A., Willem, L., Vercruysse, S., Vanhoutte, B., et al. (2020). CoMix: comparing mixing patterns in the Belgian population during and after lockdown. *Sci. Rep.* 10:21885. doi: 10.1038/s41598-020-78540-7

Creech, C. B., Walker, S. C., and Samuels, R. J. (2021). SARS-CoV-2 vaccines. *JAMA* 325:1318. doi: 10.1001/jama.2021.3199

Davis, J. T., Chinazzi, M., Perra, N., Mu, K., Pastore y Piontti, A., Ajelli, M., et al. (2021). Cryptic transmission of SARS-CoV-2 and the first COVID-19 wave. *Nature* 600, 127–132. doi: 10.1038/s41586-021-04130-w

De Clercq, E. (2006). Antiviral agents active against influenza A viruses. *Nat. Rev. Drug Discov.* 5, 1015–1025. doi: 10.1038/nrd2175

De Cock, K. M., Jaffe, H. W., and Curran, J. W. (2012). The evolving epidemiology of HIV/AIDS. *AIDS* 26, 1205–1213. doi: 10.1097/QAD.0b013e328354622a

De, L. G., Van, K. K., Coletti, P., Poletto, C., Bossuyt, N., Hens, N., et al. (2018). The impact of regular school closure on seasonal influenza epidemics: a data-driven spatial transmission model for Belgium. *BMC Infect. Dis.* 18:29. doi: 10.1186/s12879-017-2934-3

Dellicour, S., Hong, S. L., Vrancken, B., Chaillon, A., Gill, M. S., Maurano, M. T., et al. (2021). Dispersal dynamics of SARS-CoV-2 lineages during the first epidemic wave in New York City. *PLoS Pathog.* 17:e1009571. doi: 10.1371/journal.ppat.1009571

Diekmann, O., Heesterbeek, H., and Britton, T. (2013). *Mathematical Tools for Understanding Infectious Disease Dynamics.* Princeton University Press.

Dinges, W., Girard, P.-M., Podzamczer, D., Brockmeyer, N. H., García, F., Harrer, T., et al. (2016). The F4/AS01B HIV-1 vaccine candidate is safe and immunogenic, but does not show viral efficacy in antiretroviral therapy-naive, HIV-1-infected adults. *Medicine* 95:e2673. doi: 10.1097/MD.0000000000002673

Dolgin, E. (2021). The tangled history of mRNA vaccines. *Nature* 597, 318–324. doi: 10.1038/d41586-021-02483-w

Du, Z., Nugent, C., Galvani, A. P., Krug, R. M., and Meyers, L. A. (2020). Modeling mitigation of influenza epidemics by baloxavir. *Nat. Commun.* 11:2750. doi: 10.1038/s41467-020-16585-y

Eames, K. T. D., Tilston, N. L., Brooks-Pollock, E., and Edmunds, W. J. (2012). Measured dynamic social contact patterns explain the spread of H1N1v influenza. *PLoS Comput. Biol.* 8:e1002425. doi: 10.1371/journal.pcbi.1002425

Earth.Org (2022). Mapping the Spanish Flu Pandemic | Earth.Org—Past | Present | Future [Internet]. Available at: https://earth.org/data_visualization/pandemic-map-the-spanish-flu/ (Accessed February 3, 2022).

Eggo, R. M., Cauchemez, S., and Ferguson, N. M. (2011). Spatial dynamics of the 1918 influenza pandemic in England, Wales and the United States. *J. R. Soc. Interface* 8, 233–243. doi: 10.1098/rsif.2010.0216

Enger, C., Graham, N., Peng, Y., Chmiel, J. S., Kingsley, L. A., Detels, R., et al. (1996). Survival From early, intermediate, and late stages of HIV infection. *JAMA* 275, 1329–1334. doi: 10.1001/jama.1996.03530410043031

Ensoli, F., Cafaro, A., Casabianca, A., Tripiciano, A., Bellino, S., Longo, O., et al. (2015). HIV-1 tat immunization restores immune homeostasis and attacks the HAART-resistant blood HIV DNA: results of a randomized phase II exploratory clinical trial. *Retrovirology* 12:33. doi: 10.1186/s12977-015-0151-y

European Centre for Disease Prevention and Control (2022). SARS-CoV-2 variants of concern as of 03 February [Internet]. Available at: https://www.ecdc.europa.eu/en/covid-19/variants-concern (Accessed February 3, 2022).

European Medicines Agency (2022). Vaxzevria (previously COVID-19 Vaccine AstraZeneca) | European Medicines Agency [Internet]. Available at: https://www.ema.europa.eu/en/medicines/human/EPAR/vaxzevria-previously-covid-19-vaccine-astrazeneca (Accessed April 6, 2022).

Faria, N. R., Rambaut, A., Suchard, M. A., Baele, G., Bedford, T., Ward, M. J., et al. (2014). The early spread and epidemic ignition of HIV-1 in human populations. *Science* 346, 56–61. doi: 10.1126/science.1256739

Farnham, P. G., Gopalappa, C., Sansom, S. L., Hutchinson, A. B., Brooks, J. T., Weidle, P. J., et al. (2013). Updates of lifetime costs of care and quality-of-life estimates for HIV-infected persons in the United States. *J. Acquir. Immune Defic. Syndr.* 64, 183–189. doi: 10.1097/QAI.0b013e3182973966

FDA (2021). COVID-19 Vaccines | FDA [Internet]. Available at: https://www.fda.gov/emergency-preparedness-and-response/coronavirus-disease-2019-covid-19/covid-19-vaccines (Accessed March 16, 2021).

Ferdinandy, B., Mones, E., Vicsek, T., and Müller, V. (2015). HIV competition dynamics over sexual networks: first comer advantage conserves founder effects. *PLoS Comput. Biol.* 11:e1004093. doi: 10.1371/journal.pcbi.1004093

Ferguson, N. M., Cummings, D. A. T., Fraser, C., Cajka, J. C., Cooley, P. C., and Burke, D. S. (2006). Strategies for mitigating an influenza pandemic. *Nature* 442, 448–452. doi: 10.1038/nature04795

Ferretti, L., Wymant, C., Kendall, M., Zhao, L., Nurtay, A., Abeler-Dörner, L., et al. (2020). Quantifying SARS-CoV-2 transmission suggests epidemic control with digital contact tracing. *Science* 368:eabb6936. doi: 10.1126/science.abb6936

Fettig, J., Swaminathan, M., Murrill, C. S., and Kaplan, J. E. (2014). Global epidemiology of HIV. *Infect. Dis. Clin. N. Am.* 28, 323–337. doi: 10.1016/j.idc.2014.05.001

Fonner, V. A., Dalglish, S. L., Kennedy, C. E., Baggaley, R., O'Reilly, K. R., Koechlin, F. M., et al. (2016). Effectiveness and safety of oral HIV preexposure prophylaxis for all populations. *AIDS* 30, 1973–1983. doi: 10.1097/QAD.0000000000001145

Fraser, C., Cummings, D. A. T., Klinkenberg, D., Burke, D. S., and Ferguson, N. M. (2011). Influenza transmission in households during the 1918 pandemic. *Am. J. Epidemiol.* 174, 505–514. doi: 10.1093/aje/kwr122

Fraser, C., Riley, S., Anderson, R. M., and Ferguson, N. M. (2004). Factors that make an infectious disease outbreak controllable. *Proc. Natl. Acad. Sci. U. S. A.* 101, 6146–6151. doi: 10.1073/pnas.0307506101

Gallo, R. C., and Montagnier, L. (2003). The discovery of HIV as the cause of AIDS. *N. Engl. J. Med.* 349, 2283–2285. doi: 10.1056/NEJMp038194

Galvin, S. R., and Cohen, M. S. (2004). The role of sexually transmitted diseases in HIV transmission. *Nat. Rev. Microbiol.* 2, 33–42. doi: 10.1038/nrmicro794

Germann, T. C., Kadau, K., Longini, I. M., and Macken, C. A. (2006). Mitigation strategies for pandemic influenza in the United States. *Proc. Natl. Acad. Sci. U. S. A.* 103, 5935–5940. doi: 10.1073/pnas.0601266103

GOV.UK (2021). Summary of Product Characteristics for Lagevrio – GOV.UK [Internet]. Available at: https://www.gov.uk/government/publications/regulatory-approval-of-lagevrio-molnupiravir/summary-of-product-characteristics-for-lagevrio (Accessed December 10, 2021).

Graw, F., Leitner, T., and Ribeiro, R. M. (2012). Agent-based and phylogenetic analyses reveal how HIV-1 moves between risk groups: injecting drug users sustain the heterosexual epidemic in Latvia. *Epidemics* 4, 104–116. doi: 10.1016/j.epidem.2012.04.002

Greene, W. C. (2007). A history of AIDS: looking back to see ahead. *Eur. J. Immunol.* 37(SUPPL. 1), S94–S102. doi: 10.1002/eji.200737441

Hanski, I. (1999). *Metapopulation Ecology.* Oxford University Press.

Harrison, A. G., Lin, T., and Wang, P. (2020). Mechanisms of SARS-CoV-2 transmission and pathogenesis. *Trends Immunol.* 41, 1100–1115. doi: 10.1016/j.it.2020.10.004

Hazelbag, C. M., Dushoff, J., Dominic, E. M., Mthombothi, Z. E., and Delva, W. (2020). Calibration of individual-based models to epidemiological data: a systematic review. *PLoS Comput. Biol.* 16:e1007893. doi: 10.1371/journal.pcbi.1007893

Hemelaar, J. (2012). The origin and diversity of the HIV-1 pandemic. *Trends Mol. Med.* 18, 182–192. doi: 10.1016/j.molmed.2011.12.001

Hemelaar, J., Elangovan, R., Yun, J., Dickson-Tetteh, L., Fleminger, I., Kirtley, S., et al. (2019). Global and regional molecular epidemiology of HIV-1, 1990–2015: a systematic review, global survey, and trend analysis. *Lancet Infect. Dis.* 19, 143–155. doi: 10.1016/S1473-3099(18)30647-9

Hendrickx, D. M., Sousa, J. D., Libin, P. J. K., Delva, W., Liesenborgs, J., Hens, N., et al. (2021). Comparison of two simulators for individual based models in HIV epidemiology in a population with HSV 2 in Yaoundé (Cameroon). *Sci. Rep.* 11:14696. doi: 10.1038/s41598-021-94289-z

Hinch, R., Probert, W. J. M., Nurtay, A., Kendall, M., Wymant, C., Hall, M., et al. (2021). OpenABM-Covid19—an agent-based model for non-pharmaceutical interventions against COVID-19 including contact tracing. *PLoS Comput. Biol.* 17:e1009146. doi: 10.1371/journal.pcbi.1009146

HIV.gov (2021). Symptoms of HIV | HIV.gov [Internet]. Available at: https://www.hiv.gov/hiv-basics/overview/about-hiv-and-aids/symptoms-of-hiv (Accessed June 30, 2021).

Huddleston, J., Barnes, J. R., Rowe, T., Xu, X., Kondor, R., Wentworth, D. E., et al. (2020). Integrating genotypes and phenotypes improves long-term forecasts of seasonal influenza A/H3N2 evolution. *Elife* 9, 1–48. doi: 10.7554/eLife.60067

Hufsky, F., Lamkiewicz, K., Almeida, A., Aouacheria, A., Arighi, C., Bateman, A., et al. (2021). Computational strategies to combat COVID-19: useful tools to accelerate SARS-CoV-2 and coronavirus research. *Brief. Bioinform.* 22, 642–663. doi: 10.1093/bib/bbaa232

Humphreys, M. (2018). The influenza of 1918. *Evol. Med. Public Health* 2018, 219–229. doi: 10.1093/emph/eoy024

Hussain, M., Galvin, H. D., Haw, T. Y., Nutsford, A. N., and Husain, M. (2017). Drug resistance in influenza a virus: the epidemiology and management. *Infect Drug Resist.* 10, 121–134. doi: 10.2147/IDR.S105473

Jacobson, J. M., Routy, J.-P., Welles, S., DeBenedette, M., Tcherepanova, I., Angel, J. B., et al. (2016a). Dendritic cell immunotherapy for HIV-1 infection using autologous HIV-1 RNA. *J. Acquir. Immune Defic. Syndr.* 72, 31–38. doi: 10.1097/QAI.0000000000000926

Jacobson, J. M., Zheng, L., Wilson, C. C., Tebas, P., Matining, R. M., Egan, M. A., et al. (2016b). The safety and immunogenicity of an interleukin-12–enhanced multiantigen DNA vaccine delivered by electroporation for the treatment of HIV-1 infection. *J. Acquir. Immune Defic. Syndr.* 71, 163–171. doi: 10.1097/QAI.0000000000000830

Kelly, H. (2011). The classical definition of a pandemic is not elusive. *Bull. World Health Organ.* 89, 540–541. doi: 10.2471/BLT.11.088815

Kermack, W., and Mckendrick, A. (1991a). Contributions to the mathematical theory of epidemics—I. *Bull. Math. Biol.* 53, 33–55. doi: 10.1016/S0092-8240(05)80040-0

Kermack, W. O., and McKendrick, A. G. (1991b). Contributions to the mathematical theory of epidemics—II. The problem of endemicity. *Bull. Math. Biol.* 53, 57–87. doi: 10.1007/BF02464424

Kermack, W. O., and McKendrick, A. G. (1991c). Contributions to the mathematical theory of epidemics—III. Further studies of the problem of endemicity. *Bull. Math. Biol.* 53, 89–118. doi: 10.1126/science.15.367.68

Kerr, C. C., Stuart, R. M., Gray, R. T., Shattock, A. J., Fraser-Hurt, N., Benedikt, C., et al. (2015). Optima: a model for HIV epidemic analysis, program prioritization, and resource optimization. *J. Acquir. Immune Defic. Syndr.* 69, 365–376. doi: 10.1097/QAI.0000000000000605

Kerr, C. C., Stuart, R. M., Mistry, D., Abeysuriya, R. G., Rosenfeld, K., Hart, G. R., et al. (2021). Covasim: an agent-based model of COVID-19 dynamics and interventions. *PLoS Comput. Biol.* 17:e1009149. doi: 10.1371/journal.pcbi.1009149

Keshavarz, M., Solaymani-Mohammadi, F., Namdari, H., Arjeini, Y., Mousavi, M. J., and Rezaei, F. (2020). Metabolic host response and therapeutic approaches to influenza infection. *Cell. Mol. Biol. Lett.* 25:15. doi: 10.1186/s11658-020-00211-2

Kim, J., Lee, E., Park, B.-J., Bang, J. H., and Lee, J. Y. (2018). Adherence to antiretroviral therapy and factors affecting low medication adherence among incident HIV-infected individuals during 2009–2016: A nationwide study. *Sci. Rep.* 8:3133. doi: 10.1038/s41598-018-21081-x

Kompella, V., Capobianco, R., Jong, S., Browne, J., Fox, S., Meyers, L., et al. (2020). Reinforcement Learning for Optimization of COVID-19 Mitigation policies. Available at: http://arxiv.org/abs/2010.10560 (Accessed October 20, 2020).

Konda, M., Dodda, B., Konala, V. M., Naramala, S., and Adapa, S. (2020). Potential zoonotic origins of SARS-CoV-2 and insights for preventing future pandemics through one health approach. *Cureus* 12:e8932. doi: 10.7759/cureus.8932

Korber, B., Theiler, J., Gao, F., Gupta, R., Lapedes, A., Hahn, B. H., et al. (2000). Timing the ancestor of the HIV-1 pandemic strains. *Science* 288, 1789–1796. doi: 10.1126/science.288.5472.1789

Koszalka, P., Tilmanis, D., and Hurt, A. C. (2017). Influenza antivirals currently in late-phase clinical trial. *Influenza Other Respir. Viruses* 11, 240–246. doi: 10.1111/irv.12446

Kucharski, A. J., Russell, T. W., Diamond, C., Liu, Y., Edmunds, J., Funk, S., et al. (2020). Early dynamics of transmission and control of COVID-19: a mathematical modelling study. *Lancet Infect. Dis.* 20, 553–558. doi: 10.1016/S1473-3099(20)30144-4

Kumar, M., Taki, K., Gahlot, R., Sharma, A., and Dhangar, K. (2020). A chronicle of SARS-CoV-2: part-I – epidemiology, diagnosis, prognosis, transmission and treatment. *Sci. Total Environ.* 734:139278. doi: 10.1016/j.scitotenv.2020.139278

Lampejo, T. (2020). Influenza and antiviral resistance: an overview. *Eur. J. Clin. Microbiol. Infect. Dis.* 39, 1201–1208. doi: 10.1007/s10096-020-03840-9

Lauring, A. S., Tenforde, M. W., Chappell, J. D., Gaglani, M., Ginde, A. A., McNeal, T., et al. (2022). Clinical severity of, and effectiveness of mRNA vaccines against, covid-19 from omicron, delta, and alpha SARS-CoV-2 variants in the United States: prospective observational study. *BMJ* 376:e069761. doi: 10.1136/bmj-2021-069761

Lee, N., and Hurt, A. C. (2018). Neuraminidase inhibitor resistance in influenza: a clinical perspective. *Curr. Opin. Infect. Dis.* 31, 520–526. doi: 10.1097/QCO.0000000000000498

LeVasseur, M. T., Goldstein, N. D., Tabb, L. P., Olivieri-Mui, B. L., and Welles, S. L. (2018). The effect of PrEP on HIV incidence among men who have sex with men in the context of condom use, treatment as prevention, and seroadaptive practices. *J. Acquir. Immune Defic. Syndr.* 77, 31–40. doi: 10.1097/QAI.0000000000001555

Libin, P. J. K., Moonens, A., Verstraeten, T., Perez-Sanjines, F., Hens, N., Lemey, P., et al. (2020). "Deep reinforcement learning for large-scale epidemic control." in *European Conference of Machine Learning*.

Libin, P. J. K., Verstraeten, T., Roijers, D. M., Grujic, J., Theys, K., Lemey, P., et al. (2018). "Bayesian best-arm identification for selecting influenza mitigation strategies," in *European Conference of Machine Learning*. eds. U. Brefeld, E. Curry, E. Daly, B. MacNamee, A. Marascu and F. Pinelli et al. (Cham: Springer International Publishing).

Libin, P. J. K., Willem, L., Verstraeten, T., Torneri, A., Vanderlocht, J., and Hens, N. (2021). Assessing the feasibility and effectiveness of household-pooled universal testing to control COVID-19 epidemics. *PLoS Comput. Biol.* 17:e1008688. doi: 10.1371/journal.pcbi.1008688

Liljeros, F. (2011). "The web of human sexual contacts," in *The Structure and Dynamics of Networks* (Princeton University Press), 227–228.

Lipsitch, M., Cohen, T., Murray, M., and Levin, B. R. (2007). Antiviral resistance and the control of pandemic influenza. *PLoS Med.* 4:e15. doi: 10.1371/journal.pmed.0040015

Liu, S., Ji, K., Chen, J., Tai, D., Jiang, W., Hou, G., et al. (2009). Panorama phylogenetic diversity and distribution of type A influenza virus. *PLoS One* 4:e0005022. doi: 10.1371/journal.pone.0005022

Liu, D. X., Liang, J. Q., and Fung, T. S. (2021). Human coronavirus-229E, -OC43, -NL63, and -HKU1 (coronaviridae) *Encyclopedia of Virology* 428–440. doi: 10.1016/B978-0-12-809633-8.21501-X

Lopez Bernal, J., Andrews, N., Gower, C., Robertson, C., Stowe, J., Tessier, E., et al. (2021). Effectiveness of the Pfizer-BioNTech and Oxford-AstraZeneca vaccines on covid-19 related symptoms, hospital admissions, and mortality in older adults in England: test negative case-control study. *BMJ* 373:n1088. doi: 10.1136/bmj.n1088

Lotfi, M., Hamblin, M. R., and Rezaei, N. (2020). COVID-19: transmission, prevention, and potential therapeutic opportunities. *Clin. Chim. Acta* 508, 254–266. doi: 10.1016/j.cca.2020.05.044

Luk, J., Gross, P., and Thompson, W. W. (2001). Observations on mortality during the 1918 influenza pandemic. *Clin. Infect. Dis.* 33, 1375–1378. doi: 10.1086/322662

Macatangay, B. J. C., Riddler, S. A., Wheeler, N. D., Spindler, J., Lawani, M., Hong, F., et al. (2016). Therapeutic vaccination with dendritic cells loaded with autologous HIV type 1–infected apoptotic cells. *J. Infect. Dis.* 213, 1400–1409. doi: 10.1093/infdis/jiv582

Malani, P. N., and Golub, R. M. (2021). Neutralizing monoclonal antibody for mild to moderate COVID-19. *JAMA* 325:644. doi: 10.1001/jama.2021.0585

Malik, Y. A. (2020). Properties of coronavirus and SARS-CoV-2. *Malays. J. Pathol.* 42, 3–11.

Markel, H., Lipman, H. B., Navarro, J. A., Sloan, A., Michalsen, J. R., Stern, A. M., et al. (2007). Nonpharmaceutical interventions implemented by US cities during the 1918-1919 influenza pandemic. *JAMA* 298:644, –654. doi: 10.1001/jama.298.6.644

Martini, M., Gazzaniga, V., Bragazzi, N. L., and Barberis, I. (2019). The Spanish influenza pandemic: a lesson from history 100 years after 1918. *J. Prev. Med. Hyg.* 60, E64–E67. doi: 10.15167/2421-4248/jpmh2019.60.1.1205

McArthur, D. B. (2019). Emerging infectious diseases. *Nurs. Clin. North Am.* 54, 297–311. doi: 10.1016/j.cnur.2019.02.006

Medlock, J., and Galvani, A. P. (2009). Optimizing influenza vaccine distribution. *Science* 325, 1705–1708. doi: 10.1126/science.1175570

Mermel, L. A. (2018). The great influenza centennial—what have we learned about the epidemiology and prevention of transmission? *Clin. Microbiol. Infect.* 24, 1227–1228. doi: 10.1016/j.cmi.2018.07.001

Mills, C. E., Robins, J. M., and Lipsitch, M. (2004). Transmissibility of 1918 pandemic influenza. *Nature* 432, 904–906. doi: 10.1038/nature03063

Miranda, M. N. S., Pingarilho, M., Pimentel, V., Martins, M. D. R. O., Vandamme, A.-M., Bobkova, M., et al. (2021). Determinants of HIV-1 late presentation in patients followed in Europe. *Pathogens* 10:835. doi: 10.3390/pathogens10070835

Moderna, Inc. (2021). Moderna Announces First Participant Dosed in Phase 1/2 Study of Its Quadrivalent Seasonal Flu mRNA Vaccine | Moderna, Inc. [Internet]. Available at: https://investors.modernatx.com/news-releases/news-release-details/moderna-announces-first-participant-dosed-phase-12-study-its/ (Accessed July 29, 2021).

Moir, S., Chun, T. W., and Fauci, A. S. (2011). Pathogenic mechanisms of HIV disease. *Annu. Rev. Pathol. Mech. Dis.* 6, 223–248. doi: 10.1146/annurev-pathol-011110-130254

Montagnier, L., Chermann, J. C., Barré-Sinoussi, F., Klatzmann, D., Wain-Hobson, S., Alizon, M., et al. (1984). Lymphadenopathy associated virus and its etiological role in AIDS. *Princess Takamatsu Symp.* 15, 319–331.

Moore, S., Hill, E. M., Dyson, L., Tildesley, M. J., and Keeling, M. J. (2021). Modelling optimal vaccination strategy for SARS-CoV-2 in the UK. *PLoS Comput. Biol.* 17:e1008849. doi: 10.1371/journal.pcbi.1008849

Morens, D. M., and Fauci, A. S. (2007). The 1918 influenza pandemic: insights for the 21st century. *J. Infect. Dis.* 195, 1018–1028. doi: 10.1086/511989

Morens, D. M., and Fauci, A. S. (2020). Emerging pandemic diseases: how we got to COVID-19. *Cell* 182, 1077–1092. doi: 10.1016/j.cell.2020.08.021

Ngcapu, S., Theys, K., Libin, P., Marconi, V., Sunpath, H., Ndung'u, T., et al. (2017). Characterization of nucleoside reverse transcriptase inhibitor-associated mutations in the RNase H region of HIV-1 subtype C infected individuals. *Viruses* 9:330. doi: 10.3390/v9110330

Nickol, M. E., and Kindrachuk, J. (2019). A year of terror and a century of reflection: perspectives on the great influenza pandemic of 1918-1919. *BMC Infect. Dis.* 19:117. doi: 10.1186/s12879-019-3750-8

Nyberg, T., Ferguson, N. M., Nash, S. G., Webster, H. H., Flaxman, S., Andrews, N., et al. (2022). Comparative analysis of the risks of hospitalisation and death associated with SARS-CoV-2 omicron (B.1.1.529) and delta (B.1.617.2) variants in England: a cohort study. *Lancet* 399, 1303–1312. doi: 10.1016/S0140-6736(22)00462-7

O'Toole, Á., Scher, E., Underwood, A., Jackson, B., Hill, V., McCrone, J. T., et al. (2021). Assignment of epidemiological lineages in an emerging pandemic using the pangolin tool. *Virus Evol.* 7, 1–9. doi: 10.1093/ve/veab064/6315289

Oude Munnink, B. B., Worp, N., Nieuwenhuijse, D. F., Sikkema, R. S., Haagmans, B., Fouchier, R. A. M., et al. (2021). The next phase of SARS-CoV-2 surveillance: real-time molecular epidemiology. *Nat. Med.* 27, 1518–1524. doi: 10.1038/s41591-021-01472-w

Palmer, S., Cunniffe, N., and Donnelly, R. (2021). COVID-19 hospitalization rates rise exponentially with age, inversely proportional to thymic T-cell production. *J. R. Soc. Interface* 18:rsif.2020.0982, 20200982. doi: 10.1098/rsif.2020.0982

Paraschiv, S., Banica, L., Nicolae, I., Niculescu, I., Abagiu, A., Jipa, R., et al. (2017). Epidemic dispersion of HIV and HCV in a population of co-infected Romanian injecting drug users. *PLoS One* 12:e0185866. doi: 10.1371/journal.pone.0185866

Park, J. W., Lagniton, P. N. P., Liu, Y., and Xu, R.-H. (2021). mRNA vaccines for COVID-19: what, why and how. *Int. J. Biol. Sci.* 17, 1446–1460. doi: 10.7150/ijbs.59233

Pau, A. K., and George, J. M. (2014). Antiretroviral therapy: current drugs. *Infect. Dis. Clin. N. Am.* 28, 371–402. doi: 10.1016/j.idc.2014.06.001

Peeples, L. (2021). Face masks for COVID pass their largest test yet. *Nature*. doi: 10.1038/d41586-021-02457-y

Peto, T., Affron, D., Afrough, B., Agasu, A., Ainsworth, M., Allanson, A., et al. (2021). COVID-19: rapid antigen detection for SARS-CoV-2 by lateral flow assay: a national systematic evaluation of sensitivity and specificity for mass-testing. *EClinicalMedicine* 36:100924. doi: 10.1016/j.eclinm.2021.100924

Pimentel, V., Pingarilho, M., Alves, D., Diogo, I., Fernandes, S., Miranda, M., et al. (2020). Molecular epidemiology of HIV-1 infected migrants followed up in Portugal: trends between 2001–2017. *Viruses* 12:268. doi: 10.3390/v12030268

Pineda-Peña, A. C., Faria, N. R., Imbrechts, S., Libin, P., Abecasis, A. B., Deforche, K., et al. (2013). Automated subtyping of HIV-1 genetic sequences for clinical and surveillance purposes: performance evaluation of the new REGA version 3 and seven other tools. *Infect. Genet. Evol.* 19, 337–348. doi: 10.1016/j.meegid.2013.04.032

Pineda-Peña, A.-C., Pingarilho, M., Li, G., Vrancken, B., Libin, P., Gomes, P., et al. (2019). Drivers of HIV-1 transmission: the Portuguese case. *PLoS One* 14:e0218226. doi: 10.1371/journal.pone.0218226

Pingarilho, M., Pimentel, V., Diogo, I., Fernandes, S., Miranda, M., Pineda-Pena, A., et al. (2020). Increasing prevalence of HIV-1 transmitted drug resistance in Portugal: implications for first line treatment recommendations. *Viruses* 12:1238. doi: 10.3390/v12111238

Plotkin, S. (2014). History of vaccination. *Proc. Natl. Acad. Sci. U. S. A.* 111, 12283–12287. doi: 10.1073/pnas.1400472111

Pollard, R. B., Rockstroh, J. K., Pantaleo, G., Asmuth, D. M., Peters, B., Lazzarin, A., et al. (2014). Safety and efficacy of the peptide-based therapeutic vaccine for HIV-1, Vacc-4×: a phase 2 randomised, double-blind, placebo-controlled trial. *Lancet Infect. Dis.* 14, 291–300. doi: 10.1016/S1473-3099(13)70343-8

Pradhan, D., Biswasroy, P., Kumar Naik, P., Ghosh, G., and Rath, G. (2020). A review of current interventions for COVID-19 prevention. *Arch. Med. Res.* 51, 363–374. doi: 10.1016/j.arcmed.2020.04.020

Prather, K. A., Marr, L. C., Schooley, R. T., McDiarmid, M. A., Wilson, M. E., and Milton, D. K. (2020). Airborne transmission of SARS-CoV-2. *Science* 370, 303–304. doi: 10.1126/science.abf0521

Prem, K., Liu, Y., Russell, T. W., Kucharski, A. J., Eggo, R. M., Davies, N., et al. (2020). The effect of control strategies to reduce social mixing on outcomes of the COVID-19 epidemic in Wuhan, China: a modelling study. *Lancet Public Health* 5, e261–e270. doi: 10.1016/S2468-2667(20)30073-6

Requejo, H. I. Z. (2006). Worldwide molecular epidemiology of HIV. *Rev. Saude Publica* 40, 331–345. doi: 10.1590/S0034-89102006000200023

Richard, Q., Alizon, S., Choisy, M., Sofonea, M. T., and Djidjou-Demasse, R. (2021). Age-structured non-pharmaceutical interventions for optimal control of COVID-19 epidemic. *PLoS Comput. Biol.* 17:e1008776. doi: 10.1371/journal.pcbi.1008776

Riffe, T., Acosta, E., Acosta, E. J., Manuel Aburto, D., Alburez-Gutierrez, A., Altová, A., et al. (2021). Data resource profile: COVerAGE-DB: a global demographic database of COVID-19 cases and deaths. *Int. J. Epidemiol.* 50:390. doi: 10.1093/ije/dyab027

Robson, C., Baskar, S. R., Booy, R., Ferguson, P. E., Gilroy, N., Kok, J., et al. (2019). Influenza: overview on prevention and therapy. *Aust. Prescr.* 42, 51–55. doi: 10.18773/austprescr.2019.013

Saldaña, F., and Velasco-Hernández, J. X. (2021). The trade-off between mobility and vaccination for COVID-19 control: a metapopulation modelling approach. *R. Soc. Open Sci.* 8:202240. doi: 10.1098/rsos.202240

Schmid, B. V., and Kretzschmar, M. (2012). Determinants of sexual network structure and their impact on cumulative network measures. *PLoS Comput. Biol.* 8:e1002470. doi: 10.1371/journal.pcbi.1002470

Sekine, T., Perez-Potti, A., Rivera-Ballesteros, O., Strålin, K., Gorin, J.-B., Olsson, A., et al. (2020). Robust T cell immunity in convalescent individuals with asymptomatic or mild COVID-19. *Cell* 183, 158.e14–168.e14. doi: 10.1016/j.cell.2020.08.017

Simoni, J. M., Tapia, K., Lee, S.-J., Graham, S. M., Beima-Sofie, K., Mohamed, Z. H., et al. (2020). A conjoint analysis of the acceptability of targeted long-acting injectable antiretroviral therapy among persons living with HIV in the U.S. *AIDS Behav.* 24, 1226–1236. doi: 10.1007/s10461-019-02701-7

Smith, G. J. D., Vijaykrishna, D., Bahl, J., Lycett, S. J., Worobey, M., Pybus, O. G., et al. (2009). Origins and evolutionary genomics of the 2009 swine-origin H1N1 influenza A epidemic. *Nature* 459, 1122–1125. doi: 10.1038/nature08182

Sneppen, K., Nielsen, B. F., Taylor, R. J., and Simonsen, L. (2021). Overdispersion in COVID-19 increases the effectiveness of limiting nonrepetitive contacts for transmission control. *Proc. Natl. Acad. Sci. U. S. A.* 118:e2016623118. doi: 10.1073/pnas.2016623118

Spreeuwenberg, P., Kroneman, M., and Paget, J. (2018). Reassessing the global mortality burden of the 1918 influenza pandemic. *Am. J. Epidemiol.* 187, 2561–2567. doi: 10.1093/aje/kwy191

Starr, T. N., Greaney, A. J., Addetia, A., Hannon, W. W., Choudhary, M. C., Dingens, A. S., et al. (2021). Prospective mapping of viral mutations that escape antibodies used to treat COVID-19. *Science* 371, 850–854. doi: 10.1126/science.abf9302

Stoesser, G., Griffith, M., and Griffith, O. L. (2004). "HIV sequence database," in *Dictionary of Bioinformatics and Computational Biology* (Chichester, UK: John Wiley & Sons, Ltd), 52–61.

Sweeting, M. J., De Angelis, D., and Aalen, O. O. (2005). Bayesian back-calculation using a multi-state model with application to HIV. *Stat. Med.* 24, 3991–4007. doi: 10.1002/sim.2432

Taubenberger, J. K., Kash, J. C., and Morens, D. M. (2019). The 1918 influenza pandemic: 100 years of questions answered and unanswered. *Sci. Transl. Med.* 11:eaau5485. doi: 10.1126/scitranslmed.aau5485

Taubenberger, J. K., and Morens, D. M. (2006). 1918 influenza: the mother of all pandemics. *Emerg. Infect. Dis.* 12, 15–22. doi: 10.3201/eid1209.05-0979

Taubenberger, J. K., and Morens, D. M. (2020). The 1918 influenza pandemic and its legacy. *Cold Spring Harb. Perspect. Med.* 10:a038695. doi: 10.1101/cshperspect.a038695

Tebas, P., Ramirez, L., Morrow, M., Yan, J., Shah, D., Lee, J., et al. (2012). Potent cellular immune responses after therapeutic immunization of HIV-positive patients with the PENNVAX®-B DNA vaccine in a phase I trial. *Retrovirology* 9:P276. doi: 10.1186/1742-4690-9-S2-P276

Tebit, D. M., and Arts, E. J. (2011). Tracking a century of global expansion and evolution of HIV to drive understanding and to combat disease. *Lancet Infect. Dis.* 11, 45–56. doi: 10.1016/S1473-3099(10)70186-9

Theys, K., Libin, P., Pineda-Peña, A.-C., Nowé, A., Vandamme, A.-M., and Abecasis, A. B. (2018). The impact of HIV-1 within-host evolution on transmission dynamics. *Curr. Opin. Virol.* 28, 92–101. doi: 10.1016/j.coviro.2017.12.001

Theys, K., Libin, P. J. K., Van Laethem, K., and Abecasis, A. B. (2019). An evolutionary model-based approach to quantify the genetic barrier to drug resistance in fast-evolving viruses and its application to HIV-1 subtypes and Integrase inhibitors. *Antimicrob. Agents Chemother.* 63:e00539-19. doi: 10.1128/AAC.00539-19

Thomas, S. J., Moreira, E. D., Kitchin, N., Absalon, J., Gurtman, A., Lockhart, S., et al. (2021). Safety and efficacy of the BNT162b2 mRNA Covid-19 vaccine through 6 months. *N. Engl. J. Med.* 385, 1761–1773. doi: 10.1056/NEJMoa2110345

Thomson, M. M., Pérez-Álvarez, L., and Nájera, R. (2002). Molecular epidemiology of HIV-1 genetic forms and its significance for vaccine development and therapy. *Lancet Infect. Dis.* 2, 461–471. doi: 10.1016/S1473-3099(02)00343-2

Torneri, A., Libin, P., Scalia Tomba, G., Faes, C., Wood, J. G., and Hens, N. (2021). On realized serial and generation intervals given control measures: the COVID-19 pandemic case. *PLoS Comput. Biol.* 17:e1008892. doi: 10.1371/journal.pcbi.1008892

Torneri, A., Libin, P., Vanderlocht, J., Vandamme, A.-M., Neyts, J., and Hens, N. (2020). A prospect on the use of antiviral drugs to control local outbreaks of COVID-19. *BMC Med.* 18:191. doi: 10.1186/s12916-020-01636-4

Tregoning, J. S., Flight, K. E., Higham, S. L., Wang, Z., and Pierce, B. F. (2021). Progress of the COVID-19 vaccine effort: viruses, vaccines and variants versus efficacy, effectiveness and escape. *Nat. Rev. Immunol.* 21, 626–636. doi: 10.1038/s41577-021-00592-1

U.S. Food and Drug Administration (2022). Coronavirus (COVID-19) Update: FDA Authorizes First Oral Antiviral for Treatment of COVID-19 | FDA [Internet]. Available at: https://www.fda.gov/news-events/press-announcements/coronavirus-covid-19-update-fda-authorizes-first-oral-antiviral-treatment-covid-19 (Accessed February 25, 2022).

Umakanthan, S., Sahu, P., Ranade, A. V., Bukelo, M. M., Rao, J. S., Abrahao-Machado, L. F., et al. (2020). Origin, transmission, diagnosis and management of coronavirus disease 2019 (COVID-19). *Postgrad. Med. J.* 96, 753–758. doi: 10.1136/postgradmedj-2020-138234

UNAIDS (2021). Global HIV & AIDS statistics – 2020 fact sheet | UNAIDS [Internet]. Available at: https://www.unaids.org/en/resources/fact-sheet (Accessed January 4, 2021).

UNAIDS (2022). AIDSinfo | UNAIDS [Internet]. Available at: https://aidsinfo.unaids.org/ (Accessed February 3, 2022).

Ura, T., Okuda, K., and Shimada, M. (2014). Developments in viral vector-based vaccines. *Vaccine* 2, 624–641. doi: 10.3390/vaccines2030624

Valle, C., Martin, B., Touret, F., Shannon, A., Canard, B., Guillemot, J. C., et al. (2020). Drugs against SARS-CoV-2: what do we know about their mode of action? *Rev. Med. Virol.* 30, 1–10. doi: 10.1002/rmv.2143

Van De Vijver, D. A. M. C., and Boucher, C. A. B. (2018). Insights on transmission of HIV from phylogenetic analysis to locally optimize HIV prevention strategies. *Curr. Opin. HIV AIDS* 13, 95–101. doi: 10.1097/COH.0000000000000443

van Harmelen, J., Wood, R., Lambrick, M., Rybicki, E. P., Williamson, A.-L., and Williamson, C. (1997). An association between HIV-1 subtypes and mode of transmission in Cape Town, South Africa. *AIDS* 11, 81–87. doi: 10.1097/00002030-199701000-00012

Van Kerkhove, M. D., Asikainen, T., Becker, N. G., Bjorge, S., Desenclos, J.-C., dos Santos, T., et al. (2010). Studies needed to address public health challenges of the 2009 H1N1 influenza pandemic: insights from modeling. *PLoS Med.* 7:e1000275. doi: 10.1371/journal.pmed.1000275

Vandamme, A. M., Camacho, R. J., Ceccherini-Silberstein, F., De Luca, A., Palmisano, L., Paraskevis, D., et al. (2011). European recommendations for the clinical use of HIV drug resistance testing: 2011 update. *AIDS Rev.* 13, 77–108.

Vrba, S. M., Kirk, N. M., Brisse, M. E., Liang, Y., and Ly, H. (2020). Development and applications of viral vectored vaccines to combat zoonotic and emerging public health threats. *Vaccine* 8:680. doi: 10.3390/vaccines8040680

Wang, J., Wu, Y., Ma, C., Fiorin, G., Wang, J., Pinto, L. H., et al. (2013). Structure and inhibition of the drug-resistant S31N mutant of the M2 ion channel of influenza A virus. *Proc. Natl. Acad. Sci. U. S. A.* 110, 1315–1320. doi: 10.1073/pnas.1216526110

Wang, M. Y., Zhao, R., Gao, L. J., Gao, X. F., Wang, D. P., and Cao, J. M. (2020). SARS-CoV-2: structure, biology, and structure-based therapeutics development. *Front. Cell. Infect. Microbiol.* 10:587269. doi: 10.3389/fcimb.2020.587269

Wegbreit, J., Bertozzi, S., DeMaria, L. M., and Padian, N. S. (2006). Effectiveness of HIV prevention strategies in resource-poor countries: tailoring the intervention to the context. *AIDS* 20, 1217–1235. doi: 10.1097/01.aids.0000232229.96134.56

Wei, C.-J., Crank, M. C., Shiver, J., Graham, B. S., Mascola, J. R., and Nabel, G. J. (2020). Next-generation influenza vaccines: opportunities and challenges. *Nat. Rev. Drug Discov.* 19, 239–252. doi: 10.1038/s41573-019-0056-x

Weiss, S. R., and Navas-Martin, S. (2005). Coronavirus pathogenesis and the emerging pathogen severe acute respiratory syndrome coronavirus. *Microbiol. Mol. Biol. Rev.* 69, 635–664. doi: 10.1128/MMBR.69.4.635-664.2005

Welliver, R., Monto, A. S., Carewicz, O., Schatteman, E., Hassman, M., Hedrick, J., et al. (2001). Effectiveness of oseltamivir in preventing influenza in household contacts a randomized controlled trial. *JAMA* 285, 748–754. doi: 10.1001/jama.285.6.748

WHO (2004). WHO Guidelines on the Use of Vaccines and Antivirals during Influenza Pandemics Department of Communicable Disease Surveillance and Response.

WHO (2021a). Middle East respiratory syndrome coronavirus (MERS-CoV). Available at: https://www.who.int/en/news-room/fact-sheets/detail/middle-east-respiratory-syndrome-coronavirus-(mers-cov) (Accessed December 3, 2021).

WHO (2021b). Coronavirus [Internet]. Available at: https://www.who.int/health-topics/coronavirus#tab=tab_3 (Accessed March 16, 2021).

WHO (2021c). Classification of Omicron (B.1.1.529): SARS-CoV-2 Variant of Concern [Internet]. Available at: https://www.who.int/news/item/26-11-2021-classification-of-omicron-(b.1.1.529)-sars-cov-2-variant-of-concern (Accessed December 10, 2021).

WHO (2021d). Tracking SARS-CoV-2 variants [Internet]. Available at: https://www.who.int/en/activities/tracking-SARS-CoV-2-variants/ (Accessed July 29, 2021).

WHO (2022a). WHO Coronavirus (COVID-19) Dashboard | WHO Coronavirus (COVID-19) Dashboard With Vaccination Data [Internet]. Available at: https://covid19.who.int/ (Accessed February 3, 2022).

WHO (2022b). The different types of COVID-19 vaccines [Internet]. Available at: https://www.who.int/news-room/feature-stories/detail/the-race-for-a-covid-19-vaccine-explained (Accessed April 8, 2022).

WHO (2022c). The Moderna COVID-19 (mRNA-1273) vaccine: what you need to know [Internet]. Available at: https://www.who.int/news-room/feature-stories/detail/the-moderna-covid-19-mrna-1273-vaccine-what-you-need-to-know (Accessed May 1, 2022).

WHO/Europe (2021). WHO/Europe | Types of seasonal influenza vaccine [Internet]. Available at: https://www.euro.who.int/en/health-topics/communicable-diseases/influenza/vaccination/types-of-seasonal-influenza-vaccine (Accessed June 30, 2021).

Willem, L., Abrams, S., Libin, P. J. K., Coletti, P., Kuylen, E., Petrof, O., et al. (2021). The impact of contact tracing and household bubbles on deconfinement strategies for COVID-19. *Nat. Commun.* 12:1524. doi: 10.1038/s41467-021-21747-7

Williams, B. G., Lloyd-Smith, J. O., Gouws, E., Hankins, C., Getz, W. M., Hargrove, J., et al. (2006). The potential impact of male circumcision on HIV in sub-Saharan Africa. *PLoS Med.* 3:e262. doi: 10.1371/journal.pmed.0030262

Wu, J. T., Cowling, B. J., Lau, E. H. Y., Ip, D. K. M., Ho, L.-M., Tsang, T., et al. (2010). School closure and mitigation of pandemic (H1N1) 2009, Hong Kong. *Emerg. Infect. Dis.* 16, 538–541. doi: 10.3201/eid1603.091216

Wu, J., Xu, F., Lu, L., Lu, M., Miao, L., Gao, T., et al. (2010). Safety and effectiveness of a 2009 H1N1 vaccine in Beijing. *N. Engl. J. Med.* 363, 2416–2423. doi: 10.1056/NEJMoa1006736

Xu, Z., Shi, L., Wang, Y., Zhang, J., Huang, L., Zhang, C., et al. (2020). Pathological findings of COVID-19 associated with acute respiratory distress syndrome. *Lancet Respir. Med.* 8, 420–422. doi: 10.1016/S2213-2600(20)30076-X

Xu, X., Zhu, X., Dwek, R. A., Stevens, J., and Wilson, I. A. (2008). Structural characterization of the 1918 influenza virus H1N1 neuraminidase. *J. Virol.* 82, 10493–10501. doi: 10.1128/JVI.00959-08

Zhang, H., Jia, Y., Ji, Y., Cong, X., Liu, Y., Yang, R., et al. (2022). Inactivated vaccines against SARS-CoV-2: neutralizing antibody titers in vaccine recipients. *Front. Microbiol.* 13:816778. doi: 10.3389/fmicb.2022.816778

Zhou, B., Thao, T. T. N., Hoffmann, D., Taddeo, A., Ebert, N., Labroussaa, F., et al. (2021). SARS-CoV-2 spike D614G change enhances replication and transmission. *Nature* 592, 122–127. doi: 10.1038/s41586-021-03361-1

Conflict of Interest: The authors declare that the research was conducted in the absence of any commercial or financial relationships that could be construed as a potential conflict of interest.

Publisher's Note: All claims expressed in this article are solely those of the authors and do not necessarily represent those of their affiliated organizations, or those of the publisher, the editors and the reviewers. Any product that may be evaluated in this article, or claim that may be made by its manufacturer, is not guaranteed or endorsed by the publisher.

frontiers | Frontiers in Microbiology

ORIGINAL RESEARCH
published: 25 July 2022
doi: 10.3389/fmicb.2022.963901

The Assessment on Synergistic Activity of Ebselen and Silver Ion Against *Yersinia pseudotuberculosis*

Chuanjiang Dong[1†], Wei Chen[2,3†], Lili Zou[1,2,3], Binbin Liu[1,2,3], Kaihong Deng[1,2,3], Dingrui Guo[2,3], Peng Wang[1], Hao Chen[4], Helen Wang[5*] and Jun Wang[6*]*

[1] The First College of Clinical Medical Science, China Three Gorges University, Yichang, China, [2] Hubei Key Laboratory of Tumor Microenvironment and Immunotherapy, Medical College, China Three Gorges University, Yichang, China, [3] The Institute of Infection and Inflammation, Medical College, China Three Gorges University, Yichang, China, [4] Affiliated Second People's Hospital of China Three Gorges University, Yichang, China, [5] Department of Medical Biochemistry and Microbiology, Uppsala University, Uppsala, Sweden, [6] The People's Hospital of China Three Gorges University, Yichang, China

OPEN ACCESS

Edited by:
Hongliang Chai,
Northeast Forestry University, China

Reviewed by:
Dharmender K. Gahlot,
Umeå University, Sweden
Ekaterina Psareva,
I. M. Sechenov First Moscow State Medical University, Russia

***Correspondence:**
Lili Zou
zoulili@ctgu.edu.cn
Helen Wang
helen.wang@imbim.uu.se
Jun Wang
wangjfox@ctgu.edu.com

[†] *These authors have contributed equally to this work*

Specialty section:
This article was submitted to Infectious Agents and Disease, a section of the journal Frontiers in Microbiology

Received: *08 June 2022*
Accepted: *24 June 2022*
Published: *25 July 2022*

Citation:
Dong C, Chen W, Zou L, Liu B, Deng K, Guo D, Wang P, Chen H, Wang H and Wang J (2022) The Assessment on Synergistic Activity of Ebselen and Silver Ion Against Yersinia pseudotuberculosis. Front. Microbiol. 13:963901. doi: 10.3389/fmicb.2022.963901

Yersinia pseudotuberculosis is a foodborne zoonotic bacterium that is pathogenic to guinea pigs, rabbits, and mice. It also causes pseudotuberculosis in humans. However, it still lacked the scientific basis for control. Here, we found out that Ebselen (EbSe) exhibited synergistic antibacterial activity with silver nitrate (Ag^+) against *Y. pseudotuberculosis* YpIII strain with high efficacy *in vitro* using UV-visible light absorption spectrum, 5,5'-dithiobis-(2-nitrobenzoic acid), laser scanning confocal microscope, flow cytometry, transmission electron microscopy and Western blotting assays. The depletion of total glutathione (GSH) amount and inhibition of thioredoxin reductase (TrxR) activity in thiol-dependent redox system revealed the destructiveness of EbSe-Ag^+-caused intracellular oxidative stress. Furthermore, a YpIII-caused mice gastroenteritis model was constructed. EbSe-Ag^+ significantly reduced bacterial loads with low toxicity. It also down-regulated the expression levels of interferon (IL)-1β and tumor necrosis factor-α, up-regulated the expression level of IL-10 on-site. All the *in vivo* results demonstrated the antibacterial activity and immune-modulatory property of EbSe-Ag^+. Collectively, these results provided academic fundament for further analysis and development of EbSe-Ag^+ as the antibacterial agents for pseudotuberculosis control.

Keywords: *Yersinia pseudotuberculosis*, Ebselen, silver nitrate, antibacterial activity, immune-modulatory property

INTRODUCTION

Yersiniosis, one of the "other infectious diarrheas" in humans, is an important foodborne zoonosis with wide range of clinical symptoms caused by the enteric pathogens *Yersinia enterocolitica* and *Yersinia pseudotuberculosis*, which is the third most common bacterial enteritis disease in European countries (Mecsas, 2019). Although human *Y. pseudotuberculosis* infections are less frequent than those caused by *Y. enterocolitica* worldwide, it has a wide animal reservoir, mostly in temperate and cold countries (Voskresenskaya et al., 2014). Pseudotuberculosis in animals can lead to tuberculosis-like symptoms, including localized tissue necrosis and granulomas in the liver, spleen, and lymph nodes (Aswal et al., 2020). *Y. pseudotuberculosis* infections in humans are acquired

through the gastrointestinal tract by the ingestion of contaminated food products and the clinical manifestations of pseudotuberculosis are diarrhea, abdominal pain, and fever (Ohnishi et al., 2021; Rivas et al., 2021). The frequency of human infection caused by certain yersinia subgroups might be related to the frequency of exposure to specific animal sources (Le Guern et al., 2016). In some specific areas, *Y. pseudotuberculosis* may also cause a specific disease known as Far East scarlet-like fever for its clinical similarities to scarlet fever caused by group A streptococci (Dakić et al., 2005; Amphlett, 2016). Such atypical infections are severe, characterized by a strong inflammatory syndrome accompanying intestinal disorders (Eppinger et al., 2007).

As a "generalist," *Y. pseudotuberculosis* deploys sophisticated virulence factors to effectively evade the host immune system (Bergsbaken et al., 2009; Lima-Junior et al., 2013; Reinhardt et al., 2018; Schneiders et al., 2021), and host factors are also essential for pathogen-induced cell death (Mares et al., 2021). Hypoxic environment of the intestine is critical for nutrient absorption, intestinal barrier function, and innate and adaptive immune responses in the intestine (Singhal and Shah, 2020). The oxygen deficiency during growth promotes increasing of pathogenic potential of *Y. pseudotuberculosis* (Bakholdina et al., 2009), the outcomes of artificial oxidative stress arouse our curiosity.

Known as thiol dependent redox system (TDRS), thioredoxin (Trx) and glutathione (GSH) systems are vital defenders against oxidative stress (Ren et al., 2020). Trx system consists of Trx and thioredoxin reductase (TrxR); The GSH system be formed from GSH, glutathione reductase (GR) and glutaredoxin (Grx). Both systems work as backup to maintain the intracellular redox homeostasis, participating in signal transduction and regulation, DNA repair and protein synthesis and repair, oxidation resistance and other biological processes. Ultimately, TDRS affects bacterial survival and death, activation, and proliferation (Ren et al., 2018, 2020).

Our previous work showed that a non-toxic seleno-organic drug, Ebselen (EbSe), has antibacterial effect against Gram-positive bacteria (Lu et al., 2013; Dong et al., 2019); meanwhile, it could work synergistically with silver nitrate (Ag^+) to kill a couple of Gram-negative bacteria such as multidrug-resistant *Escherichia coli* (Zou et al., 2017) and *Acinetobacter baumannii* (Dong et al., 2020) by disrupting the TDRS and promoting the oxidative stress in bacteria (Zou et al., 2018; Dong et al., 2019). Thus, the *in vitro* and *in vivo* outcomes of EbSe-Ag^+ against *Y. pseudotuberculosis* YpIII strain have been extensively investigated to develop its scientific basis for pseudotuberculosis control.

MATERIALS AND METHODS

Mouse and Bacterial Strains

Kunming mice (male, 22–25 g) were purchased from China Three Gorges University, and the ethical permit approval of the Medical Animal Care and Welfare Committee of China Three Gorges University was obtained before using the mice for study. Every five mice were kept in an individual cage with a constant dark-light cycle in a conventional SPF animal house and were given free access to fundamental food as normal diet and water.

Yersinia pseudotuberculosis YpIII strains with different reporter systems on the virulence plasmid were constructed as described previously (Wang et al., 2016) and listed in **Table 1**. All experiments were carried out in the BSL2 laboratory.

Reagents

Luria Bertani (LB) medium (EMD Millipore), 2-phenyl-1, 2-benzisoselenazol-3(2H)-one (EbSe) (Daiichi), protease inhibitor cocktails (Roche), anti-Trx1 polyclonal antiserum (IMCO), rabbit anti-sheep IgG-HRP (Santa Cruz), goat anti-mouse H&L antibodies (Santa Cruz), IgG2a mouse monoclonal antibody (VIROGEN), CellROX^{TM} Deep Red Reagent (Invitrogen), Anti-IL-1β antibody (Proteintech), anti-TNF-α antibody (Proteintech), anti-IL-10 antibody (Proteintech). Protein inhibitor cocktail (MedChemExpress). Silver nitrate and all the other reagents were from Sigma-Aldrich.

Inhibitory Effect of EbSe-Ag$^+$ Against YpIII

The inhibitory effect of EbSe-Ag^+ on the growth of YpIII was measured by UV-Vis at A_{600}. YpIII cells were grown (26°C, 200 rpm) 8 h and diluted 1,000 times and treated with a serial concentration of EbSe-Ag^+ for 24 h at 26°C in a 96-well plate, and the A_{600} were measured.

Bactericidal Effect of EbSe-Ag$^+$ Against YpIII

The bactericidal activity of EbSe-Ag^+ against YpIII was detected by laser scanning confocal microscopy (LSCM, A1R$^+$, Nikon). YpIII cells were grown (26°C, 200 rpm) until an A_{600} of 0.4, and diluted 1,000 times, which were treated with 4 μM EbSe and 0.5 μM Ag^+ for 24 h at 26°C. The bactericidal effect was observed by LSCM.

EbSe-Ag$^+$ on YpIII Bacterial Morphology

YpIII was grown until an A_{600} of 0.4 and treated for 30 min with 80 μM EbSe and 5 μM Ag^+. Cells were obtained by centrifugation (4°C, 12,000 rpm, 15 min) and fixed with 2.5% glutaraldehyde. The morphology of YpIII cells was observed by transmission electron microscopy (TEM, Hitachi H-7500).

TABLE 1 | YpIII strains with different reporter systems.

Strain	Genotype	Experiments	Source
YpIII-GFP	YPIII (pCD1 expressing GFP, Km^r)	UV-Vis; LS-MS PAE; TEM DTNB; WB	This study
YpIII-mCherry	YPIII, (pCD1 expressing mCherry, Km^r)	UV-Vis; PAE DTNB; FCM WB	This study
YpIII-bioluminescent	YPIII, Xen4 (pCD1 with Tn1000:Tn5 luxCDABE, Km^r)	Animal experiments	Dong et al., 2020

Post-antibiotic Effect of EbSe-Ag$^+$ Against YpIII

The post-antibiotic effect (PAE) of EbSe-Ag$^+$ against YpIII was detected by UV-Vis. YpIII cells were grown (26°C, 200 rpm) until an A_{600} of 0.4, and diluted 1,000 times. Further, cells were treated with 4 μM EbSe and 0.5 μM Ag$^+$ for 32 h at 26°C, 200 rpm. Then, drugs were removed by centrifugation (4°C, 10,000 rpm, 2 min) for three times using PBS (pH 7.4). The A_{600} of YpIII cells were further measured every 1 h for 6 h.

The Rescue Effect of DTT Against EbSe-Ag$^+$-Treated YpIII

YpIII cells were grown (26°C, 200 rpm) until an A_{600} of 0.4, and diluted 1,000 times, which were treated with 4 μM EbSe and 0.5 μM Ag$^+$ after pre-incubation with 4 μM dithiothreitol (DTT) for 30 min at 26°C, 200 rpm. The A_{600} of YpIII cells were measured.

The Disruption of Thioredoxin Reductase Activity and Glutathione Amount by EbSe-Ag$^+$

YpIII cells were cultured until an A_{600} of 0.4 and incubated with 80 μM EbSe and 5 μM Ag$^+$ for 30 min. YpIII cells were obtained by centrifugation (4°C, 5,000 rpm, 5 min), and a protein inhibitor cocktail (in 50 mmol/L Tris-EDTA buffer, pH 7.4) was added to decrease the protease activity. The cells were disrupted with sonication (240 W, 10 min), and the supernatants were obtained by centrifugation (4°C, 12,000 rpm, 10 min). The TrxR activity and total glutathione amount were detected in a 96-well plate by 5, 5'-dithiobis-(2-nitrobenzoic acid) assay. The activity of the untreated group was 100%. The protocols were performed as previously described (Lu et al., 2013; Zou et al., 2017; Wang P. et al., 2020).

Protein Expression Level of Thioredoxin 1 Upon Treatment With EbSe-Ag$^+$

YpIII cells were cultured until an A_{600} of 0.4, which were incubated with 80 μM EbSe and 5 μM Ag$^+$ for 30 min. After lysis by sonication, the cell lysates were obtained by centrifugation at 12,000 rpm for 20 min. Western blotting assay was performed with anti-Trx1 polyclonal antibody.

Protein *S*-glutathionylation Level Upon Treatment With EbSe-Ag$^+$

YpIII cells were cultured until an A_{600} of 0.4, which were incubated with 80 μM EbSe and 5 μM Ag$^+$ for 30 min. After lysis by sonication, the cell lysates were obtained by centrifugation at 12,000 rpm for 20 min. Total protein *S*-glutathionylation (*S*-PSSG) of 80 μM EbSe and 5 μM Ag$^+$-treated YpIII cells were detected by Western blotting. Cells were cultured, washed, and resuspended in buffer containing 30 mmol/L Iodoacetamide (IAM). Western blotting assay was performed with IgG2a mouse monoclonal antibody for glutathione-protein complexes.

ROS Production by EbSe-Ag$^+$ Treatment

YpIII were grown until an A_{600} of 0.4 in LB medium and incubated with 80 μM EbSe and 5 μM Ag$^+$ for 30 min. The YpIII cells were stained with 5 μM CellROX^{TM} Deep Red Reagent for 30 min at 37°C. After incubation, the reactive oxygen species (ROS) production was quantified by flow cytometry (BECKMAN COULTER, AW15093).

Acute Mice Gastroenteritis Model

All experiments were performed in accordance with the relevant guidelines and regulations approved by China Three Gorges University. 60 healthy male Kunming mice were randomly divided into 5 groups randomly ($n = 12$). The mice were infected via intragastric gavage with 100 μL 2×10^9 CFU of YpIII as previously described (Wang et al., 2016) and were further administered i.p. with 20 mg/kg EbSe, 5 mg/kg Ag$^+$, 20 mg/kg EbSe and 5 mg/kg Ag$^+$ and DMSO on the 1-, 3-, and 5-days post-infection, separately.

Bioluminescent Imaging Analysis

Mice were deprived of food and water for 16 h prior to intragastric administration with YpIII-bioluminescent and were monitored for bioluminescent emission using IVIS lumina II (Caliper LifeSciences) at 1-, 4-, and 7-days post-infection. Mice were anesthetized using the XGI-8 gas anesthesia system (Caliper LifeSciences) prior to imaging with 2.5% IsoFluVet in oxygen (Orion Pharma Abbott Laboratories Ltd., Great Britain), and during imaging in 0.5% IsoFluVet. Images were acquired and analyzed using Living Image 4.5 (Caliper LifeSciences). To analyze bacterial localization within gastrointestinal tracts, mice were euthanized, the gastrointestinal tracts were removed, and imaged by bioluminescent imaging.

Immunohistochemical Analysis

Mice intestinal tracts were rolled, fixed in formalin (10%), and embedded in paraffin. Paraffin sections (4 μm thick) were used to detect cytokine levels by H&E stain and immunohistochemical (IHC) analysis. Anti-IL-1β, anti-TNF-α and anti-IL-10 antibodies were used for the analysis of cytokines in intestinal tracts.

Blood Routine Analysis

Mice blood was collected 7 days post-infection, and the white blood cells (WBCs) and neutrophils counts were detected. For investigation of liver and kidney function, blood was collected and centrifuged at 3,000 rpm for 10 min. Serum alanine transaminase (ALT), aspartate aminotransferase (AST), urea and creatinine were determined by fully automatic biochemical analyzer (Siemens, viva proE).

Statistical Analysis

Statistical analyses were performed by GraphPad Prism 6.0 (GraphPad Software). Means of data between two groups were contrasted using unpaired Student's *t* test. Sample rates between two groups were tested with chi-square analysis. *p*-values of < 0.05 were significant.

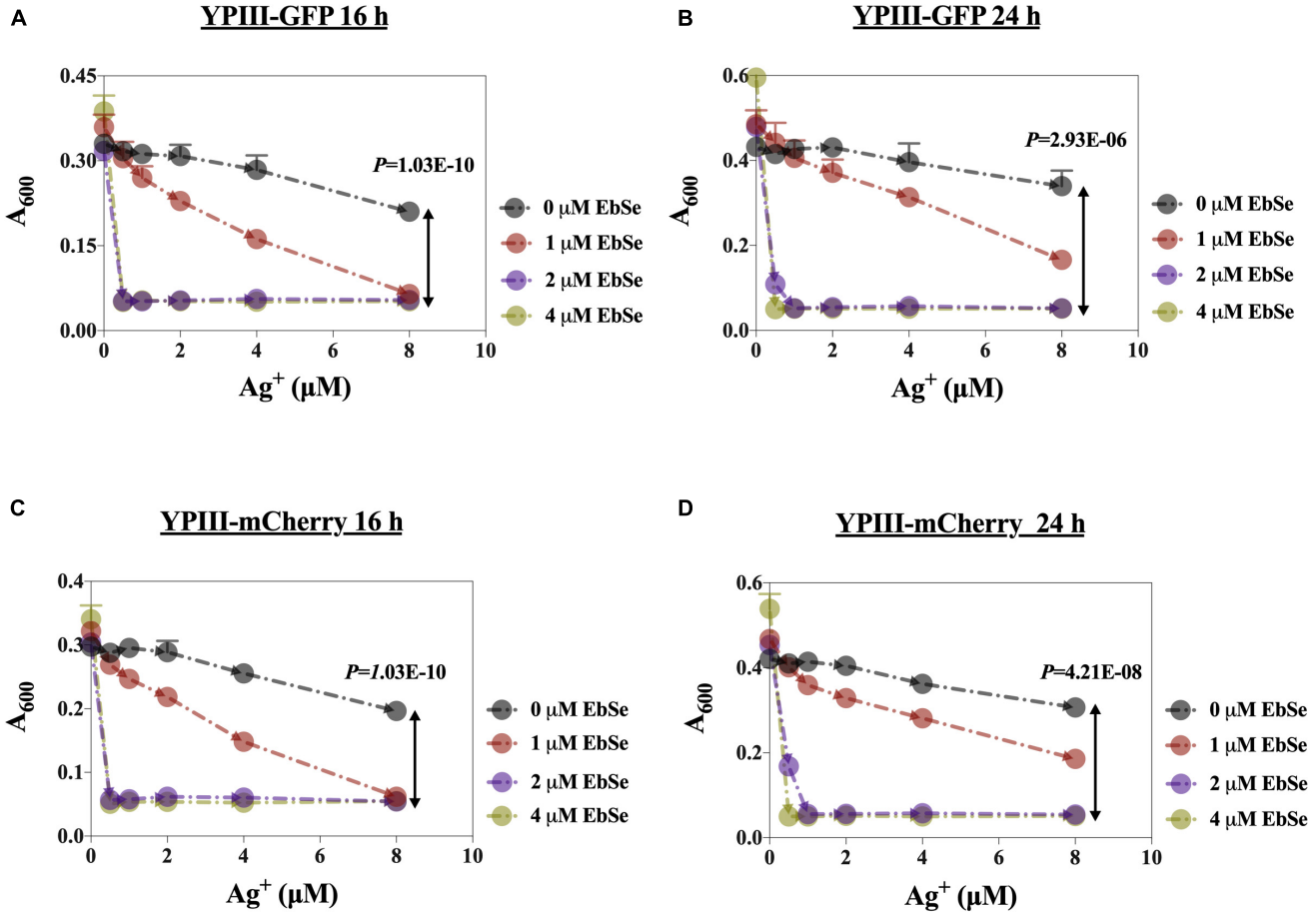

FIGURE 1 | EbSe-Ag$^+$ shows synergistic antibacterial activity against YpIII. YpIII-GFP and YpIII-mCherry were cultured to A_{600} of 0.4, diluted 1:1,000 times, and treated with EbSe-Ag$^+$. **(A,C)** At 16 h; **(B,D)** at 24 h; **(A,B)** YpIII-GFP; **(C,D)** YpIII-mCherry.

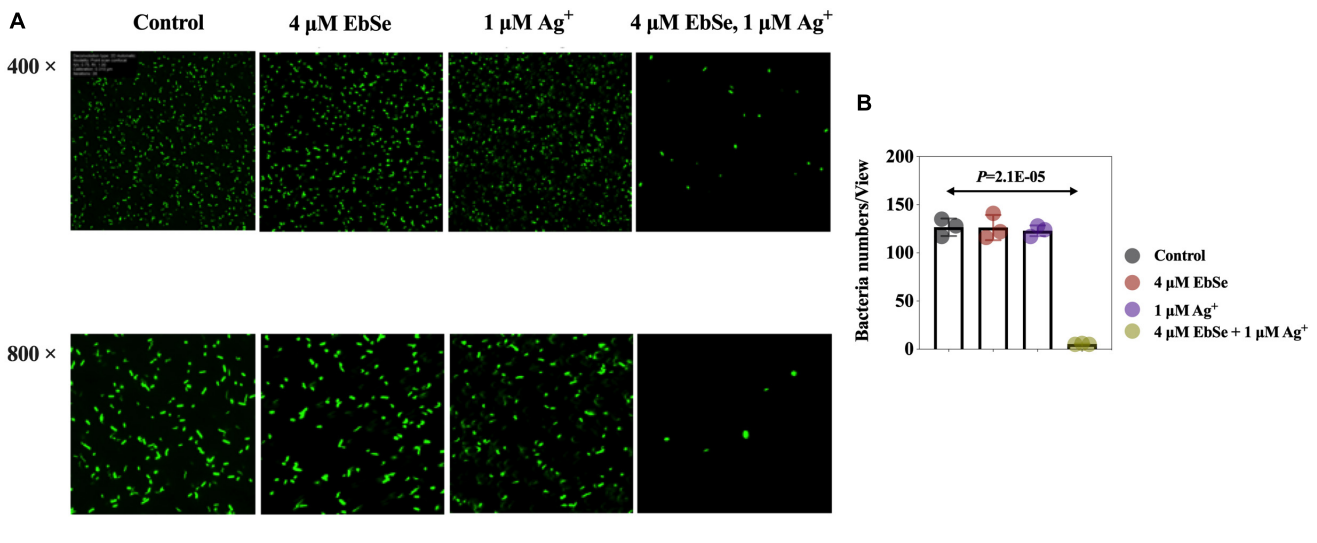

FIGURE 2 | EbSe-Ag$^+$ has a bactericidal effect against YpIII. YpIII-GFP were cultured to A_{600} of 0.4, diluted 1:1,000 times, and treated with either EbSe, Ag$^+$ or EbSe-Ag$^+$. **(A)** LSCM results showed EbSe-Ag$^+$ has a bactericidal effect against YPIII-GFP; **(B)** quantitative values.

RESULTS

EbSe-Ag^{+} Has Strong Bactericidal Activity Against YpIII

The antibacterial effects of EbSe-Ag^{+} on the growth of YpIII-GFP and YpIII-mCherry were detected by UV-Vis. As shown in **Figure 1**, Ag^{+} alone inhibited YpIII growth with a 90% minimal inhibition concentration (MIC_{90}) of 8 μM, while the addition of 2 μM EbSe effectively reduced the MIC_{90} of Ag^{+} to 0.5 μM (16 times). Meanwhile, 2 μM EbSe and 0.5 μM Ag^{+} showed no synergistic toxicity on human cells as described previously (Zou et al., 2017). In addition, the formula S = (F_{X0}/F_{00}) * (F_{Y0}/F_{00}) –

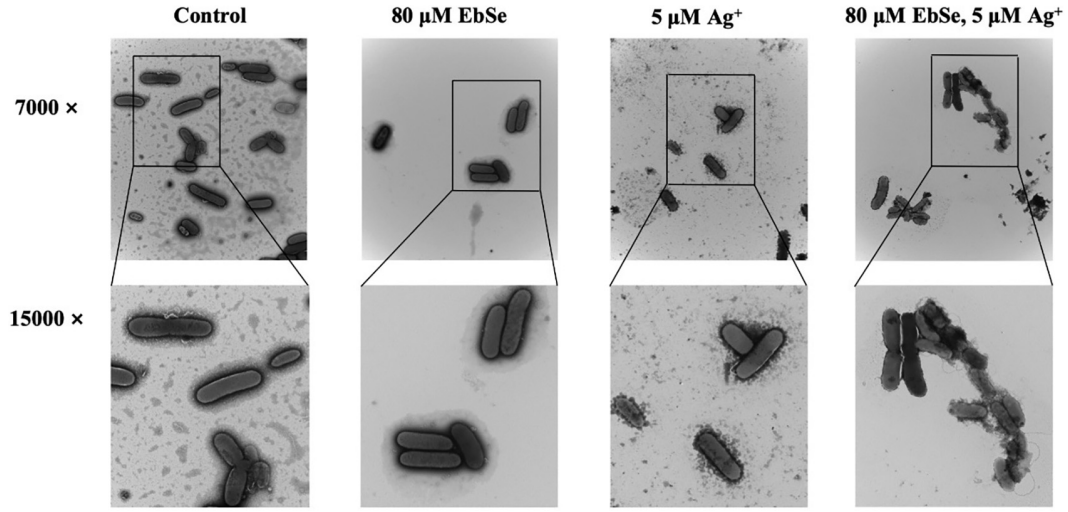

FIGURE 3 | EbSe-Ag^{+} influences YpIII morphology. YpIII-GFP were cultured to A_{600} of 0.4 and treated with EbSe-Ag^{+}. TEM results showed EbSe-Ag^{+} influences YPIII-GFP morphology.

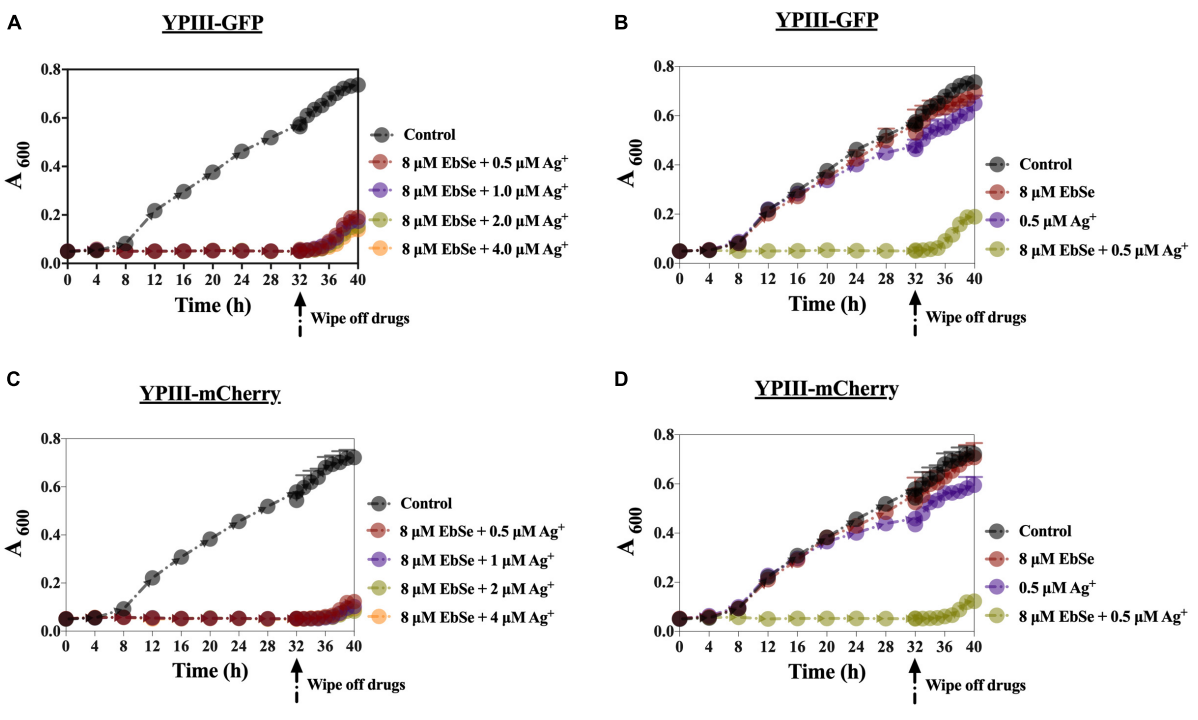

FIGURE 4 | The PAE effect of EbSe-Ag^{+} against YpIII. YpIII-GFP and YpIII-mCherry were cultured to A_{600} of 0.4, diluted 1:1,000 times, and treated with EbSe-Ag^{+}. The results showed EbSe-Ag^{+} has a PAE of 4 h. **(A,C)** 8 μM EbSe and a serial concentration of Ag^{+}; **(B,D)** 8 μM EbSe and 0.5 μM Ag^{+}; **(A,B)** YpIII-GFP; **(C,D)** YpIII-mCherry.

(F_{XY}/F_{00}) was used to calculate the synergistic effect of EbSe-Ag$^+$. The results showed that the synergy indexes were 0.97 and 0.94, respectively, indicating EbSe-Ag$^+$ has a strong synergistic antibacterial effect against YpIII (**Supplementary Figure 1**).

Whether the antibacterial effect of EbSe-Ag$^+$ is bacteriostatic or bactericidal was further investigated by LSCM and bacterial plating. 4 μM EbSe and 1 μM Ag$^+$ were inoculated with YpIII-GFP and observed by LSCM (**Figure 2**). Meanwhile, the

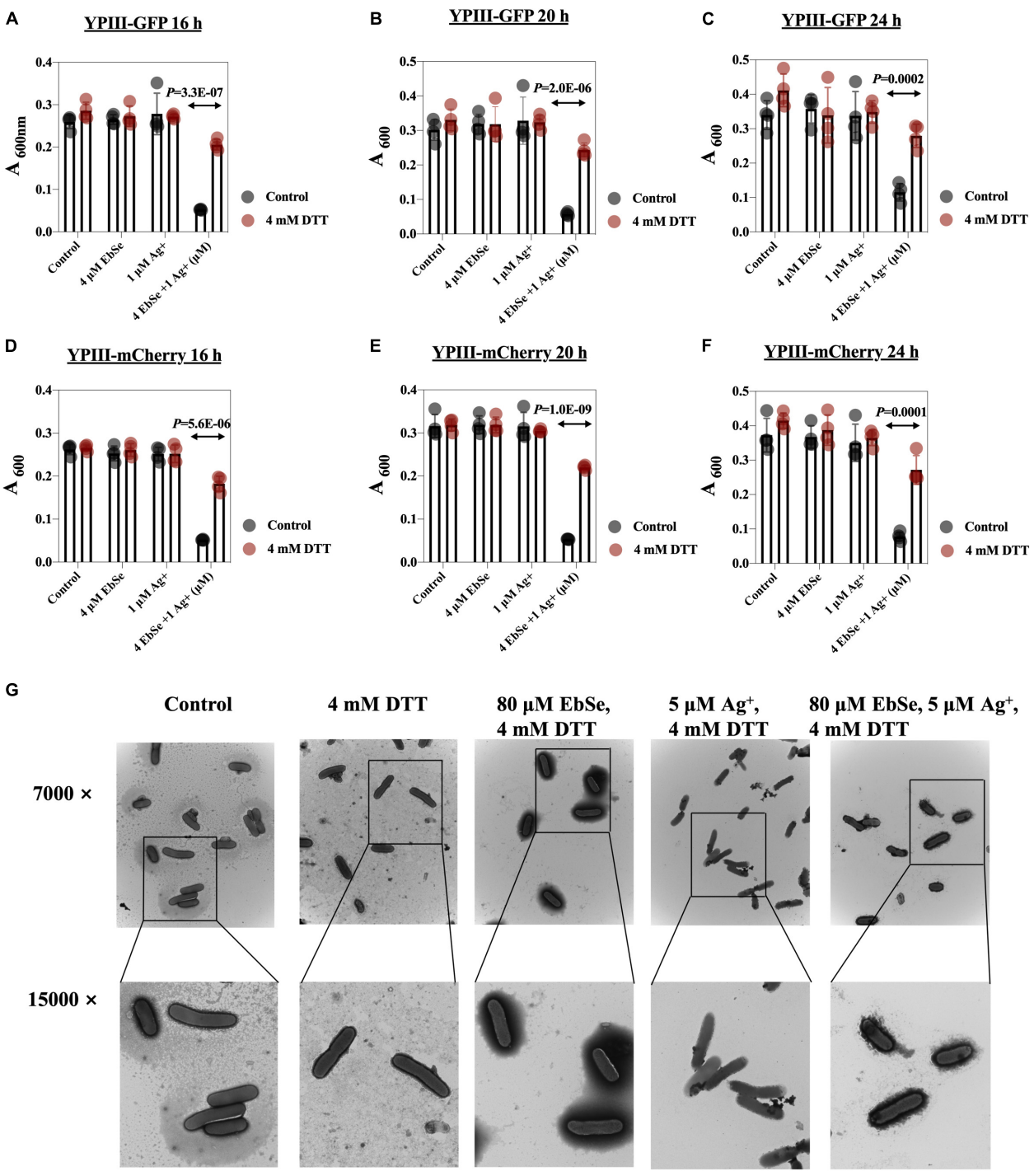

FIGURE 5 | DTT protects YpIII from EbSe-Ag$^+$. YpIII-GFP and YpIII-mCherry were cultured to A_{600} of 0.4, diluted 1:1,000 times, and treated with DTT followed with EbSe-Ag$^+$. **(A,D)** At 16 h; **(B,E)** at 20 h; **(C,F)** at 24 h; **(A–C)** YpIII-GFP; **(B–E)** YpIII-mCherry. **(G)** YpIII-GFP was cultured to 0.4 and treated with EbSe-Ag$^+$ with DTT, and the morphological changes were observed by TEM.

minimum bactericidal concentration (MBC) was calculated by plating (**Supplementary Figure 2**). Both results showed that the combination of 4 μM EbSe and 1 μM Ag$^+$ has significant bactericidal effects against YpIII-GFP.

Further, the effect of EbSe-Ag$^+$ on the morphology of YpIII was assessed by TEM. Normal YpIII-GFP has a smooth surface and a complete cell membrane and cell wall. After 30 min treatment with 80 μM EbSe and 5 μM Ag$^+$, YpIII-GFP cells were deformed, cell membranes and cell walls were ruptured, and overflow of cell contents; meanwhile, 80 μM EbSe or 5 μM Ag$^+$ treated cells showed no obvious morphological changes (**Figure 3**). The results showed that the morphology of YpIII-GFP changed significantly in EbSe-Ag$^+$ treated group compared with the control group.

EbSe-Ag$^+$ Has Outstanding Post-antibiotic Effect Against YpIII

YpIII was cultured and co-cultivated with 8 μM EbSe and 0.5 μM Ag$^+$ for 32 h. During this period, the A_{600} was measured every

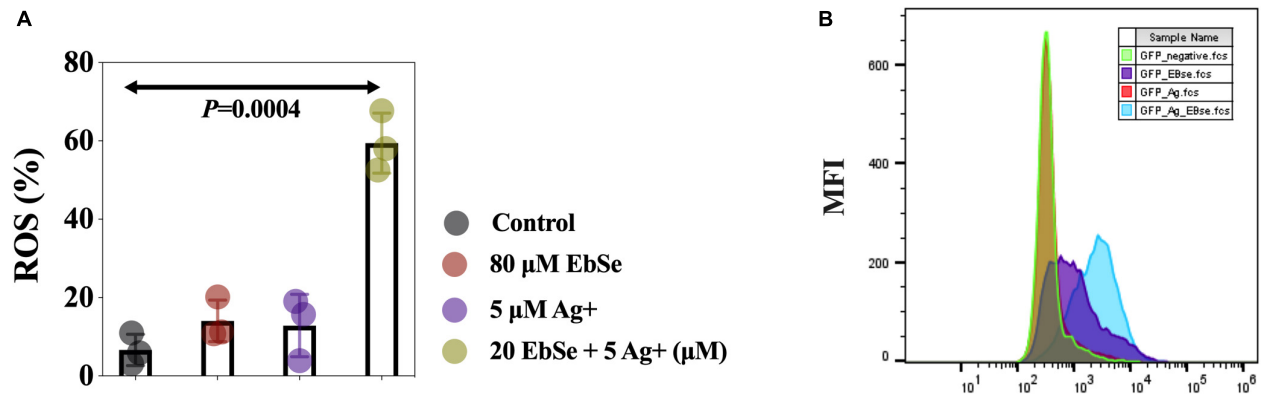

FIGURE 6 | EbSe-Ag$^+$ upregulates ROS production in YpIII. YpIII-mCherry was cultured to A_{600} of 0.4 and treated with EbSe-Ag$^+$. **(A)** Cells were stained with 5 μM CellROX^{TM} Deep Red Reagent for 30 min at 37°C and detected by FCM; **(B)** quantitative values.

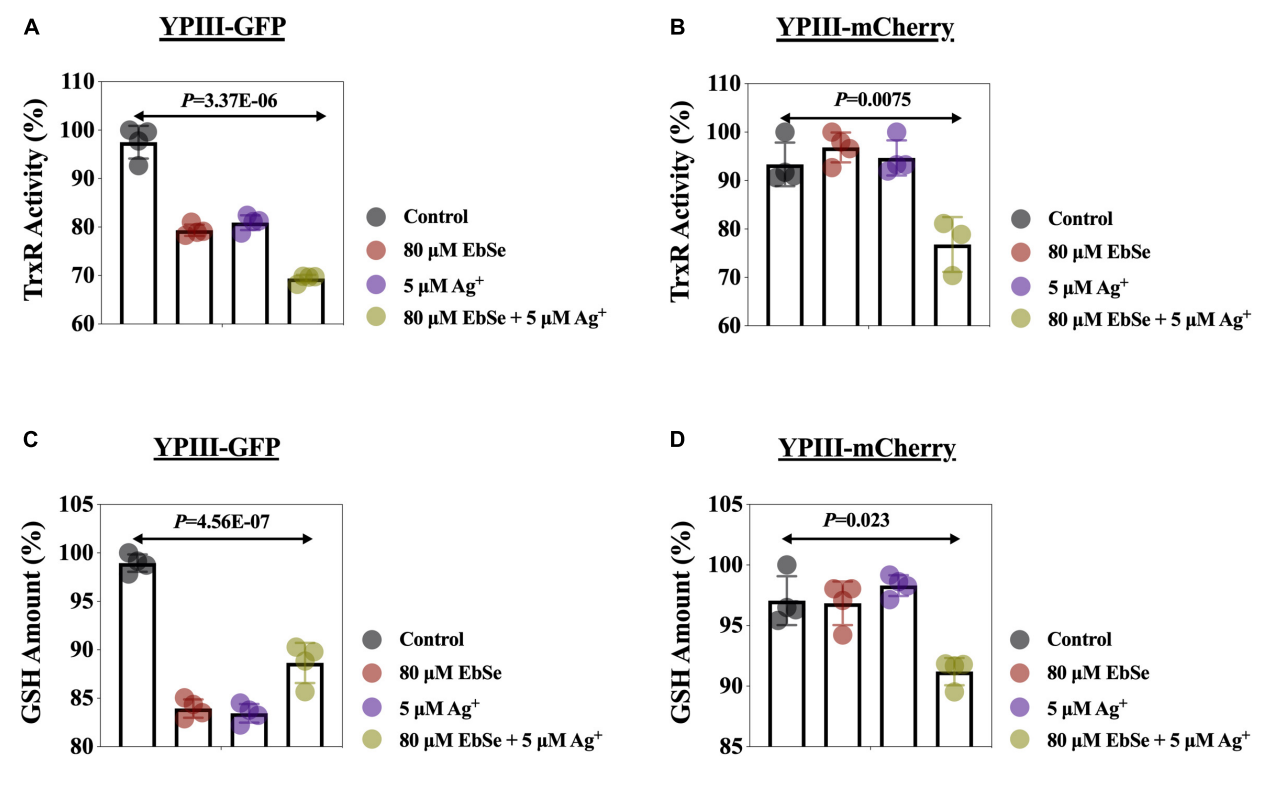

FIGURE 7 | EbSe-Ag$^+$ inhibits TrxR activity and depletes GSH in YpIII. YpIII-GFP and YpIII-mCherry were cultured to A_{600} of 0.4 and treated with EbSe-Ag$^+$. DTNB assay was used to detect the TrxR activity and GSH amount. **(A,B)** At 30 min; **(C,D)** 0–5 min slope; **(A,C)** YpIII-GFP; **(B,D)** YpIII-mCherry.

4 h. 32 h post-treatment, the bacterial solution was centrifuged and washed in PBS by 3 times, and resuspended in LB. The A_{600} was further detected every 1 h for 6 h. The results show that the post-antibiotic effect (PAE) of EbSe-Ag$^+$ was 4 h, which is longer than many clinical antibiotics, including quinolone (**Figure 4**).

DTT Rescues YpIII From EbSe-Ag$^+$ Treatment

The protective effect of DTT against EbSe-Ag$^+$-treated YpIII was evaluated by UV-Vis and TEM assays. DTT was an organic reducing agent that can remove ROS, and 4 mmol/L DTT can effectively rescue YpIII from the bactericidal effect of 4 μM EbSe and 1 μM Ag$^+$ (**Figures 5A–F**). Meanwhile, the TEM results showed that DTT could protect YpIII from EbSe-Ag$^+$ caused morphological damage (**Figure 5G**). Both results indicated that the death of YpIII caused by EbSe-Ag$^+$ was related to ROS production.

EbSe-Ag$^+$ Up-Regulates the Intracellular ROS Level in YpIII

The mean fluorescent intensity (MFI) of ROS in YpIII-mCherry cells was detected by flow cytometry (Ezraty et al., 2017; Zou et al., 2017). The result showed that the ROS production level in YpIII cells treated with 80 μM EbSe and 5 μM Ag$^+$ was significantly regulated when compared with the control (**Figure 6**).

EbSe-Ag$^+$ Disrupts YpIII Thiol-Dependent Redox System

The effects of EbSe-Ag$^+$ on bacterial TrxR activity and GSH amount in YpIII were measured by DTNB assay. The results showed that the combination of 80 μM EbSe and 5 μM Ag$^+$ could efficiently inhibit the TrxR activity and deplete GSH amount when compared with the control (**Figures 7A–D**).

Whether EbSe-Ag$^+$ could affect protein Trx1 and *S*-PSSG expression levels were also analyzed by Western blot

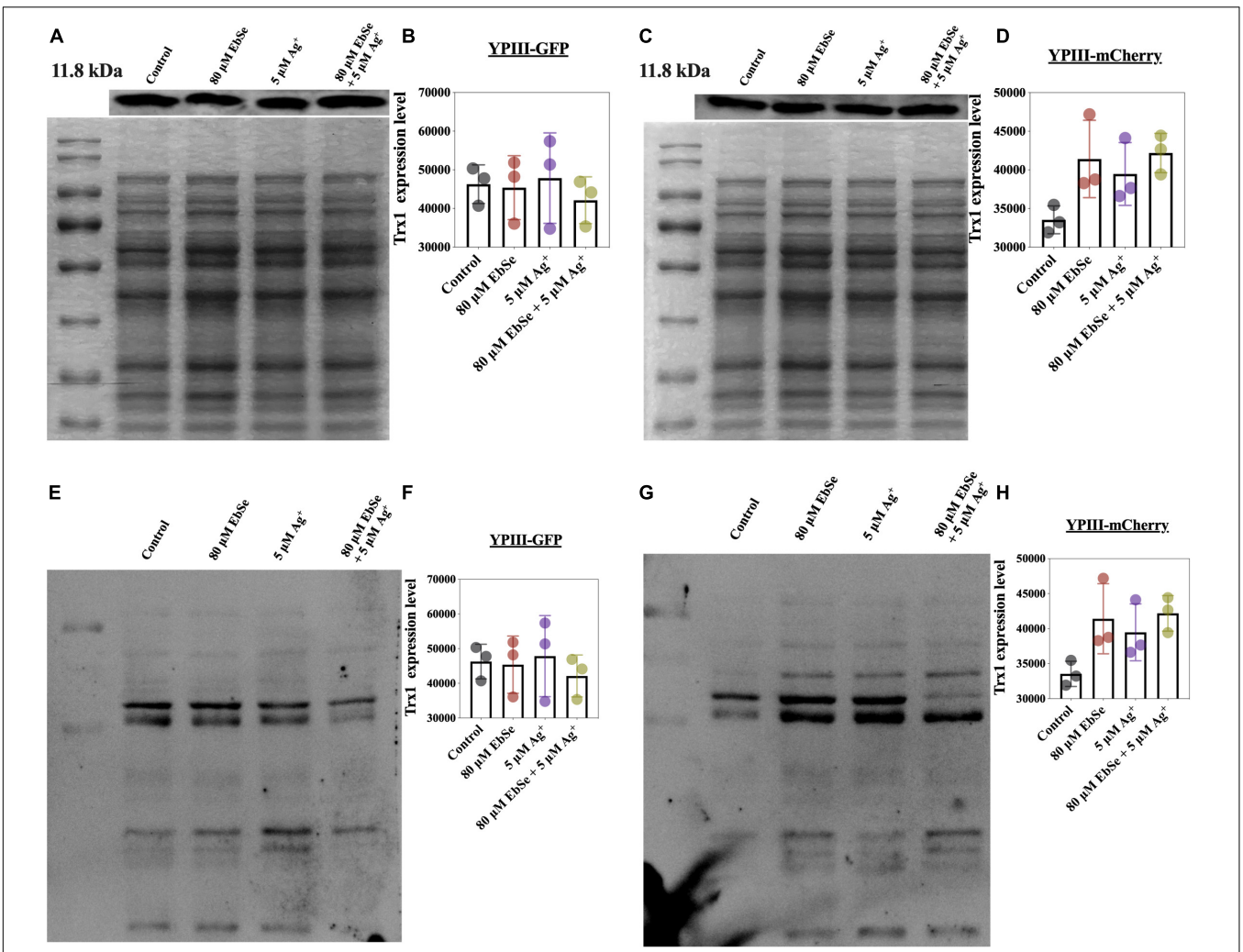

FIGURE 8 | Effect of EbSe-Ag$^+$ on Trx1 and *S*-PSSG expressions in YpIII. YpIII-GPF and YpIII-mCherry were cultured to A_{600} of 0.4 and treated with EbSe-Ag$^+$. WB assay was used to detect **(A,C)** the Trx1 expression level and **(E,G)** *S*-PSSG expression level; **(B,D)** quantitative values of the Trx1 expression level; **(F,H)** quantitative values of the *S*-PSSG expression level; **(A,B,E,F)** YpIII-GFP; **(C,D,G,H)** YpIII-mCherry.

(**Figures 8A–H**). The result showed that Trx1 protein expression level had no difference, indicating the treatment of EbSe-Ag$^+$ only influences enzyme activity. Meanwhile, protein *S*-PSSG was reduced by EbSe-Ag$^+$ treatment compared with Ag$^+$ or EbSe, which further reflected the loss of GSH.

Taken together, the above results showed that EbSe-Ag$^+$ inhibited TrxR activity and depleted GSH in YpIII. All the results suggested that EbSe-Ag$^+$ could disrupt YpIII TDRS, and ROS production is one of the key mechanisms underlying its bactericidal activity.

EbSe-Ag$^+$ Protects Mice From YpIII-Caused Gastroenteritis

Gastroenteritis is among the most common *Y. pseudotuberculosis*-caused infections (Amphlett, 2016). To evaluate whether EbSe-Ag$^+$ could protect mice from YpIII-caused gastroenteritis, 60 mice were randomly divided into five groups, and 2 × 10^9 CFU/100 μL bioluminescent-YpIII strain Xen4 (Wang et al., 2016) were orally administrated to construct gastroenteritis models. Mice were further injected i.p. with 20 mg/kg EbSe, 5 mg/kg Ag$^+$, 20 mg/kg EbSe and 5 mg/kg Ag$^+$ and DMSO on days 1-, 3-, 5-, post-infection. Mice were monitored for bioluminescent emission at 1-, 4-, and 7-days post-infection using IVIS. To further analyze bacterial localization within gastrointestinal tracts, mice were euthanized, the gastrointestinal tracts were removed, and imaged by bioluminescent imaging. The results showed that EbSe-Ag$^+$ led to a significant reduction in bacterial load on-site compared with the control group (**Figure 9**). These findings demonstrated that EbSe-Ag$^+$ could effectively protect mice from YpIII-caused gastroenteritis.

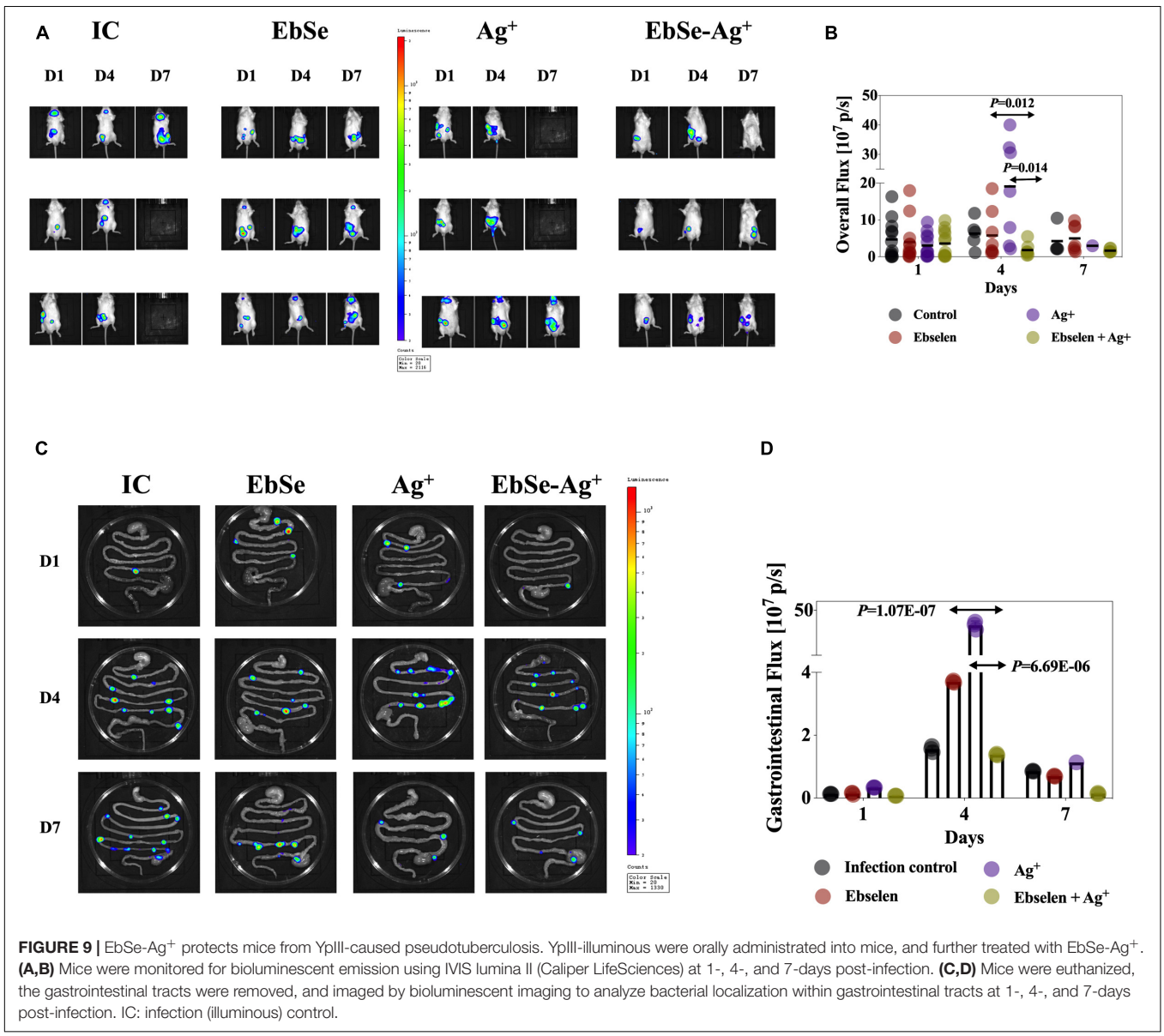

FIGURE 9 | EbSe-Ag$^+$ protects mice from YpIII-caused pseudotuberculosis. YpIII-illuminous were orally administrated into mice, and further treated with EbSe-Ag$^+$. **(A,B)** Mice were monitored for bioluminescent emission using IVIS lumina II (Caliper LifeSciences) at 1-, 4-, and 7-days post-infection. **(C,D)** Mice were euthanized, the gastrointestinal tracts were removed, and imaged by bioluminescent imaging to analyze bacterial localization within gastrointestinal tracts at 1-, 4-, and 7-days post-infection. IC: infection (illuminous) control.

EbSe-Ag$^+$ Reduces Inflammatory Responses in Gastroenteritis Mice

Hematoxylin and eosin (H&E) staining was performed using the new formative tissues. Staining revealed that control mice had increased number of inflammatory cells. Meanwhile, EbSe-Ag$^+$-treated mice had less scattered lymphocytes (**Figure 10**).

An IHC assay was used to measure the presence of pro-inflammatory cytokines IL-1β and TNF-α and anti-inflammatory cytokine IL-10. As shown in **Figure 10**, EbSe-Ag$^+$ could significantly down-regulate IL-1β and TNF-α and up-regulate IL-10 when compared to control mice.

The peripheral blood from different groups of mice was collected, and the results showed that EbSe-Ag$^+$ statistically reduced the counts of WBCs (**Figure 11A**) and neutrophils (**Figure 11B**) compared with the control. Furthermore, ALT, AST, urea, and creatinine in mice blood serum were also detected, and the results showed that EbSe-Ag$^+$ treatment reduced the ALT (**Figure 11C**), AST (**Figure 11D**) levels compared with Ag$^+$ treatment.

Overall speaking, EbSe-Ag$^+$ treatment exhibited significant effects in reducing the YpIII-caused inflammation with low toxicity.

DISCUSSION

The study of the Gram-negative zoonotic bacteria *Y. pseudotuberculosis* has been at the forefront of cellular and molecular pathogenesis for over four decades (Davidson and Davis, 2020). Since *Y. pseudotuberculosis* has a very diverse host spectrum, it can infect virtually all warm-blooded animals, including humans, livestock, pets, and wild animals (Hashimoto et al., 2021). Therefore, given the growing fascination of human populations with wildlife (such as game meat), the pseudotuberculosis can be expected to increase. Here, we showed that EbSe work synergistically with Ag$^+$ to eliminate *Y. pseudotuberculosis* YpIII strain *in vitro*. Briefly, UV-vis and LSCM assays verified that the pharmacological synergy was generated; TEM results revealed that EbSe-Ag$^+$ caused the deformation, shrinkage, and content overflow of YpIII cells, suggesting the rupture and decomposition of the bacterial cell membrane. Further, DTT was used as organic reductant, and the UV-vis, TEM, and FCM results proved that DTT can protect YpIII from the bactericidal effect of EbSe-Ag$^+$, indicating the antibacterial mechanism of EbSe-Ag$^+$ is highly related to the overmuch accumulation of ROS.

Known as a highly reactive oxygen-containing molecule, ROS is continuously produced by mitochondrial metabolism and

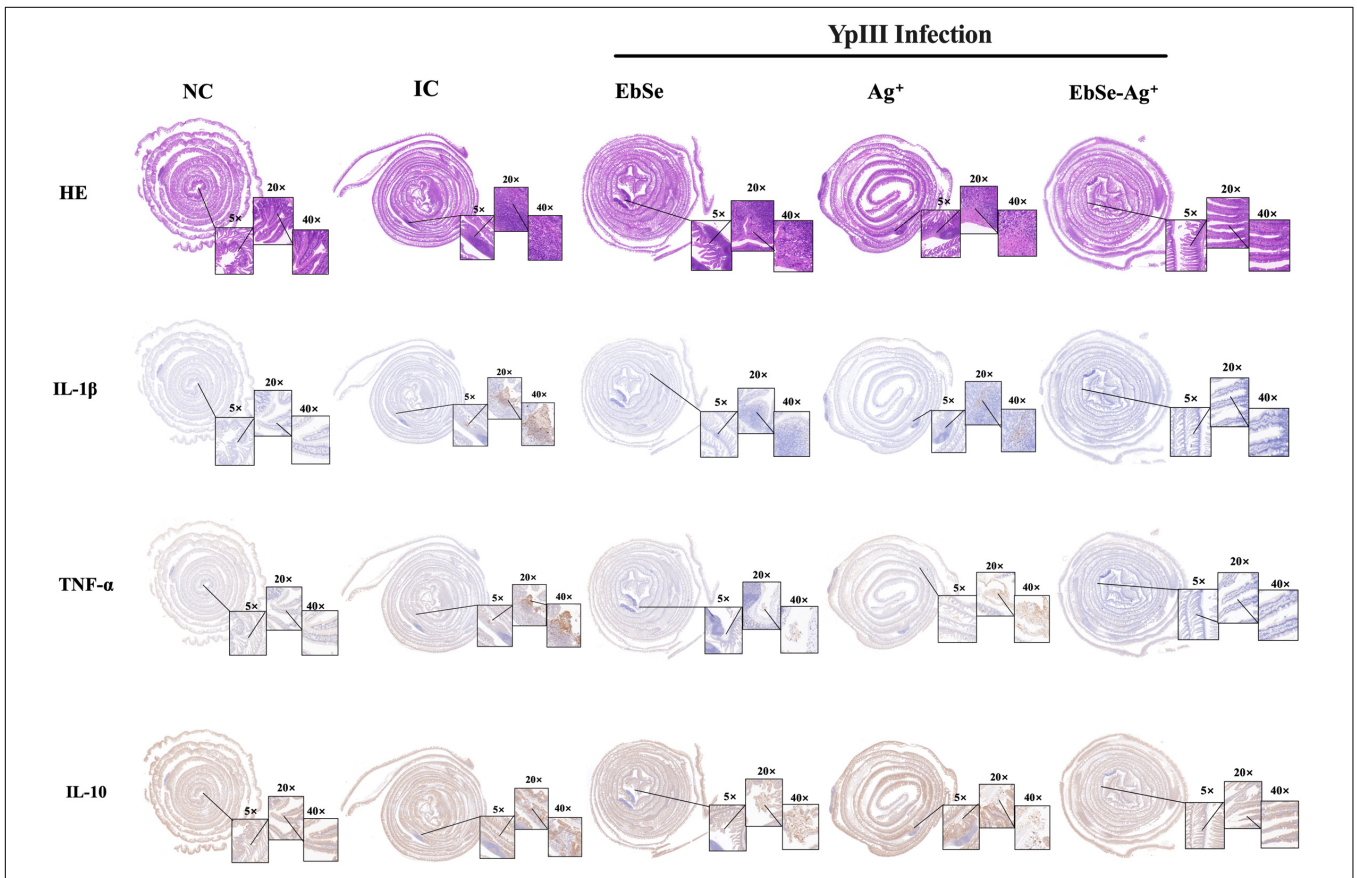

FIGURE 10 | EbSe-Ag$^+$ has immune-modulatory property. YpIII-illuminous were orally administrated into mice, and further treated with EbSe-Ag$^+$. Mice intestinal tracts were rolled, fixed, and embedded. Paraffin sections were used to perform H&E stain and detect cytokine (IL-1β, TNF-α and IL-10) levels by IHC analysis.

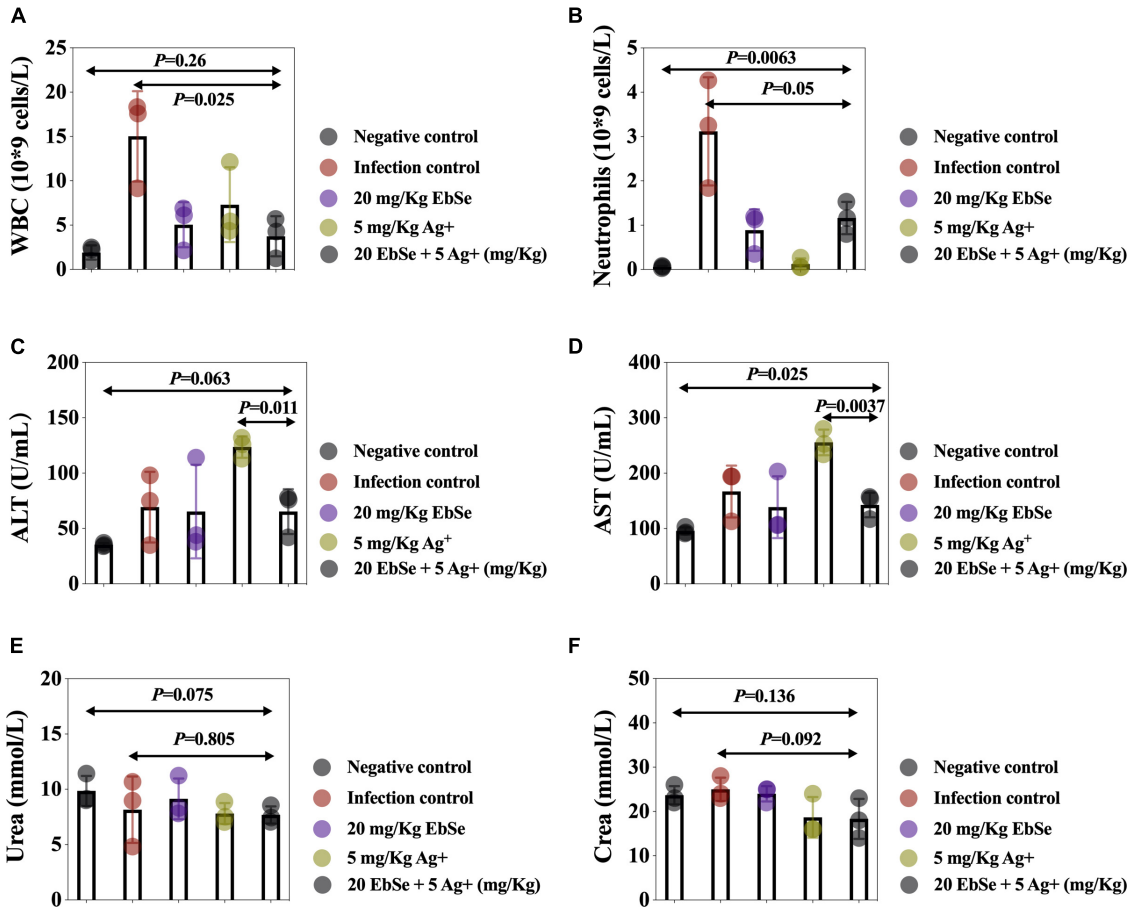

FIGURE 11 | Routine blood analysis of EbSe-Ag^{+}-treated mice. YpIII-illuminous were orally administrated into mice and further treated with EbSe-Ag^{+}. Mice blood was collected 7 days post-infection, and the numbers of **(A)** WBC and **(B)** neutrophils, the amounts of **(C)** ALT, **(D)** AST, **(E)** Urea, and **(F)** creatine were detected.

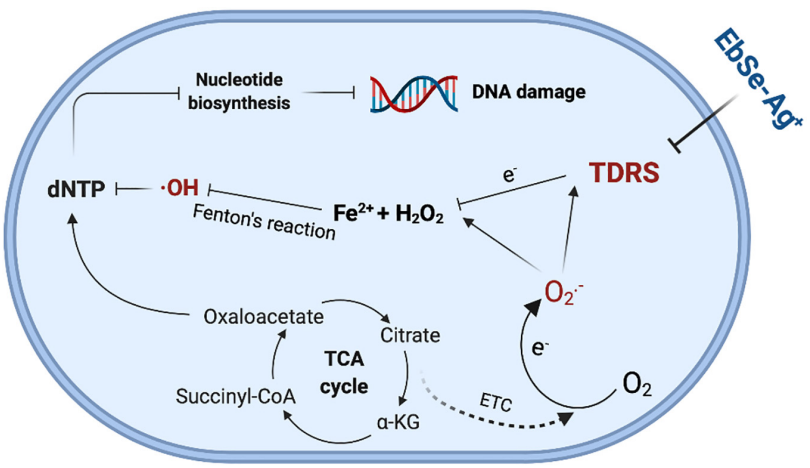

FIGURE 12 | The illustration of bactericidal effect of EbSe-Ag^{+}.

eliminated by dedicated antioxidant systems (Rabinovitch et al., 2017). Since the excessive ROS oxidize proteins, lipids, and DNA (Lei et al., 2018), its intrinsic characteristics is the basis of the mechanism necessary for the survival and growth of organisms (Li et al., 2017), and the its homeostasis in bacteria plays a crucial role in regulating diverse physiological functions

in bacteria (Zhang et al., 2017). Thus, the DTNB assays were performed, and the results showed that the activity of TrxR and the content of GSH were both significantly decreased by EbSe-Ag$^+$, indicating the disrupt of redox homeostasis. Furthermore, the expression levels of Trx1 and *S*-PSSG were detected by Western blot as described previously (Zou et al., 2017). The results showed that the expression level of Trx1 maintained, while the level of *S*-PSSG decreased significantly after EbSe-Ag$^+$ treatment. Collectively, our results indicated that EbSe-Ag$^+$ affected the activity of the enzymes in Trx system rather than its expression; meanwhile, GSH system was significantly disrupted by consumption the GSH pool (**Figure 12**).

Using well-established experimental gastroenteritis in mice offers the opportunity to evaluate the preventive strategies for pseudotuberculosis (Wang et al., 2016). In the current study, the infected mice were treated by intraperitoneal administration of EbSe-Ag$^+$. The mice were monitored for bioluminescent emission at regular intervals, and the therapeutic effect of EbSe-Ag$^+$ was verified by a significant reduction in bacterial loads (Avican et al., 2017; Brodl et al., 2018; Fleiss and Sarkisyan, 2019). Pro-inflammatory cytokines, TNF-α, and IL-1β, which are produced during intestinal inflammation have important intestinal epithelial tight junction barrier-modulating actions (Kaminsky et al., 2021), highly related to inflammatory diseases of the gut (Xu et al., 2018). Our results showed that both TNF-α, and IL-1β were down-regulated by EbSe-Ag$^+$, contributing to host defense during infection. Given that IL-10 is at the center of maintaining the delicate balance between effective immunity and tissue protection, it is not surprising that IL-10 is particularly important in maintaining the intestinal microbe-immune homeostasis, and functions to prevent excessive inflammation during the course of infection (Neumann et al., 2019). Our results showed that EbSe-Ag$^+$ up-regulated IL-10 that provide a favorable outcome in host healing, which might be highly related to its recognized immune-modulatory, anti-inflammatory, and antioxidant activities (Ren et al., 2018). Neutrophils are critical components of immunity and can rapidly migrate to infected or injured tissue, performing central roles in both the innate and the acquired immune systems (Lemaitre et al., 2022). Upon their activation, release of signaling molecules by neutrophils help combat bacterial pathogens (Borregaard, 2010; Wang L. et al., 2020). The enteropathogenic bacterium YpIII successfully persists as an extracellular bacterium during infection by virtue of its translocation of virulence effectors that act in the cytosol of host immune cells to subvert phagocytosis and proinflammatory responses (Taheri et al., 2016). In our animal trial, the peripheral blood of mice was collected, and the neutrophil counts were detected. The result showed that EbSe-Ag$^+$ can reduce the production of inflammatory cells. In addition, ALT and AST were monitored, and the results showed that the enzymes in the EbSe-Ag$^+$ group were significantly lower than that of in the Ag$^+$ group, proving that the EbSe-Ag$^+$ could reduce the hepatotoxicity caused by Ag$^+$ to a certain extent. In parallel, blood urea and serum creatinine were also monitored. The results illustrated that EbSe-Ag$^+$ in this experiment has no obvious nephrotoxicity in mice.

CONCLUSION

Our *in vitro* study demonstrated that EbSe work synergistically with Ag$^+$ to eliminate YpIII by disrupting TDRS; meanwhile, the *in vivo* experiment verified the antibacterial activity and immune-modulatory property of EbSe-Ag$^+$. Taken together, all the results help to develop its scientific basis for pseudotuberculosis control.

DATA AVAILABILITY STATEMENT

The original contributions presented in the study are included in the article/**Supplementary Material**, further inquiries can be directed to the corresponding author/s.

ETHICS STATEMENT

The animal study was reviewed and approved by the ethical permit approval of the Medical Animal Care and Welfare Committee of China Three Gorges University (2019080Q) was obtained before using the mice for study.

AUTHOR CONTRIBUTIONS

CD, WC, and PW performed *in vitro* experiments. JW and HW analyzed and interpreted the data. BL, KD, DG, and HC performed animal experiments. LZ was a major contributor in writing the manuscript. All authors read and approved the final manuscript.

FUNDING

We are grateful for the support of the National Natural Science Foundation of China (32170191 and 81903105), the Natural Science Foundation of Hubei province (2021CFB497), the Health Commission of Hubei Province Foundation (WJ2019H528), and the Swedish Research Council (2018-02376).

SUPPLEMENTARY MATERIAL

The Supplementary Material for this article can be found online at: https://www.frontiersin.org/articles/10.3389/fmicb.2022.963901/full#supplementary-material

Supplementary Figure 1 | The S degree of EbSe-Ag+ against YpIII. UV-Vis assay was used to measure the survival of bacteria and the result showed that the S degree of 4 μM EbSe and 0.5 μM Ag$^+$ was 0.97 and 0.94, respectively (in this figure). S = (F_{X0}/F_{00}) * (F_{Y0}/F_{00}) - (F_{XY}/F_{00}).

Supplementary Figure 2 | EbSe-Ag+ showed bactericidal activity against YpIII. YpIII-GFP and YpIII-mCherry were cultured to A_{600} of 0.4, diluted 1:1,000 times, treated with EbSe-Ag$^+$ and plated on LB medium.

REFERENCES

Amphlett, A. (2016). Far east scarlet-like fever: a review of the epidemiology, symptomatology, and role of superantigenic toxin: *Yersinia pseudotuberculosis*-derived mitogen A. *Open Forum Infect. Dis.* 3:ofv202. doi: 10.1093/ofid/ofv202

Aswal, M., Garg, A., Singhal, N., and Kumar, M. (2020). Comparative in-silico proteomic analysis discerns potential granuloma proteins of *Yersinia pseudotuberculosis*. *Sci. Rep.* 10:3036. doi: 10.1038/s41598-020-59924-1

Avican, U., Doruk, T., Östberg, Y., Fahlgren, A., and Forsberg, Å (2017). The tat substrate SufI is critical for the ability of *Yersinia pseudotuberculosis* to cause systemic infection. *Infect. Immun.* 85, e00867–16. doi: 10.1128/IAI.00867-16

Bakholdina, S. I., Shubin, F. N., and Solov'eva, T. F. (2009). [Oxygen deficiency increases invasive activity and resistance of *Yersinia pseudotuberculosis* to heat stress]. *Zh. Mikrobiol. Epidemiol. Immunobiol.* 3, 18–23.

Bergsbaken, T., Fink, S. L., and Cookson, B. T. (2009). Pyroptosis: host cell death and inflammation. *Nat. Rev. Microbiol.* 7, 99–109. doi: 10.1038/nrmicro2070

Borregaard, N. (2010). Neutrophils, from marrow to microbes. *Immunity* 33, 657–670. doi: 10.1016/j.immuni.2010.11.011

Brodl, E., Winkler, A., and Macheroux, P. (2018). Molecular mechanisms of bacterial bioluminescence. *Comput. Struct. Biotechnol. J.* 16, 551–564. doi: 10.1016/j.csbj.2018.11.003

Dakić, I., Vukovic, D., Stepanović, S., Hauschild, T., Jezek, P., Petrás, P., et al. (2005). Survey of genes encoding staphylococcal enterotoxins, toxic shock syndrome toxin 1, and exfoliative toxins in members of the *Staphylococcus sciuri* group. *J. Clin. Microbiol.* 43, 4875–4876. doi: 10.1128/JCM.43.9.4875-4876.2005

Davidson, R. K., and Davis, K. M. (2020). *Yersinia pseudotuberculosis*: cultivation, storage, and methods for introducing DNA. *Curr. Protoc. Microbiol.* 59:e122. doi: 10.1002/cpmc.122

Dong, C., Wang, J., Chen, H., Wang, P., Zhou, J., Zhao, Y., et al. (2020). Synergistic therapeutic efficacy of ebselen and silver ions against multidrug-resistant *Acinetobacter baumannii*-induced urinary tract infections. *Metallomics* 12, 860–867. doi: 10.1039/d0mt00091d

Dong, C., Zhou, J., Wang, P., Li, T., Zhao, Y., Ren, X., et al. (2019). Topical therapeutic efficacy of ebselen against multidrug-resistant *Staphylococcus aureus* LT-1 targeting thioredoxin reductase. *Front. Microbiol.* 10:3016. doi: 10.3389/fmicb.2019.03016

Eppinger, M., Rosovitz, M. J., Fricke, W. F., Rasko, D. A., Kokorina, G., Fayolle, C., et al. (2007). The complete genome sequence of *Yersinia pseudotuberculosis* IP31758, the causative agent of far east scarlet-like fever. *PLoS Genet.* 3:e142. doi: 10.1371/journal.pgen.0030142

Ezraty, B., Gennaris, A., Barras, F., and Collet, J. F. (2017). Oxidative stress, protein damage and repair in bacteria. *Nat. Rev. Microbiol.* 15, 385–396. doi: 10.1038/nrmicro.2017.26

Fleiss, A., and Sarkisyan, K. S. (2019). A brief review of bioluminescent systems (2019). *Curr. Genet.* 65, 877–882. doi: 10.1007/s00294-019-00951-5

Hashimoto, T., Takenaka, R., Fukuda, H., Hashinaga, K., Nureki, S. I., Hayashidani, H., et al. (2021). Septic shock due to *Yersinia pseudotuberculosis* infection in an adult immunocompetent patient: a case report and literature review. *BMC Infect. Dis.* 21:36. doi: 10.1186/s12879-020-05733-w

Kaminsky, L. W., Al-Sadi, R., and Ma, T. Y. (2021). IL-1beta and the intestinal epithelial tight junction barrier. *Front. Immunol.* 12:767456. doi: 10.3389/fimmu.2021.767456

Le Guern, A. S., Martin, L., Savin, C., and Carniel, E. (2016). Yersiniosis in France: overview and potential sources of infection. *Int. J. Infect. Dis.* 46, 1–7. doi: 10.1016/j.ijid.2016.03.008

Lei, H., Wang, G., Zhang, J., and Han, Q. (2018). Inhibiting TrxR suppresses liver cancer by inducing apoptosis and eliciting potent antitumor immunity. *Oncol. Rep.* 40, 3447–3457. doi: 10.3892/or.2018.6740

Lemaitre, J., Desjardins, D., Gallouët, A. S., Gomez-Pacheco, M., Bourgeois, C., Favier, B., et al. (2022). Expansion of immature neutrophils during siv infection is associated with their capacity to modulate T-cell function. *Front. Immunol.* 13:781356. doi: 10.3389/fimmu.2022.781356

Li, Y., Bai, H., Wang, H., Shen, Y., Tang, G., and Ping, Y. (2017). Reactive oxygen species (ROS)-responsive nanomedicine for RNAi-based cancer therapy. *Nanoscale* 10, 203–214. doi: 10.1039/C7NR06689A

Lima-Junior, D. S., Costa, D. L., Carregaro, V., Cunha, L. D., Silva, A. L., Mineo, T. W., et al. (2013). Inflammasome-derived IL-1beta production induces nitric oxide-mediated resistance to *Leishmania*. *Nat. Med.* 19, 909–915. doi: 10.1038/nm.3221

Lu, J., Vlamis-Gardikas, A., Kandasamy, K., Zhao, R., Gustafsson, T. N., Engstrand, L., et al. (2013). Inhibition of bacterial thioredoxin reductase: an antibiotic mechanism targeting bacteria lacking glutathione. *FASEB J.* 27, 1394–1403. doi: 10.1096/fj.12-223305

Mares, C. A., Lugo, F. P., Albataineh, M., Goins, B. A., Newton, I. G., Isberg, R. R., et al. (2021). Heightened virulence of *Yersinia* is associated with decreased function of the YOPJ protein. *Infect. Immun.* 89:e0043021. doi: 10.1128/IAI.00430-21

Mecsas, J. (2019). Unraveling neutrophil– *Yersinia* interactions during tissue infection. *F1000Res.* 8, F1000FacultyRev–1046. doi: 10.12688/f1000research.18940.1

Neumann, C., Scheffold, A., and Rutz, S. (2019). Functions and regulation of T cell-derived interleukin-10. *Semin. Immunol.* 44:101344. doi: 10.1016/j.smim.2019.101344

Ohnishi, T., Nakazawa, M., Wada, N., Abe, J., and Kamimaki, I. (2021). *Yersinia pseudotuberculosis* infection accompanied by intussusception and incomplete Kawasaki disease in a 7-year-old Girl. *Keio J. Med.* 71, 50–52. doi: 10.2302/kjm.2021-0002-CR

Rabinovitch, R. C., Samborska, B., Faubert, B., Ma, E. H., Gravel, S. P., Andrzejewski, S., et al. (2017). AMPK maintains cellular metabolic homeostasis through regulation of mitochondrial reactive oxygen species. *Cell Rep.* 21, 1–9. doi: 10.1016/j.celrep.2017.09.026

Reinhardt, M., Hammerl, J. A., Kunz, K., Barac, A., Nöckler, K., and Hertwig, S. (2018). *Yersinia pseudotuberculosis* prevalence and diversity in wild boars in northeast Germany. *Appl. Environ. Microbiol.* 84, e00675–18. doi: 10.1128/AEM.00675-18

Ren, X., Zou, L., and Holmgren, A. (2020). Targeting bacterial antioxidant systems for antibiotics development. *Curr. Med. Chem.* 27, 1922–1939. doi: 10.2174/0929867326661910071636 54

Ren, X., Zou, L., Lu, J., and Holmgren, A. (2018). Selenocysteine in mammalian thioredoxin reductase and application of ebselen as a therapeutic. *Free Radic. Biol. Med.* 127, 238–247. doi: 10.1016/j.freeradbiomed.2018.05.081

Rivas, L., Strydom, H., Paine, S., Wang, J., and Wright, J. (2021). Yersiniosis in New Zealand. *Pathogens* 10:191. doi: 10.3390/pathogens10020191

Schneiders, S., Hechard, T., Edgren, T., Avican, K., Fällman, M., Fahlgren, A., et al. (2021). Spatiotemporal variations in growth rate and virulence plasmid copy number during *Yersinia pseudotuberculosis* infection. *Infect. Immun.* 89, e710–e720. doi: 10.1128/IAI.00710-20

Singhal, R., and Shah, Y. M. (2020). Oxygen battle in the gut: hypoxia and hypoxia-inducible factors in metabolic and inflammatory responses in the intestine. *J. Biol. Chem.* 295, 10493–10505. doi: 10.1074/jbc.REV120.011188

Taheri, N., Fahlgren, A., and Fallman, M. (2016). *Yersinia pseudotuberculosis* blocks neutrophil degranulation. *Infect. Immun.* 84, 3369–3378. doi: 10.1128/IAI.00760-16

Voskresenskaya, E., Savin, C., Leclercq, A., Tseneva, G., and Carniel, E. (2014). Typing and clustering of *Yersinia pseudotuberculosis* isolates by restriction fragment length polymorphism analysis using insertion sequences. *J. Clin. Microbiol.* 52, 1978–1989. doi: 10.1128/JCM.00397-14

Wang, H., Avican, K., Fahlgren, A., Erttmann, S. F., Nuss, A. M., Dersch, P., et al. (2016). Increased plasmid copy number is essential for *Yersinia* T3SS function and virulence. *Science* 353, 492–495. doi: 10.1126/science.aaf7501

Wang, L., Ai, Z., Khoyratty, T., Zec, K., Eames, H. L., van Grinsven, E., et al. (2020). ROS-producing immature neutrophils in giant cell arteritis are linked to vascular pathologies. *JCI Insight* 5:e139163. doi: 10.1172/jci.insight.139163

Wang, P., Wang, J., Xie, Z., Zhou, J., Lu, Q., Zhao, Y., et al. (2020). Depletion of multidrug-resistant uropathogenic *Escherichia coli* BC1 by ebselen and silver ion. *J. Cell. Mol. Med.* 24, 13139–13150. doi: 10.1111/jcmm.15920

Xu, T., Dong, Z., Wang, X., Qi, S., Li, X., Cheng, R., et al. (2018). IL-1beta induces increased tight junction permeability in bovine mammary epithelial cells via the IL-1beta-ERK1/2-MLCK axis upon blood-milk barrier damage. *J. Cell. Biochem.* 119, 9028–9041. doi: 10.1002/jcb.27160

Zhang, J., Li, X., Han, X., Liu, R., and Fang, J. (2017). Targeting the thioredoxin system for cancer therapy. *Trends Pharmacol. Sci.* 38, 794–808.

Zou, L., Lu, J., Wang, J., Ren, X., Zhang, L., Gao, Y., et al. (2017). Synergistic antibacterial effect of silver and ebselen against multidrug-resistant Gram-negative bacterial infections. *EMBO Mol. Med.* 9, 1165–1178. doi: 10.15252/emmm.201707661

Zou, L., Wang, J., Gao, Y., Ren, X., Rottenberg, M. E., Lu, J., et al. (2018). Synergistic antibacterial activity of silver with antibiotics correlating with the upregulation of the ROS production. *Sci. Rep.* 8:11131. doi: 10.1038/s41598-018-29313-w

Conflict of Interest: The authors declare that the research was conducted in the absence of any commercial or financial relationships that could be construed as a potential conflict of interest.

Publisher's Note: All claims expressed in this article are solely those of the authors and do not necessarily represent those of their affiliated organizations, or those of the publisher, the editors and the reviewers. Any product that may be evaluated in this article, or claim that may be made by its manufacturer, is not guaranteed or endorsed by the publisher.

frontiers | Frontiers in Microbiology

TYPE Original Research
PUBLISHED 21 October 2022
DOI 10.3389/fmicb.2022.1002670

OPEN ACCESS

EDITED BY
Quan Liu,
Foshan University, China

REVIEWED BY
Zhixun Xie,
Guangxi Veterinary Research Institute, China
Xuejing Wang,
Hebei Animal Husbandry and Veterinary Research Institute, China

*CORRESPONDENCE
Zhongyi Wang
zhongyi_wang@foxmail.com
Zhendong Guo
guozd@foxmail.com
Zehui Chen
3846172@qq.com

†These authors have contributed equally to this work

SPECIALTY SECTION
This article was submitted to Infectious Agents and Disease, a section of the journal Frontiers in Microbiology

RECEIVED 25 July 2022
ACCEPTED 24 August 2022
PUBLISHED 21 October 2022

CITATION
Jiang L, Li J, Cui H, Zhang C, Jin Y, Fu Y, Ma N, Tang F, Zhang Y, Zheng J, Li L, Lu B, Chen Z, Guo Z and Wang Z (2022) Etiologic characteristics of avian influenza H11 viruses isolated from the live poultry market in southeast coastal region in China.
Front. Microbiol. 13:1002670.
doi: 10.3389/fmicb.2022.1002670

Etiologic characteristics of avian influenza H11 viruses isolated from the live poultry market in southeast coastal region in China

Lina Jiang[1†], Jiaming Li[2†], Huan Cui[3†], Cheng Zhang[3], Yifei Jin[2], Yingying Fu[2], Ningning Ma[4], Fei Tang[1], Yidun Zhang[1], Jing Zheng[1], Li Li[1], Bing Lu[2], Zehui Chen[1]*, Zhendong Guo[3]* and Zhongyi Wang[2]*

[1]Xiamen Center for Disease Control and Prevention, Xiamen, China, [2]Beijing Institute of Biotechnology, Beijing, China, [3]Changchun Veterinary Research Institute, Chinese Academy of Agriculture Sciences, Changchun, China, [4]Beijing Institute of Health Care, Beijing, China

Since it was first identified in 1956, the H11 subvariant influenza virus has been reported worldwide. However, due to the low pathogenicity of the H11 subvariant and the absence of its widespread transmission among humans, there are only a few reports on the etiology of the H11 subvariant influenza virus. Therefore, in the present study, we isolated a strain of the H11N3 avian influenza virus (AIV) from poultry feces from the live poultry market in the southeast coastal region of China. Considering that the H11 subvariant is known to cause infections in humans and to enrich the knowledge of the H11 subvariant of the avian influenza virus, the genetics, pathogenicity, and transmissibility of the isolate were studied. The phylogenetic analysis indicated that the H11N3 isolate was of Eurasian origin and carried genes closely related to duck H7N2 and H4N6. The receptor binding analysis revealed that the H11N3 isolate only acquired a binding affinity for avian-derived receptors. In the respiratory system of mice, the isolate could directly cause infection without adaptation. In addition, the results from transmission experiments and antibody detection in guinea pigs demonstrated that H11N3 influenza viruses can efficiently transmit through the respiratory tract in mammalian models. Direct infection of the H11N3 influenza virus without adaptation in the mouse models and aerosol transmission between guinea pig models confirms its pandemic potential in mammals, underscoring the importance of monitoring rare influenza virus subtypes in future studies.

KEYWORDS

H11N3 influenza virus, rare subtypes, live poultry market, mammals, transmission

Introduction

The avian influenza virus (AIV) is a member of the Orthomyxoviridae family isolated from and adapted to an avian host. Influenza A virus has 18 HA subtypes and 11 NA subtypes according to its hemagglutinin (HA) and neuraminidase (NA) differences (Spackman, 2014). Waterfowl and birds are the natural reservoirs of avian influenza viruses (Wang et al., 2018). In 1956, the H11 subtype of avian influenza virus was first isolated from domestic ducks in England (Webster et al., 1992). Following that, isolation of this subtype of the virus has been reported in several countries around the world. The H11 subtype of AIV is a low pathogenic avian influenza virus (LPAIV) covering nine different NA subtypes. Pawar et al. and Koratkar et al. isolated the H11N1 avian influenza virus from the Eurasian spoonbill in India (Koratkar et al., 2014) and from *Anas acuta* in Japan (Pawar et al., 2010), respectively. Yuee Zhang et al. isolated an H11N2 subtype influenza virus from samples collected from the live poultry market in east China and performed whole-genome sequencing (Zhang et al., 2012). The H11 subtype is most often co-infected with other subtypes of the influenza virus and has not been found to show significant clinical symptoms in infected ducks but has been reported to infect mammals—even humans (Gill et al., 2006). Data from GenBank showed that A/swine/KU/2/2001 (H11N6) was isolated from domestic pigs in Korea, proving that the subtype virus has the potential to infect mammals (Tuong et al., 2020). Antibodies to the H11 subtype virus have been repeatedly detected in the serum of poultry (Kayali et al., 2011; Luo et al., 2021). The continuous spread of this virus could pose a potential threat.

The live poultry market (LPM) is a gathering and distributing place for poultry, which is characterized by a large number of poultry species from complex sources, involving long-distance transportation and frequent contact between humans and poultry, which plays a key role in the spread and evolution of AIV (Wei et al., 2019). In the present study, a strain of the H11N3 subtype of AIV was isolated from ducks in a live poultry market in Fujian Province, China. Considering that the H11 subvariants were known to cause human infections, we investigated the viruses *in vitro* and *in vivo* (Gill et al., 2006; Kayali et al., 2011). Through whole-genome sequencing, genetic evolution analysis, and mouse infection and transmission experiments of the strain, the genetic evolution status of the virus was clarified, and the infectious risk of the virus to mammals was assessed. This study provides a reference for the comprehensive prevention and control of the H11 subtype.

Materials and methods

Ethical statement

The study was conducted strictly according to the Guidelines for the Care and Use of Laboratory Animals provided by the Ministry of Science and Technology of China. The study protocol was reviewed and approved by the Animal Experiment Ethics Committee of Changchun Veterinary Research Institute, Chinese Academy of Agricultural Sciences. The H5N1 virus experiments were conducted in an animal biosafety level 3 (ABSL-3) laboratory.

Virus isolation

We collected environmental samples on 14 January 2020 at Xindian Farmers Market, Xiang'an district, Xiamen city. After preliminary screening of the samples by real-time PCR, the influenza A virus was detected in a poultry fecal sample, which was temporarily named EV01.

After shaking and centrifugation of the virus-detected sample, the supernatant was harvested and inoculated with 10-day-old SPF chicken embryos, and allantoic fluid was collected after culturing at 37°C for 48 h. The isolated virus was serially passaged three times in 10-day-old SPF chicken embryos, and the allantoic fluid of the chicken embryos was harvested and stored at −80°C.

Genetic and phylogenetic analyses

TRIzol reagent (TaKaRa) was used to extract total RNA from the allantoic fluid, and a PrimeScript^{TM} RT Reagent Kit (TaKaRa) was used to prepare cDNA using an influenza universal oligonucleotide primer Uni12 (Supplementary Table 1). The obtained cDNA was sent to Shanghai Sangon Bioengineering Co., Ltd. for specific primer PCR of the viral genome, and the resultant PCR product was sequenced. Based on the sequences downloaded from GenBank, we compared the reference sequences of HA and NA genes with the sequences of the strains obtained in this study using the ClustalW method. The GTRGAMMA nucleotide substitution model in PhyML 3.1 software was used, and bootstrap replicates were run 1,000 times to evaluate the maximum likelihood (ML) phylogenies of codons of the two gene sequences. Phylogenetic trees were visualized using FigTree v1.4.4. The nucleotide sequences obtained in this study have been submitted to the GenBank database (accession numbers ON968457–ON968464).

Identification of receptor binding specificity

The receptor binding affinities of the EV01 virus were determined by performing HA assays using 1% desialylated chicken red blood cells (cRBCs; Zhang X. et al., 2021). Specifically, to enzymatically remove sialic acid residues from cRBCs, the cells were treated with 50 mU of vibrio cholerae neuraminidase (VCNA) for 1 h, and then, the cells were resialylated using α-2,6-(N)-sialyltransferase or α-2,3-(N)-sialyltransferase (Sigma-Aldrich) at 37°C for 3 h. In addition, an HA assay was performed on VCNA-treated cRBCs, resialylated cRBCs, and normal cRBCs using 4 different erythrocytes to analyze the receptor binding specificity of the virus. A/chicken/Hebei/HB777/2006(HB777[H5N1]) virus isolates from poultry and A/California/04/2009 (CA04[H1N1]) virus isolates from humans were used as controls for preferential binding to avian-type SA α-2,3-Gal and human-type SA α-2,6-Gal, respectively.

Growth dynamics in cells

A549 and MDCK cells were used to compare EV01 growth kinetics. A multiplicity of infection (MOI) of 0.001 was used to inoculate the virus into two cell monolayers. Infected cells were harvested at 12, 24, 36, 48, and 60 h post-inoculation (h.p.i.) and stored at −80°C, and then, virus titers were determined by median egg infective dose (EID_{50}) assays.

Experimental infection of mice

Mouse infection experiments were conducted to evaluate the pathogenicity of the virus in a mammalian host. For the experiment, 6-week-old female BALB/c mice were purchased from Beijing Vital River Laboratory Animal Technology Co., Ltd. Mice infection experiments were divided into two parts. The first part is weight monitoring, where 10 mice were equally divided into two groups: the infection group and the negative control group. The two groups of mice were anesthetized with isoflurane and were nasally inoculated with 50 μL of PBS buffer and 10^6 EID_{50} of the virus. A 14-day continuous weight monitoring program was instituted for all mice of the two groups. The second part of the mice infection experiment was the *in vivo* monitoring of virus replication. We randomly divided 15 mice into two groups, namely, the infection group and the negative control group, the same as in the first part. Virus infection was conducted based on the protocol described previously (Zhang C. et al., 2021). The mice in the infected group were euthanized at 1, 3, 5, and 7 day(s) post-inoculation (d.p.i.) to measure viral replication. A total of 10 tissue samples, namely, the heart, the liver, the spleen, the lung, the kidney, the brain, the trachea, the pancreas, the intestine, and the turbinate, were collected, and the samples were homogenized in 1 ml of PBS with 1% penicillin–streptomycin. Viral multiplication was determined in each tissue by EID_{50} assays. Then, we evaluated the clinical symptoms associated with viral infection in mouse models. For histopathological examination, a part of the lung tissue was fixed with 4% paraformaldehyde at 3 d.p.i.

Evaluation of transmissibility among guinea pigs

For the study of EV01 virus transmission in mammals, nine female guinea pigs of SPF Hartley strain weighing 300–350 g were purchased from Beijing Vital River Laboratory Animal Technology Co., Ltd. Of the nine guinea pigs, three of them were inoculated intranasally with 10^6 EID_{50} of EV01 virus at a volume of 200 μl (100 μl per nostril), which were considered the infection group. All the guinea pigs were transferred to a "tailor-made transmissibility evaluation cage" at 1 d.p.i. To study the direct contact transmission capacity of the virus, three unvaccinated guinea pigs were placed in the same isolator as the three guinea pigs of the infected group. Meanwhile, to monitor the spread of aerosols, three additional unvaccinated guinea pigs were kept in an adjacent isolator (5 cm apart). At 1, 3, 5, and 7 d.p.i., nasal wash samples were harvested using 1 ml PBS with 1% penicillin–streptomycin and titrated in SPF embryonic eggs for EID_{50} testing.

Antibody detection

Serum was collected from all guinea pigs in as mentioned previously (Section Evaluation of transmissibility among guinea pigs) at 21 d.p.i., and the HI test was conducted according to the protocol described in the OIE Manual of Diagnostic Tests and Vaccines for Terrestrial Animals. A/California/04/2009 (CA04[H1N1]) virus isolates from humans were used as the control group in this study.

Statistical analysis

GraphPad Prism was used to determine statistically significant differences using a one-way analysis of variance (ANOVA). Analyses were performed in triplicate and are representative of three separate experiments. The standard deviation is represented by error bars.

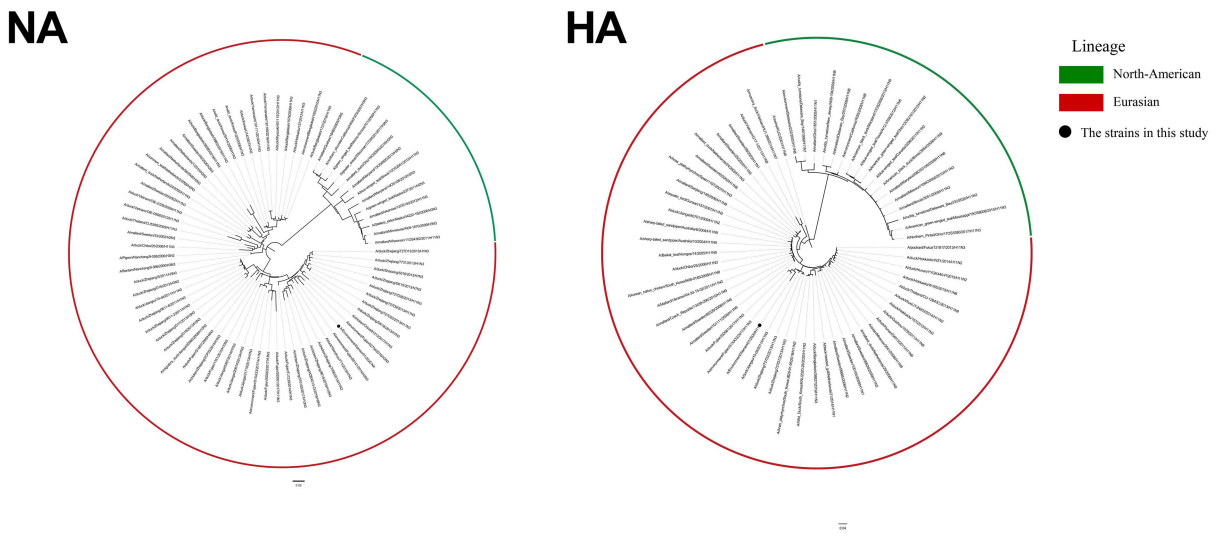

FIGURE 1
ML tree of HA and NA of H11N3 virus. The GTRGAMMA nucleotide substitution model in PhyML 3.1 software was used, and bootstrap replicates were run 1,000 times to evaluate the maximum likelihood (ML) phylogenies of codon comparison between the two gene sequences. Phylogenetic trees were visualized using FigTree v1.4.4. Black dots indicate the isolate EV01 in this study.

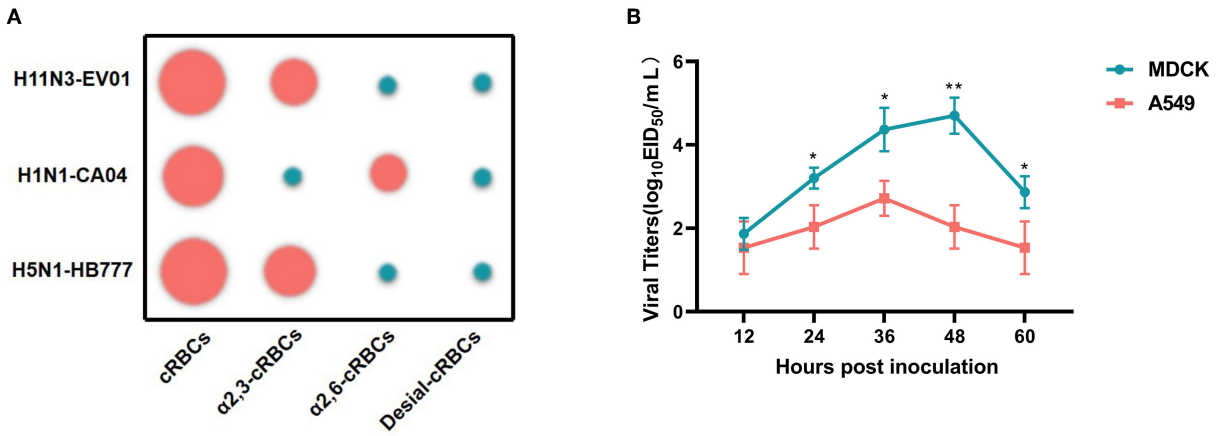

FIGURE 2
Receptor binding property of three IAV strains and replication kinetics of EV01 virus in MDCK and A549 cells. **(A)** Receptor binding property of three IAV strains. Green indicates a negative result, and red indicates a certain binding ability; the larger the circle, the stronger the binding ability. **(B)** Replication kinetics of EV01 virus in MDCK and A549 cells. The green broken line indicates the proliferation curve of EV01 in MDCK cells, and the red broken line indicates the proliferation curve of EV01 in A549 cells. Y-axis indicates viral titers in cells that have been infected with 0.001 MOI of the virus. Each data point on the polyline indicates the means and standard deviation of three independent experiments. Statistical significance between the two groups was calculated by unpaired Student's *t*-test. Values are expressed as the mean ± standard error of the mean (SEM). $*P < 0.05$, $**P < 0.01$.

Results

Phylogenetic analysis

We performed a phylogenetic analysis of the genomes of the H11N3 virus using phylogenetic trees generated by PhyML 3.1 and FigTree v1.4.4 to acquire phylogenetic information. The phylogenetic analysis indicated that the H11N3 isolate was of Eurasian origin. EV01 virus isolates of HA and NA clustered into clade A/environment/Fujian/S1XA33/2017/H11N3 and clade A/environment/Fujian/02754/2016/H3N3, respectively (Figure 1). PB1, PB2, PA, M, NS, and NP clustered into clade A/chicken/Zhejiang/51048/2015/H1N9, A/duck/Fujian/SE0195/2018/H7N2, A/duck/Fujian/SD061/2017/H11N3, A/duck/Fujian/FZHX0004-C/2017/mixed, A/duck/Mongolia/926/2019/H5N3, and A/duck/Zhejiang/422/2013/H4N6 (Supplementary Figure 1).

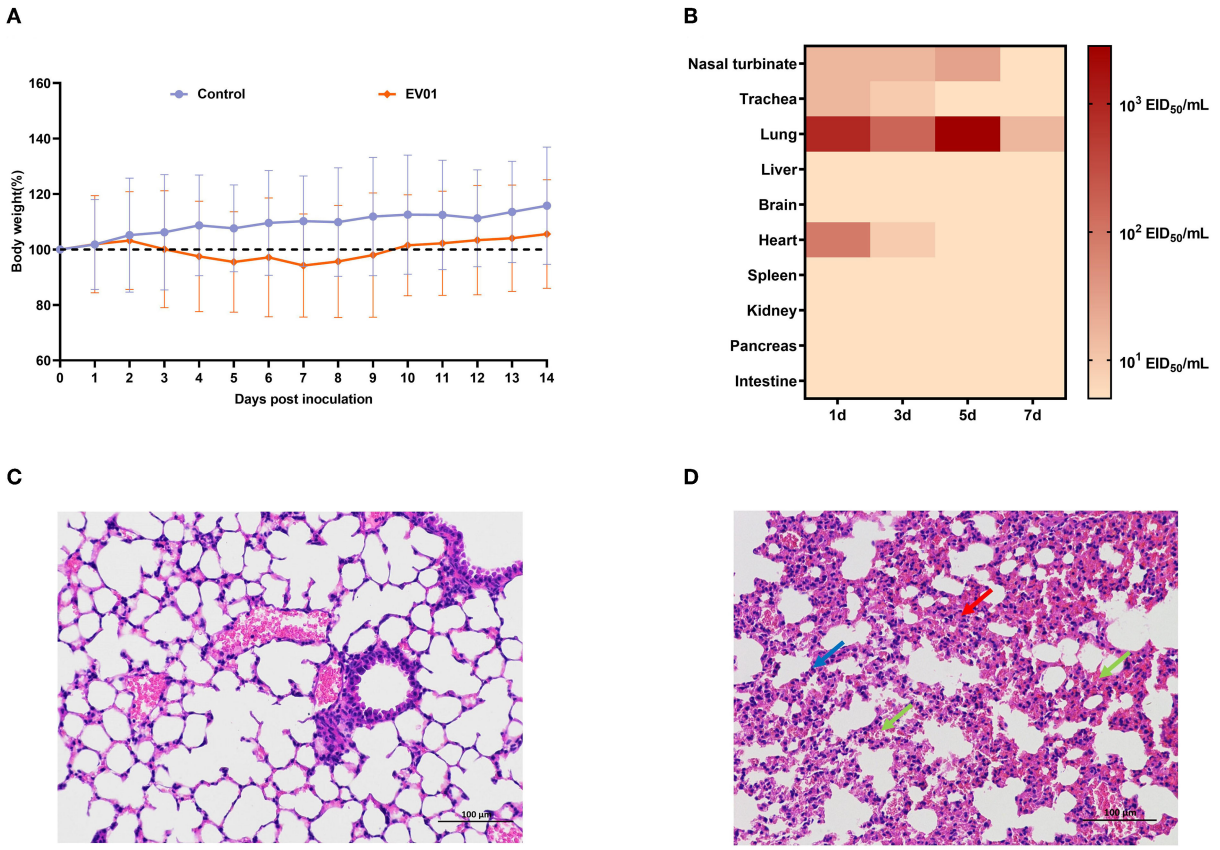

FIGURE 3
Pathogenicity of EV01 virus in mice. **(A)** Body weights were monitored daily over 14 days after inoculation. **(B)** Virus titers in different tissues of mice at 1, 3, 5, and 7 days post-inoculation with EV01 virus; darker colors indicate higher virus titers. **(C,D)** Lung tissue sections of healthy mice and mice infected with the EV01 virus. The sections were stained with H&E. The histopathological analysis of pulmonary tissues was acquired at ×20 magnification; blue arrows indicate inflammatory cell infiltration, green arrows indicate pus cells, and red arrows indicate alveolar wall thickening.

Test for receptor-binding property

The specificity of receptor binding is an important factor for IAV to cross species barriers. For avian influenza to cross species barriers, a-2,3-linked receptors must switch to a-2,6-linked receptors. HA assays were used to determine the receptor specificity of the EV01 virus, where the poultry-isolated A/chicken/Hebei/HB777/2006(HB777[H5N1]) and human-isolated A/California/04/2009 (CA04[H1N1]) viruses were used as controls for preferential binding. EV01 virus binds more readily to SA a-2,3 receptors according to the receptor binding property studies (Figure 2A, Supplementary Table 2).

Analysis of replication kinetics

A549 and MDCK cells were used to study the replication kinetics of EV01. The result indicates that the EV01 virus showed a certain proliferation ability in both cells. However, from 24 h.p.i., the proliferation ability of the virus in MDCK cells was significantly higher than that in A549 cells (Figure 2B).

Pathogenicity of EV01 virus in mice

No noticeable clinical symptoms were observed in infected mice, but the body weight of the mice decreased slightly from 3 d.p.i. and resumed slow growth to 7 d.p.i. All the infected mice survived 14 days (Figure 3A, Supplementary Table 3). Viruses were found in the turbinates, the trachea, the pulmonary tissues, and the heart but not in the liver, the brain, the spleen, the kidney, the pancreas, or the intestines. The highest viral titer was found in the pulmonary tissue at 5 d.p.i., with a value of $10^{3.53}$ EID_{50}/ml. The viral titer was lower in the trachea, consistent with the receptor-binding property test results in Section Test for receptor-binding property (Figure 3B, Supplementary Table 4). The pathological damage of the mice inoculated with either EV01 or PBS virus was assessed by

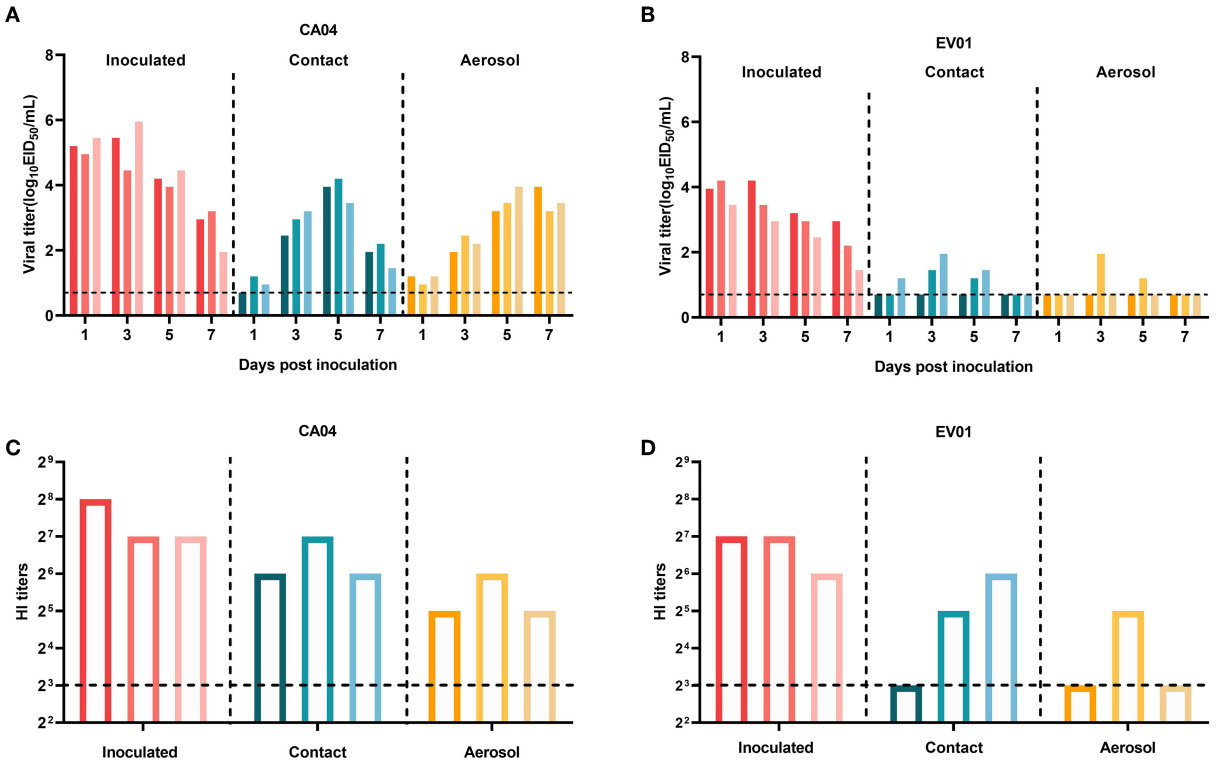

FIGURE 4
Evaluation of the transmissibility of the EV01 virus among guinea pigs. **(A)** Viral titers of the CA04 group. **(B)** Viral titers of the EV01 group. **(C)** Serum detection of each guinea pig in the CA04 group. **(D)** Serum detection of each guinea pig in the EV01 group. A total of three guinea pigs were inoculated with 200 μl of 10^6 EID_{50} viruses (100 μl per nostril). After 24 h, the three naive guinea pigs were placed in the same cage as the infected pigs to see if direct contact transmission occurs, and three other naive guinea pigs were placed in an adjacent cage (with an interval of 5 cm) to observe respiratory droplet transmission. For the detection of virus shedding, nasal washes were collected every other day after inoculation for 1, 3, 5, and 7 days after inoculation. Serum was collected at 21 d.p.i., and the HI test was conducted according to the protocol described in the OIE Manual of Diagnostic Tests and Vaccines for Terrestrial Animals. Red, green, and yellow indicate the inoculated group, the contact group, and the aerosol group, respectively. The different shades of color bars in each group indicate individual animals, and the dashed line indicates the lower limit of detection.

staining pulmonary tissues with H&E. The pulmonary tissues of the control group inoculated with PBS were normal (Figure 3C), and the pulmonary tissues from the mice inoculated with EV01 virus showed alveolar wall thickening and inflammatory cell infiltration (Figure 3D).

Transmissibility of EV01 virus in guinea pigs

The CA04 virus readily infected guinea pigs, as shown in Figure 4A. At 1 d.p.i. with CA04, guinea pigs had a nasal wash titer of 4.95–5.45 $lgEID_{50}$/ml. In the inoculated guinea pigs, the virus titer peaked at 3 d.p.i. with a titer of 5.95 $lgEID_{50}$/ml. Detectable nasal wash virus titers were relatively low in contract and exposed animals, peaking at 4.20 and 3.95 $lgEID_{50}$/ml, respectively. The virus was detected in nasal washes of all groups, indicating efficient horizontal transmission, which is consistent with previous research (Itoh et al., 2009). The seroconversion of all guinea pigs was consistent with virus transmission (Figure 4C). These findings are consistent with those of previous studies, demonstrating the validity of the research method. Figure 4B shows that the EV01 virus can also infect guinea pigs. EV01-inoculated guinea pigs showed a nasal wash titer from 3.45 to 4.20 $lgEID_{50}$/ml at 1 d.p.i. In the inoculated guinea pigs, the virus titer peaked at 3 d.p.i., with a titer of 4.20 $lgEID_{50}$/ml. Detectable nasal wash virus titers were relatively low in contract and exposed animals, and the peak value of each group was 1.95 $lgEID_{50}$/mL. In total, three of the inoculated guinea pigs were positive for the virus, due to direct contact with two pigs, and for virus shedding in one guinea pig. Seroconversion results are identical to virus-shedding test results in both groups (Figure 4D). The results showed that the EV01 virus can be aerosol-transmitted between guinea pigs. In

summary, the EV01 virus was efficient in replicating in guinea pigs as well as in transmitting efficiently in contact and exposed guinea pigs.

Discussion

Recently, some popular subtypes of the influenza virus (e.g., H9N2 and H5N6) have been confirmed to infect humans, and research on these influenza virus subtypes has also emerged endlessly (Peiris et al., 1999; Schwartz et al., 2019; Li et al., 2022). Researchers in many countries reported the H11 subtype of the avian influenza virus. However, in-depth research on the H11 subtype of the avian influenza virus is rarely reported. Therefore, in the present study, we isolated the avian influenza H11N3 virus from the poultry market environment in the southeast coastal region of China and systematically studied the evolutionary origin, pathogenicity, and transmission ability of the strain.

Phylogenetic analysis demonstrated that all eight genes of EV01 belong to the Eurasian lineage. The genes isolated in the current study have high homology with genes of some subtype strains found in Zhejiang, Mongolia, and other places. This study revealed that the H11N3 subtype of the avian influenza virus may undergo different types of recombination in different regions. This may be due to the migration of birds or the spread of the virus *via* the poultry supply chain.

The test for receptor-binding property demonstrated that EV01, like HB777[H5N1] (Zhao et al., 2013), only has α-2,3 receptor binding capacity, indicating a lower risk of cross-species infection. MDCK cells are commonly used to study influenza virus replication because they possess both avian- and human-like receptors. In previous studies, A549 cells also have been proven as a useful cell line to study the infectivity and replication of influenza viruses (Zhu et al., 2015; Shi et al., 2016). As expected, our study found that the EV01 virus showed better proliferative ability in MDCK cells than in A549 cells. These results are consistent with the receptor-binding property.

Moreover, *in vivo* study results are often inconsistent with *in vitro* study results, which necessitates the development of an ideal mammalian cell model to assess infectivity and replication. Mice and guinea pigs are considered ideal models for AIV adaptation and transmission (Schulman, 1968; Samira et al., 2009; Rodriguez et al., 2017). In our study, EV01 is pathogenic to mice and persists in their lungs for a long time. The results of the guinea pig transmission study and the serological study showed that EV01 has a certain risk of host-to-host transmission, with a direct contact transmission efficiency of 2/3 and aerosol transmission efficiency of 1/3.

Based on the aforementioned results, we speculate that H11N3 can cause disease in mammals after adaptation. Strengthening surveillance to prevent cross-species infections and human pandemics and avoiding biosafety risks are recommended. Overall, populations of RNA viruses exhibit large genetic variability; even uncommon low pathogenic influenza viruses have strong epidemic potential in a population. Rare subtypes of the virus should be monitored to prevent them from quietly developing major variants and mammalian pathogenicity due to poor surveillance.

Data availability statement

The datasets presented in this study can be found in online repositories. The names of the repository/repositories and accession number(s) can be found at: https://www.ncbi.nlm.nih.gov/genbank/, ON968457 – ON968464.

Ethics statement

The animal study was reviewed and approved by Animal Experiment Ethics Committee of Changchun Veterinary Research Institute, Chinese Academy of Agricultural Sciences.

Author contributions

ZW, ZG, and ZC contributed to conception and design of the study. LJ, HC, CZ, FT, YZ, JZ, and LL performed some of the experiments. NM performed the statistical analysis. JL wrote the first draft of the manuscript. YJ, YF, and BL wrote sections of the manuscript. All authors contributed to manuscript revision, read, and approved the submitted version.

Funding

This study was financially supported by the Beijing Science and Technology New Star Program (Z211100002121064), the Fujian Province Health Science and Technology Project (2020CXB050), and the Key Specialty of Clinical Medicine of Xiamen, China (Xiamen Health Commission Science and Education Department [2021] No. 215).

Conflict of interest

The authors declare that the research was conducted in the absence of any commercial or financial relationships that could be construed as a potential conflict of interest.

Publisher's note

All claims expressed in this article are solely those of the authors and do not necessarily represent those

of their affiliated organizations, or those of the publisher, the editors and the reviewers. Any product that may be evaluated in this article, or claim that may be made by its manufacturer, is not guaranteed or endorsed by the publisher.

Supplementary material

The Supplementary Material for this article can be found online at: https://www.frontiersin.org/articles/10.3389/fmicb.2022.1002670/full#supplementary-material

References

Gill, J. S., Webby, R., Gilchrist, M. J., and Gray, G. C. (2006). Avian influenza among waterfowl hunters and wildlife professionals. *Emerg. Infect. Dis.* 12, 1284. doi: 10.3201/eid1708.060492

Itoh, Y., Shinya, K., Kiso, M., Watanabe, T., Sakoda, Y., Al, E., et al. (2009). *In vitro* and *in vivo* characterization of new swine-origin H1N1 influenza viruses. *Nature* 460, 1021–1025. doi: 10.1038/nature08260

Kayali, G., Ba Rbour, E., Dbaibo, G., Tabet, C., Saade, M., Shaib, H. A., et al. (2011). Evidence of infection with H4 and H11 avian influenza viruses among lebanese chicken growers. *PLoS ONE* 6, e26818. doi: 10.1371/journal.pone.0026818

Koratkar, S. S., Pawar, S. D., Shelke, V. N., and Kale, S. D. (2014). Pathogenicity of avian influenza H11N1 virus isolated from wild aquatic bird Eurasian Spoonbill (*Platalea leucorodia*). *Ind. J. Medical Res.* 139, 782–785. Available online at: https://pubmed.ncbi.nlm.nih.gov/25027092/

Li, J., Fang, Y., Qiu, X., Yu, X., Cheng, S., Li, N., et al. (2022). Human infection with avian-origin H5N6 influenza a virus after exposure to slaughtered poultry. *Emerg. Microbes Infect* 11, 807–810. doi: 10.1080/22221751.2022.2048971

Luo, S., Xie, Z., Li, M., Li, D., Xie, L., Huang, J., et al. (2021). Survey of low pathogenic avian influenza viruses in live poultry markets in Guangxi Province, Southern China, 2016-2019. *Sci. Rep.* 11, 23223. doi: 10.1038/s41598-021-02639-8

Pawar, S., Chakrabarti, A., Cherian, S., Pande, S., Nanaware, M., Raut, S., et al. (2010). An avian influenza A(H11N1) virus from a wild aquatic bird revealing a unique Eurasian-American genetic reassortment. *Virus Genes* 41, 14–22. doi: 10.1007/s11262-010-0487-2

Peiris, M., Yuen, K. Y., Leung, C. W., Chan, K. H., Ip, P., Lai, R., et al. (1999). Human infection with influenza H9N2. *Lancet* 354, 916. doi: 10.1016/S0140-6736(99)03311-5

Rodriguez, L., Nogales, A., and Martinez-Sobrido, L. (2017). Influenza A virus studies in a mouse model of infection. *J. Vis. Exp.* 127, 55898. doi: 10.3791/55898

Samira, M., Lowen, A. C., Steel, J., Coates, A. L., García-Sastre, A., Palese, P., et al. (2009). Transmission of influenza virus *via* aerosols and fomites in the guinea pig model. *J. Infect. Dis.* 199, 858–865. doi: 10.1086/597073

Schulman, J. L. (1968). The use of an animal model to study transmission of influenza virus infection. *Am. J. Public Health* 58, 2092–2096. doi: 10.2105/AJPH.58.11.2092

Schwartz, I. S., Govender, N. P., Sigler, L., Jiang, Y., Maphanga, T. G., Toplis, B., et al. (2019). Human infection with avian influenza A (H9N2) virus, Cambodia, February 2021. *PLoS Pathog.* 15, e1007977. doi: 10.1371/journal.ppat.1007977

Shi, Q., Wang, Q., Ju, L., Xiong, H., and Jiang, Q. (2016). Biological characteristics of H9N2 avian influenza viruses from healthy chickens in Shanghai, China. *Medical Sci. Monitor Int. Medical J. Exp. Clin. Res.* 22, 4844–4853. doi: 10.12659/MSM.902284

Spackman, E. (2014). A brief introduction to avian influenza virus. *Methods Mol. Biol.* 1161, 61. doi: 10.1007/978-1-4939-0758-8_6

Tuong, H. T., Nguyen, N. M., Sung, H. W., Park, H., and Yeo, S. J. (2020). Genetic characterization of avian influenza A (H11N9) virus isolated from mandarin ducks in South Korea in 2018. *Viruses* 12, 20203. doi: 10.3390/v12020203

Wang, D., Wang, J., Bi, Y., Fan, D., Liu, H., Luo, N., et al. (2018). Characterization of avian influenza H9N2 viruses isolated from ostriches (*Struthio camelus*). *Sci. Rep.* 8, 2273. doi: 10.1038/s41598-018-20645-1

Webster, E. R. R. G., Bean, W. J., and Gorman, O. T. (1992). Evolution and ecology of influenza A viruses. *Microbiol. Rev.* 179, 1992. doi: 10.1128/mr.56.1.152-179.1992

Wei, J., Zhou, J., Liu, Y., Wu, J., Jin, T., Li, Y., et al. (2019). A novel partial lid for mechanical defeatherers reduced aerosol dispersion during processing of avian influenza virus infected poultry. *PLoS ONE.* 14, e0216478. doi: 10.1371/journal.pone.0216478

Zhang, C., Guo, K., Cui, H., Chen, L., Zhang, C., Wang, X., et al. (2021). Risk of environmental exposure to H7N9 influenza virus *via* airborne and surface routes in a live poultry market in Hebei, China. *Front. Cell. Infect. Microbiol.* 11, 503. doi: 10.3389/fcimb.2021.688007

Zhang, X., Li, Y., Jin, S., Wang, T., and Gao, Y. (2021). H9N2 influenza virus spillover into wild birds from poultry in China bind to human-type receptors and transmit in mammals via respiratory droplets. *Transbound. Emerg. Dis.* 2021, 14033. doi: 10.1111/tbed.14033

Zhang, Y., Teng, Q., Ren, C., Li, G., and Li, X. (2012). Complete genome sequence of a novel reassortant H11N2 avian influenza virus isolated from a live poultry market in Eastern China. *J. Virol.* (2012) 2012, 12. doi: 10.1128/JVI.02236-12

Zhao, H., Zhou, J., Jiang, S., and Zheng, B. J. (2013). Receptor binding and transmission studies of H5N1 influenza virus in mammals. *Emerg. Microbes Infect.* 2013, 89. doi: 10.1038/emi.2013.89

Zhu, Y., Yang, Y., Liu, W., Liu, X., Yang, D., Sun, Z., et al. (2015). Comparison of biological characteristics of H9N2 avian influenza viruses isolated from different hosts. *Archiv. Virol.* 160, 917–927. doi: 10.1007/s00705-015-2337-y

frontiers | Frontiers in Microbiology

TYPE Perspective
PUBLISHED 10 November 2022
DOI 10.3389/fmicb.2022.1037583

OPEN ACCESS

EDITED BY
Natasha N. Gaudreault,
Kansas State University,
United States

REVIEWED BY
Maria Fernanda Perdomo,
University of Helsinki,
Finland
Emmanuel Couacy-Hymann,
Laboratoire National d'Appui au Développement Agricole, Côte d'Ivoire

*CORRESPONDENCE
Se Chan Kang
sckang@khu.ac.kr

SPECIALTY SECTION
This article was submitted to Infectious Agents and Disease, a section of the journal Frontiers in Microbiology

RECEIVED 06 September 2022
ACCEPTED 18 October 2022
PUBLISHED 10 November 2022

CITATION
Karim AM, Kwon JE, Karim MA, Iftikhar H, Yasir M, Ullah I and Kang SC (2022) Comprehensive update on the monkeypox outbreak.
Front. Microbiol. 13:1037583.
doi: 10.3389/fmicb.2022.1037583

Comprehensive update on the monkeypox outbreak

Asad Mustafa Karim[1], Jeong Eun Kwon[1], Mujahid Aizaz Karim[2], Haseeb Iftikhar[2], Muhammad Yasir[3,4], Irfan Ullah[5] and Se Chan Kang[1]*

[1]Department of Oriental Medicine Biotechnology, College of Life Science, Kyung Hee University, Yongin, Gyeonggi, South Korea, [2]Sheikh Zayed Hospital and Medical College, Rahim Yar Khan, Punjab, Pakistan, [3]Special Infectious Agents Unit, King Fahd Medical Research Center, King Abdulaziz University, Jeddah, Saudi Arabia, [4]Department of Medical Laboratory Sciences, Faculty of Applied Medical Sciences, King Abdulaziz University, Jeddah, Saudi Arabia, [5]Department of Internal Medicine, Section of Infectious Diseases, Yale University School of Medicine, New Haven, CT, United States

Monkeypox (MPX) was first reported in 1970 in humans and outbreaks were restricted and highly localised to endemic regions of western and central Africa. However, after the first reported case in the UK in early May, 2022, the pattern of epidemic spreading in the geographical regions was much larger compared to past, posing a risk MPX might become entrenched beyond endemic areas. This virus is less transmissible than SARS-CoV-2, as it transmitted mainly through personal, close, often skin-to-skin contact with infectious MPX rash, body fluids, or scabs from an individual with MPX. Infections usually present with chills, fever, fatigue, muscle aches, headache, sore throat, skin lesions, and lymphadenopathy. Currently, there are no antivirals approved for MPX. However, an antiviral drug called "tecovirimat," approved for the treatment of smallpox, has been made accessible to treat MPX. Moreover, to prevent MPX, there are two vaccines available which are approved by FDA: Bavarian Nordic JYNNEOS, and ACAM2000 vaccine. Contact tracing is absent in case of MPX outbreak and there is lack of information from the data systems in rapid manner. Additionally, test capacity needs to be increased. Like SARS-CoV-2, global MPX outbreak demand for vaccines far exceeds availability.

KEYWORDS

monkeypox virus, monkeypox vaccine, monkeypox outbreak, tecovirimat, orthopoxvirus infections

Introduction

Human monkeypox virus (MPXV) is spreading in the USA and Europe among people who have not travelled to endemic areas. On July 23, 2022, monkeypox (MPX) outbreak was declared a public health emergency of international concern by WHO and called for a coordinated international response to slow the spread of disease (Nuzzo et al., 2022). It is the second time in 2 years that WHO has taken this step, ranking MPXV amongst 2 other diseases, polio and COVID-19, that currently carry the classification (Nuzzo et al., 2022). MPX is caused by virus transmitted between animals and humans and from humans to

humans by close contact with lesions, body fluids, respiratory droplets and contaminated materials (Guarner et al., 2022). As of September 6, 2022, there have been 42,516 confirmed cases from 93 nonendemic countries which have not historically reported MPX (Figure 1; CDC, 2022a). MPXV was first reported in 1970 in humans and outbreaks were restricted and highly localised to endemic regions of western and central Africa. In 2003, the first monkeypox outbreak was reported in United States but it linked to animals imported from Ghana. However, after the first reported case in the UK in early May, 2022, the pattern of epidemic spreading in the geographical regions was much larger compared to past, posing a risk MPXV might become entrenched beyond endemic areas. Since May, the highest number of cases have been reported in nonendemic countries like US (n = 19,996), Spain (n = 6,543), Germany (n = 3,493), Brazil (5037), and the UK (n = 3,413) and these clusters represent "an extraordinary event" (Figure 1; CDC, 2022a). However, these reported cases are likely to be an underestimation of the actual numbers because of inadequate clinical recognition of MPXV infection and the long incubation period of the virus (5–21 days; WHO, 2022). Given the rapid pace with which cases are being diagnosed, a coordinated international response is essential.

Monkeypox transmission

As MPX cases continue to soar, scientists are learning more about the spread of disease. Early claims that the virus spreads mainly through repeated skin-to-skin contact among individuals have largely borne out, according to a tranche of new studies (Guarner et al., 2022). The pattern of spread and symptoms do not look like what we had observed in endemic West and Central Africa. Though some children and women have been infected, men who have sex with men (MSM) have affected the most so far. The more the MPXV continues to transmit, the more threats it will pose to infect other populations, including wild animals, consequently, establishing viral reservoirs that might infect humans repetitively.

There are two genetic clades of this virus that include the West African clade and the Central African clade. Human-to-human transmission is not documented in case of West African clade and it has a case fatality rate of less than 1%. In case of Central African clade, human-to-human transmission has been reported with a case fatality rate of up to 10% (Moyo et al., 2022). West African clade may cause substantial sickness and it is typically self-limiting. Children are more susceptible for in case of Central African clade. MPXV exposure during pregnancy may result in difficulties, congenital monkeypox, or stillbirth (Moyo et al., 2022). The effect of MPXV disease on pregnancy outcomes with vertical transmission of viral infection to the fetus has also been reported (Mbala et al., 2017).

MPXV is less transmissible than SARS-CoV-2, as it transmitted mainly through personal, close, often skin-to-skin contact with infectious MPX rash, body fluids, or scabs from an individual with MPX (Guarner et al., 2022; Lapa et al., 2022). Direct contact can happen during intimate contact including; oral, anal, vaginal sex or touching the genitals (labia, vagina, penis, and testicles) or anus of a person infected with MPXV (Lapa et al.,

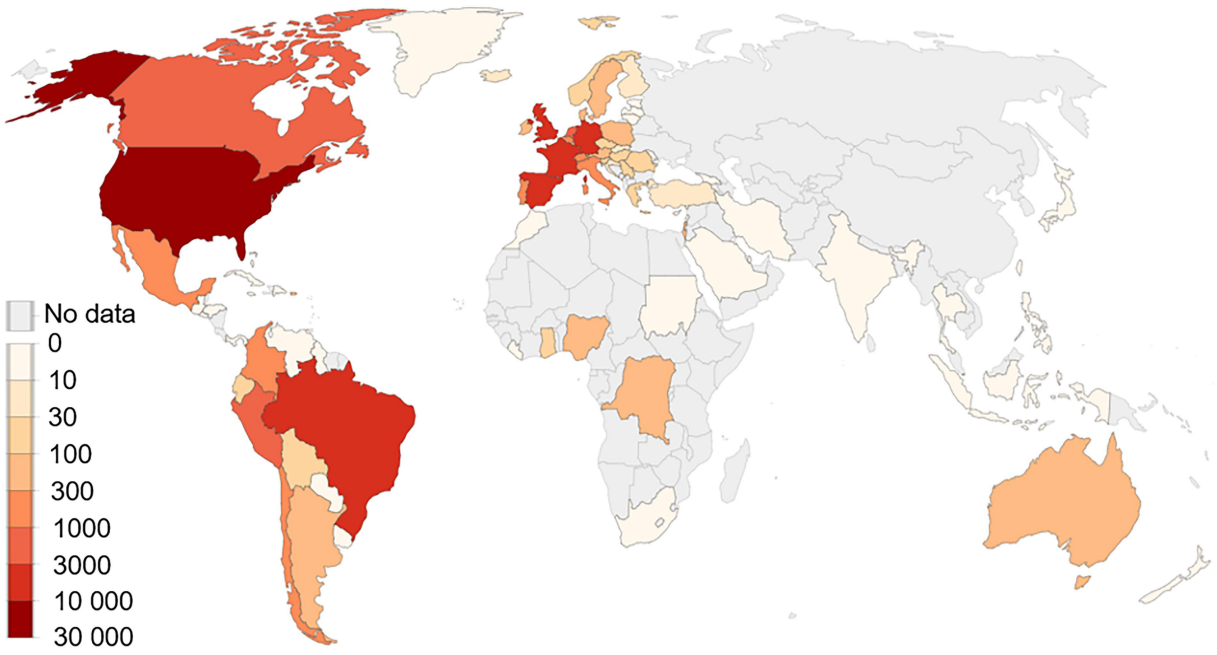

FIGURE 1
Global map of cumulative confirmed cases in endemic and non-endemic countries.

2022). It also spreads by massage, hugging, kissing, touching clothing, towels, bedding, and fetish gear of the infected individual (CDC, 2022a). MPXV is not known to linger in the air like SARS-CoV-2. In the existing outbreak, most cases have happened among MSM (CDC, 2022a). MPXV can spread through sexual activity, however it is not considered to be a sexually transmitted disease as it can be acquired without having sex. Furthermore, although the MPXV DNA has been detected in saliva, semen, and other clinical samples, it is yet unclear if MPX can spread through vaginal secretions, semen, urine, or feces (Lapa et al., 2022). In a study by J Tarín-Vicent et al., it was reported that having a larger number of lesions in and around the anus was associated with anal-receptive sex while having more number of lesions in mouth and throat was linked to oral sex (Tarín-Vicente et al., 2022). Given all these findings, the virus transmission at this point is not as simple as reported in earlier monkeypox outbreaks. Moreover, the spread of MPXV can occur across the placenta to the fetus in pregnant women (Tarín-Vicente et al., 2022). In a recent report, human-to-dog transmission of MPXV has been confirmed, suggesting a real canine disease (Seang et al., 2022). Therefore, it is imperative for the scientific community to investigate physical, serological, PCR-based and epidemiological assessments of both symptomatic and close contacts to answer what percentage of infections are asymptomatic; what body sites are infectious; and importance of condoms in sexually active communities.

Clinical characteristics

MPX has a long incubation period ranging from 5 days to 3 weeks (WHO, 2022). Infections usually present with chills, fever, fatigue, muscle aches, headache, sore throat, skin lesions, and lymphadenopathy (CDC, 2022a). The lesions develop from macules and papules to vesicles and pustules that ulcerate and crust before healing over several weeks (CDC, 2022b). The skin lesions usually happen in crops (CDC, 2022b). The primary rash and lesions are generally located at the site of inoculation (on or near the anus or genitalia). MPX is a self-limited infection and typically lasts for 2–4 weeks.

In addition, recent studies have also shown the presence of virus in asymptomatic individuals with history of contact with known cases (WHO, 2022). Recently, two monkeypox cases have been reported in infants in the USA most likely *via* household transmission. However, most of the cases have occurred among MSM (CDC, 2022a). Moreover, nearly 13 infections have been described among females, including one pregnant women, and at least 2 children have become infected. The mean incubation period from time of exposure to first symptom onset has been estimated at 7.6 days, with 95% of individuals developing symptoms within 17.1 days (CDC, 2022a). The symptoms usually start with all-over feeling of being ill. The characteristic features of MPXV infection include fever, lethargy, chills, headaches, asthenia, myalgia, backaches, and lymph node swellings. After the appearance of prodromal rash, lesions start as macules that grow to papules, vesicles, and then pustules and resolves with crust and scab formation, which spontaneously exfoliate on recovery (CDC, 2022a). Penile edema, anorectal pain, proctitis with bleeding, and balanitis and phimosis are also common symptoms in the present MPX outbreak (Tarín-Vicente et al., 2022). Moreover, epiglottitis, odynophagia sore throat, and tonsillitis also have been reported in patients. According to a study, the most common locations of lesions were anogenital region (73%), trunk, legs, or arms (55%), face (25%), and palms and soles (10%) [9]. Encephalitis, pneumonia, and eye infections are other known complications of MPX, which occur in children, immunocompromised individuals, and pregnant women (Thornhill et al., 2022). Hospitalization is rare but patients with anorectal or oral pain require pain management in hospitals. Individuals infected with MPXV should quarantined or advised to self-isolate themselves for 2–4 weeks. Inflammation of the pharyngeal, genital mucosa, conjunctival are additional symptoms of MPX (Tarín-Vicente et al., 2022).

Diagnostics and therapeutics

The distinction between monkeypox, chickenpox, and herpesvirus disease remains clinically challenging during outbreaks. The lesions of the MPX vary from those in chickenpox in their extent of skin invasion, and distribution which is very important with MPX lesions. Additionally, in case of chickenpox, the lesions appear denser on the trunk and do not spread throughout the face and extremities as in case of MPX. A clinically distinguishing symptom of MPX infection is lymphadenopathy. Any unfamiliar skin lesion, specifically in the anogenital region, should be examined. The diagnosis of MPXV is based on clinical symptoms and examinations. These include viral culture of anogenital lesion swabs, nasopharyngeal or oropharyngeal swabs and laboratory analysis of skin specimens and exudates from the lesions. Moreover, polymerase chain reaction (PCR) assays using samples from skin lesions (fluid from vesicles and pustules) can be employed for detection. However, blood PCR is not recommended because of its limitations of short duration of viremia. In US, during the current monkeypox outbreak, PCR testing is being used in commercial as well as public health laboratories. Testing should be considered in patients with clinically compatible lesions and an epidemiologic risk factor as well as any patient with a characteristic lesion (deep-seated vesicle or pustule with central umbilication). Non-variola Orthopoxvirus real-time PCR test cleared by CDC's FDA can detect MPXV and is being used in during the current outbreak. Unfortunately, no data on the use of other sample types such as saliva, blood, or genital secretions for testing is available.

MPXV belongs to *Orthopoxvirus* genus and another member of this genus called as variola virus, causes smallpox. Currently, there are no antivirals approved for MPX. However, an antiviral drug called "tecovirimat," also known as ST-246 or TPOXX approved for the treatment of smallpox, has been made accessible to treat MPXV through an expanded access

Investigational New Drug (IND) protocol (CDC, 2022c; Almehmadi et al., 2022). Tecovirimat is accessible as an injectable drug for intravenous administration and as an oral capsule (Almehmadi et al., 2022). Currently, tecovirimat is only suggested for patients with severe MPX disease or who are at higher risk for severe MPX (immunocompromised people, pregnant or lactating women, or children with atopic dermatitis) and those with concurrent illnesses (CDC, 2022c). Mechanism of action of Tecovirimat includes targeting and inhibition of the activity of the orthopoxvirus VP37 protein (encoded by and highly conserved in all members of the orthopoxvirus genus) and blocking its interaction with cellular Rab9 GTPase and TIP47, which prevents the formation of egress competent enveloped virions necessary for cell to cell and long-range dissemination of virus. Furthermore, numerous clinical trials such as PLATINUM PALM-007, ACTG5418, WHO/ARNS) are underway to provide required data on the efficacy and safety tecovirimat for MPX (CDC, 2022c). For maximum absorption of oral drug, simultaneous intake of a high-fat meal, ideally about 600 calories and 25 g of fat is required (CDC, 2022c). Other possible antiviral agents (such as cidofovir and brincidofovir) could be treatment options in life-threatening cases. However, these antivirals should be used under an IND protocol available from the CDC (CDC, 2022c).

Vaccines

To prevent MPX, there are two vaccines available which are approved by FDA: Bavarian Nordic JYNNEOS vaccine, and ACAM2000 (CDC, 2022d). ACAM2000 was permitted only for smallpox however, it was granted an expanded-access to use it against MPX. In case of JYNNEOS vaccine, an attenuated, live vaccinia virus, incapable of replicating, is administered as a 2-dose series with high antibody response in 2 weeks after the second dose of vaccine (CDC, 2022d). While ACAM2000 vaccine uses a live vaccinia virus capable of replicating and is administered as a single dose but requires multiple skin punctures (CDC, 2022d). Both vaccines are 85% effective in preventing MPX and can be administered as post exposure prophylaxis.

Among these two vaccines, administration of ACAM2000 has higher risk of adverse events in immunocompromised or people with eczema. ACAM2000 vaccination also has side effects such as myocarditis, lymphadenitis, pericarditis and constitutional symptoms, such as fatigue, malaise, myalgia, fever, and headache. ACAM2000 generates cellular type of immunity in vaccinated individuals. According to a study, in a Phase I clinical trial, ACAM2000 vaccination has been reported to induce positive responses in cell-mediated immunity in 100% of subjects. Hence, post-exposure vaccination can be effective both for preventing the disease and reducing the disease severity. It also has some operational issues such as its administration involves a bifurcated needle (CDC, 2022d). However, JYNNEOS is a better choice. Currently, because of limited supplies of JYNNEOS, health departments in US and Europe are only administering a single dose of vaccine by intradermal injection to high risk people for MPX aged 18 years or older (CDC, 2022d). In near future, it is expected that the total number of doses available for use may increase up to 5-fold because the lower dose is immunologically noninferior to the standard dose, but with more reactogenicity.

Preventing the spread of MPXV

Appropriate and consistent use of personal protective equipment (PPE) when examining MPX patient is highly protective and prevents transmission to healthcare personnel (HCP; CDC, 2022e). According to the recommendations by CDC, HCP who enter the patient's room should use gloves, gown, eye protection (i.e., goggles or a face shield that covers the front and sides of the face), and a NIOSH-approved particulate respirator equipped with N95 filters or higher (CDC, 2022e). Confirmed or suspected patients should wear mask and should be placed in a single-person room (CDC, 2022e). Lesions should be covered with a gown or sheet. Individuals with MPX infection should avoid sexual or close contact with others until the rash and lesions are absolutely healed (CDC, 2022e). There are no data available about protection from subsequent MPX infection but because of limited supply of vaccine, persons previously infected should not be prioritized for vaccination.

Lessons from current outbreaks

After the WHO recommendation, there is growing concern that the MPXV can find an animal reservoir outside Africa. MPX outbreak shows why global health cannot be overlooked. Thus, there is a dire need for global collaboration between public health and veterinary authorities working from a 'One Health' perspective. It is very important to manage exposed animals especially pets to prevent the MPXV from being spread to wildlife. MPXV can infect a wide range of mammal species, including anteaters, hedgehogs, prairie dogs, squirrels, shrews and dogs and these animals can be natural hosts and can transmit the disease to humans. Although MPX is endemic in different parts of Africa for decades, however, there was no progress on vaccine development and clinical trials on treatments. After the global MPX outbreak, there is much more to learn. Contact tracing is absent in case of MPX outbreak and there is lack of information from the data systems in rapid manner. Additionally, test capacity needs to be increased. Many persons who are at risk of MPX may not be involved with the health care system, making diagnosis, containment, and prevention challenging. Like SARS-CoV-2, global MPX outbreak demand for vaccines far exceeds availability. Though the supply of tecovirimat has increased, this drug must still be used under an IND protocol, which limits access.

Discussion

MPX and smallpox vaccines are formulated based on a vaccinia virus and give cross-protection due to immune response to *orthopoxviruses*. Occurrence of current MPX outbreak is likely due to abandonment of the global smallpox vaccination programs, rendering a massive proportion of the world population vulnerable to monkeypox because of loss of immunity against *orthopoxviruses*. Thus, clinical, public-health, and vaccination strategies against members of *orthopoxviruses* should be revisited and reinvigorated.

Data availability statement

The raw data supporting the conclusions of this article will be made available by the authors, without undue reservation.

Author contributions

AMK, SCK, and MY: conceived and planned this study. SCK and JEK: supervision, investigation, and resources. AMK, MAK, HI, IU, MY, and JEK: writing – original draft and writing – review and editing.

Funding

This research was supported by the Ministry of Trade, Industry & Energy (MOTIE), Korea Institute for Advancement of Technology (KIAT).

Conflict of interest

The authors declare that the research was conducted in the absence of any commercial or financial relationships that could be construed as a potential conflict of interest.

Publisher's note

References

Almehmadi, M., Allahyani, M., Alsaiari, A. A., Alshammari, M. K., Alharbi, A. S., Hussain, K. H., et al. (2022). A glance at the development and patent literature of tecovirimat: the first-in-class therapy for emerging monkeypox outbreak. *Viruses* 14:1870. doi: 10.3390/v14091870

CDC (2022a). U.S. monkeypox outbreak. Available at: https://www.cdc.gov/poxvirus/monkeypox/response/2022/index.html (Accessed September 4, 2022).

CDC (2022b). Clinical Recognition. Key Characteristics for Identifying Monkeypox. Available at: https://www.cdc.gov/poxvirus/monkeypox/clinicians/clinical-recognition.html (Accessed September 4, 2022).

CDC (2022c). Guidance for tecovirimat use under expanded access investigational new drug protocol during 2022 U.S. Monkeypox cases. Available at: https://www.cdc.gov/poxvirus/monkeypox/clinicians/Tecovirimat.html (Accessed September 4, 2022).

CDC (2022d) Interim clinical considerations for use of JYNNEOS and ACAM2000 vaccines during the 2022 U.S. Monkeypox Outbreak. Available at: https://www.cdc.gov/poxvirus/monkeypox/considerations-for-monkeypox-vaccination.html (Accessed September 4, 2022).

CDC (2022e) Interim infection prevention and control recommendations for healthcare personnel during the coronavirus disease 2019 (COVID-19) pandemic. Available at: https://www.cdc.gov/coronavirus/2019-ncov/hcp/infection-control-recommendations.html (Accessed September 4, 2022).

Guarner, J., Del Rio, C., and Malani, P. N. (2022). Monkeypox in 2022: what clinicians need to know. *JAMA* 328, 139–140. doi: 10.1001/jama.2022.10802

Lapa, D., Carletti, F., Mazzotta, V., Matusali, G., Pinnetti, C., Meschi, S., et al. (2022). Monkeypox virus isolation from a semen sample collected in the early phase of infection in a patient with prolonged seminal viral shedding. *Lancet. Infect. Dis.* 22, 1267–1269. doi: 10.1016/S1473-3099(22)00513-8

Mbala, P. K., Huggins, J. W., Riu-Rovira, T., Ahuka, S. M., Mulembakani, P., Rimoin, A. W., et al. (2017). Maternal and fetal outcomes among pregnant women with human monkeypox infection in the Democratic Republic of Congo. *J. Infect. Dis.* 216, 824–828. doi: 10.1093/infdis/jix260

Moyo, E., Musuka, G., Murewanhema, G., Moyo, P., and Dzinamarira, T. (2022). Monkeypox outbreak: a perspective on Africa's diagnostic and containment capacity. *Int. J. Infect. Dis.* 123, 127–130. doi: 10.1016/j.ijid.2022.08.016

Nuzzo, J. B., Borio, L. L., and Gostin, L. O. (2022). The WHO declaration of monkeypox as a global health emergency. *JAMA* 328, 615–617. doi: 10.1001/jama.2022.12513

Seang, S., Burrel, S., Todesco, E., Leducq, V., Monsel, G., Pluart, D. L., et al. (2022). Evidence of human-to-dog transmission of monkeypox virus. *Lancet* 400, 658–659. doi: 10.1016/S0140-6736(22)01487-8

Tarín-Vicente, E. J., Alemany, A., Agud-Dios, M., Ubals, M., Suner, C., Anton, A., et al. (2022). Clinical presentation and virological assessment of confirmed human monkeypox virus cases in Spain: a prospective observational cohort study. *Lancet* 400, 661–669. doi: 10.1016/S0140-6736(22)01436-2

Thornhill, J. P., Barkati, S., Walmsley, S., Rockstroh, J., Antinori, A., Harrison, L., et al. (2022). Monkeypox virus infection in humans across 16 countries: N. *Engl. J. Med.* 387, 679–691. doi: 10.1056/NEJMoa2207323

WHO. (2022). Multi-country monkeypox outbreak: situation update. Available at: https://www.who.int/emergencies/disease-outbreak-news/item/2022-DON396 (Accessed August 29, 2022).

frontiers | Frontiers in Microbiology

TYPE Original Research
PUBLISHED 11 November 2022
DOI 10.3389/fmicb.2022.1008274

OPEN ACCESS

EDITED BY
Quan Liu,
Foshan University, China

REVIEWED BY
Yong Fu,
Washington University in St. Louis, United States
Namrata Anand,
University of Kentucky, United States

*CORRESPONDENCE
Ting Zhang
zhangting@nipd.chinacdc.cn
Wei Hu
huw@fudan.edu.cn

†These authors have contributed equally to this work

SPECIALTY SECTION
This article was submitted to Infectious Agents and Disease, a section of the journal Frontiers in Microbiology

RECEIVED 31 July 2022
ACCEPTED 24 October 2022
PUBLISHED 11 November 2022

CITATION
Gao H, Huo L, Mo X, Jiang B, Luo Y, Xu B, Li J, Ma X, Jing T, Feng Z, Zhang T and Hu W (2022) Suppressive effect of pseudolaric acid B on *Echinococcus multilocularis* involving regulation of TGF-β1 signaling *in vitro* and *in vivo*. *Front. Microbiol.* 13:1008274. doi: 10.3389/fmicb.2022.1008274

Suppressive effect of pseudolaric acid B on *Echinococcus multilocularis* involving regulation of TGF-β1 signaling *in vitro* and *in vivo*

Haijun Gao[1,2,3†], Lele Huo[1†], Xiaojin Mo[1†], Bin Jiang[1], Yanping Luo[2], Bin Xu[1], Jingzhong Li[4], Xingming Ma[2], Tao Jing[2], Zheng Feng[1], Ting Zhang[1,4*] and Wei Hu[1,5*]

[1]National Institute of Parasitic Diseases, Chinese Center for Disease Control and Prevention (Chinese Center for Tropical Diseases Research), NHC Key Laboratory of Parasite and Vector Biology, WHO Collaborating Center for Tropical Diseases, National Center for International Research on Tropical Diseases, Shanghai, China, [2]School of Basic Medical Sciences, Lanzhou University, Lanzhou, Gansu, China, [3]Ganzr Tibetan Autonomous Prefecture Center for Disease Control and Prevention, Kangding, Sichuan, China, [4]National Health Commission Key Laboratory of Echinococcosis Prevention and Control, Tibet Autonomous Region Center for Disease Control and Prevention, Lhasa, Tibet, China, [5]Department of Microbiology and Microbial Engineering, School of Life Sciences, Fudan University, Shanghai, China

Echinococcus multilocularis, the causative agent of alveolar echinococcosis (AE), severely threats human health and livestock farming. The first line of chemotherapeutic drug for AE is albendazole, which limits rapid extension of *E. multilocularis* metacestodes, but is rarely curative for AE, with severe side effects in long-term use, thus development of new anti-echinococcal drugs is mandated. Pseudolaric acid B (PAB) has long been used to treat fungal-infected dermatosis, and exerted anti-tumor, -fertility, -angiogenesis, -tubulin and antiparasitic activity. However, the effect of PAB against *Echinococcus* spp. remains unclear. The present study is to understand the effect of PAB against *E. multilocularis in vitro* and *in vivo*, and identify potential anti-echinococcal mechanism, as well as its toxicity. After exposure to PAB at 20 μg/ml, significant reduction of the survival rate and substantial ultrastructural destructions in *E. multilocularis* protoscoleces were observed *in vitro*. Furthermore, the wet weight of *E. multilocularis* cysts in the infected mice was significantly decreased after treatment with PAB (40, 20 or 10 mg/kg) for 12 weeks. Meanwhile, significant increase of both protein and mRNA expression of transforming growth factor beta 1 (TGF-β1) was detected in the serum and liver of the infected mice, whereas PAB administration lowered its expression significantly. The toxicity tests demonstrated that PAB displayed lower cytotoxicity to human liver and kidney cells (HL-7702 and HK-2 cell) with IC_{50}=25.29 and 42.94 μg/ml than albendazole with IC_{50}=3.71 and 21.22 μg/ml *in vitro*, and caused lower hepatoxicity and nephrotoxicity in mice than ABZ. Our findings indicated that PAB possesses potent anti-echinococcal effect, with lower toxicity than albendazole, implying a potential chemotherapeutic agent for AE. Additionally, the present study demonstrated that the suppressive effect of PAB on the parasite may involve down-regulation of TGF-β1 signaling.

KEYWORDS

alveolar echinococcosis, pseudolaric acid B, *Echinococcus multilocularis*, protoscoleces, TGF-β1

Introduction

Alveolar echinococcosis (AE) is a neglected zoonotic parasitosis caused by the larval stage of *Echinococcus multilocularis*. It is a cosmopolitan public health issue posing severe harm to human and livestock health, mainly spreading in Central Asia and Tibetan plateau of Western China, Europe and North America (Deplazes et al., 2017). It was reported that more than 91% of annual new AE cases worldwide occurred in rural communities on the Qinghai-Tibet Plateau of Western China, which causes more than 90% of the global disease burden (Kern et al., 2017). *E. multilocularis* metacestodes often reside in the liver of human and rodents as the intermediate host, and show tumor-like infiltrative growth, leading to liver fibrosis and organ-failure, which is often termed "parasitic cancer" (Wang et al., 2016; Gao et al., 2021). If untreated or insufficiently treated, AE patients prognose a mortality rate of > 90% within 10–15 years after diagnosed (Cheng et al., 2020; Wang et al., 2020). Currently, clinical therapeutic strategies of AE include radical resection, liver transplantation and chemotherapy, in which, drug treatment is indispensable for AE patients before and after the surgical treatment (Stamatakos et al., 2009; Kern et al., 2017). Albendazole (ABZ), a derivative of benzimidazole, is the first choice for treatment of AE, while it disrupts the microtubule polymerization and interferes with its energy metabolism (Horton, 2000; Hemphill et al., 2014). However, even if ABZ limits the rapid extension of *E. multilocularis* metacestodes, the curative effect is poor, and its long-term use produces severe adverse reactions (Hemphill and Muller, 2009). Therefore, development of new and effective treatment drugs for AE is urged.

Pseudolaric acid B (PAB), a diterpene acid extracted from the root of *Pseudolarix kaempferi Gordon*, is a traditional Chinese medicine that has been used for treatment of fungal-infected dermatosis for many years (Zhang et al., 2014; Liu et al., 2017). Increasing evidences indicated that PAB have a wide range of antitumor effects. For example, in a nude mouse experiment, PAB inhibits gastric cancer cell lung metastasis, inducing cell apoptosis by suppressing phosphatidylinositol-4,5-bisphosphate 3-kinases and protein kinase B (PI3K/Akt), ERK1/2 and mitochondrial signaling pathways (Wang D. et al., 2017). In addition, our recent study has demonstrated that PAB blocks hepatocellular carcinoma (HCC) cells proliferation and invasion through inhibiting Notch1/Akt signaling pathway (Gao et al., 2022). Moreover, PAB inhibited immunomodulatory functions in T regulatory cells by reducing the expression of protein kinase B (PKB or Akt) and mitogen activated protein kinases (MAPK; Li et al., 2014; Liu et al., 2017), and a derivant of PAB was also evidenced to boost the expression of TGF-β1 in regulatory T cells (Li et al., 2014). Overall, PAB may be a novel effective candidate agent in treatment of cancer, immune disorders, inflammatory diseases, and immunosuppression, even though the mechanism responsible for PAB exerting the biological functions is still poorly understood. For instance, it was noted that PAB has a strong insecticidal effect described in ancient book-Compendium of Materia Medica (Yao et al., 2014), and later studies found it has a strong anti-parasitic effect on flatworm *Dactylogyrus* in fish (Ji, 2013). More importantly, the excessive disorder of transforming growth factor beta 1 (TGF-β1) and many other signaling pathways, such as Notch/Akt, PI3K/Akt, and MAPKs signaling, were found to cross-drive the initiation and progression of many liver diseases, such as liver fibrosis induced by *Echinococcus* infection (Brehm and Koziol, 2017; Wang Y. et al., 2017; Chen et al., 2022). However, the information of PAB against *E. multilocularis* metacestodes and the underlying anti-echinococcal mechanism remain unclear as yet.

The present study is to explore the anti-echinococcal activity of PAB on *E. multilocularis in vitro* and *in vivo*, and the target signaling regulated by PAB during this process. In addition, the cytotoxicity of PAB in normal liver and kidney cell line *in vitro*, and its sub-acute hepatotoxicity and nephrotoxicity in the mice will be assessed.

Materials and methods

Biochemical reagents

PAB, ABZ and ABZ sulfoxide (ABZ-SO, an anthelmintic active form of ABZ) were purchased from Aladdin Industrial Corporation (Shanghai, China) and Sigma-Aldrich (St. Louis, MO, United States); cell culture media were obtained from Gibco (Wisent, Canada); human liver cancer cell line (HepG2 cell) and normal human renal epithelial cell line (HK-2 cell) were purchased from Cell bank of Chinese Academy of Sciences (Shanghai, China), and human normal liver cell line (HL-7702 cell) was warmly presented by Dengfeng Yang from Gangxi Academy of

Abbreviations: *E. multilocularis*, *Echinococcus multilocularis*; AE, alveolar echinococcosis; PAB, pseudolaric acid B; TGF-β1, transforming growth factor-beta 1; ABZ, albendazole; PSC, protoscoleces; ABZ-SO, albendazole sulfoxide; ELISA, enzyme-linked immunosorbent assay; PBS, phosphate buffer saline; SEM, scanning electron microscopy; TEM, transmission electron microscopy; IHC-P, immunohistochemistry-paraffin; RT-qPCR, real-time quantitative polymerase chain reaction; WB, Western blot; ALP, alkaline phosphatase.

Sciences. Mongolian gerbils were purchased from Zhejiang Academy of Medical Sciences (Hangzhou, China).

Isolation and culture of *Echinococcus multilocularis* protoscoleces

E. multilocularis protoscoleces (PSC) were separated from the metacestodes in *E. multilocularis*-infected Mongolian gerbils, and rinsed with dulbecco's modified eagle's medium (DMEM) containing 1% of penicillin–streptomycin (P-S) until the viability of > 97%, and then seeded into 24-well culture plates (120 PSC per well) to be incubated under the condition of 37°C and 5% CO_2, as described previously (Gao et al., 2021).

Drug treatment of *Echinococcus multilocularis* protoscoleces *in vitro*

The experimental group was assigned as follows: (i) the vehicle group treated with 0.1% dimethyl sulfoxide (DMSO) ($n = 3$); (ii) the ABZ-SO group treated with ABZ-SO of 40, 20 and 10 μg/ml resolved in 0.1% DMSO ($n = 3$), respectively; (iii) the PAB group treated with PAB of 80, 40, 20, 10, 5, 2, 1 and 0.5 μg/ml resolved in 0.1% DMSO ($n = 3$), respectively. After treatment with different doses of drugs for 48 h, the PSC were stained with 0.4% trypan blue and examined morphologically under an inverted light microscope (BX43, Olympus, Japan). The survival rate of PSC were calculated as follows: PSC survival rate (%) = (live PSC count/total PSC count) × 100, with three independent biological replicates, as described previously (Gao et al., 2021), and half maximal inhibitory concentration (IC_{50}) values were calculated from the graph plotted inhibition percentage against the concentration of sample solution using the Graphpad/Prism program version 8.0 (San Diego, CA). Further, the PSC exposed to different compounds were fixed with 4% glutaraldehyde to observe the ultrastructural alterations under scanning electron microscope (SEM, JSM-5600LV, JEOL, Japan) and transmission electron microscope (TEM, HT7800, Hitachi Consumer Marketing, Japan), as described previously (Gao et al., 2021).

Culture and treatment of *Echinococcus multilocularis* microcyst *in vitro*

After PSC co-cultured with the nurse cell (HepG2 cell) for 4 weeks in complete culture media containing 89% DMEM, 1% P-S and 10% fetal bovine serum (FBS) at 37°C, 5% CO_2, the microcyst developed from PSC were seeded into 24-well culture plate with 3 microcysts per well. The test groups were assigned as: (i) the vehicle group treated with 0.1% DMSO, (ii) the PAB group treated with PAB of 40 and 20 μg/ml resolved in 0.1% DMSO, respectively. The vitality and morphology of *E. multilocularis* microcysts after treatment with PAB for 1, 2, and 4 weeks were inspected, respectively. On wk. 1, alkaline phosphatase (ALP) activity in the culture supernatant of the microcysts was examined using chemiluminescence method under a multifunctional microplate reader (BioTek, US), according to the manufacturer's reagent specification (Solarbio Science & Technology Co., Ltd., Beijing, China). On week 4 after treatment with PAB, these microcysts were stained by 0.4% trypan blue to observe the morphological alterations by inverted microscopy.

Echinococcus multilocularis infection and drug treatment *in vivo*

Kunming mice ($n = 30$) were infected with *E. multilocularis* PSC (2000 PSC per mouse) by *in situ* surgical intrahepatic implantation in Specific Pathogen Free (SPF) laboratory for 3 months, and meanwhile, other healthy mice ($n = 5$) were processed with a sham procedure as a negative control group. After 3 months post-infection, the infected mice were divided into: (i) the untreated group ($n = 5$), daily treated with only honey/PBS (1:1 v/v), (ii) the ABZ group ($n = 5$), treated with ABZ daily of 40 mg/kg in honey/PBS (1:1 v/v), (iii) the PAB group ($n = 5$), daily treated with PAB (40, 20, 10 and 5 mg/kg) in honey/PBS (1:1 v/v), respectively, and at the same time, the uninfected mice were only administrated with honey/PBS (1:1 v/v). After oral administration of different drugs for 12 weeks, the wet weight of *E. multilocularis* cysts was weighed, the serum and the liver of the mice were collected to examine the expression of TGF-β1.

Examination of TGF-β1 protein expression in *Echinococcus multilocularis* PSC by immunofluorescence assay

To examine the expression of TGF-β1 by immunofluorescence (IF) assay, *E. multilocularis* PSC in the vehicle (0.1% DMSO) group and PAB-treated (20 μg/ml) group were rinsed with phosphate buffer saline (PBS), and then fixed with 4% paraformaldehyde, as described previously (Wang et al., 2022). The paraffin-embedded PSC sections were blocked with 20% normal goat serum and incubated with rabbit anti-TGF-β1 antibody (1:100) overnight at 4°C. After reaction with Cy3 conjugated goat anti-rabbit IgG (H + L) (1:200; Servicebio technology Co., LTD., Wuhan, China) and DAPI (1:100; abcam, Cambridge, UK), these slides were imaged under a fluorescence microscope (Olympus, Japan). Mean fluorescence intensity indicating TGF-β1 protein expresssion in the images were calculated using ImageJ software (ImageJ, RRID:SCR_003070), as described previously (Jansen et al., 2016).

Analysis of TGF-β1 protein expression by ELISA, immunohistochemistry-paraffin, and Western blot assays

TGF-β1 level in the serum of the mice was measured by enzyme-linked immunosorbent assay (ELISA), following the

manufacturer's instructions (CUSABIO, Wuhan, China). The content of TGF-β1 was presented as ng/ml after the subtraction of the appropriate control. Further, to observe the expression of TGF-β1 in *Echinococcus* metacestodes and the mice after treatment with PAB, *E. multilocularis* cysts and the liver tissues were fixed with 4% paraformaldehyde for immunohistochemistry-paraffin (IHC-P) examination, as described previously (Liu et al., 2021). Brifely, the slides coated with *E. multilocularis* cysts and the liver tissues were reacted with rabbit anti-TGF-β1 polyclonal antibody (Bioss Co., Beijing, China) and goat anti-rabbit IgG (ZSGB-BIO, Beijing, China) at the dilution of 1:200 and 1:800, respectively, and then these slides were imaged under a light microscope (Olympus, Japan) (10 fields/group), and the semi-quantitative analysis of TGF-β1 protein expression in each field was performed by ImageJ software (National Institutes of Health, Bethesda, MD, USA), as described previously (Antarianto et al., 2022).

Western blot (WB) was used to examine the TGF-β1 expression, briefly, *E. multilocularis* cysts and the liver tissues of the mice were lysed by tissue homogenizer (Tiangen biotech Co., LTD, Beijing, China), the total protein was extracted using Nuclear and Cytoplasmic Protein Extraction Kit (Yeasen Biotechnology (Shanghai) Co., Ltd.), and the protein concentration was detected using BCA Assay Kit (Servicebio, Wuhan, China), as described previously (Wang et al., 2022). Every sample of 60 μg per lane was separated by 12% SDS-PAGE, and then transferred to a polyvinylidene difluoride membrane, and blocked with 5% non-fat milk for 2 h at room temperature. The membrane was incubated with 1:500 diluted rabbit anti-TGF-β1 antibodies overnight at 4°C, and then with 1:2000 diluted goat anti-rabbit IgG for 2 h at room temperature. In addition, the rabbit anti-β-actin antibody was used as an internal standard at the dilution of 1:300 (Bioss, Beijing, China). Semiquantitative analysis was performed by ImageJ software, as described previously (Jansen et al., 2016).

Determination of TGF-β1 mRNA expression by real-time quantitative PCR

Total RNA in mice livers and *E. multilocularis* cysts was extracted using TRIzol reagent (Invitrogen, San Diego, USA), and reverse-transcribed into cDNA, referring to the reagent instruction (No. RR036A). The RT-qPCR was performed according to the protocols as described (Liu et al., 2021), and the used primers were as follows: mouse *TGF-β1* (forward, 5′-CTTCAATACGTCAG ACATTCGGG-3′; reverse, 5′-GTA ACGCCAGGAATTGTTGCTA-3′), mouse *β-actin* (forward, 5′-TTGTTACCAACTGGGACG-3′; reverse, 5′-GGCATAGAG GTCTTTACGG-3′). The semi-quantitative analysis of cDNA was performed by the SYBR Green PCR Master Mix (TaKaRa, Tokyo, Japan), following the manufacturer's protocols. The relative expression level of *TGF-β1* mRNA was normalized to that of *β-actin*, and the comparison of cycle threshold (CT) values of each group was measured using the $2^{-\Delta\Delta CT}$ method (Xiao et al., 2022).

Assessment of cytotoxicity of PAB on human normal hepatocytes and kidney cell *in vitro*

To assess the cytotoxicity of PAB, human normal hepatocyte (HL-7702 cell line) and renal cell line (HK-2 cell) were seeded into 96-well culture plates (5×10^3 cells per well) and 24-well culture plates (2×10^4 cells per well) with complete culture media, and followed by incubation at 37°C and 5% CO_2 for 6 h. PAB and ABZ-SO at a final concentration of 80, 40, 20, 10, 5, 2, 1, 0.5, 0.2 and 0 μg/ml were added into the cell culture plates, respectively ($n = 6$). After treatment with PAB and ABZ-SO for 48 h, cell counting kit-8 (CCK-8) solution (10 μl per well) was added into 96-well culture plates to continuously incubate for 2 h, and the optical density was read under a multifunctional enzyme marking instrument (BioTek, US), and then cell viability was calculated using the following formula: cell viability = $[(OD_{treatment} - OD_{blank})/(OD_{control} - OD_{blank})] \times 100\%$, and IC50 values were calculated using the Graphpad/Prism software. In addition, cell morphologic alterations in 24-well culture plates were observed after staining with 1% crystal violet (Solarbio Co., Ltd., Beijing, China) under the indicated inverted microscope. These experimental processes were conducted with three independent biological replicates following the manufacturer's specifications (Beyotime Biotechnology Co., Ltd., Shanghai, China).

Evaluation of sub-acute hepatotoxicity and nephrotoxicity of PAB in mice

To evaluate the sub-acute hepatotoxicity and nephrotoxicity of PAB *in vivo*, 15 healthy Kunming mice were assigned as: (i) the control group ($n = 5$), orally administrated with honey/PBS daily (1:1 v/v), (ii) the PAB group ($n = 5$), orally administrated with PAB at 40 mg/kg in honey/PBS daily (1:1 v/v), and (iii) the ABZ group ($n = 5$), orally administrated with ABZ at 100 mg/kg (the dosage of 136.3 mg/kg for mice calculated by the recommended dosage for human with 10 mg/kg; Kern et al., 2017) in honey/PBS daily (1:1 v/v). After treatment with PAB and ABZ for 6 weeks, those mice sera were collected to detect 11 biochemical indexes that were related to the liver and kidney function by chemiluminescent immunoassay (CLIA). At the same time, the liver and kidney tissues of those mice were fixed with 4% paraformaldehyde to observe the pathological alterations by hematoxylin–eosin (HE) staining.

Statistics

The experimental data were described as the mean ± standard deviation (mean ± SD). The different reading in fluorescence intensity between two groups was analyzed by student's *t*-test, and

the differences in cysts weight, TGF-β1 level, and biochemical indexes among three or more groups were assessed by one-way ANOVA with multiple comparisons. Statistical analysis was performed using GraphPad Prism version 8.0 (San Diego, CA) and SPSS version (IBM, Chicago, IL). $p < 0.05$ indicates significant difference.

Results

Effect of PAB on the activity of *Echinococcus multilocularis* protoscoleces *in vitro*

To investigate insecticidal effect of PAB on *E. multilocularis in vitro*, the survival rate and morphological alterations in PSC were measured after treatment with PAB at different concentrations. The survival rate of PSC showed a time- and dose-dependent decreasing after treatment with 0.5–80 μg/ml PAB within 7 days. All PSC examined were killed by 1–80 μg/ml PAB in 1 week. Among them, all PSC were killed after treatment with PAB at 10, 20 and 40 μg/ml for 3, 2 and 1 day, respectively (Figure 1A). Treatment with PAB (IC_{50} = 12.63 μg/ml) at 40, 20 and 10 μg/ml for 3 days significantly reduced the PSC survival rate in comparison with ABZ-SO treatment at the same concentrations, respectively (all $p < 0.0001$) (Figure 1B).

Light microscopy indicated that structural damage was observed in the PSC after treatment with 20 μg/ml PAB, showing disappearance of calcareous corpuscles, breakage of tegument and suckers, but not seen in the vehicle group with typan blue staining (Figures 2D–F) or not (Figures 2A–C). Furthermore, SEM assay revealed that the ultrastructure of PSC treated with 20 μg/ml PAB was different from that treated with 20 μg/ml ABZ-SO or DMSO. The PSC exposed to 20 μg/ml PAB exhibited ultrastructural destructions, including shedding of tegument, breakage of rostellum and suckers (Figures 2G–I). At the same time, TEM assay indicated that in comparison with the microstructure of PSC treated with ABZ-SO and DMSO, the PSC exposed to PAB showed disappearance of periodic acid-Schiff stain (PAS) positive materials, microvillus and syncytial layer (SL), contraction of parenchymal cells, and presentation of abundant cytoplasm vacuolization, condensed chromatin and apoptotic bodies (Figures 2J–L).

Effect of PAB on the development of *Echinococcus multilocularis* protoscoleces *in vitro*

To further investigate anti-echinococcal effect of PAB *in vitro*, the development of *E. multilocularis* PSC after treatment with PAB was measured. Microscopic observation at week 1 of *in vitro* test found that, *E. multilocularis* microcysts upon exposure to PAB of 20 and 40 μg/ml showed morphological alterations, including collapse of the microcyst, shrinking of the germinal layer from the laminated layer, but not in the vehicle group. At weeks 2 and 4, the solid protrusions (SP) and new PSC in the microcysts were observed in the vehicle group, but the microcysts treated with PAB exhibited breakage. At week 4, *E. multilocularis* microcysts after treatment with PAB were found stained by trypan blue and no new PSC was found inside (Figure 3A). In addition, after treatment with 40 and 20 μg/ml PAB for 1 week, the activity of ALP in the culture supernatant of the microcysts exhibited significant increase from (0.42 ± 0.04) U/L in the vehicle group to (0.76 ± 0.08) U/L and (0.89 ± 0.04) in 20 and 40 μg/ml PAB-treated groups, respectively ($p = 0.0002$ and $p = 0.0085$; Figure 3B).

Effect of PAB against *Echinococcus multilocularis* metacestodes *in vivo*

Furthermore, *in vivo* anti-echinococcal effect of PAB was evaluated in a mouse model with liver echinococcosis. The wet

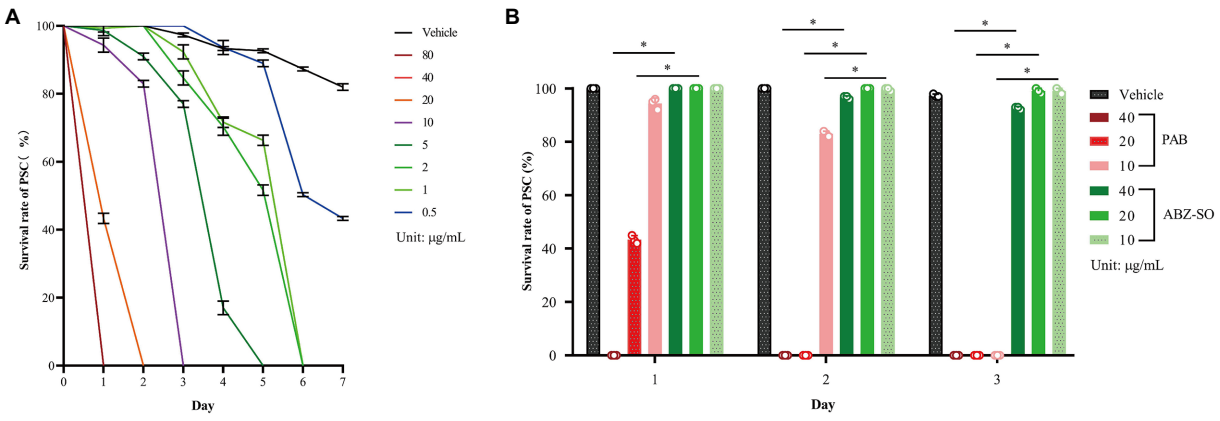

FIGURE 1
Changes in survival rate of *E. multilocularis* PSC before and after PAB treatment *in vitro*. **(A)** Survival rate of *E. multilocularis* PSC of the vehicle group exposed to 0.5–80 μg/ml PAB for 7 days, and **(B)** 10, 20 and 40 μg/ml PAB and ABZ-SO for 3 days, as measured by morphological alterations under a light microscope. Data are expressed as mean±SD, n=3. The independent experiments were processed in triplicate.

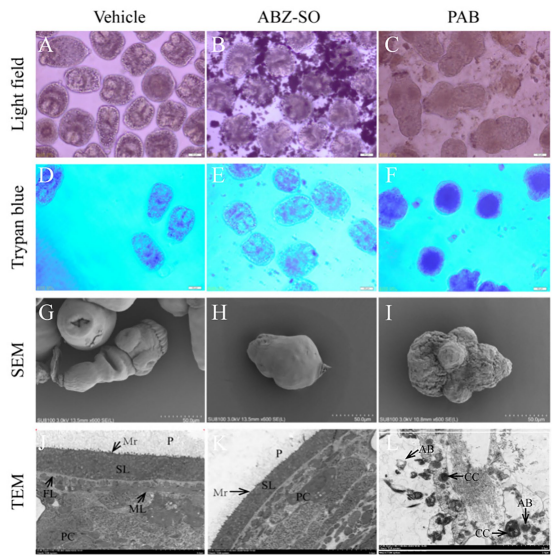

FIGURE 2
Structural morphology changes of *E. multilocularis* PSC after treatment with PAB *in vitro*. The PSC treated with PAB (20 μg/ml) and ABZ-SO (20 μg/ml) for 2 days were observed using trypan blue staining **(D–L)** or unstained **(A–C)** under light microscope **(A–F)**, 200×magnification, SEM **(G–I)**, scale-bars: 50 μm and TEM **(J–L)**, scale-bars: 5 μm. Abbreviations: P, periodic acid-schiff stain positive material; Mv, microvillus; SL, syncytial layer, FL, fibrous layer, ML, muscular layer, AB, apoptotic bodies, CC, condensed chromatin.

weight of *E. multilocularis* cysts isolated from the group treated with 40, 20 and 10 mg/kg PAB was (1.94 ± 0.30) g, (2.38 ± 0.22) g and (2.64 ± 0.48) g, respectively, which were significantly lower than those from the infected group [(3.82 ± 0.44) g] ($p < 0.0001$, $p < 0.0001$ and $p = 0.0002$), respectively, but not seen in 5 mg/kg PAB treatment group [(3.16 ± 0.37) g] ($p = 0.0597$). In addition, the wet weight of the cysts from 40 mg/kg ABZ treatment group [(2.29 ± 0.15) g] was significantly lower than that in the infected group [(3.82 ± 0.44) g] ($p = 0.011$), but no significant difference was seen when compared with the 40 mg/kg PAB treatment group ($p = 0.6091$; Table 1).

PAB down-regualting TGF-β1 protein and mRNA expression in *Echinococcus multilocularis* metacestodes

Possible anti-echinococcal mechanism of PAB was investigated by observing the expression of TGF-β1 protein and mRNA in *E. multilocularis*. By immunofluorescence assay, red fluorescence-stained TGF-β1 was found widely distributed in the natural parenchymatous tissue of the PSC, but the distribution was diminished after treatment with 20 μg/ml PAB *in vitro* (Figure 4A), and the semiquantitative analysis indicated that compared with the vehicle group, PSC in the PAB-treated group showed a significant decrease of fluorescence-labeled TGF-β1 ($p < 0.0001$; Figure 4B).

IHC-P assay revealed that the expression of TGF-β1 in *E. multilocularis* cysts [(6.29 ± 1.37)% and (6.29 ± 1.37)%] exhibited a significant decrease after treatment with 40 and 20 mg/kg PAB ($p = 0.0211$ and $p = 0.0499$), respectively, but 10 and 5 mg/kg of PAB caused no change [(7.30 ± 1.21)% and (7.58 ± 1.40)%] ($p = 0.6247$ and $p = 0.9168$) (Figures 5Aa–f), in comparison with that in the infected mice [(7.95 ± 1.10)%].

Furthermore, WB assay showed that the expression of TGF-β1 in *E. multilocularis* cysts [(0.60 ± 0.04), (0.75 ± 0.04) and (0.79 ± 0.02)], were significantly lower after treatment with 40, 20 and 10 mg/kg of PAB (all $p < 0.0001$), respectively, than those in the PAB-untreated mice (1.00 ± 0.03), but no significant reduction was observed at 5 mg/kg of PAB (0.87 ± 0.06) ($p = 0.0649$; Figures 5Ba–b).

Detected by RT-qPCR, expression of *TGF-β1* mRNA in the cysts of infected mice with 40 and 20 mg/kg PAB were reduced to 54.49% and 32.40% ($p = 0.0024$ and $p = 0.0015$), respectively, comparing with the non-treated infected group, but the expression in the group treated with 10 and 5 mg/kg of PAB only showed mild reduction at 64.80% and 84.91% ($p = 0.1196$ and $p = 0.3189$; Figure 5C).

PAB down-regualting TGF-β1 protein and mRNA expression in the liver of *Echinococcus multilocularis*-infected mice

Furthermore, the expression of TGF-β1 protein and mRNA in *Echinococcus*-infected mouse was also assessed after treatment with PAB. Detected by ELISA, the level of TGF-β1 protein in the serum of the mice was elevated 1.7-fold after infection of *E. multilocularis* ($p < 0.0001$). However, compared with that of the uninfected group, TGF-β1 level in the serum of the infected mice after treatment with 40, 20 and 10 mg/kg of PAB were reduced by 1.9-fold, 1.6-fold and 1.3-fold ($p < 0.0001$, $p < 0.0001$ and $p = 0.0035$), respectively, but 5 mg/kg of PAB treatment group only showed 1.1-fold decrease ($p = 0.2239$; Table 2).

Furthermore, IHC-P assay indicated that the expression of TGF-β1 in the mice liver was boosted fivefold after the infection of *E. multilocularis* ($p < 0.0001$). However, the expression of TGF-β1 in the infected mice treated with 40 and 20 mg/kg PAB was decreased significantly ($p < 0.0001$ and $p = 0.0167$), whilst no significant reduction was found in 10 and 5 mg/kg PAB groups ($p = 0.999$ and $p = 0.9979$; Figures 6Aa–g).

Western blot revealed that the TGF-β1 expression in the liver of *E. multilocularis* infected mouse was significantly increased ($p < 0.0001$), but significantly decreased after treatment with PAB of 40, 20, 10 and 5 mg/kg (all $p < 0.0001$), respectively (Figures 6Ba–b).

In addition, RT–qPCR indicated that the expression of *TGF-β1* mRNA in the liver of the mice was elevated 5.5-fold after infection of *E. multilocularis* ($p < 0.0001$). However, compared with that in *Echinococcus*-infected mice, RT-qPCR indicated that the expression of *TGF-β1* mRNA in the liver of the infected mice treated with 40, 20, 10 and 5 mg/kg of PAB was decreased to

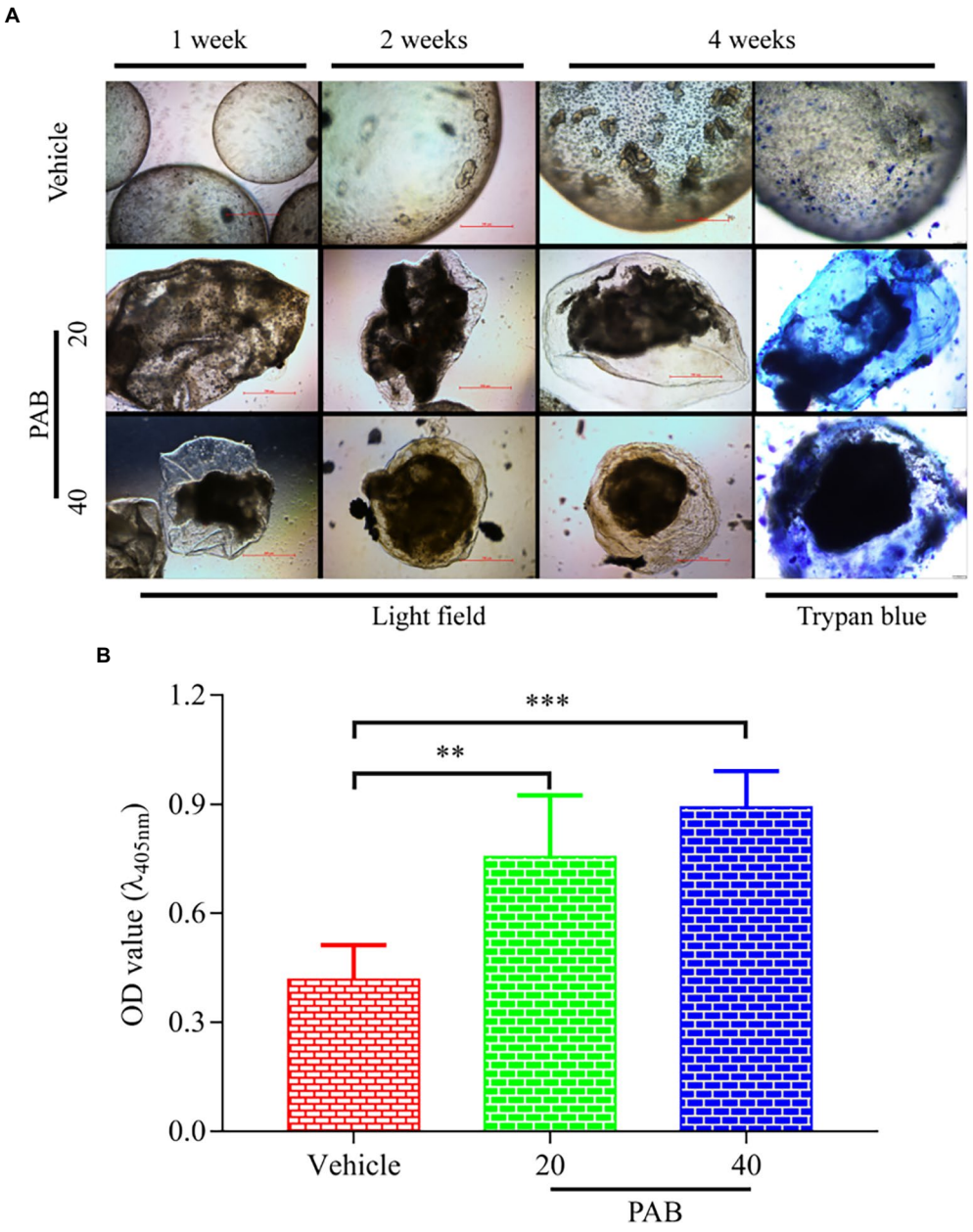

FIGURE 3
Viability changes of *E. multilocularis* microcysts after treated with PAB *in vitro*. **(A)** Microcysts exposed to 20 and 40 μg/ml PAB for 4 weeks showed ultrastructural damage, such as detachment of the germinal layer from the laminated layer, however the typical germinal layer (GL) (week 1) producing solid protrusions (SP) (week 2), present of daughter PSC (week 4) in the vehicle group. Images were measured by light microscopy at weeks 1, 2 and 4 without any staining; and at week 4 with trypan blue staining. **(B)** ALP levels in the culture supernatants of *E. multilocularis* microcysts after treatment with 20 and 40 μg/ml PAB for 1 week, as measured by chemiluminescence method. All data were assessed using One-way ANOVA with multiple comparisons. The independent experiments were processed in triplicate.

be 2.9-, 3.5-, 3.6- and 3.7-folds ($p = 0.0006$, $p = 0.0059$, $p = 0.012$ and $p = 0.0136$), respectively (Figure 6C).

Hepatorenal cytotoxicity of PAB *in vitro*

To assess the toxicity of PAB, *in vitro* the proliferation and morphology of the normal liver and kidney cell were first measured using cell counting kit (CCK-8) assay and crystal violet staining. CCK-8 indicated the survival rates of HL-7702 cell showed a dose-dependent decrease after treatment with different concentrations of PAB and ABZ-SO at 0.2, 0.5, 1, 2, 5, 10, 20, 40 and 80 μg/ml (Figure 7Aa). Among them, treated with 10 μg/ml PAB ($IC_{50} = 25.29$ μg/ml), the cell survival rate showed a significant increase [(50.79 ± 1.80)%] in comparison with that [(26.9 ± 0.81)%] using the same concentration of ABZ-SO ($IC_{50} = 3.71$ μg/ml)

($p = 0.0001$). When the concentrations of PAB and ABZ-SO reached 40 μg/ml, the cell survival rate in PAB-treated group [(46.07 ± 1.77)%] was also significantly higher than that in ABZ-SO-treated group [(24.65 ± 0.93)%] ($p = 0.0001$). In addition, crystal violet staining assay showed reduction in the number of viable HL-7702 cells after treated with 10 and 40 μg/ml PAB or ABZ-SO. Among them, ABZ-SO presented a stronger inhibitory effect than the same concentrations of PAB (Figure 7Ab).

Furthermore, CCK-8 assay indicated dose-dependent inhibitory effect of both PAB and ABZ-SO at 0.2, 0.5, 1, 2, 5, 10, 20, 40 and 80 μg/ml on HK-2 cells, respectively. Among them, the survival rate of HK-2 cells exposed to 40 μg/ml PAB ($IC_{50} = 42.94$ μg/ml) was (50.16 ± 1.82)%, whereas, showing no significant difference in comparison with that [(45.73 ± 3.52)%] upon the same concentration of ABZ-SO ($IC_{50} = 21.22$ μg/ml) ($p = 0.2907$) (Figure 7Ba). Similar to the response of HL-7702 cells, the number of HK-2 cells also decreased by crystal violet staining after treatment with 10 and 40 μg/ml PAB and ABZ-SO, respectively (Figure 7Bb).

TABLE 1 Changes in the wet weight of *E. multilocularis* metacestodes in mice orally treated with PAB for 12 weeks after 3 months post-infection.

Group	No. of mice	Dose	Cyst weight (g) (mean ± SD)
Untreated	5	5% honey/PBS	3.82 ± 0.44
ABZ	5	40 mg/kg	2.29 ± 0.15*
PAB	5	40 mg/kg	1.94 ± 0.30*
	5	20 mg/kg	2.38 ± 0.22*
	5	10 mg/kg	2.64 ± 0.48*
	5	5 mg/kg	3.16 ± 0.37

ABZ, albendazole; PAB, pseudolaric acid B; PBS, phosphate buffer saline. All data were analyzed using one-way ANOVA with multiple comparisons.
*$p < 0.05$ (compared to the untreated group).

Hepatotoxicity and nephrotoxicity of PAB in mice

To assess the sub-acute hepatotoxicity and nephrotoxicity of PAB *in vivo*, Kunming mice were orally administrated with

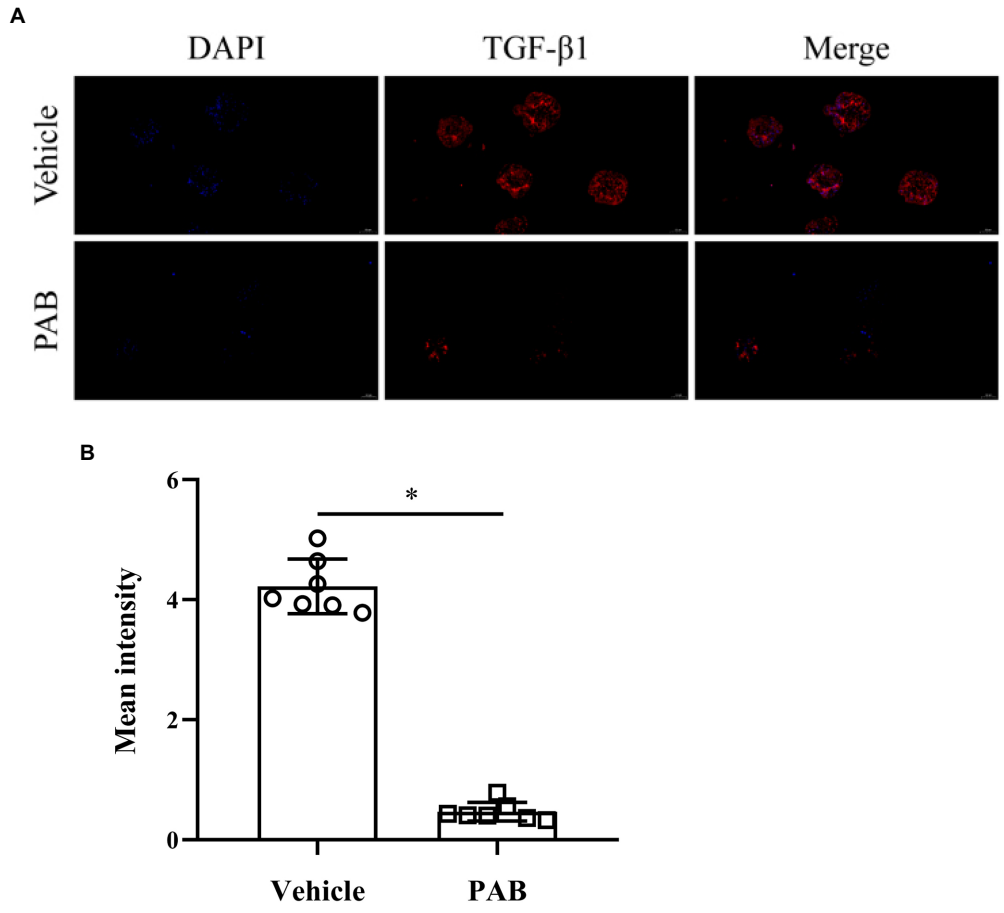

FIGURE 4
Expression of TGF-β1 in *E. multilocularis* PSC after treatment with 20 μg/ml PAB for 2 days by immunofluorescence assay. **(A)** Location of TGF-β1 protein (red) and DAPT-indicated DNA (blue) in the PSC in immunofluorescence staining images. Scale-bars: 50 μm. **(B)** Analysis of mean fluorescence intensity indicated TGF-β1 protein expression, as measured by ImageJ software. The data was assessed using *t*-test.

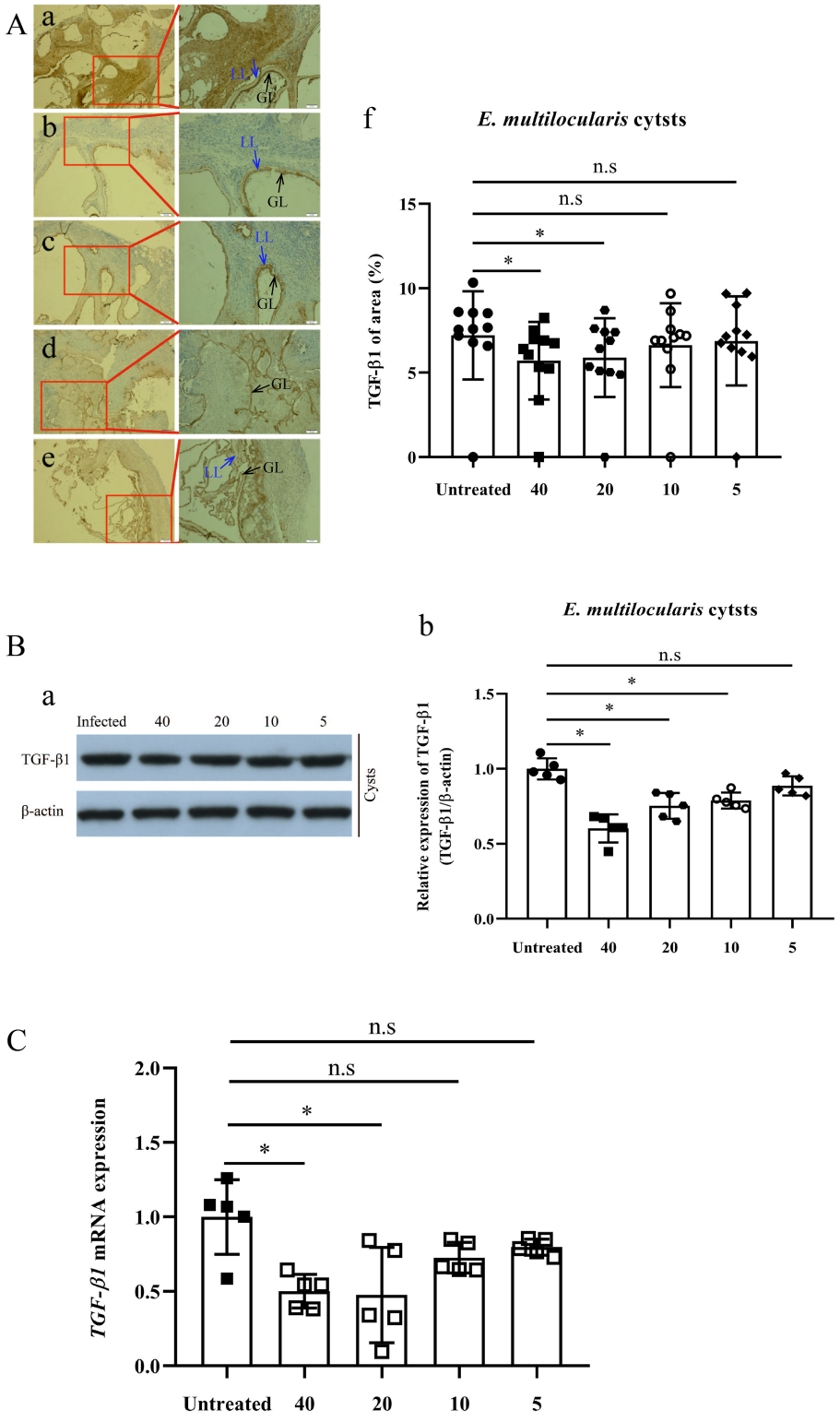

FIGURE 5
Expression of TGF-β1 protein and mRNA in *Echinococcus multilocularis* cysts after treatment with PAB for 12 weeks, as measured by immunohistochemistry-paraffin (IHC-P), Western blot (WB) and real-time quantitative PCR (RT-qPCR) assay. **(A)** Images of TGF-β1 protein expression in *E. multilocularis* cysts from the mice **(a)** untreated, and treated with PAB **(b)** 40, **(c)** 20, **(d)** 10, and **(e)** 5 mg/kg, as measured by IHC-P assay; and **(f)** semi-quantitative analysis of TGF-β1 protein, as measured by ImageJ software. Brown area indicates expression of TGF-β1 protein, Laminated layer (LL, blue arrow) and germinal layer (GL, black arrow) in *E. multilocularis* cysts. Magnification,×100 and×200. **(B)** WB analysis of **(a)** TGF-β1 and β-actin expression in *E. multilocularis* cysts in the untreated, and treated with PAB of 40, 20, 10, and 5 mg/kg PAB mice, and **(b)** the semi-quantitative analysis of TGF-β1 protein, as measured by ImageJ software. **(C)** Analysis of TGF-β1 mRNA expression in *E. multilocularis* cysts by RT-qPCR. All data were assessed using One-way ANOVA with multiple comparisons. LL, laminated layer; GL, germinal layer.

TABLE 2 Changes of TGF-β1 content in the serum of *E. multilocularis*-infected mouse orally treated with PAB for 12 weeks after 3 months post-infection.

Group	No. of mice	Dose	TGF-β1 content (ng/ml, Mean ± SD)
Control	5	5% honey/PBS	13.78 ± 2.16
Untreated[a]	5	5% honey/PBS	23.73 ± 2.56*
PAB[b]	5	40 mg/kg	12.08 ± 2.22*
	5	20 mg/kg	14.67 ± 1.98*
	5	10 mg/kg	18.08 ± 3.10*
	5	5 mg/kg	20.89 ± 1.67

PAB, pseudolaric acid B; TGF-β1, transforming growth factor beta 1. [a]Compared with the control group, and [b]compared with the untreated group. All data were analyzed using one-way ANOVA with multiple comparisons. *$p < 0.05$.

PAB for 6 weeks. Compared with the control group, the PAB group showed significant difference in serum direct bilirubin (DBIL) content with 79.68% decrease ($p = 0.0015$), total protein (TP) content with 1.1-fold increase ($p = 0.0012$), aspartate aminotransferase (AST) content with 1.1-fold increase ($p = 0.0038$), but the ABZ group showed significant difference in serum DBIL content with 79.69% decrease ($p = 0.0015$), indirect bilirubin (IBIL) content with 1.2-fold increase ($p = 0.0063$), TP content with 1.1-fold increase ($p = 0.0027$), alanine aminotransferase (ALT) content with 1.1-fold increase ($p < 0.0001$), AST content with 1.1-fold increase ($p = 0.0373$), alkaline phosphatase (ALP) with 1.2-fold increase ($p = 0.0007$). When compared with the PAB group, the ABZ group showed significance increase in serum IBIL content ($p = 0.0408$), ALT level ($p = 0.0002$), ALP content ($p = 0.0005$). Additionally, compared with the control group, the PAB group showed significant difference in serum creatinine (CRE) content with 1.2-fold increase ($p = 0.0013$) and blood urea nitrogen (BUN) content with 1.1-fold increase ($p = 0.0329$), and the ABZ group showed significant difference in serum CRE content with 1.2-fold increase ($p = 0.0032$) and BUN content with 1.1-fold increase ($p < 0.0001$). When compared with the PAB group, the ABZ group showed significance increase in serum BUN content ($p = 0.0005$; Table 3). In addition, no death and adverse reactions were observed in mice during treatment with PAB and ABZ.

It was demonstrated that pathological changes of the liver and kidney tissues in the mice after treatment with PAB were examined by HE staining. In comparison with that in the liver of untreated mice, the liver in the mice treated with PAB or ABZ for 6 weeks did not show obvious pathological damage, such as infiltration of inflammatory cells in portal area, disorganization of hepatic lobule structure and ballooning or fatty degeneration of hepatocytes (Figure 8A). As well, compared with the liver of untreated mice, the kidney in PAB- or ABZ-treated mice did not show obvious pathological damage, such as renal tubular lesions, interstitial edema and accumulation of inflammatory cells (Figure 8B).

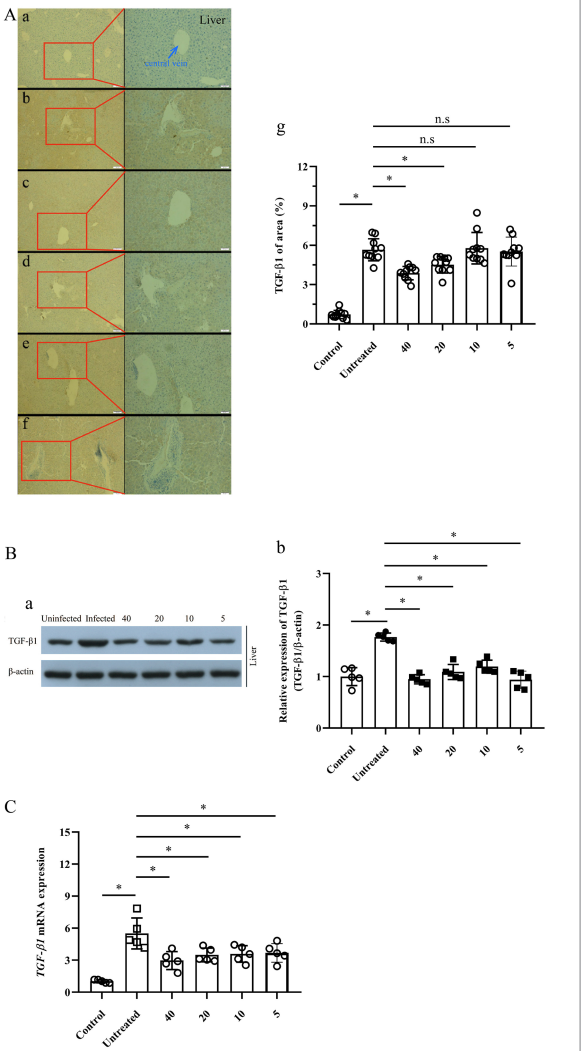

FIGURE 6
Expression of TGF-β1 protein and mRNA in the liver of *Echinococcus*-infected mouse after treatment with PAB for 12 weeks, as measured by IHC-P, WB and RT-qPCR assay. **(A)** Images of TGF-β1 protein expression in the liver of the mice, **(a)** uninfected, **(b)** untreated, and treated with PAB of **(c)** 40, **(d)** 20, **(e)** 10 and **(f)** 5 mg/kg, as measured by IHC-P assay; and **(g)** the semi-quantitative analysis of TGF-β1 protein, as measured by ImageJ software. Brown area indicates expression of TGF-β1 protein, central vein (blue arrow) in the liver of *E. multilocularis*-infected mice. Magnification,×100 and×200. **(B)** WB analysis of **(a)** TGF-β1 and β-actin expression in the mice liver, and **(b)** the semi-quantitative analysis of TGF-β1 protein, as measured by ImageJ software. **(C)** Analysis of TGF-β1 mRNA expression in the liver of the mice by RT-qPCR. All data were assessed using One-way ANOVA with multiple comparisons.

Discussion

E. multilocularis metacestodes often reside in the liver of humans and plateau pikas, and is also termed "parasitic cancer" due to its tumor-like invasive growth pattern, causing a great concern in public health (Li et al., 2018; Gao et al., 2021). Currently, the drug of choice for AE is ABZ, which can limit rapid

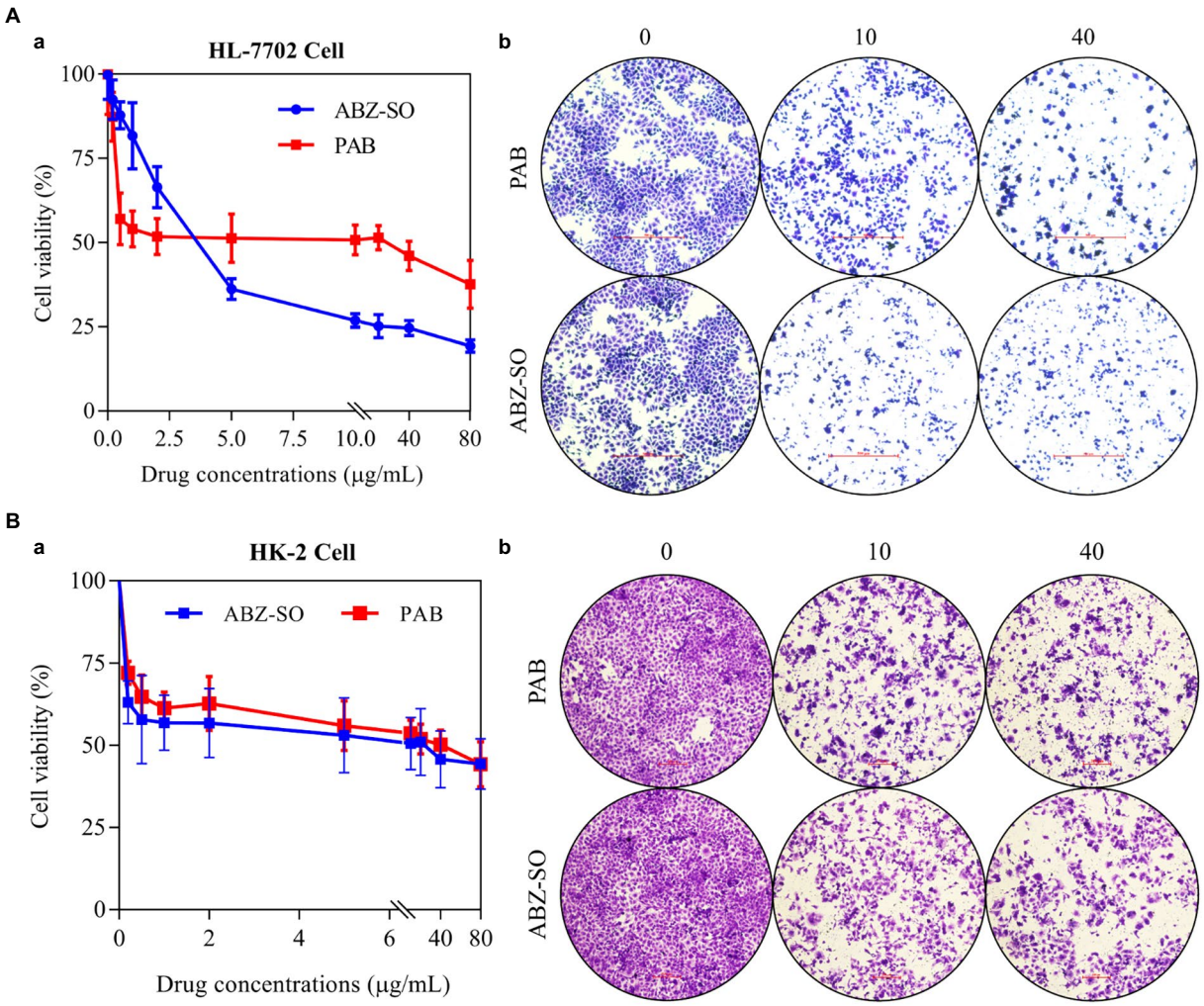

FIGURE 7
Cytotoxicity of PAB on human hepatocytes and renal cells *in vitro*. The cell livability **(a)** and number **(b)** of HL-7702 cell **(A)** and HK-2 cell **(B)** after treatment with different concentrations of PAB and ABZ-SO (0–80 μg/ml) for 48 h by CCK-8 assay **(A)** and crystal violet staining **(B)**. The independent experiments were processed in triplicate.

extension of *E. multilocularis* metacestodes, but it is difficult to meet curative goal for AE, and its long-term use produces strong adverse reactions (Liu et al., 2020b). Hence, development of new and effective anti-echinococcal drugs is imperative.

In the present study, the survival rate of *E. multilocularis* PSC exhibited a time- and dose-dependent decrease *in vitro* after treatment with PAB. Observed by SEM and TEM, we found that PSC upon exposure to PAB exhibited ultrastructural destructions, such as disappearance of syncytial layer, PAS stained materials and microvillus, collapse of parenchymae cells, and presentation of cytoplasm vacuolization, condensed chromatin and apoptotic bodies, which is similar to the pro-apoptotic activity of PAB in HCC cells (Gao et al., 2022). It is documented that *E. multilocularis* PSC has a duality: developing into an adult worm with sexual reproduction pattern in the definitive host, and initiating new cycles of asexual multiplication in the intermediate host, including development into microcyst, mature microcyst (production of cellular protrusions and brood capsules) and multiple cysts (production of abundant new PSC and multiple cysts) (Wang et al., 2016; Li et al., 2018). In the *in vitro* experiment, we observed that PSC grew into microcyst and completed a new cycle of asexual multiplication under the support of HepG2 cells, but this asexual cycle of PSC was blocked by PAB, showing collapse of microcyst, shrinking of germinal layer from the laminated layer after treatment with PAB. In addition, we found that after treatment with PAB, ALP activity in the culture supernatants of PSC *in vitro* was elevated significantly, which indicated a serious damage to *E. mutilocularis* metacestodes by PAB (Xin et al., 2020; Gao et al., 2021). At the same time, in the *in vivo* experiment, we also observed that the growth of *E. multilocularis* metacestodes was inhibited by PAB with a dose-dependent manner, evidenced by significant lower cyst weight after treatment with PAB. In short, PAB exhibits a strong parasiticidal effect on *E. multilocularis* larvae both *in vitro* and *in vivo*.

Previous study demonstrated that PAB exerts antitumor effects by activated apoptosis, autophagy and cell cycle arrest in certain types of cancer cells (Yu et al., 2008, 2016, Liu et al., 2020a). It was recognized that TGF-β1 signaling could trigger a variety of cellular responses, including inhibition of cell growth, migration, differentiation and apoptosis (Sanchez-Capelo, 2005). Later research exhibited that overexpressed TGF-β1 causes epithelial-mesenchymal transition (EMT), extracellular matrix (ECM) deposition and cancer-associated fibroblast (CAF) formation, which lead to fibrotic disease, and cancer (Peng et al., 2022). Thus, use of TGF-β1 chemical inhibitors as appears to be a new line of defenses against fibrotic disorders or cancer (Caja et al., 2018). Genome study indicated that *E. multilocularis* possesses TGF-β1, MAPK and Akt signaling pathways (Tsai et al., 2013; Zheng et al., 2013), beyond that, strong evidence suggest that during echinococccosis, the impaired host immune response is paralleled by an increased expression of TGF-β1 signaling components in periparasitic host cells and tissues (Nono et al., 2020). A later study on AE transplant treatment showed that through modulating the activity level of the TGF-β/Smad7 signaling pathway, liver fibrosis induced by *E. multilocularis* infection can be alleviated (Yang et al., 2022). In the present study, we observed apoptotic bodies in *E. multilocularis* PSC after treatment with PAB *in vitro*, referring apoptosis might be triggered. It was also demonstrated in our *in vitro* test that the TGF-β1 expression in the PSC was significantly reduced after treatment with PAB. On the other hand, we noted that the infection of *E. multilocularis* could induce over-expression of TGF-β1 protein and/or mRNA in the serum and liver of the mice, which was similar to the previous descriptions (Dissous et al., 2006; Brehm and Koziol, 2017). However, the over-expression of TGF-β1 in infected mice was significantly decreased after treatment with PAB, and meanwhile, the growth and proliferation of cysts was significantly inhibited *in vivo*. We thus deemed that the anti-parasite effect of PAB on *E. multilocularis* metacestodes was associated with the down-regulation of TGF-β1 signaling. Nevertheless, future study needs to elucidate the mechanism on how PAB regulate TGF-β1

TABLE 3 Changes of biochemical indexes in the serum of *E. multilocularis*-infected mice after treatment with PAB for 6 weeks (n=5).

Test indexes	Control group (mean ± SD)	PAB group (mean ± SD)	ABZ group (mean ± SD)
TBIL (μM/L)	1.58 ± 0.10	1.71 ± 0.09	1.51 ± 0.22
DBIL (μM/L)	0.64 ± 0.05	0.51 ± 0.05*	0.51 ± 0.03*
IBIL (μM/L)	0.59 ± 0.05	0.62 ± 0.06	0.70 ± 0.01*,#
TP (g/L)	68.99 ± 2.18	77.18 ± 2.50*	76.35 ± 3.31*
ALT (U/L)	41.10 ± 1.08	42.53 ± 1.01	45.75 ± 0.15*,#
AST (U/L)	157.85 ± 8.22	176.70 ± 8.34*	170.82 ± 4.47*
ALP (U/L)	222.26 ± 9.06	219.78 ± 5.38	272.44 ± 24.89*,#
γ-GGT (U/L)	26.88 ± 2.06	26.59 ± 0.82	27.35 ± 0.60
CRE (μM/L)	12.93 ± 0.59	15.27 ± 1.21*	15.01 ± 0.15*
BUN (mM/L)	9.99 ± 0.18	10.52 ± 0.27*	11.48 ± 0.38*,#

PAB, pseudolaric acid B; TBIL, total bilirubin; DBIL, direct bilirubin; IBIL, indirect bilirubin; TP, total protein; ALT, alanine aminotransferase; AST, aspartate aminotransferase; ALP, alkaline phosphatase; γ-GGT, γ-gamma-glutamyl transpeptidase; CRE, creatinine; BUN, blood urea nitrogen. The data were assessed using one-way ANOVA with multiple comparisons.
*$p < 0.05$ (compared to the control group), and #$p < 0.05$ (compared to the PAB group).

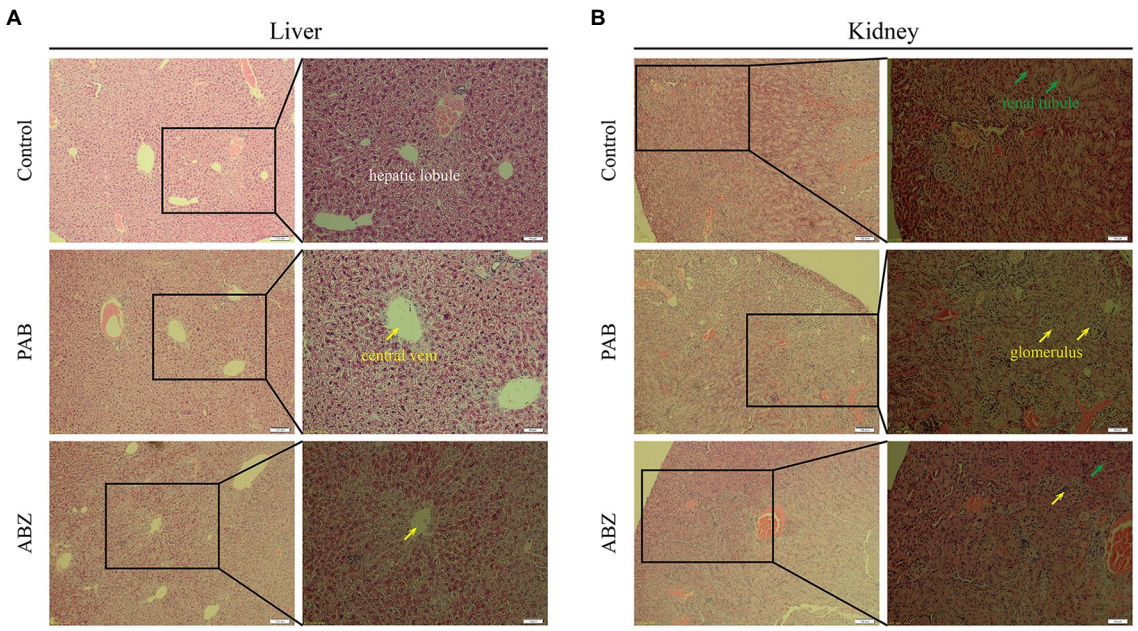

FIGURE 8
Hepatotoxicity and nephrotoxicity of PAB in mice. **(A)** Liver and **(B)** kidney histopathological images from Kunming mice treated with 40 mg/kg PAB and 100 mg/kg ABZ for 6 weeks (100×and 200× magnification), as detected by HE staining assay.

signaling pathway to exert suppressive effect on the growth and proliferation of *E. multilocularis*. Current studies suggest that PAB is a promising immunosuppressive and anti-inflammatory agent candidate. It was evidenced that the derivative of PAB can promotes the production of Tregs and this inductive effect on Tregs production might be TGF-β1 dependent (Li et al., 2014). Some experiments demonstrated that TGF-β1 is secreted into the granuloma area around *E. multilocularis*, and the signaling may contribute to parasitic evasion of the host's immunity (Zhang et al., 2008; Anthony et al., 2010). It was indicated that Treg/Th17 imbalance was observed at the middle and even late stage of *E. multilocularis* infection and it may be regulated by the TGF-β/Smad signaling pathway. TGF-β1 alone supports Treg cell expansion, TGF-β1 together with IL-6 promotes Th17 expansion (Gottstein et al., 2017; Wang et al., 2018). We expect future study on the action mechanism of PAB may include specific target effectors in TGF-β1 signaling possibly regulated by PAB, and other cytokine signaling pathway contributing to PAB's suppressive effect on the growth and development of *Echinococcus* parasite.

PAB possesses potent cytotoxic effects to target cells; however, its cytotoxicity to the host is a research concern for future clinical application. To this end, a PAB derivative, hexahydropseudolaric acid B (HPAB) was synthesized and was demonstrated to be able to substantially reduce the cytotoxicity, while its inhibitory efficacy on T cell proliferation remains high (Li et al., 2014). Another experimental study indicated that PAB displays potent anti-chronic myeloid leukaemia (CML) cells activity and inhibits the growth of the tumors, but without being toxic to mice, suggesting PAB could be used as a potential treatment for CML patients (Liu et al., 2017; Choi et al., 2019; Jiang et al., 2020). In the present study, *in vitro* PAB showed inhibitory effect in human normal liver and kidney cells with IC_{50} = 25.29 and 42.94 μg/ml, which was in agree with the previous findings of the cytostatic effect of PAB on mouse liver and renal cells (Mei, 2011). Interestingly, the cytotoxicity of PAB to the two cells exhibited a weak effect superior to ABZ with IC_{50} = 3.71 and 21.22 μg/ml. Furthermore, we assessed the sub-acute hepatotoxicity and nephrotoxicity of PAB in the healthy mice, and found significant increase of serum IBIL, ALT, ALP and BUN level in mice treated with ABZ compared to PAB, which further indicates that PAB exerts a weaker hepatotoxicity and nephrotoxicity than ABZ. However, further studies are needed to elucidate whether chronic and genetic toxicity of PAB is also weaker than ABZ.

In conclusion, PAB exhibited evident suppressive effect on *E. multilocularis* metacestodes in our *in vitro* and *in vivo* tests. Meanwhile, we found that PAB reduces the expression of TGF-β1 protein and mRNA in *E. multilocularis* metacestodes *in vitro* and in infected mice, indicative of the anti-echinococcal effect may involve the reduction of the expression of TGF-β1. In addition, PAB exhibits lower cytotoxicity than ABZ-SO in the normal liver and kidney cell lines *in vitro*, and presents no sub-acute hepatic and renal toxicity in the healthy mice. Our study suggests the potential of PAB to be developed as a therapeutic agent. However, the chronic toxicity of PAB needs clarified. Moreover, future study is expected to further elucidate the mechanism of PAB exerting suppressive effect on the growth and proliferation of *E. multilocularis* metacestodes to gain insight into the passway of TGF-β1 signaling involved.

Data availability statement

The original contributions presented in the study are included in the article/supplementary material, further inquiries can be directed to the corresponding authors.

Ethics statement

The animal study was reviewed and approved by The Experimental Animal Ethics Committee of School of Basic Medical Sciences, Lanzhou University, and the Ethics Committee of the National Institute of Parasitic Diseases, Chinese Center for Disease Control and Prevention (Chinese Center for Tropical Diseases Research).

Author contributions

TZ, HG, TJ, and WH designed the study. HG, XMo, BJ, YL, and BX carried out the experiments. HG, LH, and XMo analyzed data. TZ, WH, XMa, and JL provided experimental material. HG, TZ, and LH wrote the manuscript. HG, TZ, and ZF revised the manuscript. All authors contributed to the article and approved the submitted version.

Funding

This work was supported by the National Key Research and Development Program of China (grant no. 2021YFC2300800 and 2021YFC2300802), NHC Key Laboratory of Parasite and Vector Biology (National Institute of Parasitic Diseases, Chinese Center for Diseases Control and Prevention; grant no. NHCKFKT2022-02), the Non-profit Central Research Institute Fund of Chinese Academy of Medical Sciences (grant no. 2019PT320004), NHC Key Laboratory of Echinococcosis Prevention and Control (grant no. 2021WZK1003) and the foundation of Shanghai Municipal Health Commission (grant no. 201940302). The funders had no role in the study design, data collection, data analysis, data interpretation, or the writing of this report.

Conflict of interest

The authors declare that the research was conducted in the absence of any commercial or financial relationships that could be construed as a potential conflict of interest.

Publisher's note

References

Antarianto, R. D., Pragiwaksana, A., Septiana, W. L., Mazfufah, N. F., and Mahmood, A. (2022). Hepatocyte differentiation from iPSCs or MSCs in decellularized liver scaffold: cell-ECM adhesion, spatial distribution, and hepatocyte maturation profile. *Organogenesis* 18:2061263. doi: 10.1080/15476278.2022.2061263

Anthony, B., Allen, J. T., Li, Y. S., and McManus, D. P. (2010). Hepatic stellate cells and parasite-induced liver fibrosis. *Parasit Vectors* 3:60. doi: 10.1186/1756-3305-3-60

Brehm, K., and Koziol, U. (2017). *Echinococcus*-host interactions at cellular and molecular levels. *Adv. Parasitol.* 95, 147–212. doi: 10.1016/bs.apar.2016.09.001

Caja, L., Dituri, F., Mancarella, S., Caballero-Diaz, D., Moustakas, A., Giannelli, G., et al. (2018). TGF-β and the tissue microenvironment: relevance in fibrosis and cancer. *Int. J. Mol. Sci.* 19:E1294. doi: 10.3390/ijms19051294

Chen, Z., Lin, Z., Yu, J., Zhong, H., Zhuo, X., Jia, C., et al. (2022). Mitofusin-2 restrains hepatic stellate cells' proliferation via PI3K/Akt signaling pathway and inhibits liver fibrosis in rats. *J. Healthc. Eng.* 2022:6731335. doi: 10.1155/2022/6731335

Cheng, Z., Xu, Z., Tian, H., Liu, F., Li, X., Luo, D., et al. (2020). *In vitro* and *in vivo* efficacies of the EGFR/MEK/ERKh signaling inhibitors in the treatment of alveolar echinococcosis. *Antimicrob. Agents Chemother.* 64:e00341–20. doi: 10.1128/AAC.00341-20

Choi, S.-J., Ahn, C.-H., Yang, I.-H., Jin, B., Lee, W. W., Kim, J.-H., et al. (2019). Pseudolaric acid B induces growth inhibition and caspase-dependent apoptosis on head and neck cancer cell lines through death receptor 5. *Molecules* 24, 24:3715. doi: 10.3390/molecules24203715

Deplazes, P., Rinaldi, L., Alvarez Rojas, C. A., Torgerson, P. R., Harandi, M. F., Romig, T., et al. (2017). Global distribution of alveolar and cystic echinococcosis. *Adv. Parasitol.* 95, 315–493. doi: 10.1016/bs.apar.2016.11.001

Dissous, C., Khayath, N., Vicogne, J., and Capron, M. (2006). Growth factor receptors in helminth parasites: signalling and host-parasite relationships. *FEBS Lett.* 580, 2968–2975. doi: 10.1016/j.febslet.2006.03.046

Gao, H., Sun, X., Luo, Y., Pang, H., Ma, X., Zhang, T., et al. (2021). Anti-echinococcal effect of verapamil involving the regulation of the calcium/calmodulin-dependent protein kinase II response *in vitro* and in a murine infection model. *Parasit Vectors* 14:108:108. doi: 10.1186/s13071-021-04618-4

Gao, H., Zhang, Y., Mo, X., Huo, L., Luo, Y., Zhang, T., et al. (2022). Antitumor effect of pseudolaric acid B involving regulation of notch1/Akt signaling response in human hepatoma cell *in vitro*. *Evid. Based Complement. Altern. Med.* 2022:5353686, –5353611. doi: 10.1155/2022/5353686

Gottstein, B., Soboslay, P., Ortona, E., Wang, J., Siracusano, A., and Vuitton, D. A. (2017). Immunology of alveolar and cystic echinococcosis (AE and CE). *Adv. Parasitol.* 96, 1–54. doi: 10.1016/bs.apar

Hemphill, A., and Muller, J. (2009). Alveolar and cystic echinococcosis: towards novel chemotherapeutical treatment options. *J. Helminthol.* 83, 99–111. doi: 10.1017/S0022149X0928936X

Hemphill, A., Stadelmann, B., Rufener, R., Spiliotis, M., Boubaker, G., Muller, J., et al. (2014). Treatment of echinococcosis: albendazole and mebendazole--what else? *Parasite* 21:70. doi: 10.1051/parasite/2014073

Horton, J. (2000). Albendazole: a review of anthelmintic efficacy and safety in humans. *Parasitology* 121, S113–S132. doi: 10.1017/s0031182000007290

Jansen, S. R., Poppinga, W. J., Jager, W., Lezoualc'h, F., Cheng, X., Wieland, T., et al. (2016). Epac1 links prostaglandin E2 to β-catenin-dependent transcription during epithelial-to-mesenchymal transition. *Oncotarget* 7, 46354–46370. doi: 10.18632/oncotarget.10128

Ji, J. (2013). Study on active constituents from Pseudolarix kaempferi against Dactylogyrus infecting fish. *North West agriculture and forestry university*. (In Chinese).

Jiang, L., Wen, C., He, Q., Sun, Y., Wang, J., Lan, X., et al. (2020). Pseudolaric acid B induces mitotic arrest and apoptosis in both imatinib-sensitive and -resistant chronic myeloid leukaemia cells. *Eur. J. Pharmacol.* 876:173064. doi: 10.1016/j.ejphar.2020.173064

Kern, P., Menezes da Silva, A., Akhan, O., Mullhaupt, B., Vizcaychipi, K. A., Budke, C., et al. (2017). The echinococcoses: diagnosis, clinical management and burden of disease. *Adv. Parasitol.* 96, 259–369. doi: 10.1016/bs.apar.2016.09.006

Li, L., Chen, B., Yan, H., Zhao, Y., Lou, Z., Li, J., et al. (2018). Three-dimensional hepatocyte culture system for the study of *Echinococcus multilocularis* larval development. *PLoS Negl. Trop. Dis.* 12:e0006309. doi: 10.1371/journal.pntd.0006309

Li, T., Chen, H., Yang, Z., Wang, W., Wang, Y. T., Zhang, L. M., et al. (2014). A novel pseudolaric acid B derivative, Hexahydropseudolaric acid B, exterts an immunomodulatory effect *in vitro*/*in vivo* evaluation. *Eur. J. Pharmacol.* 745, 10–18. doi: 10.1016/j.ejphar.2014.10.009

Liu, F., Sun, C., Chen, Y., Du, F., Yang, Y., and Wu, G. (2021). Indole-3-propionic acid-aggravated CCl4-induced liver fibrosis via the TGF-beta1/Smads signaling pathway. *J. Clin. Transl. Hepatol.* 9, 917–930. doi: 10.14218/JCTH.2021.00032

Liu, M. L., Sun, D., Li, T., and Chen, H. (2017). A systematic review of the immune-regulating and anticancer activities of pseudolaric acid B. *Front. Pharmacol.* 8:394. doi: 10.3389/fphar.2017.00394

Liu, C., Wang, F., Wang, B., Wu, T., Wang, Y., Huo, W., et al. (2020a). Pseudolaric acid B induces apoptosis in human rhabdomyosarcoma RD cells. *Oncol. Lett.* 20:1. doi: 10.3892/ol.2020.12222

Liu, C., Yin, J., Hu, W., and Zhang, H. (2020b). Glycogen phosphorylase: a drug target of amino alcohols in *Echinococcus granulosus*, predicted by a computer-aided method. *Front. Microbiol.* 11:557039. doi: 10.3389/fmicb.2020.557039

Mei, X. (2011). Research on treatment effect of pseudolaric acid B on the murine allergic contact dermatitis and its mechanism. *Hebei Medical University*. In Chinese

Nono, J. K., Lutz, M. B., and Brehm, K. (2020). Expansion of host regulatory T cells by secreted products of the tapeworm *Echinococcus multilocularis*. *Front. Immunol.* 11:798. doi: 10.3389/fimmu.2020.00798

Peng, D., Fu, M., Wang, M., Wei, Y., and Wei, X. (2022). Targeting TGF-β signal transduction for fibrosis and cancer therapy. *Mol. Cancer* 21:104. doi: 10.1186/s12943-022-01569-x

Sanchez-Capelo, A. (2005). Dual role for TGF-beta1 in apoptosis. *Cytokine Growth Factor Rev.* 16, 15–34. doi: 10.1016/j.cytogfr.2004.11.002

Stamatakos, M., Sargedi, C., Stefanaki, C., Safioleas, C., Matthaiopoulou, I., and Safioleas, M. (2009). Anthelminthic treatment: an adjuvant therapeutic strategy against *Echinococcus granulosus*. *Parasitol. Int.* 58, 115–120. doi: 10.1016/j.parint.2009.01.002

Tsai, I. J., Zarowiecki, M., Holroyd, N., Garciarrubio, A., Sanchez-Flores, A., Brooks, K. L., et al. (2013). The genomes of four tapeworm species reveal adaptations to parasitism. *Nature* 496, 57–63. doi: 10.1038/nature12031

Wang, J., Cardoso, R., Marreros, N., Müller, N., Lundström-Stadelmannet, B., Siffert, M., et al. (2018). Foxp3+ T regulatory cells as a potential target for immunotherapy against primary infection with *Echinococcus multilocularis* eggs. *Infect. Immun.* 86, e00542–e00518. doi: 10.1128/iai.00542-18

Wang, H., Li, J., Guo, B., Zhao, L., Zhang, Z., McManus, D. P., et al. (2016). *In vitro* culture of *Echinococcus multilocularis* producing protoscoleces and mouse infection with the cultured vesicles. *Parasit Vectors* 9:411. doi: 10.1186/s13071-016-1687-y

Wang, Y., Shen, R. W., Han, B., Li, Z., Xiong, L., Zhang, F. Y., et al. (2017). Notch signaling mediated by TGF-beta/Smad pathway in concanavalin A-induced liver fibrosis in rats. *World J. Gastroenterol.* 23, 2330–2336. doi: 10.3748/wjg.v23.i13.2330

Wang, D., Xin, Y., Tian, Y., Li, W., Sun, D., and Yang, Y. (2017). Pseudolaric acid B inhibits gastric cancer cell metastasis *in vitro* and in haematogenous dissemination model through PI3K/AKT, ERK1/2 and mitochondria-mediated apoptosis pathways. *Exp. Cell Res.* 352, 34–44. doi: 10.1016/j.yexcr.2017.01.012

Wang, X. J., Xue, Y. Q., Zhang, H. L., Yu, Y., and Liu, P. (2022). PINK1 deficiency aggravates the β-amyloid-attenuated Mitophagy-lysosomal degradation in PC12 cells. *J. Explor. Res. Pharmacol.* 7, 30–36. doi: 10.14218/jerp.2021.00053

Wang, H., Zhang, C. S., Fang, B. B., Hou, J., Li, W. D., Li, Z. D., et al. (2020). Dual role of hepatic macrophages in the establishment of the *Echinococcus multilocularis* metacestode in mice. *Front. Immunol.* 11:600635. doi: 10.3389/fimmu.2020.600635

Xiao, Y., Wang, Y. J., Xie, J. G., and Wang, X. C. (2022). Transcriptomic identification of key genes in human peripheral blood mononuclear cells for the prognosis of sepsis. *J. Explor. Res Pharmacol.* doi: 10.14218/JERP.2022.00023

Xin, Q., Yuan, M., Li, H., Song, X., Lu, J., and Jing, T. (2020). *In vitro* effects of lonidamine and 6-aminonicotinamide against *Echinococcus granulosussensu*

stricto and *Echinococcus multilocularis*. *Vet. Res.* 51:29. doi: 10.1186/s13567-020-00744-6

Yang, N., Ma, W., Ke, Y., Liu, H., Chu, J., Sun, L., et al. (2022). Transplantation of adipose-derived stem cells ameliorates *Echinococcus multilocularis*-induced liver fibrosis in mice. *PLoS Negl. Trop. Dis.* 16:e0010175. doi: 10.1371/journal.pntd.0010175

Yao, G., Qi, M., Ji, X., Fan, S., Xu, L., Hayashi, T., et al. (2014). ATM-p53 pathway causes G2/M arrest, but represses apoptosis in pseudolaric acid B-treated HeLa cells. *Arch. Biochem. Biophys.* 558, 51–60. doi: 10.1016/j.abb.2014.05.029

Yu, J., Chen, C., Xu, T., Yan, M., Xue, B., Wang, Y., et al. (2016). Pseudolaric acid B activates autophagy in MCF-7 human breast cancer cells to prevent cell death. *Oncol. Lett.* 11, 1731–1737. doi: 10.3892/ol.2016.4103

Yu, J. H., Wang, H. J., Li, X. R., Tashiro, S. I., Onodera, S., and Ikejima, T. (2008). Protein tyrosine kinase, JNK, and ERK involvement in pseudolaric acid B-induced apoptosis of human breast cancer MCF-7 cells. *Acta Pharmacol. Sin.* 29, 1069–1076. doi: 10.1111/j.1745-7254.2008.00835.x

Zhang, S., Hüe, S., Sène, D., Penfornis, A., Bresson-Hadni, S., Kantelip, B., et al. (2008). Expression of major histocompatibility complex class I chain-related molecule a, NKG2D, and transforming growth factor-beta in the liver of humans with alveolar echinococcosis: new actors in the tolerance to parasites? *J. Infect. Dis.* 197, 1341–1349. doi: 10.1086/586709

Zhang, J., Yan, L. T., Yuan, E. L., Ding, H. X., Ye, H. C., Zhang, Z. K., et al. (2014). Antifungal activity of compounds extracted from cortex pseudolaricis against *Colletotrichum gloeosporioides*. *J. Agric. Food Chem.* 62, 4905–4910. doi: 10.1021/jf500968b

Zheng, H., Zhang, W., Zhang, L., Zhang, Z., Li, J., Lu, G., et al. (2013). The genome of the hydatid tapeworm *Echinococcus granulosus*. *Nat. Genet.* 45, 1168–1175. doi: 10.1038/ng.2757

frontiers | Frontiers in Microbiology

TYPE Original Research
PUBLISHED 25 November 2022
DOI 10.3389/fmicb.2022.1039665

OPEN ACCESS

EDITED BY
Hongliang Chai,
Northeast Forestry University, China

REVIEWED BY
Ryan Oliver Marino Rego,
Academy of Sciences of the Czech Republic (ASCR), Czechia
Paulo Eduardo Velho,
State University of Campinas, Brazil
Jana Radzijevskaja,
Vytautas Magnus University, Lithuania

*CORRESPONDENCE
Wen-Ping Guo
guowenping@nwsuaf.edu.cn

†These authors have contributed equally to this work

SPECIALTY SECTION
This article was submitted to Infectious Agents and Disease, a section of the journal Frontiers in Microbiology

RECEIVED 08 September 2022
ACCEPTED 07 November 2022
PUBLISHED 25 November 2022

CITATION
Jian R, Ren Q, Xue J, Xie G-C, Wang J, Chen G-Q, Du L and Guo W-P (2022) Genetic diversity of *Bartonella* infection in residential and field rodents in Hebei, China. *Front. Microbiol.* 13:1039665. doi: 10.3389/fmicb.2022.1039665

Genetic diversity of *Bartonella* infection in residential and field rodents in Hebei, China

Rui Jian[1†], Qing Ren[1†], Jing Xue[1], Guang-Cheng Xie[1], Jiangli Wang[2], Guo-Qing Chen[3], Luanying Du[1] and Wen-Ping Guo[1*]

[1]Department of Pathogenic Biology, College of Basic Medicine, Chengde Medical University, Chengde, Hebei, China, [2]Laboratory of Microbiology Detection, Chengde Center for Disease Control and Prevention, Chengde, China, [3]Yancheng Center for Disease Control and Prevention, Yancheng, China

Rodents are the primary natural reservoirs of *Bartonella* spp., and some of which are zoonotic causative agents. Hence, surveillance of *Bartonella* sp. infection in rodents is very important for the prevention of human bartonellosis caused by them. In this study, rodents were captured, and their spleen samples were collected for *Bartonella* sp. DNA detection and identification by amplifying the 16S rRNA, *gltA*, and *ftsz* genes using semi-nested polymerase chain reaction (PCR). The results indicated that *Bartonella* sp. DNA was detected in seven *Rattus norvegicus* individuals with a detection rate of 6.7% in Chengde City and bacterial DNA in 31 *Apodemus agrarius* individuals with a detection rate of 28.4% in Handan City. The DNA detection rate across the genders and ages of rodents was not found to be statistically significant. Furthermore, sequence analysis of the above-mentioned three genes demonstrated that at least eight *Bartonella* species were circulating in Hebei Province, of which three, including *Bartonella rattimassiliensis*, *Bartonella grahamii*, and *Bartonella tribocorum*, are human pathogens, thus suggesting the existence of a major public health risk. Overall, these results revealed the detection rate and genetic diversity of *Bartonella* species infection in rodents in Hebei Province, which could be potentially helpful for the prevention of bartonellosis caused by rodent-associated *Bartonella* species. This study highlights the urgent need for the surveillance of *Bartonella* infections in rodents and ectoparasites that affect both rodents and humans and can cause fever of unknown origin or endocarditis.

KEYWORDS

***Bartonella*, epidemiology, genetic diversity, human-pathogenic, rodents**

Introduction

Bartonella spp. belong to the genus *Bartonella* within the family Bartonellaceae and are Gram-negative facultative intracellular alphaproteobacteria (Okaro et al., 2017). Before the reclassification of *Bartonella* in 1993, only one species, *B. bacilliformis*, was recorded. After that, the number of *Bartonella* spp. has continued to increase rapidly over the past 30 years, with currently more than 50 validated species and more than 10 candidate species (Okaro et al., 2017; Krügel et al., 2022). In addition, some complete genome sequences representing potential novel species are likely to further expand the number of species in the genus *Bartonella* (Lin et al., 2008; Sato et al., 2012). *Bartonella* spp. can infect a wide range of different domestic and wild animals, including cats, dogs, rodents, cattle, sheep, and bats (Okaro et al., 2017). Moreover, an increasing variety of animals have been confirmed as hosts of *Bartonella* spp., such as the beluga whale (Maggi et al., 2008), kangaroo (Fournier et al., 2007), camel (Rasis et al., 2014), and wild carnivores (Marciano et al., 2016; López-Pérez et al., 2017). *Bartonella* spp. are zoonotic bacteria and can be transmitted from animals to humans indirectly by blood-sucking arthropods (Deng et al., 2012), as well as through direct contact through the scratch of an infected cat or with the infected feces of a vector (Krügel et al., 2022). *Bartonella henselae* and *Bartonella quintana*, which mainly cause cat scratch disease (CSD) and trench fever in humans, respectively, have attracted more attention due to more patients being attributed as having the infections (Okaro et al., 2017). More seriously, at least another 18 species are considered to be human pathogens or have been identified in humans with the clinical symptom of fever (Maggi et al., 2009; Chomel and Kasten, 2010; Vayssier-Taussat et al., 2016; Okaro et al., 2017; Krügel et al., 2022).

Rodents are the natural reservoir of many human pathogens, including viruses, bacteria, and protozoans (Meerburg et al., 2009). There is no doubt that rodents play an important role in the maintenance and transmission of *Bartonella* spp., and at least 40 *Bartonella* species have been identified in a great diversity of rodents (Okaro et al., 2017; do Amaral et al., 2022; Krügel et al., 2022). Among them, eight have been proven to be pathogenic to humans and are hosted by rodents. These include *Bartonella doshiae* (Vayssier-Taussat et al., 2016), *Bartonella elizabethae* (Daly et al., 1993), *Bartonella grahamii* (Kerkhoff et al., 1999), *Bartonella rattimassiliensis* (Kosoy et al., 2010), *Bartonella rochalimae* (Eremeeva et al., 2007), *Bartonella tribocorum* (Kosoy et al., 2010), *Bartonella vinsonii* (Roux et al., 2000), and *Bartonella washoensis* (Kosoy et al., 2003). In addition, *B. henselae*, mainly hosted by cats, has also been detected in several rodent species, although their role in the maintenance and transmission of *B. henselae* remains unclear (Helan et al., 2018; Divari et al., 2020; Böge et al., 2021). In China, at least 22 species, including eight human pathogens, have been reported in rodents, with infection rates ranging from 6.4% to 57.7% to date (Saisongkorh et al., 2009; Li et al., 2015; Xia et al., 2015; Qin et al., 2019; Rao et al., 2021; Krügel et al., 2022; Yao et al., 2022). Therefore, we speculate that the Chinese population could be at risk of being affected by rodent-associated *Bartonella* spp., although human infections have not yet been identified.

Rodent-associated *Bartonella* spp. have been found to be widely distributed around the world, as well as in China, and a number of previous studies have mainly focused on the field environment (Okaro et al., 2017; Krügel et al., 2022). Hebei Province has a complex and varied terrain consisting of plateaus, mountains, and plains, which are beneficial to rodent colonization and survival. Moreover, closer contact between humans and rodents in residential areas, as well as diverse human activities that continue to invade the wild habitat of rodents, can significantly increase the transmission risk of *Bartonella* spp. from rodents to humans. Bartonellosis, which is caused by the rodent-associated *Bartonella* spp., is a natural focal disease, and thus investigations of the epidemiology and genetic diversity of *Bartonella* spp. infection in rodents can be of great significance for the prevention of human bartonellosis. Therefore, in this study, rodent samples were collected from Hebei Province to analyze the *Bartonella* sp. infection in the rodent populations, especially those pathogenic to humans. The results of this study will not only benefit the prevention and control of human bartonellosis in the local population but will also be helpful for the accurate diagnosis of diseases with fever of unknown origin (FUO).

Materials and methods

Rodent sample collection and deoxyribonucleic acid extraction

During 2020, rodents were captured using live capture traps baited with peanuts in residential areas of Chengde City and field areas of Handan City in Hebei Province, and two sampling sites were established in each city (**Figure 1**). The species, age, and sex of all the captured rodents were identified and recorded (Chen, 1987; Wang, 2003). All the captured rodents were euthanized, and the spleen specimens were aseptically collected.

Total DNA was extracted from the spleen samples using a DNA extraction kit (OMEGA, Doraville, CA, USA) in a fume hood in a separate room. The extracted DNA was eluted with 50 μl of double-distilled water and stored at−20°C before analysis. In addition, the identification of the rodent species was further confirmed by sequence analysis of the mt-*cyt* b gene obtained by PCR using the extracted DNA as the template (Guo et al., 2013).

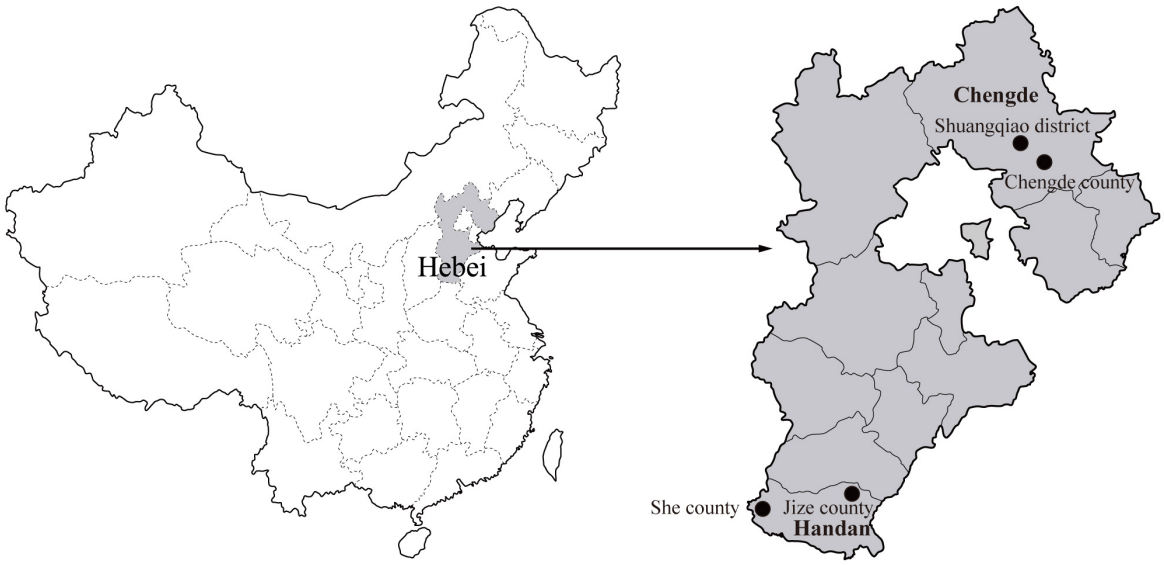

FIGURE 1
Geographical distribution of the rodent sampling sites (black dots) in Hebei Province, China. The map of China was obtained freely from http://english.freemap.jp/item/asia/china.html. The map of Hebei Province was generated using ArcGIS.

Detection and molecular characterization of *Bartonella* spp.

The presence of *Bartonella* spp. in rodents was detected by amplifying part of the 16S rRNA gene using a semi-nested polymerase chain reaction (PCR) and subsequently confirmed by further sequencing. The primer pairs Bar-SF1/Bar-SR and Bar-SF2/Bar-SR designed in this study were used for the first and second rounds of PCR to amplify an 813-bp 16S rRNA gene fragment.

In addition, the nearly complete 16S rRNA, the partial citrate synthase gene (*gltA*), and the cell division protein gene (*ftsZ*) were obtained from the *Bartonella* sp. DNA-detected samples to better determine and characterize the *Bartonella* species. Briefly, the primer pairs Bar-SF/Bar-SR1 and Bar-SF/Bar-SR2 were used to obtain the rest of the 16S rRNA with a length of 712 bp. The partial *gltA* gene (1,036 bp) was amplified with the primer pairs Bar-gltA-F/Bar-gltA-R1 and Bar-gltA-F/Bar-gltA-R2 for the primary and secondary rounds of the semi-nested PCR, respectively. The partial *ftsz* gene (860 bp) was amplified with the primer pairs Bar-ftsz-F1/Bar-ftsz-R and Bar-ftsz-F2/Bar-ftsz-R for the primary and secondary rounds of the semi-nested PCR, respectively. Alternatively, Bar-gltA-FM and Bar-ftsz-RM, instead of Bar-gltA-F and Bar-ftsz-R, were employed to amplify the shorter *gltA* (476 bp) and *ftsz* (575 bp) genes, respectively. All the primer sequences used in the present study are shown in Table 1.

The PCR reaction for the first round of the nested PCR was performed in a 20 μl reaction volume, containing 10 μl *Premix Taq* (Takara, Dalian, China), 1.5 μl extracted DNA, 0.8 μl of each primer (10 pmol), and 6.9 μl water. For the second round, the PCR mixture contained 25 μl *Premix Taq* (Takara, Dalian, China), 3 μl of the first-round PCR products, 2 μl of each primer (10 pmol), and 18 μl water for a final volume of 50 μl. The same thermal cycling condition was used for both rounds, including a denaturation at 94°C for 5 min, 30 cycles of denaturation at 94°C for 40 s, annealing at 56°C for 40 s, and elongation at 72°C for 1 min, followed by a final extension at 72°C for 7 min. In addition, to prevent contamination, the PCR mixture preparation, template addition, and agarose gel electrophoresis were performed in a fume hood in three separate rooms, and

TABLE 1 Primers used in this study.

Gene	Primers	Sequences (5′ → 3′)	Tm
16S rRNA	Bar-SF1	GGAAGAGGTGAGTGGAATTC	52°C
	Bar-SF2	GGAATTCCSAGTGTAGAGGT	
	Bar-SR	TCGCTGACCCTACCGTGGT	
	Bar-SF	CYGGCTCAGAACGAACGCTG	52°C
	Bar-SR1	CGTGGACTACCAGGGTATCT	
	Bar-SR2	GGTATCTAATCCTGTTTGCTC	
gltA	Bar-gltA-FM	GCHGATCAYGARCAAAATGC	54°C
	Bar-gltA-F	TTACYTAYGAYCCYGGBTTTA	
	Bar-gltA-R1	CYTCRATCATTTCTTTCCAYTG	
	Bar-gltA-R2	GCAAAVAGAACMGTRAACAT	
Ftsz	Bar-ftsz-F1	ATGACGATTAATCTGCATCG	50°C
	Bar-ftsz-F2	ATTAATCTGCATCGGCCAGA	
	Bar-ftsz-R	TCTTCRCGRATACGATTRGC	
	Bar-ftsz-RM	TAAAGHACTTGRTCAGCCAT	

filter tips were also used in each assay. Furthermore, ddH_2O was used as a negative control.

The PCR product was electrophoresed on a 1.0% agarose gel, and the amplicon of the expected size was purified using the Takara MiniBEST Agarose Gel DNA Extraction Kit Version 4.0 (Takara, Dalian, China). The purified PCR product was subjected to bidirectional sequencing with the PCR primers. Alternatively, the purified PCR product was ligated into the pGEM-T vector for sequencing when it produced complex sequence chromatograms in direct sequencing. The PCR products were sequenced using the ABI-PRISM Dye Termination Sequencing Kit and the ABI 3730 genetic analyzer. All the newly generated sequences in this study were submitted to GenBank under the accession numbers OP363479-OP363516 for the *rrs* gene, OP382327-OP382454 for the *gltA* gene, and OP382391-OP382426 for the *ftsZ* gene.

Sequence analysis

The nearly complete 16S rRNA gene was assembled by partially overlapping oligonucleotides using BioEdit version 7.1.11 (Hall, 1999). The nucleotide identities of the 16S rRNA, *gltA*, and *ftsZ* genes were calculated using the MegAlign program within the DNASTAR Lasergene software (Burland, 2000). Phylogenetic trees based on the 16S rRNA, *gltA*, and *ftsZ* gene sequences were reconstructed using the maximum-likelihood (ML) method within PhyML version 3.2, and the reliability of branches in the tree was evaluated by calculating the bootstrap values with 1,000 replicates (Guindon et al., 2010). The general time-reversible (GTR) substitution model with a gamma (Γ) model of rate heterogeneity and a proportion of invariable sites (GTR + Γ + I) determined by MEGA 7.0 was found to be the best fit model for the phylogenetic analysis (Kumar et al., 2016). The ML tree was rooted at its midpoint using MEGA 7.0.

Statistical analyses

The *P*-value with the chi-square test was calculated using SPSS 21.0 software for the statistical analyses to determine the association between the detection rate and the gender and age of the rodents. A *P*-value of less than 0.05 was considered to be statistically significant.

Ethics statement

This study was approved by the ethics committee of the Chengde Medical University (No. 202004). All the rodent experiments were performed in strict accordance with the Guidance for Experimental Animal Welfare and Ethical Treatment by the Ministry of Science and Technology of China. In addition, the rodents were anesthetized with ether and dissected to collect spleen samples for the detection of *Bartonella* sp. DNA, and analgesics were administered to minimize the suffering of the captured rodents.

Results

Sample collection and detection of *Bartonella* sp. deoxyribonucleic acid in rodents

A total of 223 rodents were captured from four sampling sites in Chengde and Handan cities in Hebei Province, China (**Table 2**). The collected rodents were identified into five distinct species comprising *Rattus norvegicus*, *R. tanezumi*, *Mus musculus*, *Apodemus agrarius*, and *Cricetulus triton*. In Chengde City, the rodents were sampled in residential areas, and *R. norvegicus* was found to be the most abundant species, while *A. agrarius* was the predominant species in Handan, where it was captured in the field.

Based on the amplification of the 16S rRNA gene, PCR products of the expected sizes were detected in 38 spleen samples collected from the 223 rodents. After sequencing of the PCR products, all the obtained 16S rRNA gene sequences were blasted against the GenBank nucleotide database, and the results showed that all of them shared more than 99.4% nucleotide identity with the most closely related 16S rRNA gene sequence of a *Bartonella* species. Hence, the DNA detection rate was found to be 17.0%. Specifically, seven of the *Bartonella* sp. DNA-detected samples were identified as being from *R. norvegicus* in Chengde with a detection rate of 6.7% and 31 from *A. agrarius* in Handan with a detection rate of 28.4%. Furthermore, the infection rates in female and male rodents were observed to be 16.7% (95% CI: 4.3–29.1%) and 17.3% (95% CI: 6.0–27.4%), respectively, which were not statistically significant ($\chi^2 = 0.808$, $P = 0.567$). Similarly, no significant difference ($\chi^2 = 0.887$, $P = 0.538$) was noted in the infection rates between juvenile (12.4%, 95% CI: 5.5–26.8%) and adult rodents (20.6%, 95% CI: 6.5–30.1%).

Molecular characterization of the *Bartonella* species

To better identify and characterize the *Bartonella* species in the current study, 37 nearly complete 16S rRNA gene sequences (with a length of approximately 1,400 bp), 28 partial *gltA* gene sequences (16 with a length of approximately 1,000 bp and 12 others with a length of approximately 440 bp), and 36 partial *ftsZ* gene sequences (31 with a length of approximately 830 bp and 5 others with a length of approximately 550 bp)

TABLE 2 *Bartonella* sp. DNA detection in rodents collected in Hebei, China.

Parameters	Location				Total
	Chengde City		Handan City		
	Shuangqiao District	Chengde County	Jize County	She County	
Species					
R. norvegicus	4/48	3/43	0/2	0/1	7/94
R. tanezumi	0/2	0/3	–	–	0/5
M. musculus	0/1	0/5	0/3	0/1	0/10
A.agrarius	–	0/2	12/49	19/51	31/102
C. triton	–	–	–	0/2	0/2
Gender					
Female	1/11	2/38	4/20	8/21	15/90 (95% CI: 4.3-29.1)
Male	3/40	1/15	8/34	11/34	23/133 (95% CI: 6.0-27.4)
Age					
Juvenile	2/24	2/41	3/17	5/15	12/97 (95% CI: 5.5-26.8)
Adult	2/37	1/12	9/37	14/40	26/126 (95% CI: 6.5-30.1)

were obtained from all the samples with *Bartonella* sp.-DNA detection. The sequencing and BLAST analyses based on three gene sequences indicated that all the *Bartonella* strains identified in this study were classified into at least eight different *Bartonella* species, namely, *B. japonica*, *Bartonella* sp. 1-1C (a *B. rochalimae*-like species), *B. rattimassiliensis*, *B. grahamii*, *B. taylorii*, *B. tribocorum*, *B. mastomydis*, and *B. kosoyi*. In addition, a 770-bp 16S rRNA gene sequence of Shexian-Aa46 from *A. agrarius* in Handan shared the highest nucleotide identity with *B. vinsonii* (99.5%), while its *ftsZ* gene exhibited the highest nucleotide identity with that of *Bartonella* sp. 1-1C (99.6%), which might have been caused by coinfection with two different *Bartonella* species. Due to a failure to obtain the *gltA* and *ftsZ* gene sequences resembling those of *B. vinsonii* from Shexian-Aa46, *B. vinsonii* or *B. vinsonii*-like bacteria could have been circulating in *A. agrarius* in local areas.

Specifically, five distinct *Bartonella* species, including *B. japonica* (n = 1), *Bartonella* sp. 1-1C (*n* = 2), *B. rattimassiliensis* (*n* = 2), *B. grahamii* (*n* = 1) and *B. taylorii* (*n* = 1), were detected in *R. norvegicus* in Chengde City. In Handan City, *Bartonella* sp. 1-1C, *B. tribocorum*, *B. mastomydis*, and *B. kosoyi* were identified from 6, 10, 1, and 12 *A. agrarius*, respectively. For Jize-Aa8 belonging to *B. mastomydis* in *A. agrarius*, only an approximate 1,000-bp *gltA* gene sequence was obtained, which shared the highest nucleotide identity of 99.4% with that of the *B. mastomydis* strain 008 (KY555066), while its 1,400-bp 16S rRNA belonged to *B. tribocorum*, which also may have been potentially caused by co-infection with *B. mastomydis* and *B. tribocorum*. Of the eight *Bartonella* species, only one, *Bartonella* sp. 1-1C, was detected in both *R. norvegicus* in Chengde City and *A. agrarius* in Handan City.

The strain Chengde-Rn16 shared the highest nucleotide identities of 99.6% and 97.9% with the *B. japonica* strain Fuji 18-1 for the 16S rRNA and *gltA* genes, respectively. The strain Chengde-Rn85 shared the highest nucleotide identities of 100%, 99.6%, and 99.6% with the *B. grahamii* strain as4aup for the 16S rRNA, *gltA*, and *ftsz* genes, respectively. The strain Chengde-Rn40 showed the highest nucleotide identity of 100% with the *B. taylorii* strain IBS296 for the 16S rRNA, 100% with the *B. taylorii* strain Far East I for the *gltA*, and 98.9% with the *B. taylorii* strain M1 for the *ftsz* genes. The two *B. rattimassiliensis* strains, Shuangqiao-Rn48 and Chengde-Rn25, displayed the highest nucleotide identities of 99.9% and 99.9%, respectively, with the *B. rattimassiliensis* strain 15908 for the 16S rRNA and *ftsz* genes, and 99.1% and 98.9%, respectively, with the *B. rattimassiliensis* strain SD-10 for the *gltA* gene. The seven *Bartonella* sp. 1-1C strains identified here shared 99.8–100%, 98.9–100%, and 97.6–100% nucleotide identities with each other and the highest nucleotide identities of 99.9–100%, 99.3–100%, and 97.0–100% with the *Bartonella* sp. 1-1C for the 16S rRNA, *gltA*, and *ftsz* genes, respectively. The 10 *B. tribocorum* strains identified here shared 99.9–100%, 99.3–100%, and 99.5–100% nucleotide identities with each other and the highest nucleotide identities of 99.9%, 99.6–99.0%, and 99.6–100% with the known *B. tribocorum* strains for the 16S rRNA, *gltA*, and *ftsz* genes, respectively. The 13 *B. kosoyi* strains identified here shared 99.6–100%, 99.5–99.8%, and 99.8–100% nucleotide identities with each other and the highest nucleotide identities of 99.7–100%, 99.6–99.8%, and 99.8–100% with the *B. kosoyi* strain Tel Aviv for the 16S rRNA, *gltA*, and *ftsz* genes, respectively.

Phylogenetic trees based on the 16S rRNA, *gltA*, and *ftsz* gene sequences were reconstructed, and these three trees presented similar topologies. Consistent with the genetic analysis, all sequences in the three trees were divided into eight different groups that corresponded to *B. japonica*, *Bartonella* sp.

1-1C, *B. rattimassiliensis*, *B. grahamii*, *B. taylorii*, *B. tribocorum*, *B. mastomydis*, and *B. kosoyi* (**Figures 2-4**). Moreover, the 16S rRNA gene sequence of Shexian-Aa46 clustered with that of *B. vinsonii* in the 16S rRNA tree (**Figure 2**). However, in the phylogenetic tree of *ftsz*, all sequences obtained in this study were classified into six different groups due to the absence of the *ftsz* gene sequence in the *B. japonica* strain Chengde-Rn16 and the *B. mastomydis* strain Handan-Aa8.

Discussion

Over the past 30 years, an increasing number of rodent-borne *Bartonella* species and associated patients with fever or endocarditis have been reported, suggesting more common human exposures to these agents than previously suspected (Daly et al., 1993; Kerkhoff et al., 1999; Roux et al., 2000; Kosoy et al., 2003, 2010; Eremeeva et al., 2007; Vayssier-Taussat et al., 2016; Okaro et al., 2017; Krügel et al., 2022). In addition, some species that were not previously thought to infect humans have now been confirmed to be human pathogens (Eremeeva et al., 2007; Vayssier-Taussat et al., 2016; Krügel et al., 2022). Hence, human-pathogenic *Bartonella* spp. are being considered emerging zoonotic causative agents, and more attention should be paid to their infection in reservoirs, vectors, and humans for the better prevention of bartonellosis.

Rodents are considered to be the primary natural hosts of *Bartonella* spp., and most known species have been detected in a wide variety of rodents. In China, more than half of the rodent-associated *Bartonella* species have been identified from rodents in residential and field areas (Saisongkorh et al., 2009; Xia et al., 2015; Rao et al., 2021; Krügel et al., 2022). *R. norvegicus* and *A. agrarius* are the predominant species found in residential areas and the wild, respectively, and they can also act as the hosts of *Bartonella* spp. In previous studies, at least seven validated *Bartonella* species, namely, *B. elizabethae*, *B. grahamii*, *B. rattimassiliensis*, *B. rochalimae*, *B. tribocorum*, *B. mastomydis*, and *B. queenslandensis*, were identified in *R. norvegicus* (Qin et al., 2019; An et al., 2020; Liu et al., 2022; Yao et al., 2022; Yu et al., 2022c), and six species, namely, *B. fuyuanensis*, *B. grahamii*, *B. phoceensis*, *B. japonica*, *B. taylorii*, and *B. coopersplainsensis*, were identified in *A. agrarius* (Li et al., 2015; Qin et al., 2019; Lu et al., 2022; Yu et al., 2022b). In the present study, eight official or candidate *Bartonella* species, in addition to *B. vinsonii*-like species, were identified in rodents. The findings indicated that genetically diverse *Bartonella* species are circulating in rodent populations in Hebei Province, China. In addition, this was the first identification of *B. kosoyi* in China.

Consistent with the previous study, no significant difference in the detection rate was associated with either the gender or the age of the rodents (Yao et al., 2022). In this study, it was found that the overall detection rate of *Bartonella* sp. infection in rodents was 17.0%, lower than that in rodents from the Qinghai-Tibetan Plateau (30.1%, Yu et al., 2022a), the Shangdang Basin (37.4%, Yu et al., 2022b), the Qaidam Basin (38.6%, Rao et al., 2021), Heixiazi Island (57.7%, Li et al., 2015), Shaanxi (26.1%, An et al., 2020), Zhongtiao Mountain (49.5%, Yu et al., 2022c), Zhejiang (31.4%, Liu et al., 2010), and South China (43.5%, Ying et al., 2002), while higher than that in rodents from eastern China (8.4%, Qin et al., 2019) and Guangzhou (6.4%, Yao et al., 2022). In addition, similar detection rates to those found in the present study were observed in rodents from Guizhou (16.1%; Lu et al., 2022) and southeastern China (14.9%; Liu et al., 2022). The discrepancy might have been due to the rodent species, habitats, and arthropod vector populations (Meheretu et al., 2013). In addition, compared to rodents collected in residential areas, a higher detection rate was observed in rodents collected in the wild (Yu et al., 2022b). Similarly, in this study, a *Bartonella* sp. DNA detection rate of 28.4% was observed in *R. norvegicus* in residential areas, while a 6.7% rate was found in *A. agrarius* in the field. However, *R. norvegicus* and *A. agrarius* were captured from different areas; thus, it was not clear whether the rodent species or the habitat was the factor that affected the detection rate, which is a limitation of this study.

In China, all eight rodent-related *Bartonella* species pathogenic to humans have been identified, mostly in the past 10 years (Li et al., 2015; Su et al., 2020; Yao et al., 2022). In this study, three human-pathogenic *Bartonella* species were detected, including *B. rattimassiliensis* and *B. grahamii* in Chengde and *B. tribocorum* in Handan. More importantly, the presence of *B. tribocorum* should be of concern due to the high detection rate of *A. agrarius*. In addition, attention should be paid to *B. rattimassiliensis* and *B. grahamii* due to the close association between their host, *R. norvegicus*, and humans, though they displayed a relatively low detection rate in rodents. *Bartonella* spp. are mainly transmitted from rodents to humans by blood-sucking arthropod vectors (Deng et al., 2012). In China, diverse *Bartonella* spp. have been identified in ectoparasites such as ticks, lice, and fleas (Li et al., 2007, 2013; Hao et al., 2020). Unfortunately, we failed to collect ectoparasites from the sampled rodents, which is another limitation of our study. Therefore, ectoparasites should be collected and analyzed in future studies. Furthermore, the presence of *Bartonella* spp. should be monitored and investigated in humans with fever of unknown origin or endocarditis in the local population.

As the natural reservoir hosts of many different types of microorganisms, rodents are considered to have a long-term co-divergence or co-speciation with the pathogens they carry, such as hantaviruses (Guo et al., 2013) and arenaviruses (Gonzalez et al., 2007). In terms of *Bartonella* species, Kosoy et al. also considered that they present potential co-evolution or co-speciation with their rodent hosts according to the host specificity (Kosoy et al., 2000). In addition, some previous studies have also demonstrated the host specificity of *Bartonella*

FIGURE 2
Maximum-likelihood (ML) tree reconstructed based on the 16S rRNA gene sequences of *Bartonella* species. Bootstrap values were calculated with 100 replicates and only > 70% are shown. Sequences of human-pathogenic *Bartonella* species determined herein are marked as black squares and others as black circles.

sp. infection in rodents (Telfer et al., 2007; Abreu-Yanes et al., 2018; Qin et al., 2019; Divari et al., 2021). However, an increasing amount of evidence has suggested a lack of host specificity because the same *Bartonella* species can be identified from a diversity of rodent hosts, even from those belonging to different families (Billeter et al., 2014; Krügel et al., 2022). In

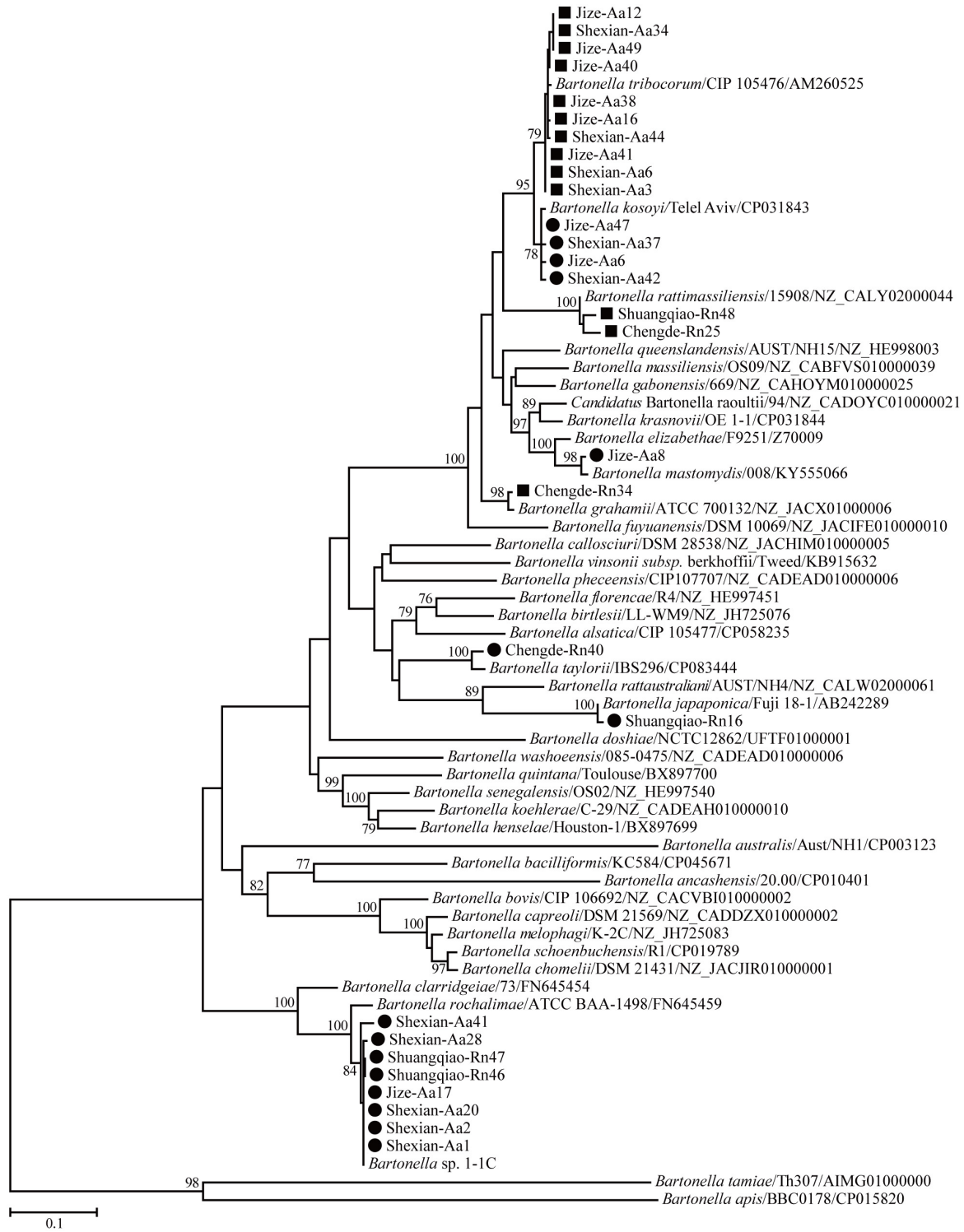

FIGURE 3
Maximum-likelihood (ML) tree reconstructed based on the *gltA* gene sequences of *Bartonella* species. The legend follows that of **Figure 2**.

the current study, *B. japonica*, *B. rattimassiliensis*, *B. grahamii*, and *B. taylorii* only in *R. norvegicus* and *B. tribocorum*, *B. mastomydis*, and *B. kosoyi* only in *A. agrarius* appear to support the view that *Bartonella* infection in rodents can exhibit host specificity. However, the *R. norvegicus* and *A. agrarius* in this study were sampled from different cities. In addition, the

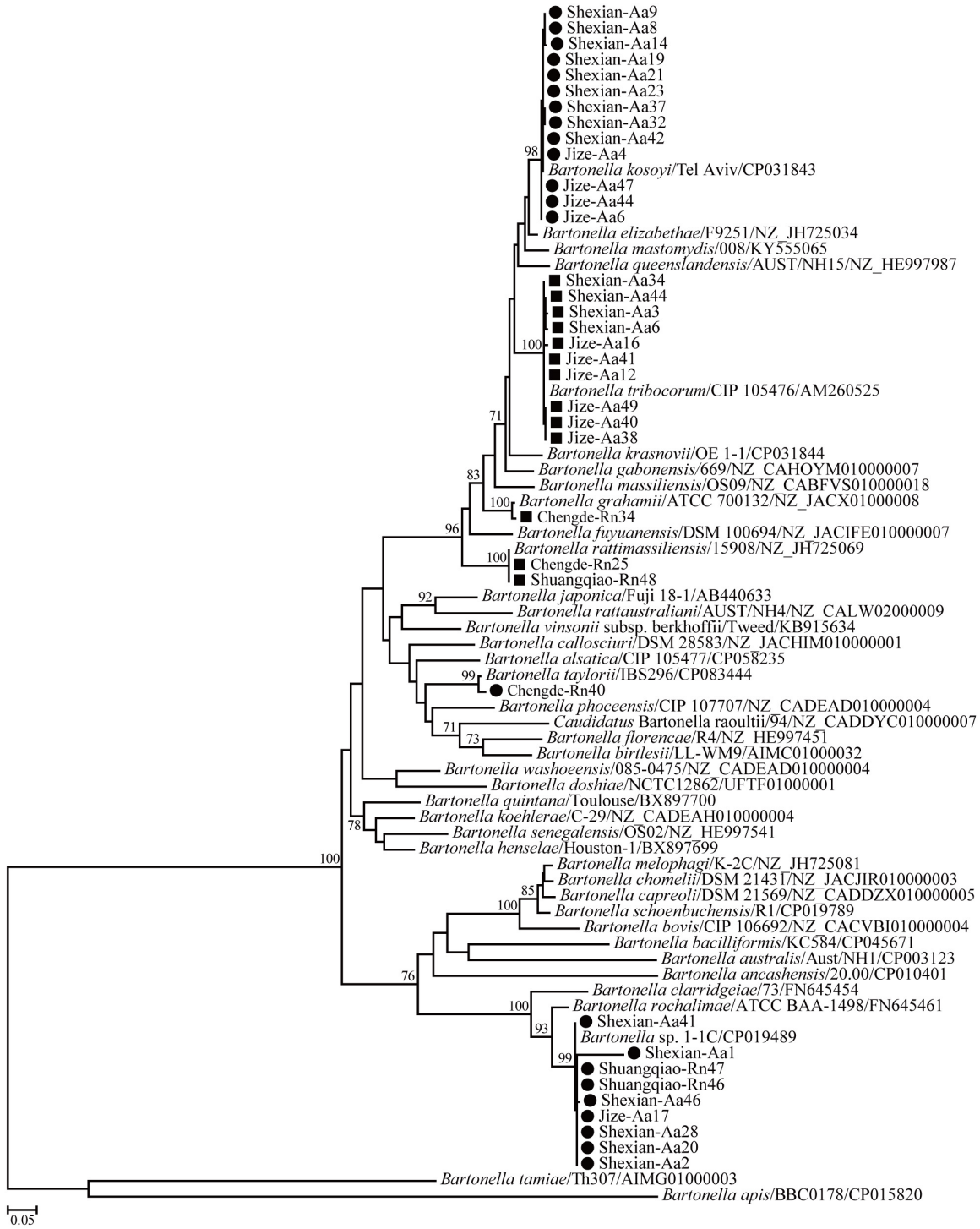

FIGURE 4
Maximum-likelihood (ML) tree reconstructed based on the *ftsz* gene sequences of *Bartonella* species. The legend follows that of **Figure 2**.

Bartonella species identified in this study were found to be carried by various rodents, as shown in previous studies. Hence, the apparent host specificity observed in this study might have been caused by the different habitats of the rodents.

Conclusion

At least eight *Bartonella* species, including three human causative agents, were identified in two rodent species in Hebei

Province, China. In addition, *Bartonella* sp. DNA detection rates of 28.4% and 6.7% were observed in *A. agrarius* in Handan City and in *R. norvegicus* in Chengde City, respectively. Our results also indicated a lack of host specificity for *Bartonella* sp. infection in rodents. Overall, our results indicate that more attention should be paid to the surveillance of rodent-associated *Bartonella* species.

Data availability statement

The datasets presented in this study can be found in online repositories. The names of the repository/repositories and accession number(s) can be found in the article/ **Supplementary material**.

Ethics statement

This animal study was reviewed and approved by Ethics Committee of the Chengde Medical University.

Author contributions

W-PG conceived and designed the experiments and contributed to writing, reviewing, and editing the manuscript. RJ, QR, JX, G-CX, G-QC, and LD performed the experiments and analyzed the data. W-PG and JW helped to collect the samples. W-PG and RJ participated in writing the original draft. All authors contributed to the article and approved the submitted version.

Funding

This study was funded by the Young Talent Program of Higher School in Hebei Province (No. BJ2020024), the Natural Science Foundation of Hebei Province (No. C2022406003), the Scientific Research Foundation for High-level Talents of Chengde Medical University (No. 202001), and key discipline construction of colleges and universities in Hebei Province (Ji Jiao Gao No. [2013]4).

Conflict of interest

The authors declare that the research was conducted in the absence of any commercial or financial relationships that could be construed as a potential conflict of interest.

Publisher's note

All claims expressed in this article are solely those of the authors and do not necessarily represent those of their affiliated organizations, or those of the publisher, the editors and the reviewers. Any product that may be evaluated in this article, or claim that may be made by its manufacturer, is not guaranteed or endorsed by the publisher.

Supplementary material

The Supplementary Material for this article can be found online at: https://www.frontiersin.org/articles/10.3389/fmicb.2022.1039665/full#supplementary-material

References

Abreu-Yanes, E., Martin-Alonso, A., Martin-Carrillo, N., Livia, K. G., Marrero-Gagliardi, A., Valladares, B., et al. (2018). *Bartonella* in rodents and ectoparasites in the Canary Islands, Spain: New insights into host-vector-pathogen relationships. *Microb. Ecol.* 75, 264–273. doi: 10.1007/s00248-017-1022-y

An, C. H., Chen, B. B., Lyu, W., Nie, S. M., Li, S. Z., Fan, S. P., et al. (2020). *Bartonella* species investigated among rodents from Shaanxi province of China. *Biomed. Environ. Sci.* 33, 201–205. doi: 10.3967/bes2020.028

Billeter, S. A., Borchert, J. N., Atiku, L. A., Mpanga, J. T., Gage, K. L., and Kosoy, M. Y. (2014). *Bartonella* species in invasive rats and indigenous rodents from Uganda. *Vector Borne Zoonotic Dis.* 14, 182–188. doi: 10.1089/vbz.2013.1375

Böge, I., Pfeffer, M., Htwe, N. M., Maw, P. P., Sarathchandra, S. R., Sluydts, V., et al. (2021). First detection of *Bartonella* spp. in small mammals from rice storage and processing facilities in Myanmar and Sri Lanka. *Microorganisms* 9:658. doi: 10.3390/microorganisms9030658

Burland, T. G. (2000). DNASTAR's lasergene sequence analysis software. *Methods Mol. Biol.* 132, 71–91.

Chen, H. X. (1987). *Classification and identification of medical animals*. Beijing: The Institute of Epidemiology and Microbiology, Chinese Academy of Preventive Medicine, 123–125. (in Chinese).

Chomel, B. B., and Kasten, R. W. (2010). *Bartonellosis*, an increasingly recognized zoonosis. *J. Appl. Microbiol.* 109, 743–750. doi: 10.1111/j.1365-2672.2010.04679.x

Daly, J. S., Worthington, M. G., Brenner, D. J., Moss, C. W., Hollis, D. G., Weyant, R. S., et al. (1993). Rochalimaea elizabethae sp. nov. isolated from a patient with endocarditis. *J. Clin. Microbiol.* 31, 872–881. doi: 10.1128/jcm.31.4.872-881.1993

Deng, H., Le Rhun, D., Buffet, J. P., Cotté, V., Read, A., Birtles, R. J., et al. (2012). Strategies of exploitation of mammalian reservoirs by *Bartonella* species. *Vet. Res.* 43:15. doi: 10.1186/1297-9716-43-15

Divari, S., Danelli, M., Pregel, P., Ghielmetti, G., Borel, N., and Bollo, E. (2021). Biomolecular investigation of *Bartonella* spp. in wild rodents of two swiss regions. *Pathogens* 10:1331. doi: 10.3390/pathogens10101331

Divari, S., Pregel, P., Zanet, S., Ferroglio, E., Giannini, F., Scaglione, F. E., et al. (2020). Molecular evidence of *Bartonella* spp. in rodents: A study in Pianosa Island, Italy. *Animals (Basel)* 10:2070. doi: 10.3390/ani10112070

do Amaral, R. B., Cardozo, M. V., Varani, A. M., Gonçalves, L. R., Furquim, M. E. C., Dias, C. M., et al. (2022). *Bartonella* machadoae sp. nov. isolated from

wild rodents in the Pantanal wetland. *Acta Trop.* 229:106368. doi: 10.1016/j.actatropica.2022.106368

Eremeeva, M. E., Gerns, H. L., Lydy, S. L., Goo, J. S., Ryan, E. T., Mathew, S. S., et al. (2007). Bacteremia, fever, and splenomegaly caused by a newly recognized *Bartonella* species. *N. Engl. J. Med.* 356, 2381–2387. doi: 10.1056/NEJMoa065987

Fournier, P. E., Taylor, C., Rolain, J. M., Barrassi, L., Smith, G., and Raoult, D. (2007). *Bartonella australis* sp. nov. from kangaroos, Australia. *Emerg. Infect. Dis.* 13, 1961–1962. doi: 10.3201/eid1312.060559

Gonzalez, J. P., Emonet, S., de Lamballerie, X., and Charrel, R. (2007). Arenaviruses. *Curr. Top. Microbiol. Immunol.* 315, 253–288. doi: 10.1007/978-3-540-70962-6_11

Guindon, S., Dufayard, J. F., Lefort, V., Anisimova, M., Hordijk, W., and Gascuel, O. (2010). New algorithms and methods to estimate maximum-likelihood phylogenies: Assessing the performance of PhyML 3.0. *Syst. Biol.* 59, 307–321. doi: 10.1093/sysbio/syq010

Guo, W. P., Lin, X. D., Wang, W., Tian, J. H., Cong, M. L., Zhang, H. L., et al. (2013). Phylogeny and origins of hantaviruses harbored by bats, insectivores, and rodents. *PLoS Pathog.* 9:e1003159. doi: 10.1371/journal.ppat.1003159

Hall, T. A. (1999). BioEdit: A user-friendly biological sequence alignment editor and analysis. *Nuclc. Acids Symp.* 41, 95–98.

Hao, L., Yuan, D., Guo, L., Hou, W., Mo, X., Yin, J., et al. (2020). Molecular detection of *Bartonella* in ixodid ticks collected from yaks and plateau pikas (*Ochotona curzoniae*) in Shiqu County, China. *BMC Vet. Res.* 16:235. doi: 10.1186/s12917-020-02452-x

Helan, J. V. G., Grinberg, A., Gedye, K., Potter, M. A., and Harrus, S. (2018). Molecular detection of *Bartonella coopersplainsensis* and B. henselae in rats from New Zealand. *N. Z. Vet. J.* 66, 257–260. doi: 10.1080/00480169.2018.1483781

Kerkhoff, F. T., Bergmans, A. M., van Der Zee, A., and Rothova, A. (1999). Demonstration of *Bartonella grahamii* DNA in ocular fluids of a patient with neuroretinitis. *J. Clin. Microbiol.* 37, 4034–4038. doi: 10.1128/JCM.37.12.4034-4038.1999

Kosoy, M., Bai, Y., Sheff, K., Morway, C., Baggett, H., Maloney, S. A., et al. (2010). Identification of *Bartonella* infections in febrile human patients from Thailand and their potential animal reservoirs. *Am. J. Trop. Med. Hyg.* 82, 1140–1145. doi: 10.4269/ajtmh.2010.09-0778

Kosoy, M., Murray, M., Gilmore, R. D. Jr., Bai, Y., and Gage, K. L. (2003). *Bartonella* strains from ground squirrels are identical to *Bartonella washoensis* isolated from a human patient. *J. Clin. Microbiol.* 41, 645–650. doi: 10.1128/JCM.41.2.645-650.2003

Kosoy, M. Y., Saito, E. K., Green, D., Marston, E. L., Jones, D. C., and Childs, J. E. (2000). Experimental evidence of host specificity of *Bartonella* infection in rodents. *Comp. Immunol. Microbiol. Infect. Dis.* 23, 221–238. doi: 10.1016/s0147-9571(99)00075-2

Krügel, M., Król, N., Kempf, V. A. J., Pfeffer, M., and Obiegala, A. (2022). Emerging rodent-associated *Bartonella*: A threat for human health? *Parasit. Vectors* 15:113. doi: 10.1186/s13071-022-05162-5

Kumar, S., Stecher, G., and Tamura, K. (2016). MEGA7: Molecular evolutionary genetics analysis version 7.0 for bigger datasets. *Mol. Biol. Evol.* 33, 1870–1874. doi: 10.1093/molbev/msw054

Li, D. M., Hou, Y., Song, X. P., Fu, Y. Q., Li, G. C., Li, M., et al. (2015). High prevalence and genetic heterogeneity of rodent-borne *Bartonella* species on Heixiazi Island, China. *Appl. Environ. Microbiol.* 81, 7981–7992. doi: 10.1128/AEM.02041-15

Li, D. M., Liu, Q. Y., Yu, D. Z., Zhang, J. Z., Gong, Z. D., and Song, X. P. (2007). Phylogenetic analysis of *Bartonella* detected in rodent fleas in Yunnan, China. *J. Wildl. Dis.* 43, 609–617. doi: 10.7589/0090-3558-43.4.609

Li, H., Liu, W., Zhang, G. Z., Sun, Z. Z., Bai, J. Y., Jiang, B. G., et al. (2013). Transmission and maintenance cycle of *Bartonella quintana* among rhesus macaques, China. *Emerg. Infect. Dis.* 19, 297–300. doi: 10.3201/eid1902.120816

Lin, J. W., Chen, C. Y., Chen, W. C., Chomel, B. B., and Chang, C. C. (2008). Isolation of *Bartonella* species from rodents in Taiwan including a strain closely related to '*Bartonella rochalimae*' from *Rattus norvegicus*. *J. Med. Microbiol.* 57, 1496–1501. doi: 10.1099/jmm.0.2008/004671-0

Liu, H., Han, T., Liu, W., Xu, G., Zheng, K., and Xiao, F. (2022). Epidemiological characteristics and genetic diversity of *Bartonella* species in rodents from southeastern China. *Zoonoses Public Health* 69, 224–234. doi: 10.1111/zph.12912

Liu, Q., Sun, J., Lu, L., Fu, G., Ding, G., Song, X., et al. (2010). Detection of *Bartonella* species in small mammals from Zhejiang province. *China J. Wildl. Dis.* 46, 179–185. doi: 10.7589/0090-3558-46.1.179

López-Pérez, A. M., Osikowicz, L., Bai, Y., Montenieri, J., Rubio, A., Moreno, K., et al. (2017). Prevalence and phylogenetic analysis of *Bartonella* species of wild carnivores and their fleas in northwestern Mexico. *Ecohealth* 14, 116–129. doi: 10.1007/s10393-017-1216-2

Lu, M., Tang, G., Ren, Z., Zhang, J., Wang, W., Qin, X., et al. (2022). *Ehrlichia*, *Coxiella* and *Bartonella* infections in rodents from Guizhou province, Southwest China. *Ticks Tick Borne Dis.* 13:101974. doi: 10.1016/j.ttbdis.2022.101974

Maggi, R. G., Kosoy, M., Mintzer, M., and Breitschwerdt, E. B. (2009). Isolation of Candidatus *Bartonella melophagi* from human blood. *Emerg. Infect. Dis.* 15, 66–68. doi: 10.3201/eid1501.081080

Maggi, R. G., Raverty, S. A., Lester, S. J., Huff, D. G., Haulena, M., Ford, S. L., et al. (2008). *Bartonella henselae* in captive and hunter-harvested beluga (*Delphinapterus leucas*). *J. Wildl. Dis.* 44, 871–877. doi: 10.7589/0090-3558-44.4.871

Marciano, O., Gutiérrez, R., Morick, D., King, R., Nachum-Biala, Y., Baneth, G., et al. (2016). Detection of *Bartonella* spp. in wild carnivores, hyraxes, hedgehog and rodents from Israel. *Parasitology* 143, 1232–1242. doi: 10.1017/S0031182016000603

Meerburg, B. G., Singleton, G. R., and Kijlstra, A. (2009). Rodent-borne diseases and their risks for public health. *Crit. Rev. Microbiol.* 35, 221–270. doi: 10.1080/10408410902989837

Meheretu, Y., Leirs, H., Welegerima, K., Breno, M., Tomas, Z., Kidane, D., et al. (2013). *Bartonella* prevalence and genetic diversity in small mammals from Ethiopia. *Vector Borne Zoonotic Dis.* 13, 164–175. doi: 10.1089/vbz.2012.1004

Okaro, U., Addisu, A., Casanas, B., and Anderson, B. (2017). *Bartonella* species, an emerging cause of blood-culture-negative endocarditis. *Clin. Microbiol. Rev.* 30, 709–746. doi: 10.1128/CMR.00013-17

Qin, X. R., Liu, J. W., Yu, H., and Yu, X. J. (2019). *Bartonella* species detected in rodents from eastern China. *Vector Borne Zoonotic Dis.* 19, 810–814. doi: 10.1089/vbz.2018.2410

Rao, H., Li, S., Lu, L., Wang, R., Song, X., Sun, K., et al. (2021). Genetic diversity of *Bartonella* species in small mammals in the Qaidam Basin, western China. *Sci. Rep.* 11:1735. doi: 10.1038/s41598-021-81508-w

Rasis, M., Rudoler, N., Schwartz, D., and Giladi, M. (2014). *Bartonella* dromedarii sp. nov. isolated from domesticated camels (*Camelus dromedarius*) in Israel. *Vector Borne Zoonotic Dis.* 14, 775–782. doi: 10.1089/vbz.2014.1663

Roux, V., Eykyn, S. J., Wyllie, S., and Raoult, D. (2000). *Bartonella vinsonii* subsp. berkhoffii as an agent of afebrile blood culture-negative endocarditis in a human. *J. Clin. Microbiol.* 38, 1698–1700. doi: 10.1128/JCM.38.4.1698-1700.2000

Saisongkorh, W., Rolain, J. M., Suputtamongkol, Y., and Raoult, D. (2009). Emerging *Bartonella* in humans and animals in Asia and Australia. *J. Med. Assoc. Thai.* 92, 707–731.

Sato, S., Kabeya, H., Yamazaki, M., Takeno, S., Suzuki, K., Kobayashi, S., et al. (2012). Prevalence and genetic diversity of *Bartonella* species in sika deer (*Cervus nippon*) in Japan. *Comp. Immunol. Microbiol. Infect. Dis.* 35, 575–581. doi: 10.1016/j.cimid.2012.07.001

Su, Q., Chen, Y., Wang, B., Huang, C., Han, S., Yuan, G., et al. (2020). Epidemiology and genetic diversity of zoonotic pathogens in urban rats (*Rattus* spp.) from a subtropical city, Guangzhou, southern China. *Zoonoses Public Health* 67, 534–545. doi: 10.1111/zph.12717

Telfer, S., Clough, H. E., Birtles, L. R., Bennett, M., Carslake, D., Helyar, S., et al. (2007). Ecological differences and coexistence in a guild of microparasites: *Bartonella* in wild rodents. *Ecology* 88, 1841–1849. doi: 10.1890/06-1004.1

Vayssier-Taussat, M., Moutailler, S., Féménia, F., Raymond, P., Croce, O., La Scola, B., et al. (2016). Identification of novel zoonotic activity of *Bartonella* spp., France. *Emerg. Infect. Dis.* 22, 457–462. doi: 10.3201/eid2203.150269

Wang, Y. X. (2003). *A complete checklist of mammal species and subspecies in China - a taxonomic and geographic reference*. Beijing: China Forestry Publishing House, 27–59. (in Chinese).

Xia, X., Liu, S., Zhang, L., Dai, M., Zhang, J., and Zhu, H. (2015). Tick infestation and tick-borne pathogen infection in human and ticks in a military camp and nearby area in Xiaogan, Hubei. *Int. J. Med. Parasit. Dis.* 42, 337–340. (in Chinese), doi: 10.3760/cma.j.issn.1673-4122.2015.06.007

Yao, X. Y., Liu, H., Sun, J., Zhang, Y. Q., Lv, Z. H., Zhang, X. L., et al. (2022). Epidemiology and genetic diversity of

Bartonella in rodents in urban areas of Guangzhou, southern China. *Front. Microbiol.* 13:942587. doi: 10.3389/fmicb.2022.942587

Ying, B., Kosoy, M. Y., Maupin, G. O., Tsuchiya, K. R., and Gage, K. L. (2002). Genetic and ecologic characteristics of *Bartonella* communities in rodents in southern China. *Am. J. Trop. Med. Hyg.* 66, 622–627. doi: 10.4269/ajtmh.2002.66.622

Yu, J., Zhang, X. Y., Chen, Y. X., Cheng, H. B., Li, D. M., and Rao, H. X. (2022c). Molecular detection and genetic characterization of small rodents associated *Bartonella* species in Zhongtiao Mountain, China. *PLoS One.* 17:e0264591. doi: 10.1371/journal.pone.0264591

Yu, J., Xie, B., Bi, G. Y., Zuo, H. H., Du, X. Y., Bi, L. F., et al. (2022b). Prevalence and diversity of small rodent-associated *Bartonella* species in Shangdang Basin, China. *PLoS Negl. Trop. Dis.* 16:e0010446. doi: 10.1371/journal.pntd.0010446

Yu, J., Li, Q., Lu, L., Li, S., Song, X., Li, D., et al. (2022a). Detection and genetic diversity of *Bartonella* species in small mammals from the central region of the Qinghai-Tibetan Plateau, China. *Sci. Rep.* 12:6996. doi: 10.1038/s41598-022-11419-x

Frontiers in Microbiology

Explores the habitable world and the potential of microbial life

The largest and most cited microbiology journal which advances our understanding of the role microbes play in addressing global challenges such as healthcare, food security, and climate change.

Discover the latest Research Topics

See more →

Frontiers

Avenue du Tribunal-Fédéral 34
1005 Lausanne, Switzerland
frontiersin.org

Contact us

+41 (0)21 510 17 00
frontiersin.org/about/contact